On the role of entanglement in the out-of-equilibrium dynamics of many-body quantum systems

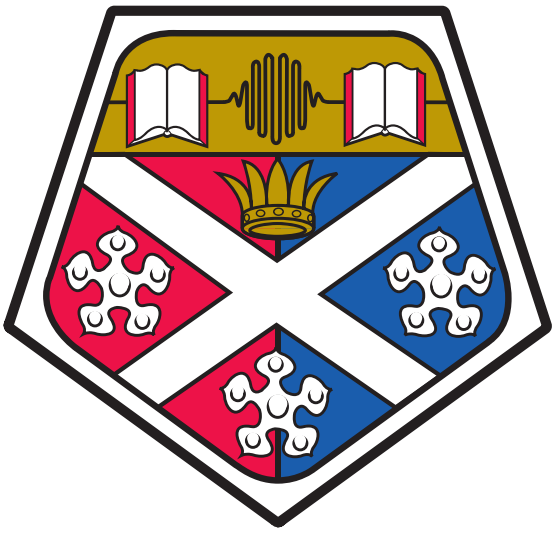

Jacopo Surace

Thesis submitted in partial fulfilment of requirements for the degree of Doctor of Philosophy

University of Strathclyde
Department of Physics and SUPA

September 2020

Abstract

Understanding the behaviour of many-body quantum systems is one of the great challenges in physics. Both at and out of equilibrium, besides few exactly solvable cases, our understanding relies on numerical simulations. Unfortunately, simulating many-body quantum systems is a hard computational problem. The standard lore is that this problem is exponentially hard in the case of simulating many-body quantum systems out-of-equilibrium. Even for simple systems, such as 1D spin chains, the current algorithms, based on the time-dependent density matrix renormalization group, are exponentially expensive in the amount of entanglement in the system. In generic out-of-equilibrium scenarios, the amount of entanglement grows linearly with time, resulting in exponentially expensive simulations. In the last years, however, the developments of the experimental techniques for controlling many-body quantum systems have pushed the exploration of out-of-equilibrium many-body quantum systems further. A critical assessment of the scope and limitations of classical numerical simulations that could help to both validate and understand the new experiments is thus necessary.

In this thesis we address this issue by unveiling the real role entanglement has in limiting our ability to simulate many-body quantum systems out-of-equilibrium. In particular, we first develop the tools for numerical computations. We build a comprehensive library for the manipulation of Fermionic Gaussian States with the programming language `Julia`. Then, we proceed to design and characterize a specific algorithm that allows to systematically approximate the equilibration value of local operators after a quantum quench. At the core of this algorithm there is the idea of transforming entanglement between distant parts of the system into mixture, while at the same time preserving the local reduced density matrices. Finally, we show that, for the Ising model, during the out-of-equilibrium evolution the entanglement spectrum allows us to obtain universal information. This information encodes the data of the underlying conformal field theory describing the system at the critical point, suggesting that it should be possible to adopt an analytical approach based on conformal field theories to obtain information about the out-of-equilibrium dynamics.

Contents

List of Figures

List of Tables

Acknowledgements

Phding has been long. It started with Luca Tagliacozzo being my supervisor, oscillated between Luca Tagliacozzo being the inspiring person able to share and to infect me and the people around him with his curiosity and Luca Tagliacozzo being an infinite dwell dragging me in a chaotic world I don't want to live in. It continued with me realising how much Luca taught me during these years, he allowed me to grow both academically and humanly. It ended up with me being grateful for having had Luca as my supervisor. Thank you Luca, you have been a mentor in all the aspects of my life, and this makes me feel really lucky.

Secondly I would like to thanks Antonio Acìn, he welcomed me in his group, giving me resources to expand towards new fields and consolidate on my old grounds.

Thank you also to Erling Riis and Gabriele De Chiara, my Phd Viva commision. I was really scared before Viving, but then it has actually been an almost fun and pleasant experience! And thanks to Marco Piani, Erik Tonni, Gian-Luca Oppo, Gordon Robb and Audrey McKinnon.

I here start a long list of thank-yous. First of all, even if she almost came last of all, I would like to thanks a girl with a super tiny head for pushing herself in my life with the greatest bravery I've ever seen. You have been and you are keeping being what makes me solid and strong. Hai un divano nel mio cuore, siediti. Then thanks to my best friend in Glasgow, really, thank you for everything, you are a sweet memory. Thank you to Zaragoza of London street, you have been patient, a lot, because of this now I feel emotionally attached to you. Then I thanks in order of importance Matteo,Tomohiro, Liviu and in sparse order Enrico,Joan (Gioan?), Tom, Jack, Laoganma, Andreas, Anton, Araceli and all the CNQO people. Then thank you

to Festinalente, since the first time I met you, I felt you close, Spain is beautiful with you. Thanks to @ddaarriiooddss, you are the first that welcomed me at ICFO, sei un figo. Thanks to @Qottmann, you are worthier than just a chandelier, thanks to the best couple Paolo and Arturo and the poor Erika. Thanks to @Wegophy, you are the angel of my focolar and the dj of my nights and merci to mamacitaataraxia, to both: it is beatutyuful living with you.

Lastly, thanks to my two best friends in alphabetical order: franz903@hotmail and @gatto_per_pranzo. You have supported me in your own ways in every moment, you are my best friends even though I am not the best friend you can have. <3

Thanks to Tàlia and Ginnywinnypinny.

Super lastly, thanks to my parents. To Camilla e Nicolò, I feel you are the best treasure I have in the world. To NaPi for creating all of this, for supporting all of this, believing in me and for showing me with real examples how with love you can find infinite strength. I hope one day saprò essere una persona di valore quanto voi.

And thanks to my english and mio espanolito and mio italjano.

Saying thank you is beatiful.

Chapter 1

Introduction

Understanding many-body systems is one of the great challenges driving research in physics. Many-body systems are composed of a large number of constituents which we can characterise singularly and for which we know the laws of interactions. A description of a many-body system involving the details of each of its constituents is called a microscopic description. The complexity of a microscopic description is notoriously computationally expensive. This can easily be seen by considering that the number of interactions can grow as the factorial of the number of constituents.

In this thesis, we are going to consider closed many-body quantum systems. These are systems where the constituents behave according to the laws of quantum mechanics and that are not in contact with any external environment. The study of these systems presents many challenges both experimentally and theoretically. Experimentally, isolating a system from the environment and observing the quantum behaviour of its constituents requires the abilities to work at really low temperatures and to keep a great degree of control on single atomic systems. Theoretically, the vast majority of quantum many-body systems are not analytically solvable and their investigation requires numerical studies. Numerical studies, in turn, are often impossible due to the exponential growth of the Hilbert space with the number of constituents of the system.

Due to the above mentioned limitations, the research in this field progressed slowly until not long ago.

This changed since the beginning of the '90s. The first Bose-Einstein condensate has been observed in 1995 [2–4]. This discovery marked the starting point of the fast development of the study of cold atoms systems. Indeed, in the subsequent decades, the joint development of experimental cooling techniques [5–8] together with methods for trapping and manipulating cold atoms (see e.g. [9] for a review) radically improved the ability of controlling many body quantum systems.
The fast development of experimental techniques contributed to pushing for the development of advanced numerical methods for simulating many-body quantum systems. In 1992 S. R. White developed the Density Matrix Renormalization Group (DMRG) [10], allowing the computation, with a limited amount of resources, of the ground state of particular one-dimensional many-body systems. In the same years and together with the flourishing of the field of many-body physics there has been the birth of the field of quantum information. The field of quantum information studies how the information is encoded and stored in quantum states, and subsequently how such information is processed during the dynamics. The central object of study in quantum information is the entanglement. It is from the cross-fertilisation of the study of many-body quantum systems and the study of quantum systems as information processing systems that in 2003 G. Vidal introduced the so-called Matrix Product States (MPS) as a fundamental tool for the study of many-body quantum systems [11, 12] (MPSs have been originally discovered in 1988 [13–15], while the first connection between MPS and DMRG was found by [16]).

Matrix product states provide a particular encoding of quantum states. Consider the state vector $|\psi\rangle$ of a many-body quantum system with N constituents. Generally, this vector is characterised by the collection of the coefficients obtained by projecting $|\psi\rangle$ on a specific basis of the Hilbert space associated with the system. The number of these coefficients is exponential in N. Matrix product states, instead, are characterised by a collection of N matrices, each associated with each constituent of the system. The dimension of these matrices is exponential with the amount of entanglement of the state. The discovery of the MPS encoding allowed to represent low-entangled quantum states with few computational resources, elevating entanglement to one of the most important

concepts in quantum many-body simulations and making the physics of many-body low entangled states tractable.

Coincidentally, following a series of theoretical results [17–19], it has been found that ground states of one-dimensional gapped many-body local Hamiltonian are all low-entanglement states. Thus, ground states of one-dimensional gapped Hamiltonians belong to the set of states efficiently tractable with MPS. Being able to solve the ground state physics of a big class of systems with MPS pushed for the development of new and sophisticated tensor network techniques (see [20–23] for a review) that allowed the computation of relevant equilibrium states as well as the simulation of the dynamics of some many-body quantum systems for short times. The necessity of extending MPS to the description of matrices gave birth to the Matrix Product Operators (MPO) formalism [24–26]. This allowed to efficiently study Hamiltonians with long-range interactions [27–30] and density matrices of mixed states, which made it possible to perform calculations at finite temperatures [25, 31]. Tensor network techniques fastly became the standard tools for condensed matter simulations.

The strong development of experimental and theoretical methods for the physics at equilibrium prepared the ground for the study of many-body closed quantum systems out-of-equilibrium. Together with the fundamental questions about the statistical mechanics of quantum systems [32–36], many other reasons pushed the research in this direction. For instance, we have witnessed over the last years, a huge development of quantum technologies. In this context, the majority of quantum processes are out-of-equilibrium [37]. Moreover, from a perspective of condensed matter physicists, looking at out-of-equilibrium physics we can explore an even richer zoo of phenomena that may not be present at equilibrium.

Furthermore, one can be interested in non-thermal equilibrium states as they can be considered as a resource [38]. It is clear, thus, that being able to simulate many-body systems out-of-equilibrium can have a big impact in many different fields.

Unfortunately, while experimental results on the out-of-equilibrium physics of many-body quantum systems proceeded fast [39–50] (see [51] for a review), the

numerical methods developed for the study of equilibrium physics started to fail in the out-of-equilibrium regime. In fact, moving out of equilibrium, the entanglement of the evolving state grows [52–58] and standard tensor networks techniques become too computational expensive. A faithful description of a general highly entangled state is in general impossible with standard numerical tools.

The combination of new experimental and numerical capabilities, nonetheless, lead to a parallel resurgence of the study of quantum statistical mechanics. Two topics, in particular, will be relevant for us. The study of the process of equilibration and thermalisation of closed quantum systems, a field until recent times inaccessible to experiments, and the study of universal properties of many-body quantum systems with the tools of conformal field theories.

In chapter 4 we will introduce quantum quenches [59], the standard protocol for investigating the out-of-equilibrium properties of closed quantum systems. Starting from the ground state $|\psi_0\rangle$ of a parameter-dependent local Hamiltonian $H(\lambda_0)$, one obtains its out-of-equilibrium evolution evolving it with the Hamiltonian $H(\lambda_1)$ obtained with the change of parameter $\lambda_0 \to \lambda_1$. For a broad class of systems, in the long-time regime, the state is expected to equilibrate *in some sense* to a stationary state. Generally, this state is expected to be a thermal state of the Hamiltonian, but, for closed quantum systems, this cannot be the case. In fact, since in closed quantum systems the time evolution is unitary, starting from a pure state (as the ground state of a Hamiltonian) it is impossible to obtain a mixed state, thus the system cannot relax to a Gibbs State. As said, though, these systems are expected to equilibrate *in some sense*. In these cases, one defines a *local* notion of equilibration. While a global relaxation is impossible, focussing on the local degrees of freedom makes it possible to recover a notion of relaxation [60–64].

These ideas suggest novel approaches for the numerical simulation of many-body quantum systems out-of-equilibrium. Instead of focussing on the microscopic dynamics, and thus on the faithful description of the state at each instant of time, we can instead individuate some relevant quantities that we are interested in and find the most efficient description capturing their behaviour. Focussing on local properties, we

have the intuition that the entanglement possibly does not have a crucial role in encoding information about relevant quantities. If this is true, it would imply that it is not necessary to be able to encode highly entangled states in order to simulate an approximation of the evolution out of equilibrium. This would allow to devise a computationally efficient approximate description of the dynamics out of equilibrium. In chapter 6 we will present an algorithm that exploits these ideas. In particular, this algorithm will transform entanglement between distant parts of the system into mixture, while at the same time preserving the local reduced density matrices of the system. This will allow the algorithm to compute an approximate description of the equilibration process at a low computational cost.

In chapter 5 we will introduce quantum conformal field theories. We have said that at equilibrium the wave-functions of quantum many-body systems characterised by gapped Hamiltonians contain a limited amount of entanglement that allows us to efficiently represent them with tensor networks. At quantum critical points this fact does not happen anymore [65]. Here the Hamiltonians become gapless and the entanglement of the ground state grows. Again we are in a situation where standard MPSs fail to encode the state of the system efficiently. In 2003 Vidal et al. [66] found that this growth of the entanglement follows universal laws. This means that this growth can be explained by an underlying theory independent of the particular details of the system one is considering. Here, the underlying theory is a conformal field theory [67–69]. In general, with the concept of universality one refers to the possibility for different systems to exhibit the same behaviour (evaluated with some defined quantity) if they present some same qualitative properties. When two systems exhibit the same behaviour, those systems are said to belong to the same universality class. Discovering that a system belongs to a known universality class allows us to compute some of its properties by working out the analogous calculations on the simplest system belonging to the same universality class. In this sense, the system becomes as difficult to treat as the simplest system in the same universality class. In the case of ground states of Hamiltonians at the quantum critical point, the study of the growth of the entanglement in the ground state as the dimension of the system

grows, allows unveiling some of the data of the underlying conformal field theory. Thus, studying the behaviour of the entanglement we can connect the system to its simpler description in terms of conformal field theory. In chapter 7 we will find that, even during the complex out-of-equilibrium dynamics, systems appear to always retain a universal behaviour associated to the critical point of the Hamiltonian and its underlying conformal field theory. As from chapter 6, also in this case, we will find that during the equilibration process, some relevant quantities of the system can be computed without the complete description of the higly-entangled state. In particular, in this case, we will need to know just the data specifying the particular underlying theory.

For dealing with these questions and investigating many-body quantum systems out-of-equilibrium it is essential to equip ourself with the necessary instruments. With this purpose, in chapter 3 we will develop the numerical tools for the treatment of Fermionic Gaussian systems. Fermionic Gaussian systems are completely solvable and it is possible to simulate their dynamics out of equilibrium with a memory cost linearly dependent on the number of constituents of the system. Some spin models, like the celebrated Ising model, are mappable to Fermionic Gaussian systems. The ability to easily manipulate these systems, allows us to explore the out-of-equilibrium dynamics easily. In general, the use of non-interacting systems is often seen as a first benchmark for tensor network algorithms (see e.g. [70]). This is because the strength of the interactions in a specific Hamiltonian does not necessarily affect the amount of entanglement between the constituents in its ground state. For example, ground states of free systems can be robustly entangled, thus highly entangled Fermionic Gaussian states are efficiently computable. Recently, several authors have realised that it is also possible to directly implement tensor network algorithms at the level of the correlation matrices (see e.g [71–75]). The numerical tools we will present include also part of these algorithms, together with our implementation of the time evolving block decimation algorithm [12] directly on the correlation matrices and other algorithms useful for mimicking tensor networks with Fermionic Gaussian states. These tools are collected in a package for `Julia` called `F_utilities` released on

Github.

1.1 Overview

This thesis is organised as follows.

In chapter 2 we present an overview of the standard methods used for encoding quantum systems. The chapter is divided into two parts. The first part presents methods dealing with the full Hilbert space, while the second one introduces methods for the reduced Hilbert space (reduced bond dimension). We present the topics highlighting the approximations and methodologies that fail when trying to simulate systems out of equilibrium and that will be treated in the second part of the thesis.

In chapter 3, we present the Julia library `F_utilities` together with a practical review of Fermionic Gaussian systems. Our aim with this chapter is presenting the main numerical tools developed for this thesis, that is a complete library, written in the proramming language `Julia`, for the manipulation of Fermionic Gaussian states. Starting from the basics of Fermionic Gaussian states, we develop the chapter including many relevant results from the literature, presenting useful models, experimental codes and new algorithms that we developed. Fermionic Gaussian states are an essential tool for numerical experiments, explorations and benchmarkings. Alongside the relevant theory, we present an explanation of examples of code and numerical experiments with the intention of realising a self-consistent chapter that can be used as a reference for the Julia library `F_utilities`.

In chapter 4 we introduce the topic of the out-of-equilibrium evolution in the context of quantum quenches and equilibration of closed quantum systems. We present the main equilibrium ensembles for equilibrated closed many-body quantum systems together with the fundamental mechanisms responsible for the equilibration. We pay special attention to quadratic systems, with explicit examples.

In chapter 5, we summarize important concepts, tools and quantities of quantum conformal field theories. In particular, we focus on conformal field theories in two dimensions, giving relevance to the quantities studied in chapter 7 and to the Ising model.

In chapter 6, we present our algorithm for predicting the value of some relevant quantities in the long-time regime of the out-of-equilibrium evolution. At the core of our proposal, there is the idea of transforming entanglement between distant parts of the system into mixture, while at the same time preserving the local reduced density matrices. We benchmark the algorithm by studying quenches of quadratic Fermionic Hamiltonians.

In chapter 7, we present our results on the universal information encoded in the out-of-equilibrium evolution of the Ising model. We consider the time evolution of the gaps of the entanglement spectrum for a block of consecutive sites in finite transverse field Ising chains after sudden quenches of the magnetic field. We provide numerical evidences that, whenever we quench at or across the quantum critical point, the time evolution of the ratios of these gaps allows to obtain universal information.

In Chapter 8 we draw our conclusions and give an overview of the key findings discussed in this thesis, together with possible interesting future directions of research.

1.2 Contributions during the PhD

- J. Surace, M. Piani, and L. Tagliacozzo, *Simulating the out-of-equilibrium dynamics of local observables by trading entanglement for mixture*, Phys. Rev. B 99, 235115 (2019).
- J. Surace, L. Tagliacozzo, and E. Tonni, *Operator content of entanglement spectra in the transverse field Ising chain after global quenches* , Phys. Rev. B 101, 241107(R) (2019).
- J. Surace, `F_utilities`, https://github.com/Jacupo/F_utilities
- J. Surace, L. Tagliacozzo, and E. Tonni, *Operator content of entanglement spectra in the transverse field Ising chain during the out-of-equilibrium dynamics*, in preparation.
- J. Surace, *Practical Gaussian States: a guide for numerical simulations with Gaussian states in Julia*, in preparation.

1.3 Conference talk presentations

- *Operator content of entanglement spectra after global quenches in the transverse field Ising chain*, Barcelona Cold Atom Meeting Feb-2020, Barcelona
- *Simulating the out-of-equilibrium dynamics of local observables trading entanglement for mixture*, ICE-5 May-2019, Barcelona
- *Predicting the robust features of the out-of-equilibrium evolution of many-body quantum systems*, V Pyrenees Winter School Apr-2019, Setcases, Spain
- *Local out-of-equilibrium dynamics of many body quantum systems*, QUISCO Jan-2018, University of Edinburgh

1.4 Posters

- *On the out-of-equilibrium evolution of local operators for Gaussian states*, Quantum Correlations in Space and Time, Bad Honnef, Germany
- *On the out-of-equilibrium evolution of local operators for Gaussian states*, Tensor network school, Ghent University

Chapter 2

Encoding of quantum states

In chapter 3 we are going to give a full overview on how to describe and manipulate a special class of quantum systems with the programming language `Julia`. In this chapter we study the task of encoding a quantum system from a more general perspective. We ask how a general quantum system, described as the principles of quantum mechanics dictates, can be encoded and manipulated with a computer. We first see how the encoding of a general quantum state requires a prohibitive amount of resources already for small physical systems. Then we see various methods for compressing the encoded quantum states and review modern techniques for approaching the closed dynamic of many-body quantum systems.

2.1 From first principles

2.1.1 Quantum states

The description of a quantum system entails a memory cost exponentially bigger than the description of a classical system. Indeed, encoding the state of a classical system (a point in a classical phase space) requires a number of parameters $\sim N$.

The principles of quantum mechanics associate a (complex and separable) Hilbert space to every quantum system. The description of a specific state of the system is a ray in the Hilbert space. Let us consider the system associated to the Hilbert space $\mathcal{H}_1$ of dimension $\dim(\mathcal{H}_1) = d_1$. Any state $|\psi\rangle$ can be represented as the linear

combination $|\psi\rangle = \sum_{i=1}^{d_1} \psi_i |i\rangle$, where $\{|i\rangle\}_{i=1}^{d}$ is an orthonormal basis of $\mathcal{H}_1$ and $\psi_i = \langle i|\psi\rangle$.

Fixing a standard orthonormal basis, as for example the basis $\{|i\rangle\}_{i=1}^{d}$, every state is completely encoded by the set of d_1 coefficients ψ_i. A quantum state is encoded in d_1 complex numbers.

It is a postulate of quantum mechanics that the joint state of two quantum systems $\mathcal{H}_1$ and $\mathcal{H}_2$, is a ray of the tensor product Hilbert space $\mathcal{H}_{1,2} = \mathcal{H}_1 \otimes \mathcal{H}_2$.

If the dimension of $\mathcal{H}_2$ is $\dim(\mathcal{H}_2) = d_2$, then the dimension of the joint system is $\dim(\mathcal{H}_{1,2}) = h_1 \cdot h_2$ and any state in $\mathcal{H}_{1,2}$ is encoded by a set of $d_1 \cdot d_2$ complex coefficients.

Let us consider a joint system of N constituents, its associated Hilbert space is $\mathcal{H} = \bigotimes_{x=1}^{N} \mathcal{H}_x$, where $\mathcal{H}_x$ is the Hilbert space associated to each constituent of the system. The total dimension of $\mathcal{H}$ is $\dim(\mathcal{H}) = d = d_1 d_2 \dots d_N$, and each state will be described by $d_1 d_2 \dots d_N$ complex coefficients.

It is clear at this point that for every quantum system we are going to consider there will always be two different dimensions. A dimension N corresponding to the number of constituents of the system and a dimension d corresponding to the number of parameters necessary for encoding the state of the system. These two dimensions are generally connected by the relation $d \sim e^N$.

The same relation holds even in the case of statistical mixtures of quantum states, where each state is encoded by the d^2 complex elements of its density matrix ρ. In general, every bounded operator on $\mathcal{H}$ can be completely encoded by d^2 complex coefficients.

2.1.2 Quantum Hamiltonians

Central to our discussion, is the closed evolution of quantum states.

The postulates dictate that the dynamics of a quantum system is governed by its Hamiltonian. The Hamiltonian is an Hermitian bounded operator $H(t)$ on the Hilbert space $\mathcal{H}$ associated to the system, possibly dependent by the time parameter t.

How a quantum state $|\psi\rangle$ evolves with the given Hamiltonian H is written in the principles of quantum mechanics, it is the solution of the eigenvalues problem

$$\frac{d|\psi\rangle}{dt} = -\frac{i}{\hbar}H(t)|\psi\rangle, \tag{2.1}$$

where we chose $|\psi\rangle$ as boundary condition. For the rest of the thesis we will set $\hbar = 1$. In the case of a time-independent Hamiltonian $H(t) = H$ the solution $|\psi(t)\rangle$ is given by

$$|\psi(t)\rangle = U(t)|\psi\rangle = e^{-iHt}|\psi\rangle, \tag{2.2}$$

where $U(t)$ is called the evolution operator.

The spectral theorem tells us that there is an orhonormal basis $\{|E_j\rangle\}_{j=1}^{d}$ for $\mathcal{H}$ of eigenvectors of the Hermitian Hamiltonian H and that each associated eigenvalue is real. The time evolved state $|\psi(t)\rangle$ takes the form

$$|\psi(t)\rangle = \sum_{j=1}^{d} e^{-iE_j t}\langle E_j|\psi\rangle|E_j\rangle = \sum_{j=1}^{d} e^{-iE_j t}c_j|E_j\rangle, \tag{2.3}$$

where $\{c_j\}_{j=1}^{d}$ are the coefficients that encode the state $|\psi\rangle$ in the non-standard basis $\{|E_j\rangle\}$, called energy eigenbasis.

In order to use the energy eigenbasis for solving the time evolution of a closed quantum system, we need to first solve the eigenvalues problem

$$E_i|E_i\rangle = H|E_i\rangle \tag{2.4}$$

Solving this problem, that is diagonalising an Hermitian matrix, generally is a computationally demanding task (diagonalising an $N \times N$ matrix requires, in general, $O(N^\nu)$ operations, where $\nu \in (2, 3)$ [76]). This, in addition to the necessity of storing all the coefficients encoding the Hamiltonian and the states, makes encoding the dynamics of a system exponentially expensive in the number of consitituents of the system.

2.2 Methods in the full Hilbert space

2.2.1 Symmetries

One technique for reducing the computational cost of the diagonalisation of an Hamiltonian without any approximation, consists in exploiting the symmetries of the system. To every symmetry corresponds a conserseved quantity and thus an operator that commutes with the Hamiltonian. The fact that an operator commutes with the Hamiltonian implies that the Hamiltonian can be divided in blocks, where each block is associated to a different eigenvalue of the commuting operator. Consider for example a Hamiltonian H that commutes with the parity operator P (3.13) ($[H, P] \coloneqq HP - PH = 0$). The parity operator has two different eigenvalues $\lambda_{\pm} = \pm 1$. This tells us that Hamiltonian H is divided in two sectors as represented in the middle part of fig 2.1. Each sector can be diagonalised independently, thus in order to diagonalise H we just have to diagonalise two matrices of smaller dimension. Since the cost of diagonalisation is a power of the dimension of the matrix, this already simplifies the task of diagonalising the whole matrix. If one is able to find multiple symmetries, then, each symmetry introduces a new block factorisation of the Hamiltonian, factorising each existing block in new sub-blocks. As an example, let us suppose that Hamiltonian H additionaly commutes with an operator T with 3 different eigenvalues t_1, t_2, t_3. This would divide the matrix H in the block structure showed in the right part of figure 2.1, simplyfing further the diagonalisation process.

2.2.2 Approximate numerical methods for diagonalisation the Hamiltonian

There exists many different methods for solving the eigenvalues problem (2.4), as, for example, [77–79].

It is not always the case, though, for someone to be interested in the full spectrum of the Hamiltonian. One can be interested in just a part of the spectrum, as for example the low-lying energy eigenvalues. In this case the computational cost can be

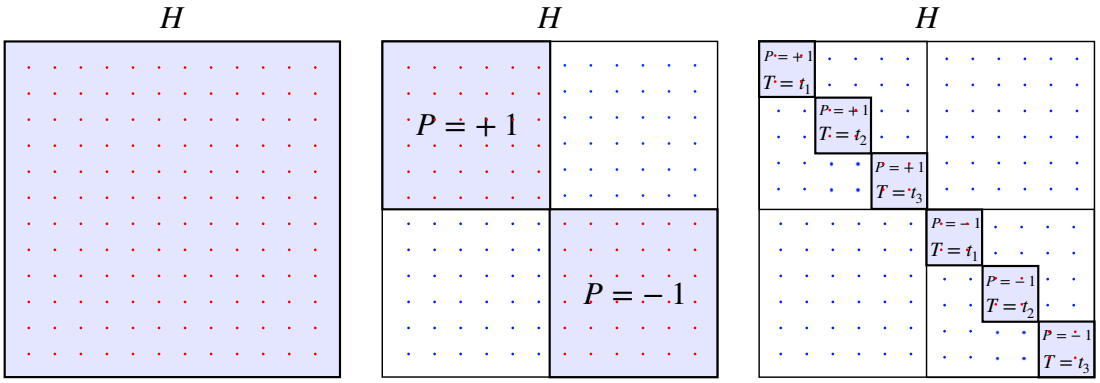

Figure 2.1: On the left we have a representation of the Hamiltonian H where each dot represents an entry. Blue dots correspond to zeroes, while red dots correspond to entries possibly different from 0. In the middle a representation of the block diagonal form on the sectors of the P operator. The operator P is such that $[H, P] = 0$ and it has just two eigenvalues $\lambda_\pm = \pm 1$. On the right we include the symmetry of T operator. Each sector is subdivided in 3 sectors corresponding to one of the three different eigenvalues of T.

significantly lowered and one can efficiently exploit the properties of the Hamiltonian such as sparsity. Iterative methods based on series expansions, as for example the Lanczos algorithm [80–82], allow us to compute the extremal parts of the spectrum (biggest or lowest eingenvalues and associated eigenvectors) with a computational cost that scales with the number of elements different from 0 in the matrix to diagonalise, thus exploiting the sparsity of the problem. These methods are the adaptations and development of the simple power method algorithm.

Power method algorithm The power method algorithm is based on the following idea. Suppose we want to find the biggest eigenvalue λ_1 and its associated eigenvector $|\lambda_1\rangle$ of a diagonalisable matrix H. We will consider the eigenvalues of H to be ordered as $\lambda_1 > \lambda_2 \geq \lambda_3 \geq \dots$. We start by choosing a random vector $|v^{[0]}\rangle$. We define the iterative algorithm

$$|v^{[n+1]}\rangle = \frac{H|v^{[n]}\rangle}{\left\| H|v^{[n]}\rangle \right\|}, \tag{2.5}$$

where $\||v\rangle\|$ is the norm of $|v\rangle$. Starting with $|v^{[0]}\rangle$, we expect that, if $\langle\lambda_1|v^{[0]}\rangle \neq 0$ and λ_1 is not degenerate, for n sufficiently big, $|v^{[n]}\rangle \sim |\lambda_1\rangle$. The fact that this algorithm converges towards $|\lambda_1\rangle$ can be easily proved by expanding $|v^{[0]}\rangle$ on the eigenbasis $\{|\lambda_i\rangle\}_i$

of H

$$|v^{[0]}\rangle = c_1|\lambda_1\rangle + c_2|\lambda_2\rangle + \dots, \tag{2.6}$$

with $c_i = \langle\lambda_i|v^{[0]}\rangle$ and thus $c_1 \neq 0$ because of the assumption $\langle\lambda_1|v^{[0]}\rangle \neq 0$. Now applying H to $|v^{[0]}\rangle$ for n times returns

$$H^n|v^{[0]}\rangle = c_1\lambda_1^n\left(|\lambda_1\rangle + \frac{c_2}{c_1}(\frac{\lambda_2}{\lambda_1})^2|\lambda_2\rangle + \dots\right). \tag{2.7}$$

Since λ_1 is the biggest eigenvalue we have that $(\frac{\lambda_i}{\lambda_1})^n \to 0$ with $n \to \infty$ for all $i \neq 1$. Because of this, we obtain that in the limit for $n \to \infty$, taking care of the normalisation, $H^n|v^{[0]}\rangle \to |\lambda_1\rangle$.
The convergence of this method is slow (it is geometric with ratio $\left|\frac{\lambda_2}{\lambda_1}\right|$) and it becomes slower as $\lambda_2 \to \lambda_1$.
We note here the importance of the value of the difference $|\lambda_1 - \lambda_2|$.

In condensed matter one is often interested in computing the ground state energy E_0 of a Hamiltonian H, that is the smallest eigenvalue of H. By adding a sufficiently big number to the Hamiltonian, one obtains that the smallest eigenvalue of H corresponds to the eigenvalue with the smallest magnitude. In order to compute the smallest eigenvalue in magnitude of H one can use the inverse power method [83] that fundamentally is the power method applied to H^{-1}. In this case the algorithm will converge geometrically with ratio $\frac{E_0}{E_1}$, where E_1 is the second smallest eigenvalue of the Hamiltonian H. If $E_1 - E_0 = 0$ then the algorithm will not converge.
Because of its importance, the difference between the two lowest eigenvalues of an Hamiltonian (that is the difference between the ground state energy and the first excited state energy) has a specific name and it is called *Hamiltonian Gap* or *spectral gap* often denoted by ΔE. In particular, definining a family of Hamiltonians dependendent on the parameter N (the dimension of the system), we call *gapless Hamiltonians* those Hamiltonians for wich the Hamiltonian Gap $\to$ 0 in the thermodynamics limit $N \to \infty$, and we call *gapped Hamiltonians* those Hamiltonians for which the spectral gap remains positive in the thermodynamic limit.

2.2.3 Approximate methods for the time evolution

Similar iterative methods used for computing the eigenvalues of the Hamiltonian can be used to compute the time evolution of a state. In fact, the Taylor expansion of the evolution operator

$$U(t) = e^{-iHt} = \mathbb{I} + \frac{(-iHt)^1}{1!} + \frac{(-iHt)^2}{2!} + \cdots + \frac{(-iHt)^n}{n!} + \ldots, \tag{2.8}$$

tells us that the time evolved state can be computed as

$$|\psi(t)\rangle = |\psi\rangle + \frac{(-iHt)^1}{1!}|\psi\rangle + \frac{(-iHt)^2}{2!}|\psi\rangle + \ldots, \tag{2.9}$$

that is just the sum of an iterative application of the Hamiltonian to the computed state. The series above can be truncated at step n leading to an approximation of the order $O(t^n)$. Methods based on this expansion, such as for example the Krylov subspace methods, suffer from the fact that they require to store the full Hamiltonian in the memory. As already said, storing the full Hamiltonian, often even when it is sparse, requires an amount of memory that scales exponentially with the dimension of the system.

To overcome these difficulties one can divide the Hamiltonian in different parts and then consider as the application of H the iterative application of each part of H. These methods are based on the Suzuki-Trotter decomposition [84, 85].

Suzuki-Trotter decomposition Let us consider two $n \times n$ matrices A and B. We are interested in computing the exponential e^{A+B} knowing e^A and e^B. In general we will have that $[A, B] \neq 0$, and thus, simply by the series expansion of e^{A+B} we notice that $e^{A+B} \neq e^A e^B$. The Trotter formula [84] tells us that

$$e^{A+B} = \lim_{n\to\infty} \left(e^{A/n} e^{B/n}\right)^n. \tag{2.10}$$

Starting from this, one can get the the Suzuki-Trotter decomposition at first order [85, 86]

$$e^{\delta(A+B)} = e^{\delta A} e^{\delta B} + O(\delta^2), \tag{2.11}$$

with δ a real number.

The Suzuki-Trotter decomposition results useful in physics as often the Hamiltonians considered have a local structure. To understand what a local structure is and how this can be exploited by a Suzuki-Trotter decomposition, it is instructive to look at an example. Let us consider a system of N constituents. To each constituent i we associate a Hilbert space of dimension d. We define the $d^N \times d^N$ Hamiltonian of the system as

$$H = \sum_{j=1}^{N-1} h_j \tag{2.12}$$

where $h_j \coloneqq \mathbb{I}_1 \otimes \cdots \otimes \mathbb{I}_{j-1} \otimes \tilde{h}_{j,j+1} \otimes \mathbb{I}_{j+1} \otimes \cdots \otimes \mathbb{I}_N$ with $\mathbb{I}_i$ the identity operator acting on the Hilbert space of the i-th constituent and $\tilde{h}_{j,j+1}$ a matrix acting on the Hilbert space of the j-th and $j+1$-th constituents. This Hamiltonian is called local because it is a sum of local terms, in the sense that each term has non trivial support on just few sites (1 site in this specific case) and thus $[h_i, h_j] = 0$ if $|i - j| > 1$. Because of this property one can associate a geometry to the Hamiltonian and imagine the label of each h_i to correspond to the site of a chain. In general, a variable is defined as k-local if it is supported on at most k sites. Using the Suzuki-Trotter decomposition we can write

$$e^{-iHt} = \prod_{j=1}^{N-1} e^{-ih_j t} + O(t^2), \tag{2.13}$$

and thus for small values of t we have a good approximation of the evolution operator as a product of the matrices $e^{-ih_j t}$. The key point of the approximation is the locality of the matrices h_j. In fact it is easy to see that

$$e^{-ih_j t} = \mathbb{I}_1 \otimes \cdots \otimes \mathbb{I}_{j-1} \otimes e^{-i\tilde{h}_{j,j+1}} \otimes \mathbb{I}_{j+1} \otimes \cdots \otimes \mathbb{I}_N, \tag{2.14}$$

thus instead of exponentiating a $d^N \times d^N$, we just need to compute N exponentiation of $d \times d$ matrices. The dimension of the matrices to exponentiate dropped exponentially. If the single terms of the Hamiltonian were not local this would have not happened.

2.3 Methods in the reduced Hilbert space

Everything we can talk about can be encoded in bits, therefore in order to understand the limitations of encoding and compressing data we can always think about binary strings.

Consider W_N the set of all binary strings of length N. The number of different elements in this set is 2^N.

We call $W_{<N}$ the set of all the binary string of length less or equal to $N-1$. Each element of this set is a couple (χ, c) where $\chi = |c|$ is a number specifying the length of the binary string c and c is the binary string, one example is $(3, 010)$. The number of different elements in this set is $2 + 2^2 + 2^3 + \cdots + 2^{N-1} = 2^N - 1$. This means that, excluding one single element of W_N, we can map W_N to $W_{<N}$. This mapping corresponds to a compression. We see that the elements of W_N mapped to elements of $W_{<N}$ with χ really small will be effectively compressed, while elements of W_N mapped to elements of $W_{<N}$ with $\chi \sim N$ will possibly requires more bit to be stored than the original string (as the description of the couple $(\chi \sim N, c)$ possibly requires more than N bits).

We also notice that sets of which the elements have shorter descriptions are set with smaller cardinality. Thus just few elements can be mapped to shorter strings and this comes at the cost of mapping other elements to longer strings.

These properties of the encoding can be exploited for compressing messages. If we define a message $\{\psi_t\}_t$ as a collection of elements $\psi_t \in W_N$ (where repetitions are allowed), we can compress the message simply assigning shorter string to elements that repeat more often and longer strings to elements that appears less often or do not appear at all. This idea is at the base of entropy encoding (see e.g. the seminal work of Huffman [87]) and it can be used for explaining why in spoken languages common

words (as for example *"yes"* and *"no"* with 3 and 2 letters respectively) are shorter than uncommon words (as for examples *"entanglement"* with 12 letters). This technique is called *entropy encoding* because the length of the compressed message is proportional to the Shannon entropy of the message [88].

In this section we present the powerful methods of matrix product states and operators, based on the tensor network representation [20–23, 89]. These methods characterise, out of all possible quantum states of a system, a restricted class of them and defines an efficient way for describing them. In analogy with the entropy encoding one can associate the set of all the states $|\psi\rangle \in \mathcal{H}$ to the set W_N and think of a message as the collection of all the states that we encounter in calculations or in experimental measurements. Matrix product states methods individuate a class of states that repeats very often in this message and tell us a method for encoding them. With an inspirational sentence we can say that tensor networks are the efficient language for describing our quantum mechanical experience.

2.3.1 Entanglement, Entropy and Spectra

In order to introuduce matrix product states, we will first review some notions of the theory of entanglement.

Entanglement

A pure state $|\psi\rangle$ on the tensor product Hilbert space $\mathcal{H} = \mathcal{H}_A \otimes \mathcal{H}_B$ is a product state if it can be written as

$$|\psi\rangle = |\psi\rangle_A \otimes |\psi\rangle_B, \tag{2.15}$$

with $|\psi\rangle_A \in \mathcal{H}_A$ and $|\psi\rangle_B \in \mathcal{H}_B$. This definition can be expanded to mixed states. A mixed state acting on the tensor product Hilbert space $\mathcal{H} = \mathcal{H}_A \otimes \mathcal{H}_B$ is a separable state if it can be written as

$$\rho = \sum_i p_i \rho_i^A \otimes \rho_i^B, \tag{2.16}$$

where $\{\rho_i^A\}_i$ and $\{\rho_i^B\}_i$ are set of density matrices acting respectively on $\mathcal{H}_A$ and $\mathcal{H}_B$ and $\{p_i\}_i$ are positive real numbers such that $\sum_i p_i = 1$.

Product states are separable. A state is entangled if it is not separable.

Entanglement entropy

Definining a resource theory of entanglement it is possible to give a meaning to a quantification of the entanglement [90, 91]. In the theory of entanglement measures, functions that quantify the amount of entanglement in a state are called *entanglement monotones*.

For pure states, an entanglement measure is the *entanglement entropy*. The definition of entanglement entropy is based on the concept of von Neumann entropy, that is the natural extension of the Shannon entropy to the context of quantum mechanics. Given a quantum state ρ the von Neumann entropy of ρ is defined as

$$S(\rho) = -\mathrm{Tr}\left[\rho \log(\rho)\right]. \tag{2.17}$$

In term of the eigenvalues ρ_i of ρ the von Neumann entropy reads as

$$S(\rho) = -\sum_i \rho_i \log(\rho_i). \tag{2.18}$$

For every state the von Neumann entropy has values in a finite interval. It is easy to see that the von Neumann entropy is always positive or zero since $\rho_i \in [0, 1]$. The von Neumann entropy of pure states is always zero. In fact the density matrix $\rho = |\psi\rangle\langle\psi|$ of a pure state is a rank 1 matrix with unit trace, thus has just one eingenvalue equal to 1. The von Neumann entropy of a state is bounded from above by the dimension of ρ as

$$S(\rho) \leq \log(\dim(\rho)), \tag{2.19}$$

where this bound is saturated in the case of a completely mixed state $\rho = \mathbb{I}/\dim(\rho)$, with $\mathbb{I}$ the identity matrix. On a lattice, where all the N local Hilbert spaces have

dimension d, the upper bound reads as

$$S(\rho) \leq N \log(d). \tag{2.20}$$

The entanglement entropy of a state is then easily defined as follows. Let us consider the pure state $\rho_{A,B} = |\psi_{AB}\rangle\langle\psi_{AB}|$ of a system on a lattice divided in two complementary partitition A and B, and its two reduced density matrices ρ_A and ρ_B respectively on A and B. The entanglement entropy $EE(\rho_{AB})$ of this state with respect to the bipartition A, B is

$$EE(\rho_{AB}) = S(\rho_A) = S(\rho_B). \tag{2.21}$$

From the observation that the von Neumann entropy of a pure state is zero, it is easy to see that the entanglement entropy of a product state is zero. The more entangled the two partitions are the higher the value of $EE(\rho_{AB})$ will be. The entanglement entropy is bounded by above by the dimension of the smaller partition as

$$EE(\rho_{AB}) \leq |A| \log(d), \tag{2.22}$$

where $|A|$ is the number of lattice sites in partition A.

2.3.2 Entanglement Contour

In the seminal work [92] Chen and Vidal introduced a fine-grained version of the entanglement entropy called *entanglement contour*.

Given a pure state decomposed in two complementary partitions A and B, the entanglement entropy $S(A) = S(B)$ is a measure of the amount of entanglement between the two partitions. The entanglement contour $s_A(x)$ (respectively $s_B(x)$) at a point x of the partition A (respectively B) is a measure of the local contribution of the site x to the entanglement between the partitons A and B. In particular the entanglement contour is not-uniquely defined by the following five properties

1. Positivity: The contribution of each site to the total entanglement must be non-

negative

$$s_A(x) \geq 0 \qquad \forall x \in A. \tag{2.23}$$

2. Normalisation: The sum of the contour $s_A(x)$ of each site of partition A must add up to the total entanglement entropy $S(A)$ of the partition

$$\sum_{x \in A} s_A(x) = S(A). \tag{2.24}$$

3. Symmetry: If T is a symmetry of ρ_A, the reduced density matrix of partition A, that is $T\rho_A T^\dagger = \rho_A$, and T exchanges site i with site j, then $s_A(i) = s_A(j)$.

4. Invariance under local unitary transformation: If U_X is a local unitary with support $X \subseteq A$ and $\rho'_A = U_X \rho_A U_X^\dagger$, then $s_A(X)$ is equal for both ρ_A and ρ'_A, where

$$s_A(X) = \sum_{x \in X} s_A(x). \tag{2.25}$$

5. Upper bound: If the Hilbert space of A is factorised as $\mathcal{H}_A = \mathcal{H}_\Omega \otimes \mathcal{H}_{\bar{\Omega}}$ and $\mathcal{H}_X$ is contained in $\mathcal{H}_\Omega$, then

$$s_X \leq S(\Omega). \tag{2.26}$$

In general it is still an open question whether more conditions may be needed in order to uniquely identify an entanglement contour. In section 3.3.10 we are going to see a particular entanglement contour defined for Fermionic Gaussian states. Other than for Fermionic Gaussian states, entanglement contours have been defined for harmonic lattices, single intervals in holographic CFTs and inhomogeneous critical systems [93–95]

Entanglement Spectrum

In order to characterise the entanglement in a system one can consider other quantities other then just the entanglement entropy. It is possible, for example, to extend the

definition of von Neumann entropy $S(\rho)$ to the family of *Renyi entropies*

$$S_\alpha(\rho) = \frac{1}{1-\alpha}\log(\mathrm{Tr}\,[\rho^\alpha]), \tag{2.27}$$

for $\alpha \geq 0$. The von Neumann entropy is the limit for $\alpha \to 1$ of the Renyi entropy.
The information content of the Renyi entropies is equivalent to the one encoded in the whole spectrum of ρ. It is thus convenient to consider directly the spectrum of the density matrices [96]. In particular the spectrum of the reduced density matrix of a system is called *entanglement spectrum* [97–101] as it encodes all the properties of the reduced states and thus the entanglement properties of the general state. The *entanglement Hamiltonian* of a state ρ_{AB} is defined as the Hermitian matrix H_A such that $\rho_A = e^{H_A}$.

2.3.3 Local Hamiltonians

In the paragraph about the Suzuki-Trotter decomposition 2.2.3 we introduced the concept of local Hamiltonians without any reference to the geometry of the system. We introduce here the concept of quantum lattice model, for which a distance between the various constituents of the system is defined.

Definition of Local Hamiltonians

A lattice model is based on the structure of a graph $G = (V, E)$ where V is the set of vertices and E is the set of edges (that is a set of couples of vertices). If we associate to each vertex a constituent of our physical system, we can define the distance between two constituents as the minimum number of edges that connects the vertices associated to each one of the two constituents.
For an example see figure 2.2. In general every kind of graph is possible, but we will will focus principally just on chains and square lattices that are two simple examples of graphs (see figure 2.2). We define a geometrically local Hamiltonian on the lattice G (from this point onwards we omit geometrically and call it just local Hamiltonian)

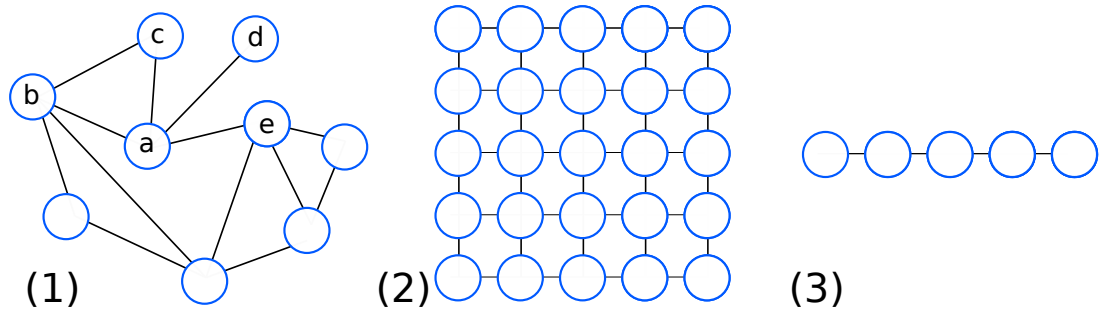

Figure 2.2: Three examples of graphs. The blue circles represent the vertices, the black lines represent the edges. In (1) we represent a generic graph, the nearest neighbours of vertex a are vertices b, c, d, e. In (2) a square lattice, in (3) a chain lattice.

an Hamiltonian of the form

$$H = \sum_{j \in V} h_j \tag{2.28}$$

where each h_j has non trivial support only on vertices at short distances from vertex j. In the case of a chain, for example, if for every $j \in V$ we have that h_j has non trivial support only on $j-1, j, j+1$ we will say that the Hamiltonian is local.

The same definition of locality applies to any observable and we will say that an observable is local if it has non trivial support only on neighbouring vertices.

Examples of local Hamiltonians are for examples the hopping model 3.4 and the transverse field Ising model 3.5.

The property for a Hamiltonian of being local has strong consequences. We remind, for example, that in the treatment of the Suzuki-Trotter decomposition 2.2.3, we have seen how the fact that the Hamiltonian H is local implies that within a good approximation we can exponentially reduce the number of parameters necessary for describing H.

Exponential decay of correlations

An important property of systems described by local and gapped Hamiltonian is that the correlation functions of the ground state decay exponentially with the distance [102, 103]. Considering a chain lattice system with ground state $|\psi\rangle$, for two local

observables O_i and O_j with support on sites i and j respectively, one has

$$|\langle\psi|O_iO_j|\psi\rangle - \langle\psi|O_i|\psi\rangle\langle\psi|O_j|\psi\rangle| \leq Ce^{-|i-j|\Delta E/2v}||O_i||||O_j||, \tag{2.29}$$

where C is a positive constant, $||\cdot||$ is the operator norm, and v is a positive constant called the Lieb-Robinson velocity [104].

The decaying rate $\xi \coloneqq \frac{2v}{\Delta E}$ defines a length scale for the correlations and it is called *correlation length*. This bound is generalised to observables with support on more than one site and for thermal states [102].

Area Law

We have seen how for local gapped Hamiltonians the correlations in the ground states decay exponentially. Because of this rapid decay of correlations, we can consider each subsystem of contiguous sites to be correlated just with the subsystems at its boundaries.

This observation gives us some intuition about the behaviour of entanglement for these states. Let us consider the ground state of a gapped local Hamiltonian on the lattice of figure 2.3. We can think about the partition A as correlated just with partitions C and C'.

Now we focus on the partition scheme $(A, B + C + C')$, which means that the system is divided in two complementary partitions, one of the elements labelled with A and the complementary with elements labelled with B, C and C' referring to figure 2.3. We ask about the amount of entanglement of the state. If, for measuring the entanglement entropy we focus on partition A, we can naively suppose that we are actually dealing with just a pure state of the system $A + C + C'$ because of the exponential decay of correlations. Let us take this supposition seriously. This would imply that A is effectively directly entangled just with C. Since $S(C + C')$ is upper bounded by $|C + C'|\log(d)$ we would have that $S(A) \leq |C + C'|\log(d)$. Thus we would expect the entropy of a partiton A of the ground state of a gapped local

Hamiltonian to be bounded by the dimension of the boundary of the partition.

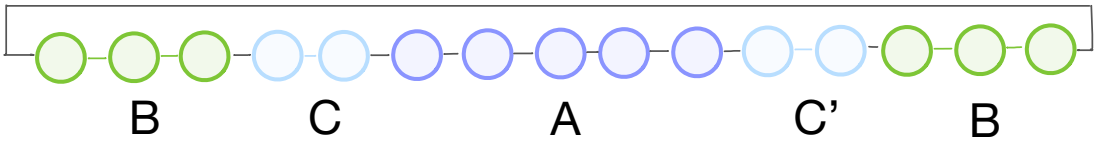

Figure 2.3: Exponentially decaying correlation on a periodic 1D lattice. Since the correlations are decaying exponentially, partition A can be considered effectively correlated just with C and C' and in a product state with partition B.

This bold statement is actually been verified in many different cases and it is an instance of the *entanglement's area law* [19]. More specifically, a generic quantum state on a lattice obeys the area law if the entanglement of two complementary partitions grows at most proportionally with the size of the boundary between the two complementary partitions. For a one-dimensional chain lattice the boundary consists only of two sites for every chosen dimension of the partition, for a $2D$ square lattice the boundary of a squared partition grows as the perimeter of the partition and so on for higher dimensions.

The fact that exponentially decaying correlation functions imply an area law has been proved only in the case of $1D$ gapped Hamiltonians [105] and it is in general not true. Nevertheless, even if it is in general not true that exponentially decaying correlations implies an entanglement's area law, still one can find many instances for which the low-lying energy state of local gapped Hamiltonians satisfy an area law.

The idea that low-lying energy states of a local gapped Hamiltonian should satisfy an area law has been supported by many evidences, starting from the work of Bekenstein on the entropy of black holes [106] to the works on spins [66, 69] and bosons [107, 108]. Inspired by these evidences, the validity of the area law has been proved for various systems. For example for the ground state of gapped one dimensional finite systems the von Neumann entropy S of a partition is bounded by [109]

$$S \leq c_0 \eta \ln(\eta) \ln(d) 2^{\eta \ln(D)}, \tag{2.30}$$

where c_0 is a constant, d is the dimension of the Hilbert space at each site of the lattice and $\eta = 6 \cdot \max(2v/\Delta E, \xi)$ with ξ the correlation length, ΔE the gap of the Hamiltonian and v is a constant of the order of the norm of the local terms of the Hamiltonian.

While in the ground state of gapped one dimensional continuous systems at the critical point the von Neumann entropy of the ground state scales as [69, 110]

$$S \sim N_b \frac{c}{6} \log(L) + c_1, \tag{2.31}$$

where N_b is the number of boundaries between the subsystems, c is the central charge of the corresponding conformal field theory (see chapter 5), L is the size of the system, and c_1 is a constant (non universal). Away from the critical point the entropy scales as in (2.31) but with the dimension of the system L substituted by the correlation lenght ξ.

The area law has been proved also for other systems as gapped quadratic fermionic and bosonic Hamiltonians [107, 111], gapless quadratic bosonic Hamiltonians for lattices of dimension bigger than 1 [112], and for a generic class of low-energy states of finite-range interactions Hamiltonians [113].

2.3.4 Matrix Product states

On average, the entropy of a partition of a pure state $|\psi\rangle$ is proportional to $|A|$ [114]. States satisfying the area law are thus a tiny fraction of all the possible states in a Hilbert space. From last section we have seen how states satisfying the area law are an interesting class of states, representing, for example, ground states of $1D$ gapped Hamiltonians.

Putting all these observations together we individuate and characterise a small set of quantum states out of the exponentially many of the full Hilbert space. We are now interested in being able to compress this class of states. One of the most efficient methods for compressing these states is using *matrix product states* [12, 115].

Let us consider an N constituents systems and a vector in its Hilbert space $\mathcal{H} = (\mathbb{C}^d)^{\otimes N}$

$$|\psi\rangle = \sum_{i_1,\ldots,i_N} c_{i_1,\ldots,i_N} |i_1,\ldots,i_N\rangle, \tag{2.32}$$

where $|i_1,\ldots,i_N\rangle = |i_1\rangle \otimes \cdots \otimes |i_N\rangle$ and for each $l = 1,\ldots,N$ $i_l \in \{1,\ldots,d\}$. In total we have d^N different coefficients. The coefficient tensor $c_{i_1,\ldots,i_N}$ can be rewritten as

$$c_{i_1,\ldots,i_N} = A^{[1]}_{i_1} A^{[2]}_{i_2} \ldots A^{[N]}_{i_N}, \tag{2.33}$$

where for $l \neq 1$ and $l \neq N$, $A^{[l]}_i$ is a $D \times D$ matrix, $A^{[1]}_i \in \mathbb{C}^{1\times D}$ is a row vector, and $A^{[N]}_i \in \mathbb{C}^{D\times 1}$ is a column vector. We encoded all the coefficients of the state in NdD^2. The state can then be written as:

$$|\psi\rangle = \sum_{i_1,\ldots,i_N} A^{[1]}_{i_1} A^{[N]}_{i_N} \ldots A^{[N]}_{i_N} |i_1,\ldots,i_N\rangle \tag{2.34}$$

Equation (2.34) is called Matrix Product State (MPS) representation of the state. The dimension D of the matrices is called *bond dimension* of the state. The faithful MPS representation of a generic state requires a bond dimension $D_{\max} = d^{\frac{N}{2}}$, thus the specification of Dd^{N+1} coefficients. We will see that the bond dimension is a measure of the entanglement across any two complementary partitions of the system, thus, the bond dimension of the MPS representation of low-entangled states is expected to be much smaller than $D_{\max}$ and in general to not depend on the system size. The power of the MPS representation is that it allows to efficiently obtain a low-entanglement approximation of states, that is an approximated MPS representation of bond dimension D smaller then the value necessary for obtaining a faithful description of the state. To have an intuition of the kind of approximation one is performing when using an MPS ansatz at lower bond dimension for representing a state, we review the basic ideas of the method for constructing an MPS in the canonical form [116].

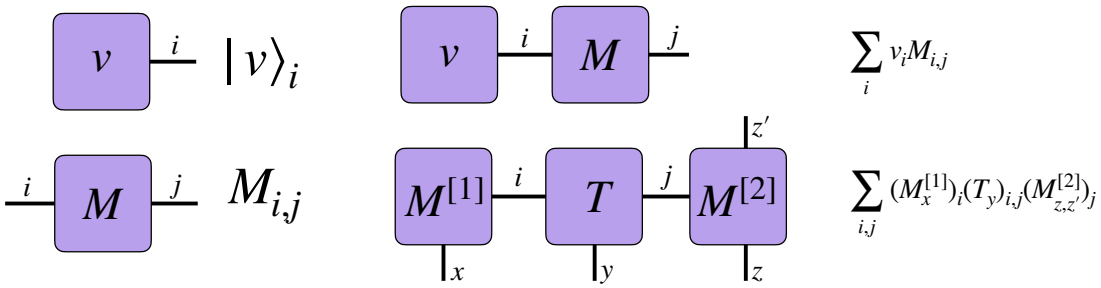

Figure 2.4: Tensor network notation. A box with n legs corresponds to a tensor with n indices. On the left, starting from the top the tensor network notation of the vector $|v\rangle$ and of the matrix M. Legs connecting two boxes correspond to summed indices of the two tensors corresponding to the two boxes. On the right a vector matrix multiplication and a more complex summation.

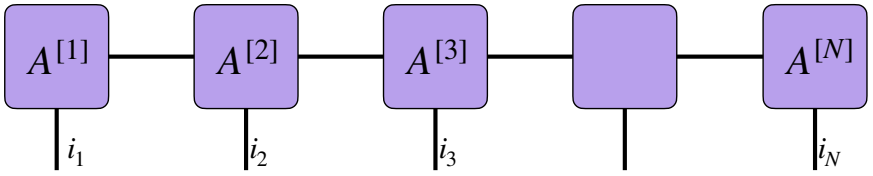

Figure 2.5: A graphical representation of the MPS representation of eq (2.34).

Schmidt decomposition and Singular Value Decomposition We first introduce two important mathematical tools at the core of MPS, the Singular Value Decomposition (SVD) and the Schmidt decomposition, we then show how this two tools are strictly connected.

Singular value decomposition Let C be an $m \times n$ matrix. It is always possible to decompose C as

$$C = USV^{\dagger}, \tag{2.35}$$

where

- U is an $m \times m$ unitary matrix.
- V is an $n \times n$ unitary matrix.
- S is an $m \times n$ real rectangular diagonal matrix, with diagonal elements $S_{\alpha,\alpha}$ called *singular values*.

Schmidt Decomposition Let $\mathcal{H}_A$ and $\mathcal{H}_B$ be two Hilbert spaces of dimension d_A and d_B respectively. Assume that $d_B \geq d_A$. Then for every $|\psi_{AB}\rangle \in \mathcal{H}_{AB} = \mathcal{H}_A \otimes \mathcal{H}_B$ there exist two orthonormal basis $\{|\psi_i^{[A]}\rangle\}_{i=1}^{d_A}$ and $\{|\psi_i^{[B]}\rangle\}_{i=1}^{d_B}$ of $\mathcal{H}_A$ and $\mathcal{H}_B$, the Schmidt basis, such that

$$|\psi_{AB}\rangle = \sum_{\alpha=1}^{d_A} \lambda_\alpha |\psi_\alpha^{[A]}\rangle \otimes |\psi_\alpha^{[B]}\rangle, \tag{2.36}$$

with Schmidt coefficients $\lambda_\alpha \geq 0$ for every α.
The number of Schmidt coefficients different from 0 is called *Schmidt rank*. A product state has Schmidt rank equal to 1.
The entanglement spectrum of partition A and partition B is equal and it is $\{|\lambda_\alpha|^2\}_\alpha$, the entanglement entropy of $|\psi_{AB}\rangle$ is $S(A) = S(B) = -2\sum_\alpha |\lambda_\alpha|^2 \log(|\lambda_\alpha|)$.

Relation between Schmidt decomposition and SVD Consider again the state $|\psi_{AB}\rangle$ of the last section. This time we consider two different basis for $\mathcal{H}_A$ and $\mathcal{H}_B$, namely $\{|i_A\rangle\}_i$ and $\{|j_B\rangle\}_j$. In general, if the chosen basis is not the Schmidt basis, the expression of the state on this basis will take the form:

$$|\psi_{AB}\rangle = \sum_{i,j} c_{i,j} |i_A\rangle \otimes |j_B\rangle. \tag{2.37}$$

We apply a SVD to the matrix of the coefficients $c_{i,j} = \sum_\alpha U_{i,\alpha} S_{\alpha,\alpha} V^\dagger_{\alpha,j}$ and we obtain

$$|\psi_{AB}\rangle = \sum_{i,j} \sum_\alpha S_{\alpha,\alpha} U_{i,\alpha} |i_A\rangle \otimes V^\dagger_{\alpha,j} |j_B\rangle. \tag{2.38}$$

Comparing this equation with equation (2.36) we can identify the singular values $S_{\alpha,\alpha}$ with the Schmidt coefficients λ_α and the two orthonormal basis $\{\sum_i U_{i,\alpha}|i_A\rangle\}_\alpha$ and $\{\sum_j V^\dagger_{\alpha,j}|j_B\rangle\}_\alpha$ with the two Schmidt Basis. The rank of the matrix S, that is the rank of matrix c is the number of Schmidt values different from 0.

Construction of an MPS in one dimension Let us imagine that the quantum state ψ of equation (2.32) is defined on a $1D$ lattice. We consider the complementary

partitioning of the system A_1 and $B_{2,\ldots,N}$, where the subindices denotes the sites of the lattice belonging to the partition. The Schmidt decomposition of $|\psi\rangle$ with respect to this partition is

$$|\psi\rangle = \sum_{\alpha_1=1}^{d} \lambda_{\alpha_1}^{[1]} |\psi_{\alpha_1}^{[1]}\rangle \otimes |\psi_{\alpha_1}^{[2,\ldots,N]}\rangle, \tag{2.39}$$

where $\{|\psi_j^{[1]}\rangle\}_j$ and $\{|\psi_j^{[2,\ldots,N]}\rangle\}_j$ are orthonormal basis of the Hilbert spaces associated to the two partitions of the lattice.

We express $|\psi_j^{[A]}\rangle$ on the original basis $\{|i_1\rangle\}$ as $|\psi_{\alpha_1}\rangle = \sum_{i_1}^{d} \Gamma_{\alpha_1}^{[1]i_1}$ and we obtain

$$|\psi\rangle = \sum_{i_1,\alpha_1} \Gamma_{\alpha_1}^{[1]i_1} \lambda_{\alpha_1}^{[1]} |i_1\rangle \otimes |\psi_{\alpha_1}^{[2,\ldots,N]}\rangle. \tag{2.40}$$

Repeating this procedure now for the system $(2,\ldots,N)$ with the partitioning A_2, $B_{3,\ldots,N}$ and then iteretively until the partitioning A_{N-1},B_N of the system $(N-1,N)$, we obtain

$$c_{i_1,\ldots,i_N} = \sum_{\alpha_1,..,\alpha_{N-1}=0} \Gamma_{\alpha_1}^{[1]i_1} \lambda_{\alpha_1}^{[1]} \Gamma_{\alpha_1\alpha_2}^{[2]i_2} \lambda_{\alpha_2}^{[2]} \Gamma_{\alpha_2\alpha_3}^{[3]i_3} \lambda_{\alpha_3}^{[3]} \cdot .. \cdot \Gamma_{\alpha_{N-2}\alpha_{N-1}}^{[N-1]i_{N-1}} \lambda_{\alpha_{N-1}}^{[N-1]} \Gamma_{\alpha_{N-1}}^{[N]i_N}. \tag{2.41}$$

This is a different notation for MPS, often called Vidal's notation. The Vidal's notation relates to the MPS notation (2.34) introduced before by the equality

$$(A_{i_l}^{[l]})_{\alpha_{l-1},\alpha_l} = \Gamma_{\alpha_{l-1},\alpha_l}^{[l]i_l} \lambda_{\alpha_l}^{[l]}. \tag{2.42}$$

From this equality we see that the bond dimension corresponds to the number of Schmidt values in the Schmidt decomposition that corresponds to the rank of the matrix S in the SVD decomposition. It is clear that the dimension of each matrix $A_{i_l}^{[l]}$ can vary fo each l, this is indeed the general case. One refers to the bond dimension of a state when the dimension of each matrix $A_{i_l}^{[l]}$ is fixed, as we will see in the case of truncated MPS representation. We remind that this is just one of the many ways of constructing MPS [12], for a more precise and complete treatment we refer to [117] or one of the many reviews already cited in this chapter.

Entanglement of an MPS Expressing the MPS with Vidal's notation is particularly convenient for understanding the entanglement properties of MPS states. Indeed, each set $\{\lambda^{[l]}_{\alpha_l}\}_{\alpha_l}$, is exactly the set of Schmidt coefficients of the partitioning $A_{1,\dots,l}B_{l+1,\dots,N}$. We note that, from equation (2.42), the dimension of the matrix associated to each site used in the MPS representation (2.34) corresponds to the number of Schmidt values for the partition scheme of the system with boundary at that site.

Eckart-Young Theorem Suppose we have a matrix C and we want to approximate it with a matrix $\tilde{C}$ of rank at most r. This approximation is called *low rank approximation.*

The Eckart-Young theorem [118] tells us that the best low rank approximated matrix $\tilde{C}$ can be obtained by performing the SVD of C and setting the smallest singular values of C to zero, leaving just r singular values different from 0.

Thus, if $C = USV^\dagger$ with singular values $\{S_{1,1}, S_{2,2}, \dots, S_{n,n}\}$ such that $S_{1,1} \geq S_{2,2} \geq \cdots \geq S_{n.n} \geq 0$, we define $\tilde{S}$ as the rectangular diagonal matrix with same dimensions of S and with diagonal elements $\{S_{1,1}, S_{2,2}, \dots, S_{r,r}, 0, \dots, 0\}$. The low rank approximated matrix is $\tilde{C} = U\tilde{S}V^\dagger$.

It is importat to keep in mind that the quality of the approximation is measured in Frobenius norm. Thus $\tilde{C}$ is defined by the equality

$$||C - \tilde{C}||_F = \min_{rank(D)=r} ||C - D||_F, \tag{2.43}$$

where the Frobenius norm is defined for a generic $m \times n$ matrix M as

$$||M||_F = \sqrt{\sum_{i=1}^{m}\sum_{j=1}^{n} |M_{i,j}|^2}. \tag{2.44}$$

The Frobenius norm weight all the elements of the matrix M equally. The same result has been generalised by Mirsky [119] to include all the unitarily invariant norms, including the spectral norm (the spectral norm of a matrix is its biggest singular value).

We will see that, many times, measuring the approximation error with other norms

can be useful. We could, for example, be interested in finding the low rank approximation of a matrix M for wich we want to preserve all the diagonal elements and at the same time we do not care about the possible changes of the out-of-diagonal elements (we will develop on this intuition in chapter 6). In this case, we would like to minimise the error of a norm that weights more the elements of the diagonal and less the out of diagonal elements. This kind of minimisation problems is known as *weighted low-rank approximation*. The general weighted low-rank approximation problem does not admit an analytic solution in term of the singular value decomposition and it is usually solved by variational methods which do not guarantee that a global optimal solution is found.
The weighted low-rank approximation problem is strictly connected to the so-called Netflix problem [120, 121] that is an active research topic in computer science.

Truncated MPS Putting the ingredients of all last paragraphs together we can finally study the MPS ansatz at lower bond dimension. In fact, if during the process of building the MPS for a state ψ we decide to always keep just the χ biggest Schmidt values at each Schmidt decomposition step, what we are are actually doing is performing a low-rank approximation of the coefficient matrix. Doing so we obtain an MPS with bond dimension χ, which we know minimises the error in Frobenius norm at each step of the construction.
This low-rank approximation, or, as it is called in condensed matter, fixed bond dimension approximation has proven to be optimal for various reasons. It is really efficient, indeed we have seen that the amount of coefficients needed to store the state of a lattice of N sites of local dimension d is $dN\chi^2$, that for small χ is much smaller than d^N. The MPS representation is also the state of the art compression of states obeying the area law, thus the relevant class of state we individuated in this section. Fixing the bond dimension of a state implies fixing the number of Schmidt coefficients of each partition, thus bounding the Entanglement Entropy of each partition. Indeed, it is easy to see that the the entanglement entropy of any partition of an MPS of fixed

bond dimension χ is bounded by

$$EE \leq 2\log(\chi). \tag{2.45}$$

From this bound on the entanglement, we obtain that the computational resources needed for encoding an MPS grow exponentially with the amount of entanglement. At this point we know that an MPS state with fixed and small bond dimension is a low entangled state. We do not know if low entangled states are always efficiently representable as an MPS.

From this intuition we expect for the MPS representation to be an efficient ansatz for representing low entangled states (as the one obeying the area law), this is indeed the case in many cases. More precisely we know that if for a state $|\psi\rangle$ the Renyi entropies for $\alpha < 1$ of any block are bounded by a constant, then an efficient approximation of $|\psi\rangle$ by a truncated MPS exists [122]. The general connections between the efficiciency of the representation of a state with a truncated MPS and its entanglement is studied in [123].

2.3.5 Matrix Product Operators

A generic operator O can be expanded on a suitable basis as

$$O = \sum_{\substack{i_1,\ldots,i_N \\ i'_1,\ldots,i'_N}} c^{i'_1,\ldots,i'_N}_{i_1,\ldots,i_N} |i_1,\ldots,i_N\rangle\langle i'_1,\ldots,i'_N|, \tag{2.46}$$

where c is a tensor of d^{2N} coefficients.

Analogously with what we have done introducing the MPS representation for quantum states, we introduce here the Matrix Product Operator (MPO) representation [124] for the general operator O as

$$O = \sum_{\substack{i_1,\ldots,i_N \\ i'_1,\ldots,i'_N}} B^{[1]}_{i_1,i'_1} B^{[2]}_{i_2,i'_2} \ldots B^{[N]}_{i_N,i'_N} |i_1,\ldots,i_N\rangle\langle i'_1,\ldots,i'_N| \tag{2.47}$$

where each $B^{[l]}_{i_l,i'_l}$ is a $D \times D$ matrix. One difference with equation (2.34) is that now we have two sub indices, thus a greater number of matrices.

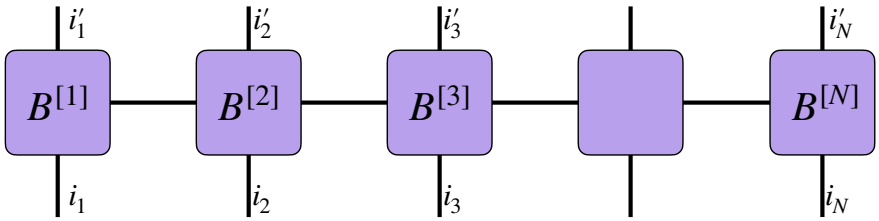

Figure 2.6: A graphical representation of the MPO representation of eq (2.47).

Matrix product operators can be used to approximately represent density matrices and Hamiltonians [25, 31]. In this context, since the state is mixed, the entanglement entropy cannot be used to measure entanglement and intuitions related to the area law and the truncation of the MPO to lower bond dimension are partially lost. Another difficulty in dealing with truncated MPO is the fact that it is difficult to control the positivity of the operator. Valid density matrices are positive semidefinite operators, the process of truncating the bond dimension of the MPO is not guaranteed to conserve the positivity and thus it is not guaranteed that the truncated version of an MPO is a valid density matrix. Furthermore, checking if the MPO is positive is a computationally inefficient task [125]. Fortunately, it has been shown that thermal states of spin lattices can efficiently be approximated by MPO [126–129] and generic thermal state can be guaranteed to be positive with a relatively efficient procedure [126].

Chapter 3

Julia library for manipulation of Fermionic Gaussian states: F_utilities

In this section we present a practical introduction to the manipulation of Fermionic Gaussian systems. In particular we will focus on the encoding of these systems in a computer using a Julia package called `F_utilities`. Starting from the basis, we will move to relevant modern results and techiques, and finish introducing novel algorithms. By the end of the chapter the reader should be able to reproduce all the results of this thesis using the package `F_utilities` and make good use of `F_utilities` for other relevant numerical simulations. It should be possible to read this chapter independently from the rest of the thesis and use it as the documentation of the package `F_utilities` and as a useful resource in the broad and fertile field of Fermionic Gaussian states.

3.1 The canonical anticommutation relations

3.1.1 The Hilbert space characterised by the canonical anticommutation relations

Consider a set of operators $\{a_i\}_{i=1}^N$ acting on a Hilbert space $\mathcal{H}$. We say that these operators satisfy the *canonical anticommutation relation* (CAR) when they satisfy

$$\{a_i, a_j^\dagger\} = \mathbb{I}\delta_{i,j}; \qquad \{a_i, a_j\} = 0, \tag{3.1}$$

with $\{a, b\} \coloneqq ab + ba$ the notation for the anticommutator.

As shown in [130] a number of properties of the set of operators $\{a_i\}_{i=1}^N$ and of the Hilbert space $\mathcal{H}$ can be inferred just by the fact that such operators exist and obey the CAR.

The $a_i^\dagger a_i$ form a set of *commuting, Hermitian, positive operators* with eigenvalues $\{0, 1\}$. We denote with $\vec{x} \in \{0,1\}^N$ a binary string of length N with the i-th elements x_i. With $|\vec{x}\rangle$ we identify one of the 2^N states that is the simultaneous eigenstate of $a_i^\dagger a_i$ for all $i = 1, \ldots, N$ with eigenvalues respectively x_i. The operator a_i acts as a *lowering operator* for $a_i^\dagger a_i$ and $a_i^\dagger$ acts as a *raising operator* for $a_i^\dagger a_i$ in the sense that

1. If $a_i^\dagger a_i |\vec{x}\rangle = |\vec{x}\rangle$, that is, $|\vec{x}\rangle$ is an eigenvector of $a_i^\dagger a_i$ with eigenvalue equal to 1, then the action of a_i on $|\vec{x}\rangle$ lowers the corresponding eigenvalue, meaning that $a_i^\dagger a_i (a_i |\vec{x}\rangle) = 0 (a_i |\vec{x}\rangle)$.

2. If $a_i^\dagger a_i |\vec{x}\rangle = 0 |\vec{x}\rangle$, that is, $|\vec{x}\rangle$ is an eigenvector of $a_i^\dagger a_i$ with eigenvalue equal to 0, then the action of $a_i^\dagger$ on $|\vec{x}\rangle$ raises the corresponding eigenvalue, meaning that $a_i^\dagger a_i (a_i^\dagger |\vec{x}\rangle) = 1 (a_i^\dagger |\vec{x}\rangle)$.

We define an *ordering* by explicitly defining $|\vec{x}\rangle \coloneqq (a_1^\dagger)^{x_1} (a_2^\dagger)^{x_2} \ldots (a_N^\dagger)^{x_N} |\vec{0}\rangle$, where $\vec{0}$ is the string of N zeros. The set $\{|\vec{x}\rangle\}_{\vec{x}\in\{0,1\}^N}$ forms an orthonormal basis. Since the dimension of the Hilbert space $\mathcal{H}$ is 2^N, then $\{|\vec{x}\rangle\}_{\vec{x}\in\{0,1\}^N}$ is an orthonormal basis of $\mathcal{H}$.

The orthonormal basis $\{|\vec{x}\rangle\}_{\vec{x}\in\{0,1\}^N}$ is called *Fock basis*. The action of the raising and

lowering operators on $|\vec{x}\rangle$ is then

$$a_i|\vec{x}\rangle = \begin{cases} -(-1)^{S^i_{\vec{x}}}|\vec{x'}\rangle \text{ with } x'_i = 0 \text{ and } x'_{j\neq i} = x_{j\neq i}, & \text{if } x_i = 1 \\ 0 & \text{if } x_i = 0 \end{cases}, \tag{3.2}$$

$$a^\dagger_i|\vec{x}\rangle = \begin{cases} 0 & \text{if } x_i = 1 \\ -(-1)^{S^i_{\vec{x}}}|\vec{x'}\rangle \text{ with } x'_i = 1 \text{ and } x'_{j\neq i} = x_{j\neq i}, & \text{if } x_i = 0 \end{cases}, \tag{3.3}$$

with $S^i_{\vec{x}} = \sum_{k=1}^{i-1} x_k$.

In appendix A we report some useful equalities valid for operators satisfying the CAR.

3.1.2 Dirac and Majorana representations

The raising and lowering operators $a^\dagger_i$,a_i are called *Dirac operators* and they represent the action of adding and removing the i-th Fermionic mode.

Both a_i and its adjoint $a^\dagger_i$ are not Hermitian. The Hermitian combinations of the raising and lowering operators

$$x_i = \frac{a_i + a^\dagger_i}{\sqrt{2}}, \qquad p_i = \frac{a_i - a^\dagger_i}{i\sqrt{2}}, \tag{3.4}$$

are called *Majorana operators*.

The inverse transformations are:

$$a_i = \frac{x_i + ip_i}{\sqrt{2}}, \qquad a^\dagger_i = \frac{x_i - ip_i}{\sqrt{2}}. \tag{3.5}$$

In terms of Majorana operators the CARs read as

$$\{x_i, x_j\} = \{p_i, p_j\} = \delta_{i,j}, \qquad \{x_i, p_j\} = 0. \tag{3.6}$$

We remark that to Majorana operators labelled by i correspond Dirac operators labelled by i. Moving between Majorana and Dirac operators does not mix modes.

Vector notation We can collect the Dirac operators of a system with N modes in the vector $\vec{\alpha}$ of length $2N$ defined as

$$\vec{\alpha} = \begin{pmatrix} a_0^\dagger \\ \vdots \\ a_{N-1}^\dagger \\ a_0 \\ \vdots \\ a_{N-1} \end{pmatrix} \quad , \quad \vec{\alpha}^\dagger = \begin{pmatrix} a_0 & \dots & a_{N-1} & a_0^\dagger & \dots & a_{N-1}^\dagger \end{pmatrix}. \tag{3.7}$$

Analogously we can collect the Majorana operators in the vector $\vec{r}$ defined as

$$\vec{r} = \begin{pmatrix} x_0 \\ \vdots \\ x_{N-1} \\ p_0 \\ \vdots \\ p_{N-1} \end{pmatrix}, \tag{3.8}$$

in terms of $\vec{r}$ the CAR are conveniently written as

$$\{r_i, r_j\} = \delta_{i,j}. \tag{3.9}$$

We define the unitary matrix Ω as

$$\Omega = \tfrac{1}{\sqrt{2}} \begin{pmatrix} \mathbb{I} & \mathbb{I} \\ i\mathbb{I} & -i\mathbb{I} \end{pmatrix} \quad , \quad \Omega^\dagger = \Omega^{-1} = \tfrac{1}{\sqrt{2}} \begin{pmatrix} \mathbb{I} & -i\mathbb{I} \\ \mathbb{I} & i\mathbb{I} \end{pmatrix} . \tag{3.10}$$

Such a matrix, applied to the vector of the Dirac operators $\vec{\alpha}$, returns the vector of Majorana operators $\vec{r} = \Omega\vec{\alpha}$.

Fermionic transformation A transformation $\vec{r} \to \vec{s} = O\vec{r}$ is said to preserve the CAR in the Majorana representation if it maps a vector of Majorana operators $\vec{r}$ to a

new one $\vec{s} = O\vec{r}$. If we explicitly impose $\vec{s} = O\vec{r}$ to preserve the CAR we obtain

$$\delta_{i,j} = \{s_i, s_j\} = \sum_{k,l} O_{i,k} O_{j,l} \{r_k, r_l\} = (OO^T)_{i,j}, \tag{3.11}$$

thus matrix O must be an orthogonal matrix.

We call *Fermionic transformation* any transformation $\vec{\alpha} \to \vec{\beta} = U\vec{\alpha}$ that preserves the CAR of the Dirac operators vectors. Matrix U has the form of $U = \Omega^\dagger O \Omega$ with O an orthogonal matrix. It has been shown in [131] that Fermionic transformations are generated by Fermionic quadratic Hamiltonian (to be defined later), thus have the general form $U = e^{-i\hat{H}}$, with $\hat{H}$ a generic Fermionic quadratic Hamiltonian.

Clifford Algebra The Majorana operators $\{r_i\}_{i=1,\dots,2N}$ are Hermitian, traceless and generate the Clifford algebra denoted by $\mathcal{C}_{2N}$.

Any arbitrary operator $X \in \mathcal{C}_{2N}$ can be represented as a polynomial of the Majorana operators as [131]

$$X = \alpha_0 \mathbb{I} + \sum_{p=1}^{2N} \sum_{1 \le q_1 < \dots < q_p \le 2N} \alpha_{q_1,\dots,q_p} r_{q_1} \dots r_{q_p}, \tag{3.12}$$

where $\mathbb{I}$ is the identity and the coefficients α_0 and $\alpha_{q_1,\dots,q_p}$ are real. When the representation of $X \in \mathcal{C}_{2N}$ involves only even powers of Majorana operators, we call it an *even operator*. If the representation of X involves only odd powers of Majorana operators, then X is called *odd* operator.

We define the *parity operator* as

$$P = (i2)^N r_1 r_2 \dots r_{2N} = \prod_{i=1}^{N} (\mathbb{I} - 2a_i^\dagger a_i) \tag{3.13}$$

Every even operator X commutes with the parity operator P. The parity p_X of an operator X is defined as $PX = p_X X$ and it can only assume the two values $p_X \in \{-1, 1\}$.

Fermionic quadratic Hamiltonians (to be defined later) are even operators. For an N-mode Fermionic system with orthonormal basis $\{|\vec{x}\rangle\}$, the matrices $|\vec{x}\rangle\langle\vec{x}|$ defined for

every $\vec{x}$ have the polynomial representation

$$|\vec{x}\rangle\langle\vec{x}| = \left(\frac{\mathbb{I}}{2} - i(-1)^{x_1} r_1 r_2\right)\left(\frac{\mathbb{I}}{2} - i(-1)^{x_2} r_3 r_4\right)\ldots\left(\frac{\mathbb{I}}{2} - i(-1)^{x_N} r_{2N-1} r_{2N}\right), \quad (3.14)$$

thus $\{|\vec{x}\rangle\langle\vec{x}|\}$ are all even operators with parity $p_{|\vec{x}\rangle\langle\vec{x}|} = -(-1)^{\sum_{i=1}^{N} x_i}$.
Mixed matrices $|\vec{x}\rangle\langle\vec{x'}|$ with $\vec{x} \neq \vec{x'}$ are odd operators if $\mathrm{mod}(d(\vec{x},\vec{x'}),2) = 1$, where $d(\vec{x},\vec{y})$ is the Hamming distance of $\vec{x}$ and $\vec{y}$, and they are even operators if $\mathrm{mod}(d(\vec{x},\vec{x'}),2) = 0$.

3.2 Fermionic Quadratic Hamiltonians

3.2.1 Dirac Representation

The general *Fermionic quadratic Hamiltonians* (f.q.h.) on a finite lattice of N sites in the Dirac operators representation can be written as

$$\hat{H} = \sum_{i,j=1}^{N} \left(A_{i,j} a_i^\dagger a_j - \bar{A}_{i,j} a_i a_j^\dagger + B_{i,j} a_i a_j - \bar{B}_{i,j} a_i^\dagger a_j^\dagger\right), \quad (3.15)$$

where A is a *Hermitian* complex matrix, $A^\dagger = A$, and B is a *skew-symmetric* complex matrix, $B^T = -B$.
Defining the matrix

$$H = \begin{pmatrix} -\bar{A} & B \\ -\bar{B} & A \end{pmatrix}, \quad (3.16)$$

the *compact form* of equation (3.15) reads

$$\hat{H} = \vec{\alpha}^\dagger H \vec{\alpha}. \quad (3.17)$$

We will call *Hamiltonians* both $\hat{H}$ and H as for a fixed choice of Dirac operators one completely identifies the other.

3.2.2 Majorana Representation

The Majorana representation of the generic f.q.h. reads as

$$\hat{H} = i \sum_{i,j=1}^{N} \left(h_{i,j}^{xx} x_i x_j + h_{i,j}^{pp} p_i p_j + h_{i,j}^{xp} x_i p_j + h_{i,j}^{px} p_i x_j \right) = i \vec{r}^{\dagger} h \vec{r}, \tag{3.18}$$

where

$$ih = \Omega H \Omega^{\dagger} = i \begin{pmatrix} \Im\{A+B\} & \Re\{A+B\} \\ \Re\{B-A\} & \Im\{A-B\} \end{pmatrix} = i \begin{pmatrix} h^{xx} & h^{xp} \\ h^{px} & h^{pp} \end{pmatrix}. \tag{3.19}$$

Where $\Im\{\cdot\}$ and $\Re\{\cdot\}$ are respectively the imaginary and the real part of their argument.

Using the properties of matrices A and B, it is easy to see that matrix h is real and skew-symmetric.

3.2.3 Diagonalisation

Diagonal form of the Hamiltonian with Dirac operators Given a particular f.q.h. $\hat{H}$ in the general form (3.15) it is always possible to find a new set of Dirac operators $\{b_k\}_{k=1}^{N}$ such that $\hat{H}$ in terms of $\{b_k\}_{k=1}^{N}$ reads as

$$\hat{H} = \sum_{k=1}^{N} \epsilon_k (b_k^{\dagger} b_k - b_k b_k^{\dagger}), \tag{3.20}$$

with $\epsilon_k \in \mathbb{R}$ for all $k = 1, 2, \ldots, N$ [132].

We call Hamiltonians in this form free-free fermion Hamiltonians.

In compact form

$$\hat{H} = \vec{\beta}^{\dagger} H_D \vec{\beta} \tag{3.21}$$

with

$$H_D = U^\dagger H U = \begin{pmatrix} -\epsilon_1 & 0 & \dots & & \dots & 0 \\ 0 & \ddots & \ddots & & & \vdots \\ \vdots & \ddots & -\epsilon_N & & & \\ & & & \epsilon_1 & \ddots & \vdots \\ \vdots & & & \ddots & \ddots & 0 \\ 0 & \dots & & & \dots 0 & \epsilon_N \end{pmatrix}, \tag{3.22}$$

where $\vec{\beta}$ is the collection of the Dirac operators $b_k, b_m^\dagger$ ordered as in $\vec{\alpha}$, and U is the Fermionic tranformation that diagonalises the Hamiltonian.
We will always order the eigenvalues in descending order ($\epsilon_1 \geq \epsilon_2 \geq \cdots \geq \epsilon_N \geq 0$).

Diagonal form of the Hamiltonian with Majorana operators In terms of Majorana operators the diagonal form of a generic f.q.h. reads as

$$\hat{H} = i \sum_{i=1}^{N} \lambda_i (\tilde{x}_i \tilde{p}_i - \tilde{p}_i \tilde{x}_i). \tag{3.23}$$

for a set of Majorana operators $\{\tilde{x}_i\}_i$, $\{\tilde{p}_i\}_i$. In compact form

$$\hat{H} = i \vec{s}^\dagger h_D \vec{s}, \tag{3.24}$$

where $\vec{s}$ is the collection of the Majorana operators $\tilde{x}_i, \tilde{p}_j$ ordered as (3.31) and where

$$h_D = O^T h O = \bigoplus_{i=1}^{N} \begin{pmatrix} 0 & \lambda_i \\ -\lambda_i & 0 \end{pmatrix} \tag{3.25}$$

is a block diagonal matrix and O the orthogonal transformation that diagonalises the Hamiltonian in the Majorana operators representation. Substituting the definition of Majorana operators (3.4) into equation (3.23) and confronting with equation (3.20) we note that $\epsilon_k = \lambda_k$.

3.2.4 Numerical diagonalisation

As seen in subsection 3.2.3, diagonalising a general f.q.h. $\hat{H}$ reduces to diagonalising (or to block diagonalise in the case of Majorana representation) the matrix H of its compact form.

We are thus interested in finding the Fermionic transformation U that maps H and the vector of Dirac operators $\vec{\alpha}$ respectively to the diagonal matrix $H_D = U^\dagger H U$ and to the vector of Dirac operators $\vec{\beta} = U\vec{\alpha}$ such that, in term of $\vec{\beta}$, the Hamiltonian is in the diagonal form (3.20).

Here we focus on the numerical approach, we diagonalise the Hamiltonian using standard matrix decomposition techniques. For a more physical approach we refer to [132].

First step in the diagonalisation procedure is moving to the Majorana representation of H

$$\begin{aligned} \hat{H} = \vec{\alpha}^\dagger H \vec{\alpha} = \vec{\alpha}^\dagger \Omega^\dagger \Omega H \Omega^\dagger \Omega \vec{\alpha} = \\ = i\vec{r}^\dagger h \vec{r}. \end{aligned} \tag{3.26}$$

The following theorem is a standard result in matrix theory [133, 134]

Theorem 1 (Block diagonal form of skew-symmetric matrices)
Let h be $2N \times 2N$ a real, skew-symmetric matrix. There exists a real special orthogonal matrix O such that

$$h = O h_D O^T, \tag{3.27}$$

with h_D a block diagonal matrix of the form

$$h_D = \bigoplus_{i=1}^{N} \begin{pmatrix} 0 & \lambda_i \\ -\lambda_i & 0 \end{pmatrix} \tag{3.28}$$

for real, positive-definite $\{\lambda_i\}_{i=1,\dots,N}$. The non-zero eigenvalues of matrix h are the imaginary numbers $\{\pm i\lambda_i\}_{i=1,\dots,N}$.

For a more general form of this theorem see appendix A.1.5.

Matrix h in (3.18) is real, skew-symmetric, thus, using theorem (3.27) we know there exists an orthogonal transformation O that diagonalises the matrix

$$\hat{H} = i\vec{r}^{\dagger} h \vec{r} = i\vec{r}^{\dagger} O O^{\dagger} h O O^{\dagger} \vec{r} = \tag{3.29}$$

$$= i\vec{s}^{\dagger} \left(\bigoplus_{i=1}^{N} \begin{pmatrix} 0 & \lambda_i \\ -\lambda_i & 0 \end{pmatrix} \right) \vec{s} = i\vec{s}^{\dagger} h_D \vec{s} \tag{3.30}$$

That is $\hat{H} = i \sum_{i=0}^{N-1} \lambda_i (\tilde{x}_i \tilde{p}_i - \tilde{p}_i \tilde{x}_i)$ once defined the new collection of Majorana operators $\vec{s} = O\vec{r}$ as

$$\vec{s} = \begin{pmatrix} \tilde{x}_0 \\ \tilde{p}_0 \\ \tilde{x}_1 \\ \tilde{p}_1 \\ \vdots \\ \tilde{x}_{N-1} \\ \tilde{p}_{N-1} \end{pmatrix}. \tag{3.31}$$

The vector of Majorana operators $\vec{s}$ has a different ordering with respect to the vector $\vec{r}$. We call the order of the operators in $\vec{s}$ an xp ordering and the ordering of the operators in $\vec{r}$ and xx ordering. The transformation matrix $\Omega^{\dagger}$ maps a vector of Majorana operators in xx ordering to a vector of Dirac operators, thus, before being able to move to the Dirac representation we have to reorder the element of vector $\vec{s}$. To do so we use the matrix

$$F_{xp \to xx} = \begin{array}{c} \\ i=0 \\ i=1 \\ \vdots \\ \vdots \\ i=N \\ i=N+1 \\ \vdots \\ i=2N+1 \end{array} \begin{pmatrix} 1 & 0 & 0 & 0 & \dots & \dots & 0 & 0 \\ 0 & \vdots & 1 & \vdots & & & \vdots & \vdots \\ \vdots & \vdots & \vdots & \vdots & & & 0 & \vdots \\ \vdots & 0 & 0 & 0 & & & 1 & \vdots \\ \vdots & 1 & 0 & 0 & & & 0 & \vdots \\ \vdots & 0 & \vdots & 1 & & & \vdots & \vdots \\ \vdots & \vdots & \vdots & 0 & & & \vdots & 0 \\ 0 & 0 & 0 & \vdots & \dots & \dots & 0 & 1 \end{pmatrix} \tag{3.32}$$

that applied to a vector $\vec{s}$ with the xp ordering returns a vector $\vec{\tilde{r}} = F_{xp\to xx}\vec{s}$ with xx ordering. Mapping back to the Dirac representation we obtain the diagonal form of the Hamiltonian in the Dirac operators representation as

$$\hat{H} = i\left(\vec{s}F^T_{xp\to xx}\Omega\right)\left(\Omega^\dagger F_{xp\to xx} h_D F^T_{xp\to xx}\Omega\right)\left(\Omega^\dagger F_{xp\to xx}\vec{s}\right) = \tag{3.33}$$

$$= \sum_{k=1}^{N} \epsilon_k (b_k^\dagger b_k - b_k b_k^\dagger) = \vec{\beta}^\dagger H_D \vec{\beta}. \tag{3.34}$$

The Fermionic transformation U that diagonalises the Hamiltonian H in the form (3.22) is

$$U = \Omega^\dagger \cdot O \cdot F^\dagger_{xp\to xx} \cdot \Omega. \tag{3.35}$$

F_utilities 3.2.1: Diag_h(H)$\to H_D, U$

This function diagonalises H. H_D is the diagonal form with the first half diagonal negative and the second one positive ordered as (3.22). U is the Fermionic transformation such that: $H = UH_DU^\dagger$.

Block-diagonal form of real skew-symmetric matrices The matrix decomposition (3.27) of theorem 1 is numerically obtained in 3 steps

1. Compute numerically a Schur decomposition (or Schur triangularisation as in [134]) of the skew-symmetric matrix h such that: $h = \tilde{O}\tilde{h}_D\tilde{O}^T$. The matrix $\tilde{h}_D$ should be a block-diagonal matrix with each block in the anti-diagonal form

$$\begin{pmatrix} 0 & \tilde{\lambda}_i \\ -\tilde{\lambda}_i & 0 \end{pmatrix}. \tag{3.36}$$

   It is not guaranteed that the $\tilde{\lambda}_i$ are positive for each i. It is necessary to reorder them as in step 2.

2. Build the orthogonal matrix $S = \bigoplus_{i=1}^{\lfloor N/2 \rfloor} s_i$ with

$$s_i = \begin{pmatrix} 0 & 1 \\ 1 & 0 \end{pmatrix} \tag{3.37}$$

if $\tilde{\lambda}_i < 0$ or

$$s_i = \begin{pmatrix} 1 & 0 \\ 0 & 1 \end{pmatrix}, \tag{3.38}$$

if $\tilde{\lambda}_i > 0$.

3. The final orthogonal transformation is $O = \tilde{O}S$ such that $h = Oh_DO^T$.

F_utilities 3.2.2: Diag_real_skew(h) $\rightarrow h_D, O$

This function implements the algorithm for the block diagonalisation of h a generic skew-symmetric real matrix. h_D is the block-diagonal matrix of (3.27) and has the following property: it is in the block diagonal form, each 2×2 block is skew-symmetric with the upper-right element positive and real and h_D is in ascending order for the upper diagonal. O is an orthogonal matrix such that: $h = Oh_DO^T$.

3.3 Fermionic Gaussian States

3.3.1 Fermionic Gaussian states

Definition 1 (Fermionic Gaussian state)

A state ρ is a Fermionic Gaussian state (f.g.s.) if it can be represented as

$$\rho = \frac{e^{-\hat{H}}}{Z} = \frac{e^{-\vec{\alpha}^\dagger H \vec{\alpha}}}{Z} \tag{3.39}$$

with $Z := Tr\left[e^{-\hat{H}}\right]$ a normalisation constant and $\hat{H}$ a Fermionic Gaussian Hamiltonian called parent Hamiltonian of ρ.

Every possible value of the norm of the Hamiltonian is admitted, $\left\|\hat{H}\right\|_1 \in [0, +\infty]$.

Both extremum values are reached with a single sided limit procedure in the definition of ρ.
All the information about the state is encoded in the $2N \times 2N$ matrix H at the exponential.

Fermionic Gaussian states have an immediate interpretation as thermal Gibbs states of f.q.h.. One can even rescale the parent Hamiltonian as $\hat{\hat{H}} = \frac{1}{\beta}\hat{H}$ such that $\left\|\hat{\hat{H}}\right\| = 1$ and $\beta = \frac{1}{\|\hat{H}\|}$. In this way the state reads as $\rho = \frac{e^{-\beta\hat{\hat{H}}}}{Z}$ with $\beta \in [0, +\infty]$. Since f.g.s are exponential of f.g.h. and f.g.h. are even operator, it follows that f.g.s are even operator.

Single mode Gaussian states Consider the single mode parent Hamiltonian $\hat{H}_1 = \epsilon(b^\dagger b - bb^\dagger)$ of the f.g.s. $\rho = \frac{1}{Z}e^{-\hat{H}_1}$. The explicit representation of ρ on the basis $\{b^\dagger|0\rangle, |0\rangle\}$ is

$$\rho = \begin{pmatrix} 1-f & 0 \\ 0 & f \end{pmatrix} \tag{3.40}$$

where $f = \langle 0|\rho|0\rangle$ and the two coherences are 0 because we cannot have the odd terms $|0\rangle\langle 1|$ and $|1\rangle\langle 0|$ in the expansion of the even operator ρ (see [1, 135] for a detailed and beautiful analysis of the admitted coherences). Using the polynomial expansion (3.14) we can see that $f = \mathrm{Tr}\left[\rho b^\dagger b\right] \coloneqq \langle b^\dagger b\rangle$, that is the occupation of the Fermionic mode, thus a single mode Gaussian state is completely characterised by the occupation $\langle b^\dagger b\rangle$.

3.3.2 Correlation Matrix

We have seen that for any f.q.h. H it is always possible to find a Fermionic transformation U that diagonalises H transforming the Dirac operators vector as $\vec{\beta} = U\vec{\alpha}$. Diagonalising the parent Hamiltonian of a f.g.s. ρ we obtain its decomposition in terms of single-mode thermal states

$$\rho = \frac{e^{-\vec{\beta}^\dagger H_D \vec{\beta}}}{Z} = \frac{1}{Z}\bigotimes_{k=1}^{N} e^{-\epsilon_k(b_k^\dagger b_k - b_k b_k^\dagger)} = \bigotimes_{k=1}^{N} \frac{e^{-\epsilon_k(b_k^\dagger b_k - b_k b_k^\dagger)}}{Z_k}, \tag{3.41}$$

where $Z_k = \mathrm{Tr}\left[e^{-\epsilon_k(b_k^\dagger b_k - b_k b_k^\dagger)}\right]$.
Each single-mode thermal state is completely characterised by its occupation number,

thus ρ is completely characterised by the set of occupations $\{\langle b_i^\dagger b_i\rangle\}_{i=1}^N$. Expressing the occupations in term of the operators $\vec{\alpha} = U^\dagger\vec{\beta}$, we find that every f.g.s. is *completely characterised* by the collection of all the correlators $\Gamma_{i,j}^{a^\dagger a} \coloneqq \langle a_i^\dagger a_j\rangle$ and $\Gamma_{i,j}^{aa} \coloneqq \langle a_i a_j\rangle$. We collect these correlators in the so called *correlation matrix*

$$\Gamma \coloneqq \langle\vec{\alpha}\vec{\alpha}^\dagger\rangle = \begin{pmatrix} \Gamma^{a^\dagger a} & \Gamma^{a^\dagger a^\dagger} \\ \Gamma^{aa} & \Gamma^{aa^\dagger} \end{pmatrix} \tag{3.42}$$

with $\Gamma_{i,j}^{aa} = -\overline{\Gamma_{i,j}^{a^\dagger a^\dagger}}$ and $\Gamma_{i,j}^{aa^\dagger} = (\mathbb{I} - \Gamma^{a^\dagger a})_{i,j}^\dagger$, where $\overline{A}$ is the conjugate of A. The correlation matrix Γ is Hermitian, Γ^{aa} and $\Gamma^{a^\dagger a^\dagger}$ are skew-symmetric, and $\Gamma^{a^\dagger a}$ and $\Gamma^{aa^\dagger}$ are Hermitian.

Expressed in term of Majorana operator the correlation matrix is defined as

$$\Gamma^{maj} \coloneqq \langle\vec{r}\vec{r}^\dagger\rangle = \Omega\Gamma\Omega^\dagger. \tag{3.43}$$

It is interesting observing that, since a f.g.s. is completely described by its correlation matrix, with the spirit of the maximum entropy principle (see [136, 137]), it is possible to equivalently define Fermionic Gaussian states as the states that maximise the von Neumann entropy given the expectation values collected in the correlation matrix.

3.3.3 Covariance matrix

The *covariance matrix* of a f.g.s. is the real, skew-symmetric matrix defined as

$$\gamma \coloneqq i\,\mathrm{Tr}\left[\rho[\vec{r}_i, \vec{r}_j]\right], \tag{3.44}$$

with $[\vec{r}_i, \vec{r}_j]$ the commutator of the two Majorana operators $\vec{r}_i$ and $\vec{r}_j$.

As for the correlation matrix, the covariance matrix of a f.g.s ρ completely describes the states. In fact γ and Γ are related by the equality

$$\gamma = -i\Omega\left(2\Gamma - \mathbb{I}\right)\Omega^\dagger = -i\left(2\Gamma^{maj} - \mathbb{I}\right). \tag{3.45}$$

In this thesis we will use both the covariance matrix and the correlation matrix approach.

3.3.4 Wick's theorem

As mentioned, f.g.s. are fully characterised by their covariance matrix. This means that it must be possible to obtain the expectation value of every operator X from γ solely. To do so we just need to take the polynomial expansion (3.12) of X and apply the celebrated Wick's theorem [138] to each monomial term. The Wick's theorem states that for a f.g.s. ρ and a monomial of Majorana operators $r_{q_1} r_{q_2} \dots r_{q_p}$ one has

$$\mathrm{Tr}\left[\rho r_{q_1} r_{q_2} \dots r_{q_p}\right] = \mathrm{Pf}(\gamma_{|_{q_1,q_2,\dots,q_p}}) \tag{3.46}$$

where $1 \leq q_1 < q_2 < \cdots < q_p \leq 2N$ and $\gamma_{|_{q_1,q_2,\dots,q_p}}$ is the restriction of the covariance matrix to all the two points correlators involving just the Majorana operators $\{r_{q_1}, r_{q_2}, \dots, r_{q_p}\}$ and Pf() is called the *Pfaffian*. Since the Pfaffian is nonvanishing only for a $2N \times 2N$ skew-symmetric matrix [139], it is clear that the expectation value of any odd operators is always zero.

Example

Consider a system composed by 2 Fermionic modes corresponding to the Dirac operators a_1 and a_2. The Majorana operators vector is $\vec{r} = (r_1, r_2, r_3, r_4)$, thus the covariance matrix takes the form

$$\gamma = \begin{pmatrix} 0 & \langle r_1, r_2\rangle & \langle r_1, r_3\rangle & \langle r_1, r_4\rangle \\ -\langle r_1, r_2\rangle & 0 & \langle r_2, r_3\rangle & \langle r_2, r_4\rangle \\ -\langle r_1, r_3\rangle & -\langle r_2, r_3\rangle & 0 & \langle r_3, r_4\rangle \\ -\langle r_1, r_4\rangle & -\langle r_2, r_4\rangle & -\langle r_3, r_4\rangle & 0 \end{pmatrix} \tag{3.47}$$

where $\langle r_i, r_j\rangle \coloneqq i\mathrm{Tr}\left[\rho[r_i, r_j]\right]$. Using Wick's theorem we have that

$$\mathrm{Tr}\left[\rho r_1 r_2 r_3 r_4\right] = \mathrm{Pf}\begin{pmatrix} 0 & \langle r_1,r_2\rangle & \langle r_1,r_3\rangle & \langle r_1,r_4\rangle \\ -\langle r_1,r_2\rangle & 0 & \langle r_2,r_3\rangle & \langle r_2,r_4\rangle \\ -\langle r_1,r_3\rangle & -\langle r_2,r_3\rangle & 0 & \langle r_3,r_4\rangle \\ -\langle r_1,r_4\rangle & -\langle r_2,r_4\rangle & -\langle r_3,r_4\rangle & 0 \end{pmatrix} = \tag{3.48}$$

$$= \langle r_1,r_2\rangle\langle r_3,r_4\rangle - \langle r_1,r_3\rangle\langle r_2,r_4\rangle + \langle r_2,r_3\rangle\langle r_1,r_4\rangle, \tag{3.49}$$

and

$$\mathrm{Tr}\left[\rho r_2 r_4\right] = \mathrm{Pf}\begin{pmatrix} 0 & \langle r_2,r_4\rangle \\ -\langle r_2,r_4\rangle & 0 \end{pmatrix} = \langle r_2,r_4\rangle, \tag{3.50}$$

and

$$\mathrm{Tr}\left[\rho r_1 r_2 r_4\right] = \mathrm{Pf}\begin{pmatrix} 0 & \langle r_1,r_2\rangle & \langle r_1,r_4\rangle \\ -\langle r_1,r_2\rangle & 0 & \langle r_2,r_4\rangle \\ -\langle r_1,r_4\rangle & -\langle r_2,r_4\rangle & 0 \end{pmatrix} = 0. \tag{3.51}$$

3.3.5 Diagonalisation of the correlation matrix

In subsection 3.3.2 we have seen that for any f.g.s. ρ there exists a Fermionic transformation U that diagonalises its parent Hamiltonian . With the new Dirac operators $\vec{\beta}$ the state can be expressed as a tensor product of single mode thermal states

$$\frac{e^{-\vec{\beta}^\dagger H_D \vec{\beta}}}{Z} = \frac{1}{Z}\bigotimes_{k=1}^{N} e^{-\epsilon_k(b_k^\dagger b_k - b_k b_k^\dagger)} = \bigotimes_{k=1}^{N}\frac{e^{-\epsilon_k(b_k^\dagger b_k - b_k b_k^\dagger)}}{Z_k}. \tag{3.52}$$

with $Z_k = \mathrm{Tr}\left[e^{-\epsilon_k(b_k^\dagger b_k - b_k b_k^\dagger)}\right]$.

Expressed with these operators the correlation matrix is diagonal. If we consider the Fock basis $\{|\vec{k}\rangle\}_{\vec{k}\in\{0,1\}^N}$ built with the action of the operators $\vec{\beta}$ on $|0\rangle$, we have that in this basis ρ assumes a diagonal form. We call U_ρ the unitary transformation that moves from the basis $\{|\vec{x}\rangle\}_{\vec{x}\in\{0,1\}^N}$ to the one of the modes $\{|\vec{k}\rangle\}_{\vec{k}\in\{0,1\}^N}$.

It is easy to see that expressed on this basis ρ has the diagonal form

$$\rho^D = U_\rho^\dagger \rho U_\rho = \bigotimes_{i=1}^{N} \begin{pmatrix} \nu_i & 0 \\ 0 & 1-\nu_i \end{pmatrix}. \tag{3.53}$$

The same Fermionic transformation U that diagonalises the parent Hamiltonian brings Γ in the diagonal form

$$\Gamma^D = U^\dagger \Gamma U = \begin{pmatrix} \nu_1 & 0 & \dots & & \dots & 0 \\ 0 & \ddots & \ddots & & & \vdots \\ \vdots & \ddots & \nu_N & & & \\ & & & 1-\nu_1 & \ddots & \vdots \\ \vdots & & & \ddots & \ddots & 0 \\ 0 & \dots & & & \dots 0 & 1-\nu_N \end{pmatrix}, \tag{3.54}$$

with $\nu_i \in [0,1]$ the occupation number of the i-th free mode. To numerically obtain the diagonal form of the correlation matrix we notice that the covariance matrix γ is a real, skew-symmetric matrix, thus using theorem 1 we know that we can find an orthogonal transformation O such that

$$\gamma = O\gamma^D O^T = O\left(\bigoplus_{i=1}^{N} \begin{pmatrix} 0 & \eta_i \\ -\eta_i & 0 \end{pmatrix}\right) O^T \tag{3.55}$$

with $\eta_i \in [-\frac{1}{2}, \frac{1}{2}]$.

Following the same procedure of subsection 3.2.4, we can write the diagonal elements of Γ^D as

$$\nu_i = \frac{1}{2} - \eta_i. \tag{3.56}$$

The elements of H_D and Γ^D are related by the following formulas

$$\epsilon_k = \frac{1}{2} \ln\left(\frac{1-\nu_k}{\nu_k}\right), \tag{3.57}$$

$$\nu_k = \frac{1}{1+e^{2\epsilon_k}}, \tag{3.58}$$

with $\nu_k \in [0,1]$ and $\epsilon_k \in [-\infty, +\infty]$, where the boundary values are taken with a limit. The complete calculation can be found in appendix A.1.1. In (3.22) we defined all the ϵ_k to be positive, to use the same notation, one just has to exchange b with $\tilde{b}^\dagger$ and $b^\dagger$ with $\tilde{b}$, that is exchanging occupations with vacancies for the mode with ϵ_k negative. This corresponds to switching ν_k with $1-\tilde{\nu}_k$ and $1-\nu_k$ with $\tilde{\nu}_k$.
In general the correlation matrix Γ and the parent Hamiltonian H are related by the formula [66, 140–142]

$$\Gamma = \frac{1}{1+e^{2H}}. \tag{3.59}$$

F_utilities 3.3.1: Diag_gamma(Γ) $\rightarrow \Gamma^D, U$

This function returns Γ^D, the diagonal form of the Dirac correlation matrix Γ and U the Fermionic transformation such that $\Gamma = U\Gamma^D U\dagger$.

Phisicality of a state It is known that a matrix ρ represents a valid physical density matrix if it is a positive semi-definite Hermitian matrix with trace equal to one. The condition for a matrix Γ to represent a valid physical correlation matrix of a f.g.s. is

$$\Gamma^2 - \Gamma \leq 0, \tag{3.60}$$

or equivalently

$$\gamma\gamma^\dagger \leq -\mathbb{I}. \tag{3.61}$$

These conditions are equivalent to the request that all the eigenvalues ν_i of matrix Γ have to belong to the interval $[0,1]$.

Ground states of Fermionic quadratic Hamiltonians Suppose we have a f.q.h. H and that we are interested in obtaining the correlation matrix Γ_0 associated to its ground state $|0\rangle$. In order to obtain Γ_0 we proceed by first finding the Fermionic transformation U that diagonalise H. Since our algorithm associates to each free mode of the diagonalised Hamiltonian a positive energy, in the diagonal basis the ground

state is $|0\rangle\langle 0|$. The correlation matrix associated to the state $|0\rangle$ is the block matrix:

$$\Gamma_{|0\rangle\langle 0|} = \begin{pmatrix} 0 & 0 \\ 0 & \mathbb{I}_{N\times N} \end{pmatrix}. \tag{3.62}$$

To obtain the ground state Γ_0 we just need to move back to the original basis, thus

$$\Gamma_0 = U\Gamma_{|0\rangle\langle 0|}U^\dagger. \tag{3.63}$$

F_utilities 3.3.2: GS_gamma(H_D, U)$\to \Gamma_0$

This function returns Γ_0, the ground state of the Hamiltonian $H = UH_DU^\dagger$.

Thermal state of Fermionic quadratic Hamiltonians Suppose we have a f.q.h. H and that we are interested in obtaining the correlation matrix Γ_0 associated to the thermal state $\rho_\beta = \frac{e^{-\beta H}}{\mathrm{Tr}[e^{-\beta H}]}$.

As we did for computing the ground state, we move to the diagonal basis with the Fermionic transformation U. In the diagonal basis the thermal state has the correlation matrix

$$\Gamma_\beta^D = \begin{pmatrix} \frac{1}{1+e^{2\beta\epsilon_1}} & 0 & \dots & & \dots & 0 \\ 0 & \ddots & \ddots & & & \vdots \\ \vdots & \ddots & \frac{1}{1+e^{2\beta\epsilon_N}} & & & \\ & & & \frac{1}{1+e^{-2\beta\epsilon_1}} & \ddots & \vdots \\ \vdots & & & \ddots & \ddots & 0 \\ 0 & \dots & & & \dots 0 & \frac{1}{1+e^{-2\beta\epsilon_N}} \end{pmatrix}. \tag{3.64}$$

To obtain the thermal state Γ_β we just need to move back to the original basis, thus

$$\Gamma_\beta = U\Gamma_\beta^D U^\dagger. \tag{3.65}$$

F_utilities 3.3.3: Thermal_fix_beta(H_D, U, β)$\to \Gamma_0$

This function returns Γ_β, the termal state at inverse temperature β of the Hamiltonian $H = UH_DU^\dagger$.

F_utilities 3.3.4: Thermal_fix_energy(H_D, U, E)$\rightarrow \Gamma_{\beta(E)}, \beta(E), \Delta(E)$

This function variationally computes and then returns $\Gamma_{\beta(E)}$, the thermal state at inverse temperature $\beta(E)$ of the Hamiltonian $H = UH_DU^\dagger$, and $\beta(E)$ the temperature such that $\mathrm{Tr}\left[\rho_{\beta(E)}H\right] = E$ and $\Delta(E)$ the difference between the required energy E and the actual energy of the state $\Gamma_{\beta(E)}$. It outputs the precision $\Delta(E)$ and $\beta(E)$.

Energy of a Fermionic Gaussian state Consider a f.q.h H and a f.g.s. Γ. The energy of Γ with respect to H is the expectation value $\mathrm{Tr}\left[\hat{H}\rho\right]$ of the associated $\hat{H}$ computed on the associated state ρ.

In order to compute this expectation value one just needs to find the Fermionic transformation U that diagonalises H. With this, one is able to find the energies ϵ_k and the occupations $\langle b_k^\dagger b_k\rangle$ and $\langle b_k b_k^\dagger\rangle$. The correlation matrix Γ is not diagonal in the diagonal basis $\vec{\beta}$ of H, but we are just interested in its diagonal elements.

The energy $E_H(\Gamma)$ of Γ is thus

$$E_H(\Gamma) = \sum_k \epsilon_k(\langle b_k^\dagger b_k\rangle - \langle b_k b_k^\dagger\rangle). \tag{3.66}$$

F_utilities 3.3.5: Energy(Γ, H_D, U)$\rightarrow E_H(\Gamma)$

This function returns $E_H(\Gamma)$ the energy of the state Γ calculated with H. Matrices H_D and U are the output of `Diag_h(H)`.

3.3.6 Eigenvalues of ρ and eigenvalues of Γ

We have seen that the diagonal form of the correlation matrix Γ and of the density matrix ρ of a f.g.s. can be obtained respectively with a Fermionic transformation U and a unitary operation U_ρ. The Fock basis in which ρ is diagonal is the one generated by the set of operators that expresses Γ in diagonal form.

In these two basis ρ and Γ assume the forms

$$\Gamma^D = \begin{pmatrix} \nu_1 & 0 & \dots & & \dots & 0 \\ 0 & \ddots & \ddots & & & \vdots \\ \vdots & \ddots & \nu_N & & & \\ & & & 1-\nu_1 & \ddots & \vdots \\ \vdots & & & \ddots & \ddots & 0 \\ 0 & \dots & & & \dots 0 & 1-\nu_N \end{pmatrix},$$

$$\rho^D = \bigotimes_{k=1}^{N} \begin{pmatrix} \nu_k & 0 \\ 0 & 1-\nu_k \end{pmatrix} = \begin{pmatrix} \pi_{\vec{0}} & 0 & \dots \\ 0 & \ddots & \vdots \\ \vdots & \dots & \pi_{\vec{1}} \end{pmatrix}. \tag{3.67}$$

Thus if we denote each of the 2^N eigenvalues $\pi_{\vec{x}}$ of ρ with a binary string $\vec{x} \in \{0,1\}^N$ we have that

$$\pi_{\vec{x}} = \prod_{k=1}^{N} \left(\vec{x}_k \nu_i + (1-\vec{x}_k)(1-\nu_k)\right). \tag{3.68}$$

It is evocative changing the order of the Dirac operators in the representation of Γ^D

$$\vec{\beta} = \begin{pmatrix} b_0^\dagger \\ \vdots \\ b_{N-1}^\dagger \\ b_0 \\ \vdots \\ b_{N-1} \end{pmatrix} \qquad \rightarrow \qquad \vec{\tilde{\beta}} = \begin{pmatrix} b_0^\dagger \\ b_0 \\ b_1^\dagger \\ b_1 \\ \vdots \\ b_N^\dagger \\ b_N \end{pmatrix}, \tag{3.69}$$

this can be easily done with the Fermionic transformation $\tilde{\Gamma}^D = F^\dagger_{xp\to xx} \Gamma^D F_{xp\to xx}$. With this ordering we have

$$\tilde{\Gamma}^D = \bigoplus_{k=1}^{N} \begin{pmatrix} \nu_k & 0 \\ 0 & 1-\nu_k \end{pmatrix}, \qquad \rho^D = \bigotimes_{k=1}^{N} \begin{pmatrix} \nu_k & 0 \\ 0 & 1-\nu_k \end{pmatrix}. \tag{3.70}$$

To tensor product of density matrices corresponds a direct sum of correlation matrices.

F_utilities 3.3.6: Eigenvalues_of_rho(Γ)$\rightarrow \vec{\nu}$

This function returns the eigenvalues of the correlation matrix ρ associated to the Fermionic Gaussian state with Dirac correlation matrix Γ.

3.3.7 Reduced density matrix and tensor product of Fermionic Gaussian states

Trying to define a partial trace over Fermionic modes subspaces one soon faces what is often called the "partial trace ambiguity" [1, 135] (see also the end of appendix A.1.6).

In the case of Fermionic Gaussian states, though, this is a much simpler task. Any reduced state formalism has to satisfy the simple criterion that the reduced density operator must contain all the information about the subsystem that can be obtained from the global state when measurements are performed only on the respective subsystem alone [1, 135].

With Wick's theorem in mind it is easy to see that the correlation matrix of the reduced state on the modes $i_1, \ldots, i_m$ is just the correlation matrix $\Gamma|_{\{i_1,\ldots,i_m\}}$ and that the reduced state of a f.g.s. is a f.g.s. too.

F_utilities 3.3.7: Reduce_gamma(Γ,m,i_1)→ $\Gamma|_{\{i_1,\dots,i_m\}}$

This function takes a Dirac correlation matrix Γ, a dimension of the partition m and the initial site of the partition i_1 and return $\Gamma|_{\{i_1,\dots,i_m\}}$, the reduced correlation matrix on the contiguous modes $\{i_1,\dots,i_m\}$ where $i_m = i_1 + m$ and periodic boundary conditions are always assumed.

Examples: the green elements of the matrix $M_{6\times6}$ are the ones returned by the function calls.

Reduce_gamma($M_{6\times6}$,2,1)→

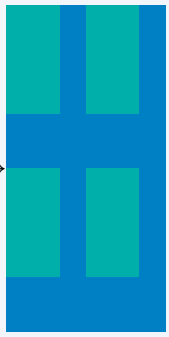

Reduce_gamma($M_{6\times6}$,2,3)→

The correlation matrix $\Gamma_{A,B}$ of the tensor product of two f.g.s. Γ_A and Γ_B is obtained simply by collecting all the elements of Γ_A and Γ_B in a single well ordered correlation matrix $\Gamma_{A,B}$. The code for obtaining $\Gamma_{A,B}$ from Γ_A and Γ_B is

```
D_A = size(Gamma_A,1);
D_B = size(Gamma_B,1);
D   = D_A+D_B;

Gamma_AB = zeros(Complex{Float64}, D,D);
Gamma_AB = Inject_gamma(Gamma_AB,Gamma_A,1);
```

```
Gamma_AB = Inject_gamma(Gamma_AB,Gamma_B,D_A+1);
```

This code makes use of the function `Inject_gamma`.

F_utilities 3.3.8: Inject_gamma(Γ, Γ_{inj}, i)→ Γ_{comp}

This function takes a $2N \times 2N$ matrix Γ and a $2n \times 2n$ matrix Γ_{inj} with $n \leq N$. It returns the $2N \times 2N$ matrix Γ_{comp} as shown in the pictures.

$\Gamma =$  , $\Gamma_{inj} =$ 

`Inject_gamma`$(\Gamma, \Gamma_{inj}, 1) \rightarrow$ 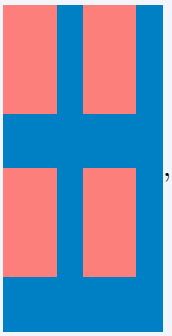 ,

`Inject_gamma`$(\Gamma, \Gamma_{inj}, 3) \rightarrow$ 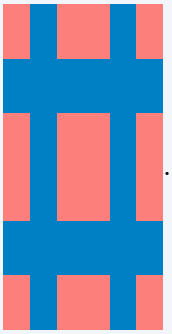 .

In the last example it is clear the systems behave with periodic boundary conditions.

If Γ is the correlation matrix of a f.g.s ρ and Γ_{inj} is the correlation matrix of a f.g.s ρ_{inj} then Γ_{comp} is the correlation matrix of the state $\mathrm{Tr}_{\texttt{i,...,i+n-1}}[\rho] \otimes \rho_{inj}$.

Figure 3.1: System with Open Boundary Conditions. If the state is translational invariant, then the reduced density matrix on sites 1 and 2 is the same as the one on sites 3 and 4, but is different from the one on sites 5 and 1

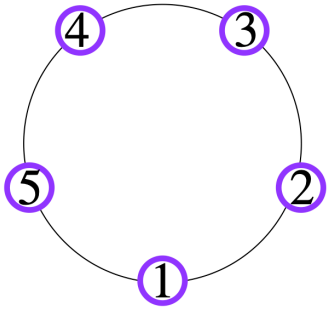

Figure 3.2: System with Periodic Boundary Conditions. If the state is translational invariant then the reduced density matrix on sites 1 and 2 or sites 3 and 4 or even sites 5 and 1 are all the same

It is clear that with the ordering (3.69), the tensor product of two f.g.s. corresponds to the direct sum of their correlation matrices

$$\rho_{A,B} = \rho_A \otimes \rho_B \;\rightarrow\; \tilde{\Gamma}_{A,B} = \tilde{\Gamma}_A \oplus \tilde{\Gamma}_B. \tag{3.71}$$

3.3.8 Correlation matrices of translational invariant states

We consider a state ρ of a system of N sites and all its reduced density matrices ρ_A, where A is any possible set of sites of the system. We denote with $A+m$ the set of sites $A+m = \{j = i+m | i \text{ is a site of } A\}$, that is a translation of all site of A by m sites. When we will assume Periodic Boundary Conditions (PBC) we will allow for translations "over the border" of the system, in the sense that when $i+m > N$ (or $i+m < 1$) we will substitute it with $i+m \rightarrow \text{mod}(i+m-1, N+1)+1$. This is interpreted as connecting the first site with the last site of the system. Thus for PBC all translations are allowed. When we will assume Open Boundary Conditions (OBC) only translations within the system. This means that if $i \in A$ and $i+m > N$ (or $i+m < 1$), then the subset $A+m$ is not an allowed subset of sites.

A *translational invariant state* is a state such that for every A we have $\rho_A = \rho_{A+m}$ for every allowed m.

This property easily translates to correlation matrices of states. For the two point correlators of a translational invariant state we have that $\langle a_j^\dagger a_l \rangle = \langle a_{j+m}^\dagger a_{l+m} \rangle$ and $\langle a_j a_l \rangle = \langle a_{j+m} a_{l+m} \rangle$ for every m. The specific correlator is thus individuated just by the difference of the sites of the first and second operator $\Delta \coloneqq l - j$ with $\Delta \in [-(N-1), N-1]$. Using this, we substitute $\langle a_j^\dagger a_l \rangle \to \langle a^\dagger a \rangle_\Delta$ and analogously $\langle a_j a_l \rangle \to \langle aa \rangle_\Delta$. We now focus on $\Gamma^{a^\dagger a}$, explicitly expressing it, we have

$$\Gamma^{a^\dagger a} \begin{pmatrix} \langle a^\dagger a \rangle_0 & \langle a^\dagger a \rangle_1 & \langle a^\dagger a \rangle_2 & \dots & \langle a^\dagger a \rangle_{N-1} \\ \langle a^\dagger a \rangle_{-1} & \langle a^\dagger a \rangle_0 & \langle a^\dagger a \rangle_1 & \dots & \langle a^\dagger a \rangle_{N-2} \\ \langle a^\dagger a \rangle_{-2} & \langle a^\dagger a \rangle_{-1} & \langle a^\dagger a \rangle_0 & \dots & \langle a^\dagger a \rangle_{N-3} \\ \vdots & \vdots & \vdots & \ddots & \vdots \\ \langle a^\dagger a \rangle_{-(N-1)} & \langle a^\dagger a \rangle_{-(N-2)} & \langle a^\dagger a \rangle_{-(N-3)} & \dots & \langle a^\dagger a \rangle_0 \end{pmatrix}. \tag{3.72}$$

Matrix with this structure are called *Toeplitz matrices*.

If we further require the system to have PBC, we have that the parameter Δ is restricted to the range $[0, N-1]$. Consider for example the specific instance of the correlator $\langle a^\dagger a \rangle_{1-N} = \langle a_N^\dagger a_1 \rangle$, because of the translational invariance property of the system and because of the PBC we know that $\langle a_N^\dagger a_1 \rangle = \langle a_{N+1}^\dagger a_{1+1} \rangle = \langle a_1^\dagger a_2 \rangle = \langle a^\dagger a \rangle_1$ (see figure 3.2).

With PBC, $\Gamma^{a^\dagger a}$ has the form

$$\Gamma^{a^\dagger a} = \begin{pmatrix} \langle a^\dagger a \rangle_0 & \langle a^\dagger a \rangle_1 & \langle a^\dagger a \rangle_2 & \dots & \langle a^\dagger a \rangle_{N-1} \\ \langle a^\dagger a \rangle_{N-1} & \langle a^\dagger a \rangle_0 & \langle a^\dagger a \rangle_1 & \dots & \langle a^\dagger a \rangle_{N-2} \\ \langle a^\dagger a \rangle_{N-2} & \langle a^\dagger a \rangle_{N-1} & \langle a^\dagger a \rangle_0 & \dots & \langle a^\dagger a \rangle_{N-3} \\ \vdots & \vdots & \vdots & \ddots & \vdots \\ \langle a^\dagger a \rangle_1 & \langle a^\dagger a \rangle_2 & \langle a^\dagger a \rangle_3 & \dots & \langle a^\dagger a \rangle_0 \end{pmatrix}. \tag{3.73}$$

We see that $\Gamma^{a^\dagger a}$ is the circulant matrix (see appendix A.1.4) characterised by the circulant vector $\langle \vec{a^\dagger a} \rangle = \big(\langle a^\dagger a \rangle_0, \langle a^\dagger a \rangle_1, \langle a^\dagger a \rangle_2, \dots, \langle a^\dagger a \rangle_{N-1}\big)$. Following the same

reasoning, we see that $\Gamma^{aa^\dagger}$ is a circulant matrix characterised by the circulant vector $\langle \vec{aa^\dagger} \rangle = \big(\langle aa^\dagger\rangle_0, \langle aa^\dagger\rangle_1, \langle aa^\dagger\rangle_2, \ldots, \langle aa^\dagger\rangle_{N-1}\big)$. Matrices Γ^{aa} and $\Gamma^{a^\dagger a^\dagger}$ are circulant skew-simmetric matrices, often called *skew-circulant matrices*. If N is even Γ^{aa} and $\Gamma^{a^\dagger a^\dagger}$ are specified by the circulant vectors

$$\langle \vec{aa} \rangle = \Big(\langle aa\rangle_0, \langle aa\rangle_1, \langle aa\rangle_2, \ldots, \langle aa\rangle_{\frac{N}{2}-1}, 0, -\langle aa\rangle_{\frac{N}{2}-1}, -\langle aa\rangle_{\frac{N}{2}-2}, \ldots, \langle aa\rangle_1\Big)$$

and

$$\langle a^\dagger \vec{a^\dagger} \rangle = \Big(\langle a^\dagger a^\dagger\rangle_0, \langle a^\dagger a^\dagger\rangle_1, \langle a^\dagger a^\dagger\rangle_2, \ldots, \langle a^\dagger a^\dagger\rangle_{\frac{N}{2}-1}, 0, -\langle a^\dagger a^\dagger\rangle_{\frac{N}{2}-1}, -\langle a^\dagger a^\dagger\rangle_{\frac{N}{2}-2}, \ldots, \langle a^\dagger a^\dagger\rangle_1\Big).$$

If N is odd Γ^{aa} and $\Gamma^{a^\dagger a^\dagger}$ are specified by the circulant vectors

$$\langle \vec{aa} \rangle = \Big(\langle aa\rangle_0, \langle aa\rangle_1, \langle aa\rangle_2, \ldots, \langle aa\rangle_{\frac{N-1}{2}}, -\langle aa\rangle_{\frac{N-1}{2}-1}, -\langle aa\rangle_{\frac{N-1}{2}-2}, \ldots, \langle aa\rangle_1\Big)$$

and

$$\langle a^\dagger \vec{a^\dagger} \rangle = \Big(\langle a^\dagger a^\dagger\rangle_0, \langle a^\dagger a^\dagger\rangle_1, \langle a^\dagger a^\dagger\rangle_2, \ldots, \langle a^\dagger a^\dagger\rangle_{\frac{N-1}{2}}, -\langle a^\dagger a^\dagger\rangle_{\frac{N-1}{2}-1}, -\langle a^\dagger a^\dagger\rangle_{\frac{N-1}{2}-2}, \ldots, \langle a^\dagger a^\dagger\rangle_1\Big).$$

Eigenvalues using the properties of circulant-matrices In appendix A.1.4 we show the general form of the eigenvalues of a circulant matrix. For Γ^{aa},$\Gamma^{a^\dagger a^\dagger}$matrices $\Gamma^{a^\dagger a}$,$\Gamma^{aa^\dagger}$ we have that their respective eigenvalues $\lambda_k^{a^\dagger a}$,$\lambda_k^{aa^\dagger}$ are

$$\lambda_k^{a^\dagger a} = \sum_{\Delta=0}^{N-1} e^{i\frac{2\pi}{N}\Delta k}\langle a^\dagger a\rangle_\Delta \qquad\qquad \lambda_k^{aa^\dagger} = \sum_{\Delta=0}^{N-1} e^{i\frac{2\pi}{N}\Delta k}\langle aa^\dagger\rangle_\Delta. \tag{3.74}$$

For matrices Γ^{aa},$\Gamma^{a^\dagger a^\dagger}$ we have that their respective eigenvalues λ_k^{aa},$\lambda_k^{a^\dagger a^\dagger}$ are

$$\begin{aligned}\lambda_k^{aa} &= \begin{cases} 2\sum_{\Delta=0}^{\frac{N}{2}-1} e^{i\frac{2\pi}{N}k\Delta}\langle aa\rangle_\Delta & \text{if } N \text{ even} \\ (1+e^{-i\frac{\pi}{N}})\sum_{\Delta=0}^{\frac{N}{2}-1} e^{i\frac{2\pi}{N}k\Delta}\langle aa\rangle_\Delta & \text{if } N \text{ odd} \end{cases}, \\ \lambda_k^{a^\dagger a^\dagger} &= \begin{cases} 2\sum_{\Delta=0}^{\frac{N}{2}-1} e^{i\frac{2\pi}{N}k\Delta}\langle a^\dagger a^\dagger\rangle_\Delta & \text{if } N \text{ even} \\ (1+e^{-i\frac{\pi}{N}})\sum_{\Delta=0}^{\frac{N}{2}-1} e^{i\frac{2\pi}{N}k\Delta}\langle a^\dagger a^\dagger\rangle_\Delta & \text{if } N \text{ odd} \end{cases}. \end{aligned} \tag{3.75}$$

We notice that the eigenvalues of Γ^{aa},$\Gamma^{a^\dagger a^\dagger}$ comes in pairs $\lambda_k^{aa} = -\lambda_{k+\lceil\frac{N}{2}\rceil}^{aa}$ and $\lambda_k^{a^\dagger a^\dagger} = -\lambda_{k+\lceil\frac{N}{2}\rceil}^{a^\dagger a^\dagger}$ as expected from the property of skew-symmetric matrices (see appendix A.1.5).

Eigenvalues using the Fourier transform on a linear lattice We introduce the Fourier transforms on a linear lattice

$$f_k = \frac{1}{\sqrt{N}}\sum_{j=1}^{N} e^{i\frac{2\pi}{N}kj}a_j, \qquad f_k^\dagger = \frac{1}{\sqrt{N}}\sum_{j=1}^{N} e^{-i\frac{2\pi}{N}kj}a_j^\dagger, \tag{3.76}$$

with inverse transformations

$$a_j = \frac{1}{\sqrt{N}}\sum_{k=1}^{N} e^{-i\frac{2\pi}{N}kj}f_k, \qquad a_j^\dagger = \frac{1}{\sqrt{N}}\sum_{k=1}^{N} e^{i\frac{2\pi}{N}kj}f_k^\dagger. \tag{3.77}$$

It is easy to see that the Fourier modes $\{f_k, f_k^\dagger\}_k$ obey to the CAR and are valid Dirac operators.

Now we perform the substitutions (3.5.1) in the expression of $\Gamma^{a^\dagger a}$ and we further exploit the translational invariance ($\langle a^\dagger a\rangle\Delta = \frac{1}{N}\sum_{j=1}^{N}\langle a_j^\dagger a_{j+\Delta}\rangle$) to obtain

$$\langle a^\dagger a\rangle_\Delta = \frac{1}{N^2}\sum_{j}^{N}\sum_{k,k'} e^{i\frac{2\pi}{N}k'\Delta}e^{i\frac{2\pi}{N}(k-k')j}\langle f_k^\dagger f_{k'}\rangle. \tag{3.78}$$

Collecting the Kronecker delta (see appendix A.2.4) we can express the elements of

$\Gamma^{a^\dagger a}$ as

$$\langle a^\dagger a\rangle_\Delta = \frac{1}{N}\sum_{k=1}^{N} e^{-i\frac{2\pi}{N}k\Delta}\langle f_k^\dagger f_k\rangle. \tag{3.79}$$

With the same procedure we obtain

$$\begin{aligned}
\langle a^\dagger a\rangle_\Delta &= \frac{1}{N}\sum_{k=1}^{N} e^{-i\frac{2\pi}{N}k\Delta}\langle f_k^\dagger f_k\rangle, & \langle aa^\dagger\rangle_\Delta &= \frac{1}{N}\sum_{k=1}^{N} e^{-i\frac{2\pi}{N}k\Delta}\langle f_k f_k^\dagger\rangle \\
\langle aa\rangle_\Delta &= \frac{1}{N}\sum_{k=1}^{N} e^{-i\frac{2\pi}{N}k\Delta}\langle f_k f_{N-k}\rangle, & \langle a^\dagger a^\dagger\rangle_\Delta &= \frac{1}{N}\sum_{k=1}^{N} e^{-i\frac{2\pi}{N}k\Delta}\langle f_{N-k}^\dagger f_k^\dagger\rangle.
\end{aligned} \tag{3.80}$$

with inverse transformations

$$\begin{aligned}
\langle f_k^\dagger f_k\rangle &= \sum_{\Delta=1}^{N} e^{i\frac{2\pi}{N}k\Delta}\langle a^\dagger a\rangle_\Delta, & \langle f_k f_k^\dagger\rangle &= \sum_{\Delta=1}^{N} e^{i\frac{2\pi}{N}k\Delta}\langle aa^\dagger\rangle_\Delta \\
\langle f_k f_{N-k}\rangle &= \sum_{\Delta=1}^{N} e^{i\frac{2\pi}{N}k\Delta}\langle a^\dagger a\rangle_\Delta, & \langle f_k^\dagger f_{N-k}^\dagger\rangle &= \sum_{\Delta=1}^{N} e^{-i\frac{2\pi}{N}k\Delta}\langle aa^\dagger\rangle_\Delta.
\end{aligned} \tag{3.81}$$

We can easily identify

$$\begin{aligned}
\lambda_k^{a^\dagger a} &= \langle f_k^\dagger f_k\rangle, & \lambda_k^{aa^\dagger} &= \langle f_k f_k^\dagger\rangle \\
\lambda_k^{aa} &= \langle f_k f_{N-k}\rangle, & \lambda_k^{a^\dagger a^\dagger} &= \langle f_k^\dagger f_{N-k}^\dagger\rangle.
\end{aligned} \tag{3.82}$$

At last, we note that the Fourier transform does not mix creation and annihilation operators and can be implemented directly on the vector of Dirac operators $\vec{\alpha}$ with the Fermionic transformation U_ω that has the block diagonal form

$$U_\omega = \begin{pmatrix} W & 0 \\ 0 & \bar{W} \end{pmatrix}, \tag{3.83}$$

where W is the matrix implementing the discrete Fourier transform (see appendix A.1.4) and it acts separately on the creation and annihilation operators sectors of $\vec{\alpha}$.

For an example of diagonalisation of translational invariant matrices see e.g. subsection 3.4

F_utilities 3.3.9: Build_Fourier_matrix(N)$\to U_\omega$

This function returns the Fermionic transformation U_ω for a system of N sites.

3.3.9 Product Rule

It will result useful to compute the product $\rho = \rho_1\rho_2$ of the density matrices of two Fermionic Gaussian states. We observe that the commutator of two quadratic terms of Majorana operators $\vec{r}$ is always again a quadratic operator or zero

$$[r_i r_j, r_k r_l] = \delta_{k,i} r_l r_j + \delta_{k,j} r_i r_l - \delta_{i,l} r_k r_j - \delta_{l,j} r_i r_k. \tag{3.84}$$

This is also valid for Dirac operators. We say that the commutator of two monomials of Dirac operators of degree at most 2 is a polynomial of Dirac operators of degree at most 2. Using this observation together with the Baker-Campbell-Hausdorff formula (equation B.C.H.0 in appendix A.2.4), it is easy to see that ρ, the product of two f.g.s., is always a f.g.s.

$$\rho = \frac{e^{-\hat{H}}}{Z}, \tag{3.85}$$

with $\hat{H}$ given by the B.C.H.0.

It is possible to derive the covariance matrix γ of ρ directly from the covariance matrices γ_1 and γ_2 of the states ρ_1 and ρ_2. This formula appears in [143] where a more detailed description, considering even pathological cases, is given. If we assume that $\mathbb{I} - \gamma_1$ and $\mathbb{I} - \gamma_2$ are invertible then we have

$$\gamma = \mathbb{I} - (\mathbb{I} - \gamma_2)\frac{1}{\mathbb{I} + \gamma_1\gamma_2}(\mathbb{I} - \gamma_1). \tag{3.86}$$

F_utilities 3.3.10: Product(Γ_1, Γ_2)$\to \Gamma$

This function returns the correlation matrix Γ corresponding to the f.g.s $\rho = \rho_1\rho_2$, where ρ_1 and ρ_2 are characterised by the correlation matrices Γ_1 and Γ_2.

3.3.10 Information measures

Von Neumann Entropies The von Neumann entropy of a quantum state described by the density matrix ρ is

$$S(\rho) = -\mathrm{Tr}\left[\rho \ln(\rho)\right]. \tag{3.87}$$

In terms of the eigenvalues λ of ρ, the von Neumann entropy reads as

$$S(\rho) = -\sum_{\lambda} \lambda \ln(\lambda) \tag{3.88}$$

If ρ is a f.g.s. of a system with N sites, since the von Neumann entropy is invariant under unitary transformation of the state, substituting in (3.87) the product form (3.70) and using the fact that the von Neumann entropy is additive for product states, the von Neumann entropy becomes a function of the eigenvalues ν_i of the correlation matrix Γ and it is the sum of just $2N$ terms

$$S(\Gamma) \equiv S(\rho) = -\sum_{k=1}^{N} \left[\nu_k \ln(\nu_k) + (1-\nu_k)\ln(1-\nu_k)\right]. \tag{3.89}$$

F_utilities 3.3.11: VN_entropy(Γ)$\to S$

This function returns S, the `Float64` value of the von Neumann Entropy of the state described by the Dirac correlation matrix Γ.

Purity A state is pure if its correlation matrix Γ is such that [144]

$$\Gamma^2 = \Gamma, \tag{3.90}$$

or, equivalently,

$$\gamma^2 = -\mathbb{I} \tag{3.91}$$

The purity of a state ρ is defined as

$$\mathrm{Purity}(\rho) \equiv Tr\left[\rho^2\right]. \tag{3.92}$$

We have that:

$$\text{Purity}(\rho) = \prod_{i=1}^{N-1} \frac{1}{2}\left(1 + \tanh(\epsilon_i)^2\right), \tag{3.93}$$

$$\text{Purity}(\Gamma) = \prod_{i=1}^{N-1} \left(2\left(\nu_i - 1\right)\nu_i + 1\right), \tag{3.94}$$

$$\text{Purity}(\gamma) = \prod_{i=1}^{N-1} \left(2\eta_i^2 + \frac{1}{2}\right), \tag{3.95}$$

the value of the purity is the same if computed with any of these equations. For more details see appendix A.1.2.

F_utilities 3.3.12: Purity(Γ)$\rightarrow p$

This function returns p the purity of the Fermionic Gaussian state with Dirac correlation matrix Γ.

Entanglement Contour In 2014 Chen and Vidal [92] introduced the entanglement contour "a tool for identifyng which real-space degrees of freedom contribute, and how much, to the entanglement of a region A with the rest of the system B". We consider the state of a system on a chain of N sites, we divide the chain into two complementary partitions, partition A and partition B. Now suppose partitions A and B are entangled and that there exists a measure $\mathcal{E}(A, B)$ that quantifies the amount of entanglement between A and B. The entanglement contour $c_A(i)$ of partition A tells us how much each site i of partition A contributes to the total amount of entanglement betwen A and B. Furthermore summing $c_A(i)$ over all the sites of A one should obtain exactly $\mathcal{E}(A, B)$.

Chen and Vidal state five reasonable properties that define when a function is a contour function. In the same paper they show that these five properties do not identify a unique contour function, but instead a class of functions. In chapter 2.3.2 we presented these five properties and introduced the general concept of entanglement contour, here we are going to focus on a specific entanglement contour defined for Fermionic Gaussian states. First of all we restrict to pure states. For a pure state, it is known that a

good measure of entanglement between two complementary partition A and B is the entanglement entropy, that is the von Neumann entropy $\mathcal{E}(A,B) = S(A)$ of the reduced state on A.

We consider an Hilbert space $\mathcal{H}$ divided in the two complementary partitions $\mathcal{H} = \mathcal{H}_A \otimes \mathcal{H}_B$, each partition with N_A and N_B sites respectively. The Schmidt decomposition (see section 2.3.4) of a pure state $|\psi^{A,B}\rangle$ in $\mathcal{H}$ is

$$|\psi^{A,B}\rangle = \sum_i \sqrt{p_i} |\psi_i^A\rangle \otimes |\psi_i^B\rangle, \tag{3.96}$$

with $p_i \geq 0$, $\sum_i p_i = 1$ and

$$\rho^A \equiv Tr_B \left[|\psi^{A,B}\rangle\langle\psi^{A,B}| \right] = \sum_i p_i |\psi_i^A\rangle\langle\psi_i^A|. \tag{3.97}$$

The entanglement entropy for this choice of partition is thus $S(A) = -\sum_i p_i ln(p_i)$.

Factorising the Hilbert space $\mathcal{H}_A$ in its tensor product structure $\mathcal{H}_A = \bigotimes_{j\in A} \mathcal{H}_j$, we individuate in each local Hilbert space $\mathcal{H}_j$ a site of the partition A. We remind that ρ^A cannot be expressed as a product state over this factorisation of $\mathcal{H}_A$ and that the von Neumann entropy is not additive. Thus the von Neumann entropy computed on each site is not a good entanglement contour function.

We know from 3.3.7 that ρ_A is a f.g.s., thus we can express the entanglement entropy $S(A)$ as the sum of the von Neumman entropy of each mode in A,

$$S(A) = \sum_{k=1}^{N_A} S_k = -\sum_{k=1}^{N_A} \left[\nu_k \ln(\nu_k) + (1-\nu_k)\ln(1-\nu_k) \right]. \tag{3.98}$$

Each mode k, associated to the Dirac operators $\beta_k = b_k^\dagger$, $\beta_{k+N_A} = b_k$, is connected to the real space modes associated the Dirac operators $\alpha_i = a_i^\dagger$, $\alpha_{i+N_A} = a_i$ by the Fermionic transformation U such that

$$\beta_k = \sum_{i=1}^{N_A} U_{k,i} \alpha_i. \tag{3.99}$$

We want to use this equation to find how much a fixed mode k contributes to a fixed site i. We call this contribution $p_i(k)$ and we define it as

$$p_i(k) \coloneqq \frac{1}{2}\left[|U_{k,i}|^2 + |U_{k+N_A,i+N_A}|^2 + |U_{k,i+N_A}|^2 + |U_{k+N_A,i}|^2\right]. \tag{3.100}$$

The entanglement contour for partition A is thus defined as

$$c_A(i) \coloneqq \sum_{k=1}^{N_A} p_i(k) S_k. \tag{3.101}$$

It is easy to see that each of the $p_i(k)$ is positive and that

$$\sum_{k=1}^{N_A} p_i(k) = 1, \tag{3.102}$$

as

$$\sum_{k=1}^{N_A} p_i(k) = \frac{1}{2}\left[\sum_{l=1}^{2N_A} U_{i,l}U^*_{l,i} + U_{i+N_A,l}U^*_{l,i+N_A}\right] = \frac{1}{2}\left((UU^\dagger)_{i,i} + (UU^\dagger)_{i+N_A,i+v}\right) = 1,$$

since U is unitary. Thus one has the desired property

$$\sum_{i=1}^{N_A} c_A(i) = S(A). \tag{3.103}$$

F_utilities 3.3.13: Contour(Γ_A)$\to \vec{c_A}$

This function returns the vector $\vec{c_A}_i = c_A(i)$ of the entanglement contour of the correlation matrix Γ_A.

3.3.11 Examples

We will use the function

F_utilities 3.3.14: Random_NNHamiltonian(N)$\rightarrow H$

Generate a random f.q.h. Hamiltonian for a system of N sites with just nearest neighbour interactions.

Computing the energies of H In this program we compute the energies ϵ_k of a random nearest neighbours Hamiltonian on a linear lattice of $N = 64$ sites generated with the function `Random_NNHamiltonian(64)`. The program generates the output figure 3.3 .

```
using F_utilities;
using PyPlot;
using LinearAlgebra;

const Fu = F_utilities;

N = 64;

#Generate and diagonalise the hamiltonian
H = Fu.Random_NNhamiltonian(N)
H_D, U_D = Fu.Diag_h(H)

#Print the energy modes epsilon_k
figure("Energies")
plot(1:N,diag(H_D)[1:N])
xlabel(L"$k$")
ylabel(L"$\epsilon_k$")
```

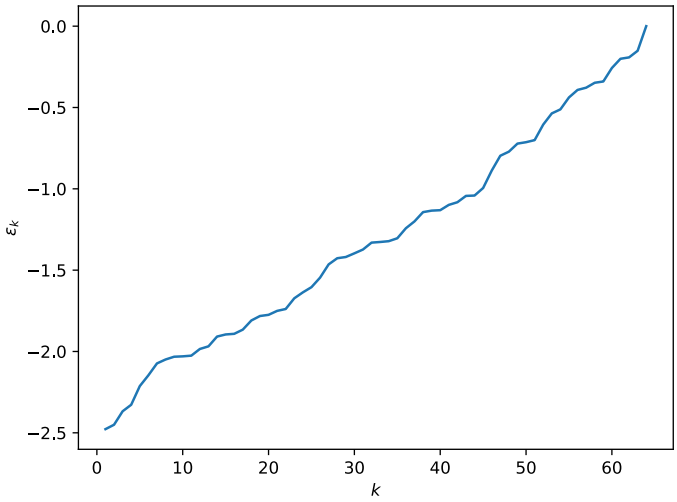

Figure 3.3: Output of examples 3.3.11. In the plot are represented the eigenvalues of a random nearest-neighbour Hamiltonian computed with the code `Random_NNHamiltonian(N)` for a system with $N = 64$ sites.

Computing the entanglement contour of a partition of a ground state In this program we compute the entanglement contour and the entropy of a partition of $N_A = 32$ sites in the bulk of the ground state of a random nearest neighbours Hamiltonian on a linear lattice of $N = 64$ sites. The program generates the output figure 3.4.

```
using F_utilities;
using PyPlot;
using LinearAlgebra;

const Fu = F_utilities;

N = 64;
H = Fu.Random_NNhamiltonian(N);
H_D, U_D = Fu.Diag_h(H);
```

```
Gamma = Fu.GS_Gamma(H_D, U_D);
println("The energy of the ground state is: ", Fu.Energy_fermions(
    ↪ Gamma,H_D, U_D));


N_A = 32;
#I consider the reduced state over the sites 17,18,...,48
Gamma_A = Fu.Reduce_gamma(Gamma,N_A,17);
#I compute the entangement entropy
S_A = Fu.VN_entropy(Gamma_A);
#I compute the contour of partition A
c_A = Fu.Contour(Gamma_A);


lbl_title   = string(L"$S(A) = $", S_A);
lbl_legend  = string(L"$\sum_{i=1}^{N_A} c_A(i) = $", sum(c_A));
figure("Contour of A")
title(lbl_title)
plot(1:N_A, c_A, marker="o", label=lbl_legend);
xlabel("i")
ylabel(L"$c_A(i)$")
legend();
```

Output:

```
The energy of the ground state is:  -83.1750144099933
```

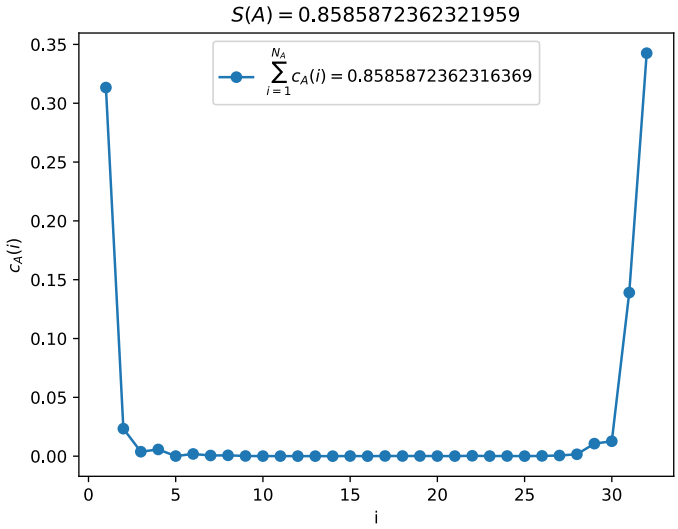

Figure 3.4: Output of examples 3.3.11. In the plot it is represented the entanglement contour of the reduced density matrix of the first 32 contiguous site of a linear chain, when the global state is the ground state of a nearest-neighbour Hamiltonian on a linear chain of $N = 64$ sites. Note how for a nearest neighbour Hamiltonian, the contour is higher on the boundary of the partition.

3.3.12 Time Evolution

We learned about Hamiltonians and states. Now it is time to put these two ingredients together and finally talk about the unitary evolution of Fermionic Gaussian states.

We start stating that *the space of Fermionic Gaussian states is closed under evolution induced by Fermionic quadratic Hamiltonians.*

The best way for seeing this is using the Majorana operators representation. We consider a general f.q.h. $\hat{H}$ and a generic f.g.s. $\rho = \frac{e^{-\hat{H}_\rho}}{Z}$ with both $\hat{H}$ and $\hat{H}_\rho$ of the form (3.18). Using standard notation we call $\rho(t)$ the state ρ at time t defined as

$$\rho(t) := e^{-it\hat{H}} \rho e^{it\hat{H}} = \frac{e^{-it\hat{H}} e^{-\hat{H}_\rho} e^{it\hat{H}}}{Z}. \tag{3.104}$$

As already observed in subsection 3.3.9, the commutator of two quadratic monomial of Dirac operators is a polynomial at most quadratic in Dirac operators. Using this

observation together with the Baker-Campbell-Hausdorff formula (equation B.C.H.0 in appendix A.2.4), it is easy to see that $\rho(t)$ has the form

$$\rho(t) = \frac{e^{-\hat{H}_{\rho(t)}}}{Z}, \tag{3.105}$$

with $\hat{H}_{\rho(t)}$ a Fermionic quadratic Hamiltonian. Thus $\rho(t)$ is again a Gaussian state proving that the space of Gaussian states is closed under evolution induced by Fermionic quadratic Hamiltonians.

We will now compute an explicit formula for the time evolution of the correlation matrix $\Gamma(t)$ of the f.g.s. state $\rho(t)$. The first step is computing the time evolution of the creation and annihilation operators in the Heisenberg picture. We denote with $\vec{\beta}$ the vector of Dirac operators that diagonalises H. The annihilation and creation operators b_k and $b_k^\dagger$ evolved at time t are (see appendix A.1.3)

$$b_k(t) = e^{-i\hat{H}t} b_k e^{i\hat{H}t} = e^{-i2\epsilon_k t} b_k, \tag{3.106}$$

$$b_k^\dagger(t) = e^{-i\hat{H}t} b_k^\dagger e^{i\hat{H}t} = e^{i2\epsilon_k t} b_k^\dagger. \tag{3.107}$$

In compact form this can be written as

$$\vec{\beta}(t) = e^{i2H_D t}\vec{\beta}. \tag{3.108}$$

It is easy now to compute the time evolution of the correlators $\langle\vec{\beta}\vec{\beta}^\dagger\rangle$

$$\langle\vec{\beta}(t)\vec{\beta}^\dagger(t)\rangle = \langle e^{i2H_D t}\vec{\beta}\vec{\beta}^\dagger e^{-i2H_D t}\rangle. \tag{3.109}$$

Thus, if U is the Fermionic transformation such that $\vec{\beta} = U\vec{\alpha}$, the Fermionic transformation implementing the time evolution of $\vec{\alpha}$ is $U^\dagger e^{i2H_D t}U = e^{i2Ht}$. We finally obtain that the correlation matrix Γ evolves with H as

$$\Gamma(t) = e^{i2Ht}\Gamma e^{-i2Ht}. \tag{3.110}$$

F_utilities 3.3.15: Evolve(Γ, H_D, U, t)$\to \Gamma(t)$

This function returns the correlation matrix Γ evolved at time t with H. Matrices H_D and U are the output of `Diag_h(H)`.

3.4 Hopping model

We consider the translational invariant hopping Hamiltonian for a system of N sites

$$\hat{H} = \sum_{i=1}^{N-1} [a_i^\dagger a_{i+1} - a_i a_{i+1}^\dagger] + \delta[a_N^\dagger a_1 - a_N a_1^\dagger], \tag{3.111}$$

with $\delta = 1$ for periodic boundary conditions and $\delta = 0$ for open boundary conditions. The compact form (3.16) of $\hat{H}$ is specified by the two circulant matrices (see A.1.4)

$$A = \begin{pmatrix} 0 & \frac{1}{2} & 0 & \dots & 0 & \delta\frac{1}{2} \\ \frac{1}{2} & 0 & \frac{1}{2} & 0 & \dots & 0 \\ 0 & \frac{1}{2} & 0 & \frac{1}{2} & 0 & \dots \\ \vdots & \vdots & \ddots & \ddots & \ddots & \vdots \\ \delta\frac{1}{2} & 0 & 0 & \dots & \frac{1}{2} & 0 \end{pmatrix} \qquad B = \begin{pmatrix} 0 & \dots & 0 \\ \vdots & \ddots & \vdots \\ 0 & \dots & 0 \end{pmatrix} \tag{3.112}$$

As seen in subsection 3.3.8 and appendix A.1.4) we know that H is diagonalised with a Fourier transformation. Indeed, if we express the hopping Hamiltonian (3.111) in term of the Fourier modes (3.5.1) we obtain

$$\hat{H} = \sum_{k=1}^{N} \phi_k (f_k^\dagger f_k - f_k f_k^\dagger), \tag{3.113}$$

where

$$\phi_k = \cos(\frac{2\pi}{N} k). \tag{3.114}$$

The Fermionic transformation that diagonalises the Hamiltonian is U_ω as defined in (3.83).

3.4.1 Numerical diagonalisation

In the following code we show how to initialise and diagonalise the hopping Hamiltonian using functions of `F-utilities`. We perform these calculations using two different methods. The energies computed with both methods are reported in figure 3.5, the ground states correlations matrices are identical.

```
using F_utilities;
using PyPlot;
using LinearAlgebra;

const Fu = F_utilities;



N =127;

H   = Fu.Build_hopping_hamiltonian(N,PBC=true);

U_omega = Fu.Build_Fourier_matrix(N);
D_omega = U_omega'*H*U_omega;
D,U = Fu.Diag_h(H);



figure("Energies")
plot(diag(real.(D_omega))[(N+1):(2*N)],label="Method Fourier");
plot(real.(diag(D))[(N+1):(2*N)], label="Method Diag_h");
xlabel(L"$k$");
ylabel(L"$\epsilon_k$");
legend();

Gamma_omega = Fu.GS_gamma(D_omega,U_omega);
Gamma   = Fu.GS_gamma(D,U);
```

```
println("")
println("Energy GS Method Fourier:      ",Fu.Energy(Gamma_omega,(
    ↪ D_omega,U_omega)))
println("En GS Method Diag_h:           ",Fu.Energy(Gamma,(D,U)))
```

Output:

```
Energy GS Method Fourier:  -80.85277253991693
En GS Method Diag_h:  -80.85277253997737
```

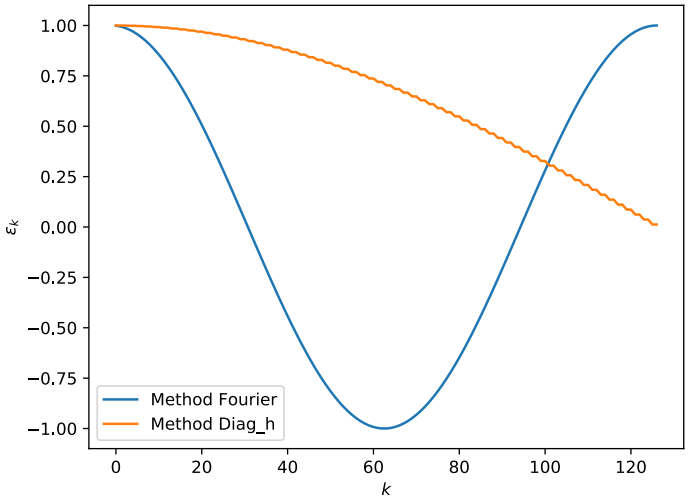

Figure 3.5: In this example we diagonalised the Hamiltonian with two different methods. Using the Fourier transform method we obtain the energies specified in (3.114). These energies are both positive and negative. Using the `Diag_h` method of `F_utilities` we obtain just positive energies. The difference in the diagonal energies comes from the fact that `Diag_h`, for every eigenmode with negative energy, substitutes creation and annihilation operators in order to redefine the energy as positive, and then reorders the modes in order to have the energies in descending order. If we diagonalise with the Fourier transform then the ground state is obtained filling all the modes with negative energy. If we diagonalise with `Diag_h` then the ground state corresponds to the empty state.

F_utilities 3.4.1: Build_hopping_Hamiltonian(N, PBC=true)$\to H$

This functions return the Hamiltonian H if dimension $2N \times 2N$ for the hopping model. If `PBC=false` it return the hopping Hamiltonian with open boundary conditions

For the numerical diagonalisation of the Hamiltonian we used two methods, the analytical one using the Fourier modes, and the numerical one introduced in the previous subsection.

These methods return the hopping Hamiltonian in the diagonal forms

$$\hat{H}_\omega = \sum_{k=1}^{N} \phi_k (f_k^\dagger f_k - f_k f_k^\dagger), \qquad \hat{H} = \sum_{k=1}^{N} \epsilon_k (b_k^\dagger b_k - b_k b_k^\dagger), \tag{3.115}$$

where the differences in the energies are due to the fact that `Diag_h` considers all the energies ϵ_k positive, thus defines $b_k = f_k^\dagger$ and $b_k^\dagger = f_k$ for each k such that $\phi_k < 0$ (that corresponds to flipping the sign of ϕ_k when it is negative, such that the corresponding $\epsilon_k = -\phi_k$), and then reorder the modes such that to modes with smaller k correspond biggest energies.

3.4.2 Time Evolution

For the hopping model we analytically obtained the Fermionic transformation U_ω that diagonalises the Hamiltonian. This allows us to give an analytical expression for the time evolution of the correlation matrix.

Expressing the correlation matrix Γ in term of the operators $\vec{\phi}$ and computing the time evolution with the diagonal Hamiltonian (3.113) we obtain

$$\langle a_l^\dagger a_m \rangle(t) = \frac{1}{N} \sum_{k,k'} \sum_{x,y} e^{i2(\phi_k - \phi_{k'})t} e^{i\frac{2\pi}{N}(k(l-x)-k'(m-y))} \langle a_x^\dagger a_y \rangle \tag{3.116}$$

$$\langle a_l a_m \rangle(t) = \frac{1}{N} \sum_{k,k'} \sum_{x,y} e^{-i2(\phi_k + \phi_{k'})t} e^{-i\frac{2\pi}{N}(k(l-x)+k'(m-y))} \langle a_x a_y \rangle. \tag{3.117}$$

Because of the block diagonal structure of U_ω there is not mixing of the two types of correlators during the evolution of the correlation matrix.

Time evolution of translational invariant states Let us consider a translational invariant state Γ. In subsection 3.3.8 we expressed Γ in term of the Fourier modes $f_k^\dagger, f_k$. Using the diagonal form (3.115) of the Hopping Hamiltonian to compute the time evolution of the correlators of Γ expressed as in (3.80) we have that Γ evolves as

$$\begin{aligned}
\langle a^\dagger a\rangle_\Delta(t) &= \frac{1}{N}\sum_{k=1}^{N} e^{-i\frac{2\pi}{N}k\Delta}\langle f_k^\dagger f_k\rangle, & \langle aa^\dagger\rangle_\Delta(t) &= \frac{1}{N}\sum_{k=1}^{N} e^{-i\frac{2\pi}{N}k\Delta}\langle f_k f_k^\dagger\rangle \\
\langle aa\rangle_\Delta(t) &= \frac{1}{N}\sum_{k=1}^{N} e^{i4\phi(k)t}e^{-i\frac{2\pi}{N}k\Delta}\langle f_k f_{N-k}\rangle, & \langle a^\dagger a^\dagger\rangle_\Delta(t) &= \frac{1}{N}\sum_{k=1}^{N} e^{-i4\phi(k)t}e^{-i\frac{2\pi}{N}k\Delta}\langle f_{N-k}^\dagger f_k^\dagger\rangle.
\end{aligned} \tag{3.118}$$

in the following program we numerically compute the time evolution induced by a hopping Hamiltonian on a random translational invariant gaussian state with exponentially decaying correlation functions. We consider a linear system of $N = 50$ sites and evolve it for $N_{\text{steps}} = 100$ steps of $\delta_{steps} = 0.1$. The program generates the output figures 3.6 and 3.7.

```
using F_utilities;
using PyPlot;
using LinearAlgebra;

const Fu = F_utilities;



N=50;
N_steps = 100;
delta_steps = 0.1;

#Build the circulant vector for the adaa part of the Gamma with
```

```
    ↪ exponential decaying correlations
adaa = zeros(Complex{Float64},N);#
for i=1:div(N,2)
    adaa[i] = exp(-i*0.15)*(rand()+im*rand())
end
adaa[((div(N,2))+1):N]= reverse(adaa[1:div(N,2)]);
#Build the translational invariant adaa part of the Gamma
Gamma_adaa = Fu.Circulant(adaa);
Gamma_adaa = (Gamma_adaa+Gamma_adaa')/2.

#Build the circulant vector for the aa part of the Gamma
aa = zeros(Complex{Float64},N);
aa[2] = rand()+im*rand();
aa[3] = rand()+im*rand();
#Build the translational invariant aa part of the Gamma
Gamma_aa = Fu.Circulant(aa)
Gamma_aa = (Gamma_aa-transpose(Gamma_aa))/2.;

#Build the translational invariant Gamma
Gamma= zeros(Complex{Float64}, 2N,2N);
Gamma[(1:N),(1:N)]          = Gamma_adaa;
Gamma[(1:N).+N,(1:N).+N]    = (I-Gamma_adaa)';
Gamma[(1:N).+N,(1:N)]       = Gamma_aa;
Gamma[(1:N),(1:N).+N]       = -conj(Gamma_aa);
Fu.Print_complex_matrix("Gamma",Gamma)

H   = Fu.Build_hopping_hamiltonian(N,PBC=true);
D,U = Fu.Diag_h(H);
```

```
Gamma_evolved   = copy(Gamma);
adaa        = zeros(Complex{Float64}, N_steps)
aa          = similar(adaa);

#Start the time evolution cycle
#at each cycle it saves the value of two correalotors
adaa[1]     = Gamma_evolved[1,2];
aa[1]       = Gamma_evolved[N+1,2];
for t=2:N_steps
    global Gamma_evolved = Fu.Evolve(Gamma_evolved,(D,U),
        ↪ delta_steps);
    adaa[t]     = Gamma_evolved[1,2];
    aa[t]       = Gamma_evolved[N+1,2];
end

figure("Evolutions")
plot(real.(adaa), color="black", label=L"$\mathfrak{R}(\langle a_1
    ↪ ^{\dagger}a_2 \rangle)(t)$");
plot(imag.(adaa), color="black",linestyle="--", label=L"$\mathfrak{
    ↪ I}(\langle a_1^{\dagger} a_2 \rangle)(t)$");
plot(real.(aa), color="purple", label=L"$\mathfrak{R}(\langle
    ↪ a_1a_2 \rangle)(t)$");
plot(imag.(aa), color="purple", linestyle="--", label=L"$\mathfrak{
    ↪ I}(\langle a_1 a_2 \rangle)(t)$");
legend()
xlabel("timestep")
```

Output:

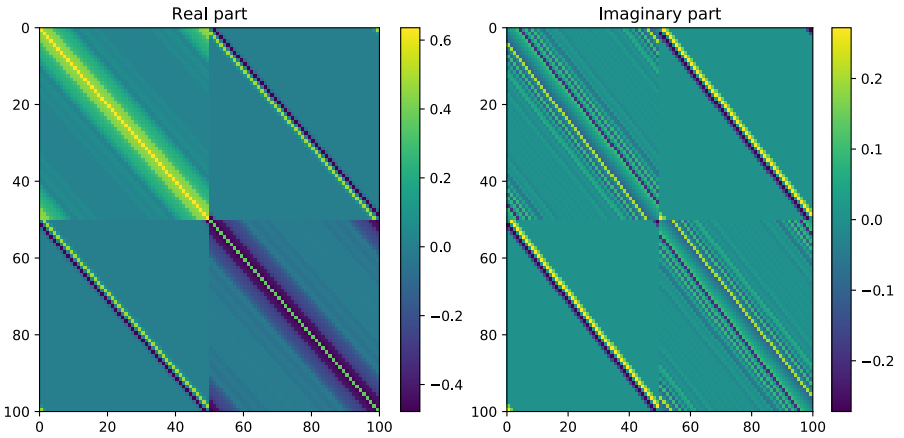

Figure 3.6: This is a representation of the real and imaginary part (left and right plots) of the elements of the correlation matrix Γ of a translational invariant state with exponentially decaying correlations. The element (i, j) corresponds to $\Gamma_{i,j}$. The exponential decay of the correlation is evident from the fading of the colours moving to matrix elements farer from the diagonal.

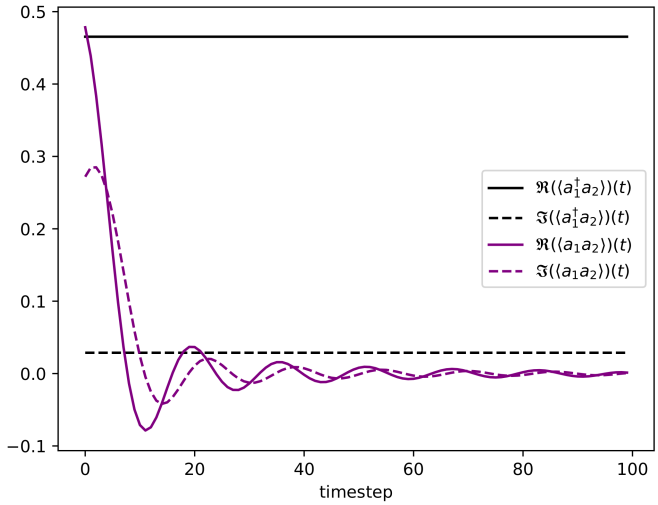

Figure 3.7: The time evolution induced by the Hopping Hamiltonian of the real and imaginary part of $\langle a_1^\dagger a_2\rangle$ and $\langle a_1 a_2\rangle$ of the translational invariant state specified in the code. The expectation values evolve as predicted by equations (3.118).

3.5 Transverse Field Ising Model

The Hamiltonian of the Transverse Field Ising model (TFI) has the form

$$\hat{H} = -\sum_{n=1}^{N-1} \sigma_n^x \sigma_{n+1}^x - g_I \sigma_N^x \sigma_1^x - \cot(\theta) \sum_{n=1}^{N} \sigma_n^z, \tag{3.119}$$

where N is the number of sites, σ_i^α with $\alpha = x, y, z$ are the Pauli matrices at the i-th site and $\cot(\theta)$ is the magnetic field, with $0 < \theta < \frac{\pi}{2}$.

The parameter g_I encodes the boundary conditions of the Ising model: here we consider $g_I = -1, 0, +1$, corresponding, respectively, to anti-periodic, open and periodic boundary conditions.

The model is called *transverse* field Ising model because the field interacts with the spins with σ_i^z, while the spins interact between each others with $\sigma_i^x \sigma_{i+1}^x$.

The TFI Hamiltonian can be exactly diagonalised using a Jordan-Wigner transformation (see appendix A.1.6) mapping spin operators to spinless fermions [68, 132, 145–150].

In term of fermions the Hamiltonian has the form

$$\hat{H} = -\sum_{n=1}^{N-1} (a_n^\dagger - a_n)(a_{n+1} + a_{n+1}^\dagger) + g_I P (a_N^\dagger - a_N)(a_1 + a_1^\dagger) - \cot(\theta) \sum_{n=1}^{N} (a_n^\dagger a_n - a_n a_n^\dagger), \tag{3.120}$$

where $P = \prod_{n=1}^{N} (1 - 2 a_n^\dagger a_n)$ is the parity operator introduced in 3.1.2.

We notice that becuase of the presence of the parity operator P, the TFI Hamiltonian cannot be directly mapped to a f.q.h.. Nonetheless, since the Hamiltonian $\hat{H}$ commutes with the parity operator P we can diagonalise $\hat{H}$ and $\hat{P}$ simultaneously. On the diagonal basis of P we have that $\hat{H}$ has the block diagonal form $\hat{H} = \hat{H}_e \oplus \hat{H}_o$, where $\hat{H}_e$, called even sector Hamiltonian, corresponds to the eigenvalue $+1$ of P and $\hat{H}_o$, the odd sector Hamiltonian, corresponds to the eigenvalue -1 of P. We can then proceed to diagonalise the Hamiltonian on the two sectors independently (see section 2.2.1 and figure 2.1).

The Hamiltonians of the two sectors are:

$$\hat{H}_{o}^{e} = -\sum_{n=1}^{N-1}(a_n^\dagger - a_n)(a_{n+1} + a_{n+1}^\dagger) \pm g_I(a_N^\dagger - a_N)(a_1 + a_1^\dagger) - \cot(\theta)\sum_{n=1}^{N}(a_n^\dagger a_n - a_n a_n^\dagger). \tag{3.121}$$

Finally, we see that on each parity sector the TFI Hamiltonian is mapped to a f.q.h.. A bit of confusion can raise from considering the boundary conditions. The boundary conditions of the TFI Hamiltonian do not correspond to the boundary conditions of the Fermionic Hamiltonian. In fact, let us consider the three f.q.h.

$$\hat{H}(g_F) = -\sum_{n=1}^{N-1}(a_n^\dagger - a_n)(a_{n+1} + a_{n+1}^\dagger) - g_F(a_N^\dagger - a_N)(a_1 + a_1^\dagger) - \cot(\theta)\sum_{n=1}^{N}(a_n^\dagger a_n - a_n a_n^\dagger), \tag{3.122}$$

where the boundary conditions are encoded by the parameter $g_F = -1, 0. + 1$ and corresponds respectively to antiperiodic, open and periodic boundary conditions of the Fermionic Hamiltonian. The correspondences between spin model and Fermionic model are collected in table 3.1. Written in compact form (3.17), Hamiltonian (3.122), is specified by the matrices

$$A = -\tfrac{1}{2}\begin{pmatrix} 2\cot(\theta) & 1 & 0 & \dots & 0 & g_F \\ 1 & 2\cot(\theta) & 1 & 0 & \dots & 0 \\ 0 & 1 & 2\cot(\theta) & 1 & 0 & \dots \\ \vdots & \vdots & \ddots & \ddots & \ddots & \vdots \\ g_F & 0 & 0 & \dots & 1 & 2\cot(\theta) \end{pmatrix} \tag{3.123}$$

and

$$B = -\tfrac{1}{2}\begin{pmatrix} 0 & -1 & 0 & \dots & 0 & g_F \\ 1 & 0 & -1 & 0 & \dots & 0 \\ 0 & 1 & 0 & -1 & 0 & \dots \\ \vdots & \vdots & \ddots & \ddots & \ddots & \vdots \\ -g_F & 0 & 0 & \dots & 1 & 0 \end{pmatrix}. \tag{3.124}$$

We already know how to numerically diagonalise this Hamiltonian. We will present here the standard method for analytical diagonalisation, introducing the Bogoliubov

$g_I = 1$ (TFI periodic)	Even sector	$g_F = -1$, (f.q.h. antiperiodic)
	Odd Sector	$g_F = +1$, (f.q.h periodic)
$g_I = 0$ (TFI open)	Even/Odd sector	$g_F = 0$, (f.q.h. open)
$g_I = -1$ (TFI antiperiodic)	Even sector	$g_F = +1$, (f.q.h. periodic)
	Odd Sector	$g_F = -1$, (f.q.h antiperiodic)

Table 3.1: Corrspondences between spin models and Fermionic models

transformations, and we will compare the results with the numerical diagonalisation.

3.5.1 Analytical diagonalisation of the TFI Hamiltonian

In this subsection we will see how to diagonalise the three Hamiltonians (3.122) analytically. For a complete and detailed treatment we refer to [132, 148] or the more recent review [150].

Antiperiodic and periodic boundary condition Fermionic Hamiltonian Let us first consider the case of antiperiodic and periodic boundary conditions, $g_F = -1, +1$ (APBC and PBC respectively). Both cases can be brought to the form:

$$\begin{aligned}\hat{H} =& -2\sum_{k>0}\left[(\cot(\theta)+\cos(\frac{2\pi}{N}k))(f_k^\dagger f_k - f_k f_k^\dagger) + i\sin(\frac{2\pi}{N}k)(f_k^\dagger f_{-k}^\dagger - f_{-k}f_k)\right] + \\ &-(1+\cot(\theta))(f_0^\dagger f_0 - f_0 f_0^\dagger) - (\cot(\theta)-1)(f^\dagger_{-\frac{N}{2}} f_{-\frac{N}{2}} - f_{-\frac{N}{2}} f^\dagger_{-\frac{N}{2}}),\end{aligned} \tag{3.125}$$

where

$$f_k = \frac{1}{\sqrt{N}}\sum_{j=1}^{N} e^{i\frac{2\pi}{N}kj}a_j, \qquad f_k^\dagger = \frac{1}{\sqrt{N}}\sum_{j=1}^{N} e^{-i\frac{2\pi}{N}kj}a_j^\dagger, \tag{3.126}$$

with inverse transformations

$$a_j = \frac{1}{\sqrt{N}}\sum_{k} e^{-i\frac{2\pi}{N}kj}f_k, \qquad a_j^\dagger = \frac{1}{\sqrt{N}}\sum_{k} e^{i\frac{2\pi}{N}kj}f_k^\dagger. \tag{3.127}$$

and

$$k = \frac{-N+1}{2}, \frac{-N+1}{2}+1, \ldots, \frac{N-1}{2} \qquad \text{for } g_F = -1 \text{ and } N \text{ even or } g_F = 1 \text{ and } N \text{ odd}$$
$$k = \frac{-N}{2}, \frac{-N}{2}+1, \ldots, \frac{N}{2}-1 \quad \text{for } g_F = +1 \text{ and } N \text{ even or } g_F = -1 \text{ and } N \text{ odd}. \tag{3.128}$$

Terms with $f_0^\dagger, f_0$ and $f_{-\frac{N}{2}}, f^\dagger_{-\frac{N}{2}}$ in (3.125) are present just when $k = 0$ and $k = -\frac{N}{2}$ are allowed.

The different quantisations of the k in the two cases are justified in [132] and can be understood by intuition noting that with the first quantisation one would have $a_{N+1} = -a_1$, while with the second $a_{N+1} = a_1$. We can write the Hamiltonian in the compact form

$$\hat{H} = \sum_{k>0} \begin{pmatrix} f_k^\dagger & f_{-k} \end{pmatrix} h_k \begin{pmatrix} f_k \\ f_{-k}^\dagger \end{pmatrix} - (1 + \cot(\theta)(f_0^\dagger f_0 - f_0 f_0^\dagger), \tag{3.129}$$

with

$$h_k = \begin{pmatrix} -2(\cot(\theta) + \cos(\frac{2\pi}{N}k)) & 2i\sin(\frac{2\pi}{N}k) \\ -2i\sin(\frac{2\pi}{N}k) & 2(\cot(\theta) + \cos(\frac{2\pi}{N}k)) \end{pmatrix}. \tag{3.130}$$

This divides the modes space in sectors that couple each k with $-k$. For each of these sectors we have the unitary transformation

$$U_k = \begin{pmatrix} s_k & -it_k \\ -it_k & s_k \end{pmatrix}, \tag{3.131}$$

such that it diagonalises h_k as

$$U_k^\dagger h_k U_k = \begin{pmatrix} \epsilon_k & 0 \\ 0 & -\epsilon_k \end{pmatrix}, \tag{3.132}$$

with eigenvalues

$$\epsilon_k = 2\sqrt{1 + \cot(\theta)^2 + 2\cot(\theta)\cos(\frac{2\pi}{N}k)}. \tag{3.133}$$

The elements of U_k are defined as

$$s_k = \frac{\sin(\frac{2\pi}{N}k)}{\sqrt{\epsilon_k(\epsilon_k/2 + \cot(\theta) + \cos(\frac{2\pi}{N}k))}}, \tag{3.134}$$

$$t_k = \frac{\epsilon_k/2 + \cot(\theta) + cos(\frac{2\pi}{N}k)}{\sqrt{\epsilon_k(\epsilon_k/2 + \cot(\theta) + cos(\frac{2\pi}{N}k))}}. \tag{3.135}$$

This defines the Fermionic transformation of all the Fourier modes that read as

$$f_k = s_k b_k - i t_k b^\dagger_{-k}, \tag{3.136}$$

$$f^\dagger_{-k} = s_k b^\dagger_{-k} - i t_k b_k. \tag{3.137}$$

This transformation is called Bogoliubov-Valatin transformation [151, 152], and sometimes s_k and t_k are expressed respectively as $\cos(\phi_k)$ and $\sin(\phi_k)$, with ϕ_k called Bogoliubov angle. One has that for PBC and APBC each f.q.h. of the form (3.125) is characterised by the choice of the quantisation of k and a particular Bogoliubov angle. We finally obtain the diagonal form of the Hamiltonian

$$\hat{H} = \sum_{k\neq -\frac{N}{2},0} \frac{\epsilon_k}{2}(b^\dagger_k b_k - b_k b^\dagger_k) - (1-\cot(\theta))(f^\dagger_0 f_0 - f_0 f^\dagger_0) - (\cot(\theta)-1)(f^\dagger_{-\frac{N}{2}} f_{-\frac{N}{2}} - f_{-\frac{N}{2}} f^\dagger_{-\frac{N}{2}}). \tag{3.138}$$

Open boundary condition Fermionic Hamiltonian For the open boundary conditions (OBC) form of Hamiltonian (3.122) there is not a clear meaning for the term a_{N+1}, thus we will not apply any Fourier transform. We will not show here the procedure for the diagonalisation, we refer to [132, 148] or the more recent [153] for it. We have that the energies ϵ_k of the Hamiltonian in diagonal form will be

$$\epsilon_k = \sqrt{1 + \cot(\theta)^2 + 2\cot(\theta)\cos(\phi_k)} \tag{3.139}$$

with $\{\phi_k\}_{k=1}^N$ the roots of equation

$$\frac{\sin((N+1)\phi)}{\sin(N\phi)} = -\frac{1}{\cot(\theta)}, \tag{3.140}$$

in the interval $0 \leq \phi_k \leq \pi$.

3.5.2 Ground state

In the case of OBC the ground state is easily found using the function `GS_gamma()` with the Hamiltonian (3.122) imposing $g_F = 0$.

For computing the ground state in the case of APBC or PBC we need to know if the ground state is even or odd or if it is a superposition of states with different parities. It is known that, at finite dimension, with N even, for the antiperiodic Ising model the ground state is in the odd sector, while for the periodic Ising model the ground state is in the even sector. When N is odd, for the antiperiodic Ising model the ground state is in the even sector and for the periodic Ising model the ground state is in the odd sector [149].

In the thermodynamic limits, the energy difference between the two sectors goes to zero, the ground state becomes degenerate. Here we present a program for finding the correct sector of the ground state and for verifying that as N grows the energy difference between the ground state of the two sectors goes to zero. The program generates the output figure 3.8.

Analitical and Numerical energies

```
using F_utilities;
using PyPlot;
using LinearAlgebra;

const Fu = F_utilities;

N   = 10;
theta   = pi/8;

H_APBC          = Fu.TFI_Hamiltonian(N, theta; PBC=-1);
HD_APBC, U_APBC = Fu.Diag_h(H_APBC);
```

```
NE_APBC          = diag(HD_APBC);

H_PBC            = Fu.TFI_Hamiltonian(N, theta; PBC=+1);
HD_PBC, U_PBC    = Fu.Diag_h(H_PBC);
NE_PBC           = diag(HD_PBC);

H_OBC            = Fu.TFI_Hamiltonian(N, theta; PBC=0);
HD_OBC, U_OBC    = Fu.Diag_h(H_OBC,2);
NE_OBC           = diag(HD_OBC);

AE_APBC = zeros(Float64, 2*N);
AE_PBC  = similar(AE_APBC);
AE_OBC  = similar(AE_APBC);

#The solutions of equation sin((N+1)*phi)/sin(N*phi)=-1/cot(theta)
phi = [0.293377974249272,0.586547314382234,
        0.879273168816649,1.17126278605144,
        1.46212217642804,1.75129510871389,
        2.03798675412035,2.32111594487769,
        2.59947341172037,2.87247738375037]
for n=1:N
    AE_APBC[n]  = sqrt(1+cot(theta)^2+2*cot(theta)*cos(2*pi*((1-N)
       ↪ /2+n-1)/N));
    AE_PBC[n]   = sqrt(1+cot(theta)^2+2*cot(theta)*cos(2*pi*((-N)
       ↪ /2+n-1)/N));
    AE_OBC[n]   = sqrt(1+cot(theta)^2+2*cot(theta)*cos(phi[n]));
end

AE_APBC[(N+1):(2*N)]    = -AE_APBC[1:N];
AE_PBC[(N+1):(2*N)]     = -AE_PBC[1:N];
```

```
AE_OBC[(N+1):(2*N)]     = -AE_OBC[1:N];



fig = plt.figure("Comparison Analitical and Numerical Results",
    ↪ figsize=(10, 6), dpi=80)
plt.subplots_adjust(wspace=0, hspace=0)
ax1 = plt.subplot2grid((21,10), (0,0), colspan=10, rowspan=7);
ax1.set_title("Comparison Analitical and Numerical")
ax1.plot(sort(AE_APBC)[11:20], color="black",  marker="o",
        markersize=10, mfc="none" ,   label="Analytical APBC");
ax1.plot(sort(NE_APBC)[11:20], color="red", marker="+",
        markersize=10,  linestyle="None", label="Numerical APBC");
ax1.xaxis.set_ticklabels([])
yticks([1.5,2,2.5,3],[L"$1.5$",L"$2$",L"$2.5$",L"$3$"],fontsize=15)
ax1.set_ylabel(L"$\epsilon_k$",fontsize=18)
legend();
ax2 = plt.subplot2grid((21,10), (7,0), colspan=10, rowspan=7);
ax2.plot(sort(NE_PBC)[11:20],  color="purple",  marker="o",
        markersize=10, mfc="none" , label="Analytical PBC" );
ax2.plot(sort(AE_PBC)[11:20], color="green", marker="+",
        markersize=10,  linestyle="None", label="Numerical PBC");
ax2.xaxis.set_ticklabels([])
yticks([1.5,2,2.5,3],[L"$1.5$",L"$2$",L"$2.5$",L"$3$"],fontsize=15)
ax2.set_ylabel(L"$\epsilon_k$",fontsize=18)
legend();
ax3 = plt.subplot2grid((21,10), (14,0), colspan=10, rowspan=7);
ax3.plot(sort(NE_OBC)[11:20],   color="blue",  marker="o",
        markersize=10, mfc="none" , label="Analytical OBC" );
ax3.plot(sort(AE_OBC)[11:20],  color="orange", marker="+",
        markersize=10,  linestyle="None", label="Numerical OBC");
```

```
ax3.set_ylabel(L"$\epsilon_k$",fontsize=18)
ax3.set_xlabel(L"$k$",fontsize=18)
xticks([0,1,2,3,4,5,6,7,8,9],[L"$1$",L"$2$",L"$3$",L"$4$",L"$5$",L"
    ↪ $6$",L"$7$",L"$8$",L"$9$",L"$10$"],fontsize=15)
yticks([1.5,2,2.5,3],[L"$1.5$",L"$2$",L"$2.5$",L"$3$"],fontsize=15)
legend();
tight_layout();


GS_APBC     = Fu.GS_gamma(HD_APBC,U_APBC);
GS_PBC      = Fu.GS_gamma(HD_PBC,U_PBC);
E_GS_APBC   = Fu.Energy(GS_APBC,(HD_APBC,U_APBC));
E_GS_PBC    = Fu.Energy(GS_PBC,(HD_PBC,U_PBC));


println("Ground State Energies");
println("G_F=-1 :       ", E_GS_APBC);
println("G_F=+1 :       ", E_GS_PBC);
```

Output:

```
Ground State Energies
G_F=-1 :  -25.18934650837823
G_F=+1 :  -25.189223629491178
```

We have $N = 10$ so the ground state is expected to be in the GF=-1 sector. The computed energies confirm this.

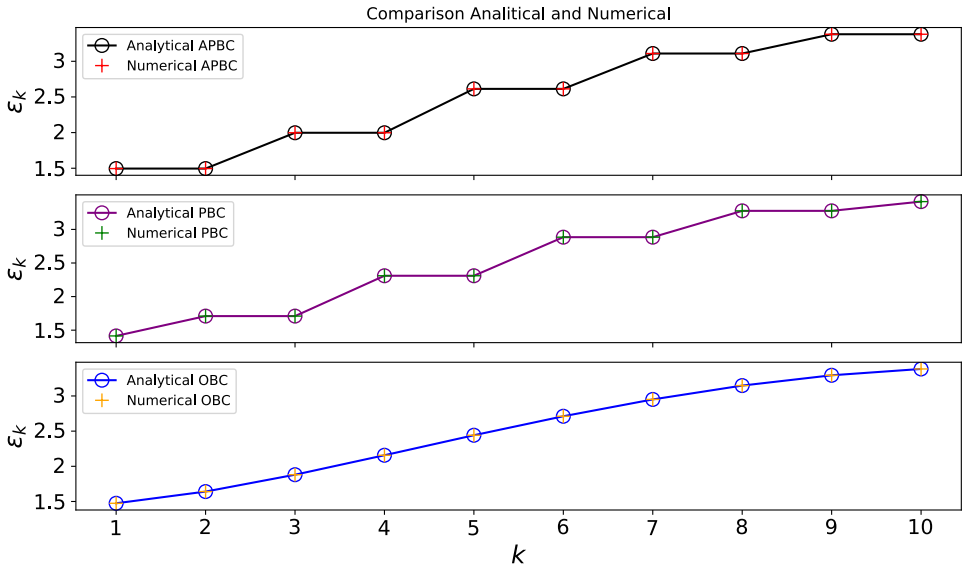

Figure 3.8: Output of the code 3.5.2. The three plots represent the analytical and numerical values of the free mode energies ϵ_k of the Hamiltonian (3.122) computed with antiperiodic, periodic and free boundary conditions. We see that the energies computed with `F_utilities` correspond to the one computed analytically.

Degenerancy of the ground state In the following program we check that the ground state energies of the TFI hamiltonians (3.122) with $g_F = \pm 1$ converge to the same value as the dimension of the system grows. The program generates the output figure 3.9.

```
using F_utilities;
using PyPlot;

const Fu = F_utilities;

theta   = pi/8;
Delta_E = zeros(Float64, 47)

for N=4:50
        H_APBC          = Fu.TFI_Hamiltonian(N, theta; PBC=-1);
```

```
        HD_APBC, U_APBC = Fu.Diag_h(H_APBC);
        H_PBC           = Fu.TFI_Hamiltonian(N, theta; PBC=+1);
        HD_PBC, U_PBC   = Fu.Diag_h(H_PBC);

        E_GS_APBC   = Fu.Energy(Fu.GS_gamma(HD_APBC,U_APBC),(
            ↪ HD_APBC,U_APBC));
        E_GS_PBC    = Fu.Energy(Fu.GS_gamma(HD_PBC,U_PBC),(HD_PBC,
            ↪ U_PBC));

        global Delta_E[N-3]= abs(E_GS_APBC-E_GS_PBC);
end

figure("|E_GS(GF=+1)-E_GS(GF=-1)|")
plot(4:50, log10.(abs.(Delta_E)));
xlabel(L"$N$");
ylabel(L"$\log|E_{GS}(g_F=+1,N)-E_{GS}(g_F=-1,N)|$");
tight_layout();
```

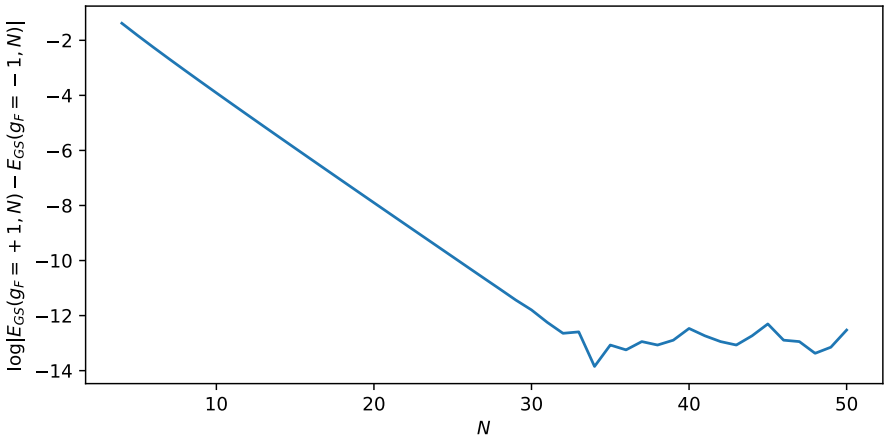

Figure 3.9: The ground states of Hamiltonians (3.122) for $g_F = \pm 1$ converge exponentially to the same value. The ground state of the antiperiodic and of the periodic transverse field Ising model is degenerate in the thermodynamic limit.

3.5.3 Time Evolution

As in the case of the Hopping model, even for the Hamiltonian (3.122) it is possible to explicitly compute the time evolution of the correlation matrix elements. We focus here on the case of $g_F = -1$ and N even in order to simplify the analitical form. The principal difference with the Hopping model is that, in the case of the Fermionic TFI, the transformation that diagonalises the Hamiltonian is not a simple Fourier transform, but it is a composition of a Fourier transform and a Bogoliubov transformation. We exemplify how to obtain an analitical form for the time evolution of the term $\langle a_1^\dagger a_1 \rangle$ of a translational invariant correlation matrix. As a first step, exploiting the translational invariance of the state and moving to the Fourier modes, we write

$$\begin{aligned}\langle a_1^\dagger a_1 \rangle = \frac{1}{N}\sum_{n=1}^{N}\langle a_n^\dagger a_n \rangle = \frac{1}{N^2}\sum_{n=1}^{N}\sum_{k=\frac{-N+1}{2}}^{\frac{N+1}{2}}\sum_{k'=\frac{-N+1}{2}}^{\frac{N+1}{2}} e^{-i\frac{2\pi}{N}n(k-k')}\langle f_k^\dagger f_{k'}\rangle = \\ = \frac{1}{N}\sum_{k=\frac{-N+1}{2}}^{\frac{N+1}{2}}\langle f_k^\dagger f_k\rangle. \end{aligned} \tag{3.141}$$

We then move to the Bogoliubov modes with the transformation (3.136) obtaining

$$\langle a_1^\dagger a_1 \rangle = \frac{1}{N}\sum_{k=\frac{-N+1}{2}}^{\frac{N+1}{2}}\left[s_k^2\langle b_k^\dagger b_k\rangle + t_k^2\langle b_{-k}b_{-k}^\dagger\rangle + i s_k t_k(\langle b_{-k}b_k\rangle - \langle b_k^\dagger b_{-k}^\dagger\rangle)\right]. \tag{3.142}$$

In this basis the Hamiltonian is diagonal, thus the time evolution easily computed as

$$\langle a_1^\dagger a_1 \rangle(t) = \frac{1}{N}\sum_{k=\frac{-N+1}{2}}^{\frac{N+1}{2}}\left[s_k^2\langle b_k^\dagger b_k\rangle + t_k^2\langle b_{-k}b_{-k}^\dagger\rangle + i s_k t_k(e^{i2\epsilon_k t}\langle b_{-k}b_k\rangle - e^{-i2\epsilon_k t}\langle b_k^\dagger b_{-k}^\dagger\rangle)\right]. \tag{3.143}$$

To obtain the expression of $\langle a_1^\dagger a_1 \rangle(t)$ in terms of correlators of the operators $a^\dagger, a$ we just have to map the $b^\dagger, b$ to $a^\dagger, a$.

3.6 Benchmarking with Fermionic Gaussian states

Fermionic Gaussian states can be used as a tool for benchmarking algorithms. We will see how tools developed for general quantum states can be translated to the language of correlation matrices. To understand the idea behind the benchmarking, let us take an explicit example. In the next subsection we are going to see the imaginary time evolution of Fermionic Gaussian states. One usually uses the imaginary time evolution of a state for computing the ground state of an Hamiltonian. Of course, in the case of f.g.s., computing the ground state is not the main purpose, as we know already how to compute it for any f.q.h.. Knowing already the exact results allows us to compare the algorithm for the imaginary time evolution with the exact results and get good insight in what we should expect in a context where the exact result is not known.
If we have an algorithm acting on some generic quantum state, we can try to translate it in the formalism of f.g.s. and benchmark it to the exact results.
In this subsection we present the translation of some well known algorithm in the language of correlation matrices. The purpose of this subsection is not to benchmark these algorithm, but instead, to translate some important existing algorithms. This will provide us the translations of the possible building blocks of any novel and more complex experimental algorithm.

3.6.1 Imaginary-time evolution

In order to find the ground state of a non-degenerate Hamiltonian H one can use the following equality

$$|GS\rangle = \lim_{\tau\to\infty} \frac{e^{-H\tau}|\psi\rangle}{||e^{-H\tau}|\psi\rangle||} \tag{3.144}$$

starting from a generic state $|\psi\rangle$ with $\langle GS|\psi\rangle \neq 0$.
To see this, let us consider the orthononormal basis $\{|E_i\rangle\}_i$ generated by the collection of the eigenvectors of H, with eigenvalues $\{E_i\}_i$ such that $0 \leq E_0 \lneq E_1 \leq E_2 \leq$, where $\mathcal{H}$ is the Hilbert space on which H act.
Expanding $|\psi\rangle$ on this basis one obtains $|\psi\rangle = \sum_i c_i|E_i\rangle$, with $c_0 \neq 0$ from the fact that

$\langle GS|\psi\rangle \neq 0$. One can thus see that eq (3.144) is just a projection to the ground state:

$$\lim_{\tau\to\infty}\frac{e^{-H\tau}|\psi\rangle}{||e^{-H\tau}|\psi\rangle||} = \lim_{\tau\to\infty}\sum_i \frac{e^{-E_i\tau}c_i}{\sqrt{\sum_i e^{-2E_i\tau}|c_i|^2}}|E_i\rangle = \tag{3.145}$$

$$= \lim_{\tau\to\infty}\sum_i \frac{e^{-\frac{E_i}{E_0}\tau}c_i}{\sqrt{\sum_i e^{-2\frac{E_i}{E_0}\tau}|c_i|^2}}|E_i\rangle = |E_0\rangle, \tag{3.146}$$

and thus that $\lim_{\tau\to\infty}\frac{e^{-H\tau}}{||e^{-H\tau}||}$ is the projector on the ground state:

$$\lim_{\tau\to\infty}\frac{e^{-H\tau}}{||e^{-H\tau}||} = \lim_{t\to\infty}\frac{\sum_i e^{-E_i\tau}|E_i\rangle\langle E_i|}{\sqrt{\sum_i e^{-2E_i\tau}}} = \tag{3.147}$$

$$= \lim_{\tau\to\infty}\frac{\sum_i e^{-\frac{E_i}{E_0}\tau}|E_i\rangle\langle E_i|}{\sqrt{\sum_i e^{-2\frac{E_i}{E_0}\tau}}} = |E_0\rangle\langle E_0|. \tag{3.148}$$

The imaginary-time evolution is directly related to the power method presented in section 2.2.2. The eigenvenvector associated to the smallest eigenvalue E_0 of H is the eigenvector associated to the biggest eigenvalue of e^{-H} and this can be approximately obtained using the power method by computing $(e^{-H})^N|\psi\rangle$, a procedure that in the limit of $N\to\infty$ is analogous to equation (3.144).

Applying the same method to the density matrix one can obtain the ground state ρ_{GS} of a non degenerate Hamiltonian H from a general density matrix ρ such that $Tr[\rho\rho_{GS}] \neq 0$ as

$$\rho_{GS} = \lim_{\tau\to\infty}\frac{e^{-H\tau}\rho e^{-H\tau}}{Tr\left[\rho e^{-2H\tau}\right]}. \tag{3.149}$$

We refer to the method for obtaining the ground state using (3.144) as performing an *imaginary time evolution*.

This is the case because, if for the time evolution operator $U(t) = e^{-iHt}$ for the Hamiltonian H, we select $t = -i\tau$ we obtain the operator $e^{-H\tau}$ that is the one of eq (3.144). One can thus write in a non-formal way $|GS\rangle = \lim_{t\to -i\infty}\frac{|\psi(t)\rangle}{||\psi(t)\rangle||}$.

It is important to keep in mind that the operator $e^{-H\tau}$ is not unitary and for this reason it does not preserve the norm of the state and one has to renormalise it.

3.6.2 Numerical Imaginary time evolution

In the numerical approach to imaginary time evolution one faces some difficulties.
Almost in all cases one is forced to evolve the state step by step renormalising every time, performing a discrete imaginary time evolution.
This procedure does not allow to reach infinite time in a finite amount of time steps, thus one has to find a criterion to stop the evolution when the convergence is accurate up to some confidence parameter. To check if the reached state is the expected state is tricky and theoretically impossible in most of the cases since one does not always have the exact value of the energy of the ground state.
A method for checking the convergence is to check the energy difference between two steps of the discrete imaginary time evolution. Once the difference in energy between two steps is lower than an acceptable value ϵ, one decides that the algorithm converged.
It is not always the case though. It is also possible that the approximate imaginary time evolution stops at some plateaux and thus it tricks the algorithm in believing in a false convergence to the ground state.

Imaginary time evolution of the correlation matrix The imaginary time evolution of the correlation matrix is defined as

$$\Gamma_{i,j}(\tau) = Tr\left[\rho(\tau)\vec{\alpha}_i\vec{\alpha}_j^\dagger\right] = \tag{3.150}$$

$$= \frac{Tr\left[e^{-\hat{H}\tau}\rho e^{-\hat{H}\tau}\vec{\alpha}_i\vec{\alpha}_j^\dagger\right]}{Tr\left[e^{-\hat{H}\tau}\rho e^{-\hat{H}\tau}\right]}. \tag{3.151}$$

Obtaining an explicit form for $\Gamma(\tau)$ just in term of H and $\Gamma(0)$ is not easy. Following the reasoning made for the real time evolution, one can compute the imaginary time evolution in Heisenberg picture with $e^{-\hat{H}\tau}$ of the operator $\vec{\alpha}_i\vec{\alpha}_j^\dagger$. Using the Baker-Campbell-Hausdorff formula (i.e. $e^A B e^A = \sum_{n=0}^{\infty}\frac{1}{n!}\underbrace{\{A,...\{A}_{n},B\underbrace{\}...\}}_{n}$ i.e. *B.C.H.2* in Appendix A.2.4) and moving in the diagonal basis with Dirac operators $\vec{\beta}$ one can write

the Hamiltonian as $\hat{H} = \sum_k \epsilon(k) \left(b_k^\dagger b_k - b_k b_k^\dagger \right)$.

Thus one has

$$e^{-\hat{H}\tau} \vec{\beta}_l \vec{\beta}_j^\dagger e^{-\hat{H}\tau} = \sum_{n=0}^{\infty} \frac{-\tau^n}{n!} \underbrace{\{\hat{H}, ...\{\hat{H}}_{n}, \vec{\beta}_l \vec{\beta}_j^\dagger \underbrace{\}...\}}_{n}. \tag{3.152}$$

Since $b_l^\dagger b_j \hat{H} = (\hat{H} + 2\Delta_{l,j}) b_l^\dagger b_j$, we cannot simplify this expression as in the case of real time evolution.

To obtain a numerical algorithm for the imaginary time evolution one has to realise that, for each value of τ, $\Gamma(\tau)$ is just the correlation matrix of the f.g.s.

$$\rho(\tau) = \frac{e^{-\hat{H}\tau} \rho e^{-\hat{H}\tau}}{\mathrm{Tr}\left[e^{-\hat{H}\tau} \rho e^{-\hat{H}\tau} \right]}, \tag{3.153}$$

and this can be seen as the state obtained by correctly normalising the matrix product of the density matrices of three states. The trick for obtaining the correlation matrix $\Gamma(\tau)$ is thus using the product rule (see subsection 3.3.9) of the initial f.g.s. ρ and the thermal state $\rho_{\beta=\tau} = \frac{e^{-H\tau}}{\mathrm{Tr}[e^{-\hat{H}\tau}]}$. This allows us to compute the imaginary time evolution of Fermionic Gaussian states.

F_utilities 3.6.1: Evolve_imag(Γ, H_D, U, τ)$\to \Gamma(\tau)$

This function returns the correlation matrix Γ evolved at imaginary time τ with H. Matrices H_D and U are the output of `Diag_h(H)`.

3.6.3 Fermionic Gaussian States with Fixed Bond Dimension

The compression of correlation matrices of f.g.s. in a similar fashion of matrix product states (MPS) has been introduced in [154].

Let us consider a pure Fermionic Gaussian state completely described by the $N \times N$ matrix $\Lambda_{i,j} = \langle a_i^\dagger a_j \rangle$. Since Λ is a pure state, its eigenvalues are either 1 (the mode is occupied) or 0 (the mode is unoccupied). This high degeneracy can be exploited mixing occupied (or unoccupied) eigenstate for finding a basis in which these modes are localised. In systems with a limited entanglement structure we expect to be able to

find a basis in which eigenstates are localised. This fact can be justified as follows. Let Λ be the ground state of a 1D local Hamiltonian. We consider the partition of the first ℓ sites of the system. The state of the partition is described by the $\ell \times \ell$ correlation matrix Λ_ℓ. In ground states of 1D local Hamiltonians, the entanglement of partitions of the systems of dimension ℓ grows at most as $\log(\ell)$. This means that for growing values of ℓ we expect to find eigenvalues of Λ_ℓ closer and closer to 1 or 0. Now suppose that diagonalising Λ_ℓ, the eigenvalue associated to the eigenvector $\vec{v}$ is ~ 1. This makes $\vec{v}$ also an approximate eingenvalue of Λ.

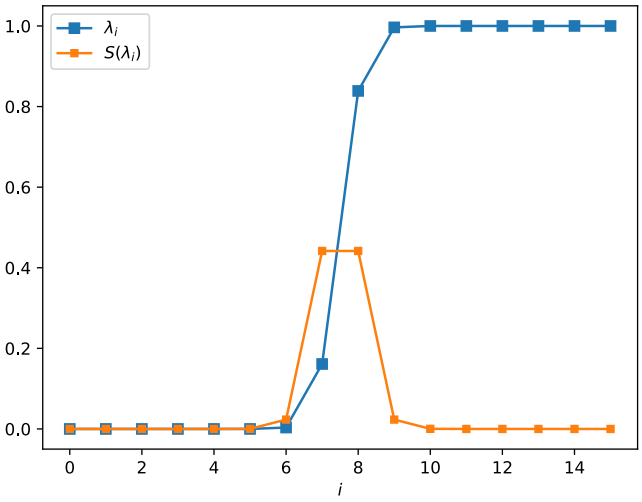

Figure 3.10: In blue the eigenvalues λ_i of the reduced state $\Lambda_{\ell=16}$ of the ground state of a hopping Hamiltonian with $N = 500$. In orange the von Neumann entropy $S(\lambda_i)$ of the mode associated to each eigenvalue λ_i. The total von Neumann entropy of the partition $\Lambda_{\ell=16}$ is given by the sum of the entropies of each mode (see (3.89)). Since the entropy of a partition Λ_ℓ is bounded by $\log(\ell)$, with growing ℓ the added modes must have associated eigenvalues close to 0 or 1.

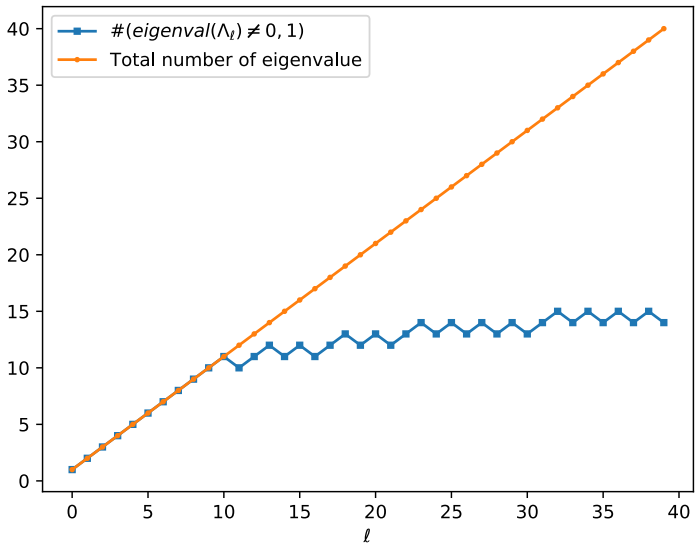

Figure 3.11: In blue the number of eigenvalues of Λ_ℓ that are 0 or 1 up to machine precision, in orange the total number of eigenvalues of Λ_ℓ in the ground state of a hopping Hamiltonian with $N = 500$. When the dimension of the partition is $\ell > 10$ the entanglement saturates and the number of eigenvalues equal to 1 or 0 starts growing linearly.

In [154], developing on this idea, the authors are able to construct a compression algorithm for correlation matrices and directly map it to the MPS representation of the state.

Here we will illustrate a method for obtaining the correlation matrix of a f.g.s. expressed as an MPS with fixed bond dimension D.

Let us consider a pure f.g.s. $|\psi\rangle$ on a system with N sites with associated $N \times N$ correlation matrix Λ. We denote with $|\psi^D\rangle$ the state obtained representing $|\psi\rangle$ with an MPS of fixed bond dimension D. We are interested in the correlation matrix Λ^D of the state $|\psi^D\rangle$.

For a bipartition having bond dimension D corresponds to having Schmidt rank D [66]. If a state $|\psi\rangle$ has bond dimension $D' > D$, we can approximate it at bond dimension D by setting to 0 the lower Schmidt coefficients and renormalising the state. With the formalism of correlation matrices we cannot directly manipulate the single Schmidt coefficients, but we can approximate low entangled modes with product modes.

Approximating an entangled mode with a product mode corresponds to setting half of the Schmidt coefficients to zero. With this insight we can devise the following algorithm for obtaining Λ^D.

We proceed as follows. We consider $\Lambda_{1,\dots,m+1}$, the correlation matrix of the partition of the first ℓ sites, where $m = \lceil \log_2(D) \rceil$. We will refer to m as the bond dimension of the correlation matrix.

We diagonalise it as $\Lambda_{1,\dots,m+1} = U_1 D^1_{1,\dots,m+1} U_1^\dagger$, the diagonal elements of $D_{1,\dots,\ell}$ are organised such that, the top left element λ_1^1 is the closest to 0 or 1. Suppose $\lambda_1^1 \sim 1$. We expand U_1 to be $N \times N$ adding ones on the diagonal and we have that the top left element of $\Lambda^1 = U_1^\dagger \Lambda U_1$ is λ_1^1. We set the first column and first row of Λ^1 to 0 and $(\Lambda^1)_{1,1}$ to 1 (because $\lambda_1^1 \sim 1$). We then proceed diagonalising $\Lambda^1_{2,\dots,m+2} = U_2 D^2_{2,\dots,m+2} U_d^\dagger$. Suppose this time the top left element of D^2 is $\lambda_1^2 \sim 0$. We set the second column and second row of $\Lambda^2 = U_2^\dagger \Lambda^1 U_2$ to 0 and $(\Lambda^2)_{2,2}$ to 0 (because $\lambda_1^2 \sim 0$). Iterating this procedure $N - \ell$ times we obtain a correlation matrix $\Lambda^{(N-m1)}$ with $N - m$ diagonal elements equal to 0 or 1. We proceed with the same procedure decreasing the dimension of the reduced system everytime until after N steps we obtain a diagonal matrix with diagonal elements equal to 0 or 1. Returning to the original basis applying all the transformation $\{U_i\}_{i=1,\dots,N}$ to Λ^N we obtain the correlation matrix associated to the state $|\psi^D\rangle$. We report a schematic representation of the algorithm in figures 3.12 and 3.13.

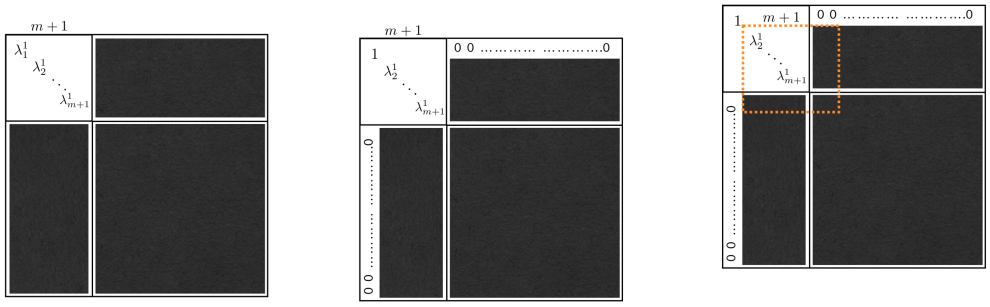

(a) Step 1: Diagonalise the subsystem $\Lambda^1_{1,\dots,m+1}$. The eigenvalues are ordered such that $\min(|1-\lambda^1_1|,|\lambda^1_1|) \leq \min(|1-\lambda^1_2|,|\lambda^1_2|) \leq \cdots \leq \min(|1-\lambda^1_{m+1}|,|\lambda^1_{m+1}|)$.

(b) Step 2: Since $\lambda^1_1 \sim 1$ ($\lambda^1_1 \sim 0$) we set it to 1 (0). We set to zero all the other elements of the first row and first column of Λ. This will be the an eigenvalue of Λ.

(c) Step 3: We move to the second subsystem $\Lambda^2_{2,\dots,m+2}$. We note that now the correalation matrix is represented in a mixed basis and the lower indices do not exactly represent the sites of the system.

Figure 3.12: Steps of the algorithm for reducing the bond dimension of a Fermionic Gaussian state. The big squares represent the correlation matrix Λ. We repeat this procedure $(N-m)$ times then we continue for m steps reducing by one the dimension of the reduced system at each step. At the end one obtain a diagonal matrix with diagonal elements equal to 1 or 0.

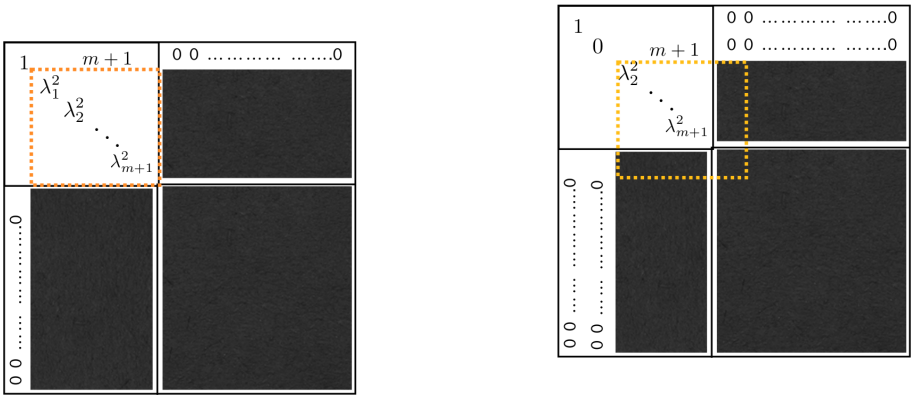

(a) Step 4: We diagonalise $\Lambda^2_{2,\ldots,\ell+1}$

(b) Step6: After resetting λ_1^2, we move to $\Lambda^3_{3,\ldots,m+3}$

.

Figure 3.13: Steps 4 and 6 of the algorithm for reducing the bond dimension of a Fermionic Gaussian state.

In figure 3.14 we plot the number of eigenvalues different from 0 and 1 for different partitions of the system for the ground state Γ of a hopping Hamiltonian of a system of $N = 100$ sites, and for Γ with bond dimension reduced to m.

We know that for ground states of $1D$ local Hamiltonians the amount of entanglement (measured by the von Neumann entropy S) of any region of an MPS of bound dimension D is bounded by $S \leq \log(D)$. In figure 3.15 we plot the value of the entropy of different regions of the ground state of a random Hamiltonian. The entropy is indeed bounded by $S \leq \log(D)$ with $D = 2^m$.

Combining this method with the imaginary time evolution algorithm one can construct the time evolving block decimation algorithms on the space of correlations matrices.

Together with the algorithm for reducing the bond dimension of one dimensional systems on the space of correlation matrices, in `F_utilities` we include the

algorithm for reducing the bond dimension of specific two dimensional systems. In particular we focussed on two dimensional systems where the Hamiltonian can be sectorised. This algorithm differs from the one for one dimensional systems in the way it handles the lowest Schmidt's coefficients of different sectors. Taking advantage of the sectorisation of the Hamiltonian, the algorithm becomes more complex, but at the same time more efficient.

3.6.4 Reduction of the bond dimension of a two dimensional system divided in sectors

We consider the Fermionic quadratic Hamiltonian

$$\hat{H} = \sum_x \sum_y \left[a^\dagger_{x,y} a_{x+1,y} + a^\dagger_{x+1,y} a_{x,y} + (-1)^x \left(a^\dagger_{x,y} a_{x,y+1} + a^\dagger_{x,y+1} a_{x,y} \right) \right], \tag{3.154}$$

defined on the on an $L \times L$ lattice on a cylinder with periodic boundary conditions along the x direction and open boundary conditions along the y direction as in figure 3.6.4. Because of the boundary conditions we have that L must be even.
Substituting the Fourier operators

$$a^\dagger_{x,y} = \frac{1}{\sqrt{L}} \sum_k e^{-i\frac{2\pi}{L}kx} c^\dagger_{k,y}, \tag{3.155}$$

where, because of the boundary conditions, we choose k as

$$k = -\frac{L}{2}, -\frac{L}{2}+1, \ldots, \frac{L}{2}-1, \tag{3.156}$$

the Hamiltonian becomes as

$$\begin{aligned} \hat{H} = \sum_{k<0} \Big[\sum_y 2\cos(\frac{2\pi}{L}k) \left(c^\dagger_{k,y} c_{k,y} - c^\dagger_{k+\frac{L}{2},y} c_{k+\frac{L}{2},y} \right) + \\ + c^\dagger_{k,y} c_{k+\frac{L}{2},y+1} + c^\dagger_{k+\frac{L}{2},y} c_{x,y+1} + c^\dagger_{k+\frac{L}{2},y+1} c_{k,y} + c^\dagger_{k,y+1} c_{k+\frac{L}{2},y} \Big]. \end{aligned} \tag{3.157}$$

In this form the Hamiltonian is divided in $\frac{L}{2}$ sectors, each one corresponding to the couples of values of $\{k, k+\frac{L}{2}\}$. This means that the eigenstates of this Hamiltonain

are product states of states defined on each $\{k, k+\frac{L}{2}\}$ sector. Thus, these eigenstates, instead of being described by a $2L^2 \times 2L^2$ correlation matrix, are instead described by just a collection of $\frac{L}{2}$ correlation matrices of dimension $2L \times 2L$, where each of these correlation matrices corresponds to a stripe of the cylinder in the (k, y) space.

We call states of this kind, sectorised states.

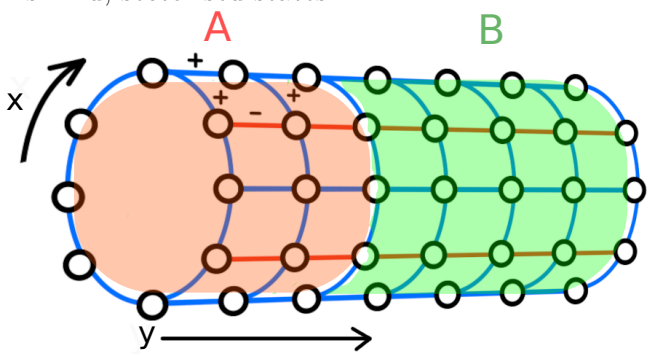

Figure 3.14: Lattice with periodic boundary conditions along the x direction. Red lines correspond to negative couplings, blue lines correspond to positive couplings. Two possible partitions A and B are higlighted in red and green respectively.

Performing the reduction of the bond dimension of a sectorised state, one can expolit the sectorisation property in order to reduce the computational cost of the operation. Consider for example the ground state of Hamiltonian (3.154). Once we move to the Fourier basis along the x direction this becomes a sectorised state. Mimicking the encoding of this quantum state with a tensor network corresponds to fixing its Schmidt rank relatively to some iterative partition scheme. We choose a partition scheme that increasingly cuts the cylinder perpendularly to y. Since the Fourier transformation we applied mixes only Dirac operator corresponding to the same value of y, this partition scheme is a geometric partition scheme (it is equivalent on the (x, y) space and the (k, y) space). Step l of the partition scheme divides the system in a partition A consisting of all the elements corresponding to $y = \{1, \ldots, l\}$ and a partition B corresponding to all the elements corresponding to $y \in \{l+1, \ldots, L\}$ analogously of the iterative partition scheme used for the one dimensional system of the last section.

Choosing this partition scheme allows us to exploit a parallel implementation of the algorithm for the reduction of the bond dimension of the state. In fact, instead of considering the full $2L^2 \times 2L^2$ correlation matrix describing the state we consider the

$\frac{L}{2}$ correlation matrices of dimension $2L \times 2L$. The first step of the algorithm consists in partitioning the system at step $m+1$ of the partition scheme. These corresponds to taking the first $2(m+1)$ elements of each correlation matrix. One then proceed diagonalising these subsystem. This step is analogous to step 1 of the one dimensional system presented in the last section, with the difference that now we are acting on $\frac{L}{2}$ correlation matrices simultaneously. This returns $L(m+1)$ eigenvalues from the $\frac{L}{2}$ sectors. Step 2 consists in considering all these $L(m+1)$ eingenvalues *together*, selecting the $2\frac{L}{2}$ closest to 0 or 1 and then approximating them with 0 or 1 respectively in the respective correlation matrix and setting them to product state with the rest of the system analogously to what was done in step 2 of the one dimensional case. Here the difference with the one dimensional case of the last section consists in the fact that we are setting to product state L modes, not just one, and that we are choosing them from all the correlation matrices. Step 3 consists in moving to the partition scheme $m+2$, enlarging the first partitions. Differently from the one dimensional case, here one has to keep track of the number of approximations performed in each sectors before diagonalising. As in the one dimensional case, the algorithm then proceed iteratively returning after at most L steps, the correlation matrix $\Gamma(m)$ of a state with reduced bond dimension with the respect to the partitions along the chosen spatial direction. Considering larger values of m, the correlation matrix $\Gamma(m)$ converges towards Γ, the exact correlation matrix.

F_utilities 3.6.2: RBD(Γ, m)$\to \Gamma(m)$

This function returns the correlation matrix $\Gamma(m)$ obtained reducing the bond dimension of Γ to m.

F_utilities 3.6.3: RBD_csectors($\vec{\Gamma}$, L_x, L_y, m)$\to \vec{\Gamma}(m)$

This function returns the correlation matrices $\vec{\Gamma}(m)$ obtained reducing the bond dimension to mL of the system on the $L_x \times L_y$ cylinder described by the correlation matrices $\vec{\Gamma}$. Each correlation matrix must cointains information of two values of k and must be organised following the order $\vec{\alpha} = (a_{k,1}, a_{k+\frac{L}{2},1}, a_{k,2}, a_{k+\frac{L}{2},2}, \dots)$

```
using F_utilities;
using PyPlot;
using LinearAlgebra;

const Fu    = F_utilities;
const LinA  = LinearAlgebra;



N           = 100;
H           = Fu.Build_hopping_hamiltonian(N);
HD, U       = Fu.Diag_h(H);
Gamma       = Fu.GS_gamma(HD,U);
Gamma_RBD   = Fu.RBD(Gamma,5)

prod_modes_border       = zeros(Int64, N);
prod_modes_RBD_border   = zeros(Int64, N);
prod_modes_bulk         = zeros(Int64, div(N,2));
prod_modes_RBD_bulk     = zeros(Int64, div(N,2));
for l=1:N
      DA,UA             = Fu.Diag_gamma(Fu.Reduce_gamma(Gamma,l,1))
          ↪ ;
      DA_RBD,UA_RBD     = Fu.Diag_gamma(Fu.Reduce_gamma(Gamma_RBD,l
          ↪ ,1));
      prod_modes_border[l]     = count(i->i!=0, round.(real.(LinA.
          ↪ diag(DA)[1:l]),digits=14));
      prod_modes_RBD_border[l] = count(i->i!=0, round.(real.(LinA.
          ↪ diag(DA_RBD)[1:l]),digits=14));
end
for l=1:div(N,2)
      DA,UA                   = Fu.Diag_gamma(Fu.Reduce_gamma(Gamma
```

```
        ↪ ,l, div(N,2)));
    DA_RBD,UA_RBD           = Fu.Diag_gamma(Fu.Reduce_gamma(
        ↪ Gamma_RBD,l, div(N,2)));
    prod_modes_bulk[l]      = count(i->i!=0, round.(real.(LinA.
        ↪ diag(DA)[1:l]),digits=14));
    prod_modes_RBD_bulk[l]  = count(i->i!=0, round.(real.(LinA.
        ↪ diag(DA_RBD)[1:l]),digits=14));
end
figure("prod_eigenvalues");
plot(1:N,prod_modes_border, marker="s", markersize=3, label=L"$\#(
    ↪ eigenval(\Gamma_{1,\dots,\ell}\neq 0,1)$");
plot(1:div(N,2),prod_modes_bulk, marker="s", markersize=3, label=L"
    ↪ $\#(eigenval(\Gamma_{\frac{N}{2},\dots,\frac{N}{2}+\ell})\
    ↪ neq 0,1)$");
plot(1:N,prod_modes_RBD_border, marker="s", markersize=3, label=L"$
    ↪ \#(eigenval(\Gamma(m=5)_{1,\dots,\ell}\neq 0,1)$");
plot(1:div(N,2),prod_modes_RBD_bulk, marker="s", markersize=3,
    ↪ label=L"$\#(eigenval(\Gamma(m=5)_{\frac{N}{2},\dots,\frac{N
    ↪ }{2}+\ell}\neq 0,1)$");
axvline(div(N,2), linestyle="--", linewidth=0.5, color="gray")
xlabel(L"$\ell$")
grid(axis="y", linestyle="--")
legend();
```

Output:

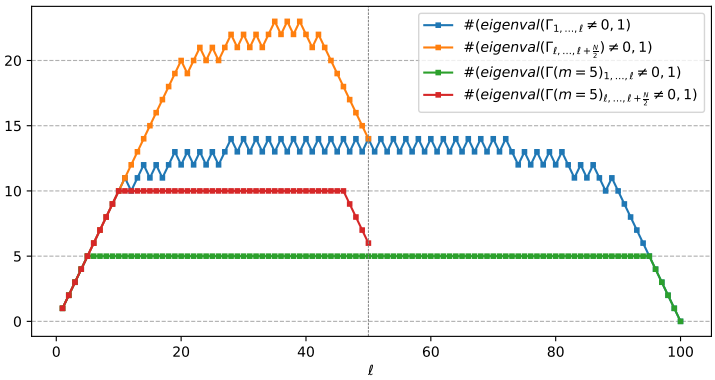

Figure 3.15: Eigenvalues different from 0 and 1 for different partitions of the system for the ground state Γ of a hopping Hamiltonian of a system of $N = 100$ sites, and for Γ with bond dimension reduced to m. The blue dots correspond to partitions of Γ with first site at the boundary of the system and with dimension ℓ. The orange dots correspond to partitions of Γ with first site at the boundary of the system and with dimension ℓ. The green dots are anologous to the blue dots, but computed for the state $\Gamma(m = 5)$ obtained reducing the bond dimension of Γ to $m = 5$. Red dots are anologous to the orange dots, but computed for $\Gamma(m = 5)$. As expected the number of eigenvalues different from 0 and 1 are bounded as $\#eigenval(\neq 0, 1) \leq 2m$.

```
using F_utilities;
using PyPlot;
using LinearAlgebra;

const Fu    = F_utilities;
const LinA  = LinearAlgebra;

function Random_hamiltonian(N)
  A   = rand(N,N)+im*rand(N,N);
  A   = (A+A')/2.;
  bd  = rand(N-1).+im*rand(N-1);
  B   = Tridiagonal(bd, zeros(Complex{Float64}, N), -bd);
  H   = zeros(Complex{Float64}, 2*N, 2*N);
  H[(1:N),(1:N)]          = -conj(A);
  H[(1:N).+N,(1:N)]       = -conj(B);
```

```
  H[(1:N),(1:N).+N]       = B;
  H[(1:N).+N,(1:N).+N]    = A;

  return H;
end

N           = 100;
H           = Random_hamiltonian(N);
HD, U       = Fu.Diag_h(H);
Gamma       = Fu.GS_gamma(HD,U);
Gamma_RBD   = Fu.RBD(Gamma,1)
S_modes_border       = zeros(Float64, N);
S_modes_RBD_border   = zeros(Float64, N);
S_modes_bulk         = zeros(Float64, div(N,2));
S_modes_RBD_bulk     = zeros(Float64, div(N,2));
for l=1:N
      S_modes_border[l]     = Fu.VN_entropy(Fu.Reduce_gamma(Gamma,l
          ↪ ,1));
      S_modes_RBD_border[l] = Fu.VN_entropy(Fu.Reduce_gamma(
          ↪ Gamma_RBD,l,1));
end
for l=1:div(N,2)
      S_modes_bulk[l]         = Fu.VN_entropy(Fu.Reduce_gamma(Gamma
          ↪ ,l, div(N,2)));
      S_modes_RBD_bulk[l]     = Fu.VN_entropy(Fu.Reduce_gamma(
          ↪ Gamma_RBD,l, div(N,2)));
end
figure("Entropies");
plot(1:N,log.(abs.(S_modes_border)), marker="s", markersize=3,
    ↪ label=L"$F=S(\Gamma_{1,\dots,\ell}\neq 0,1)$");
```

```
plot(1:div(N,2),log.(abs.(S_modes_bulk)), marker="s", markersize=3,
    ↪  label=L"$F=S(\Gamma_{\frac{N}{2},\dots,\ell+\frac{N}{2}})\
    ↪ neq 0,1)$");
plot(1:N,log.(abs.(S_modes_RBD_border)), marker="s", markersize=3,
    ↪ label=L"$F=S(\Gamma(m=1)_{1,\dots,\ell}\neq 0,1)$");
plot(1:div(N,2),log.(abs.(S_modes_RBD_bulk)), marker="s",
    ↪ markersize=3, label=L"$F=S(\Gamma(m=1)_{\frac{N}{2},\dots,\
    ↪ ell+\frac{N}{2}}\neq 0,1)$");
axvline(div(N,2), linestyle="--", linewidth=0.5, color="gray")
axhline(log(log(2)), linestyle="-.", color="red", label="F=log(D)")
axhline(log(2*log(2)), linestyle="-.", color="red", label="F=2*log(
    ↪ D)")
xlabel(L"$\ell$")
ylabel(L"$\log(F)$")
# grid(axis="y", linestyle="--")
legend();
```

Output:

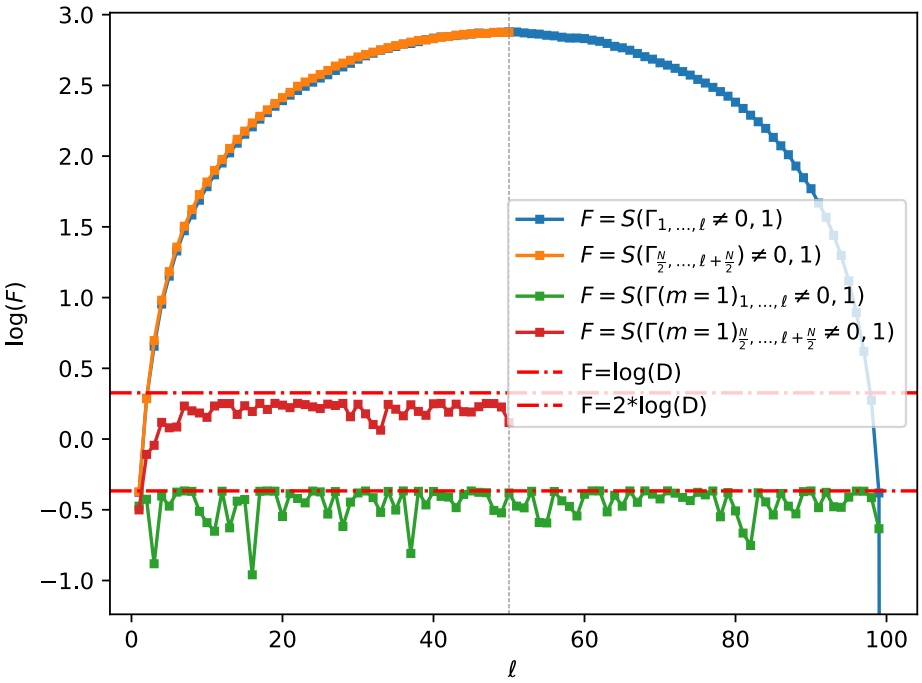

Figure 3.16: The entropy of different regions of the ground state of a random Hamiltonian. The blue dots correspond to partitions of dimension ℓ with first site at the boundary of the chain. The orange dots correspond to partitions of dimension ℓ with first site in the middle of the chain. The green dots are anologous to the blue dots but computed for the state $\Gamma(m = 1)$ obtained reducing the bond dimension of Γ to $m = 1$. Red dots are anologous to the orange dots, but computed for $\Gamma(m = 1)$. As expected since the Hamiltonian is random and long range, the entropy of the partitions almost always saturates. The red dash-dotted horizontal lines represent the upper bound for the entropy of a partition (starting at the border or not respectively for $\log(D)$ and $2\log(D)$). As we can see the entropy is always bounded by $S \leq \log(D)$ with $D = 2^m$ as expected.

Chapter 4

Equilibration in closed quantum systems

In chapter 2 we studied efficient methods for encoding a particular class of static quantum states. In this chapter we are going to study what happens when these states are free to evolve within an out-of-equilibrium dynamics. We will see that, generally, the resources needed for the description of the evolved states grow in time, posing difficult challenges in the simulation of the dynamics of many-body quantum systems.

This is not surprising, as even for classical systems, following the microscopic evolution of a many-body system is a challenging task.

As already imagined by the first works on quantum mechanics [33, 155], closed quantum systems can equilibrate towards stationary states in a similar fashion of thermalising dynamics in classical physics.

In this chapter will see how the concept of thermalisation and equilibration emerges in the context of many-body quantum physics and how it differs from its classical counterpart. In particular we will focus on the locality properties of the spreading of correlations paving the way for understanding how these can be exploited for simplifying the description of the out of equilibrium dynamics.

4.0.1 Quantum Quenches

In order to study systems out of equilibrium we need to decide a method for moving out of equilibrium.

The simplest protocol (that makes sense theoretically and experimentally) for the out-of-equilibrium dynamics is that of quantum quenches [63]. A quench protocol consists in considering an eigenstate (most of the time the ground state) $|\psi\rangle$ of an Hamiltonian H_0 (most of the time a local Hamiltonian) and studying its evolution after a sudden quench of the Hamiltonian $H_0 \to H_1$. The out of equilibrium dynamics is

$$|\psi\rangle(t) = e^{-iH_1 t}|\psi\rangle. \tag{4.1}$$

Quantum quenches are categorised as of two different types. There are local quenches, where the difference between the Hamiltonian pre-quench H_0 and the Hamiltonian after-quench H_1 is local. An example of local quench is changing a particular interaction between two specific lattice sites. There are global quenches where the after-quench Hamiltonian can differ in any way from H_0.

The categorisation of the quenches is strictly connected with the possible experimental implementation of the out-of-equilibrium dynamics.

In the following we will consider local Hamiltonians parametrised by a real number (this number can for example correspond to the strength of nearest neighbour interaction). We will quench the system by changing the value of this parameter. Since the properties of ground states are in many cases efficiently computable, we will have the advantage of starting from a state we can characterise efficiently.

In the following we will consider the Fermionic Ising transverse field Hamiltonian H of eq (3.122) with $N = 200$ and $g_F = 1$ for periodic boundary conditions. The Hamiltonian is dependent on the parameter $\theta \in [0, \frac{\pi}{2}]$. A quench protocol would consist in computing the ground state of $H(\theta_0)$ with $\theta_0 = \frac{\pi}{128}$ and then evolve it with $\theta = \frac{\pi}{8}$ with timesteps $\delta = 0.25$.

4.0.2 Entanglement and complexity

The computational resources needed by matrix product states techniques grow exponentially with the amount of entanglement in the system (see equation (2.45)). If we want to be able to efficiently simulate systems out of equilibrium we should hope for the entanglement to remain bounded during the evolution. Unfortunately, this is not the case.

In fact, the post quench dynamics spreads the initially localised correlations to arbitrarily large distances [156, 157] leading to a fast growth of entanglement with time [54–58, 158].

The speed of the dynamical growth of entanglement is upper bounded by a linear growth in time t [159–161], a result that is the consequence of the finite velocity of the propagation of correlation derived from the Lieb-Robinson bounds [162]. This upper bound can be tight for quadratic models [149, 156, 163, 164].

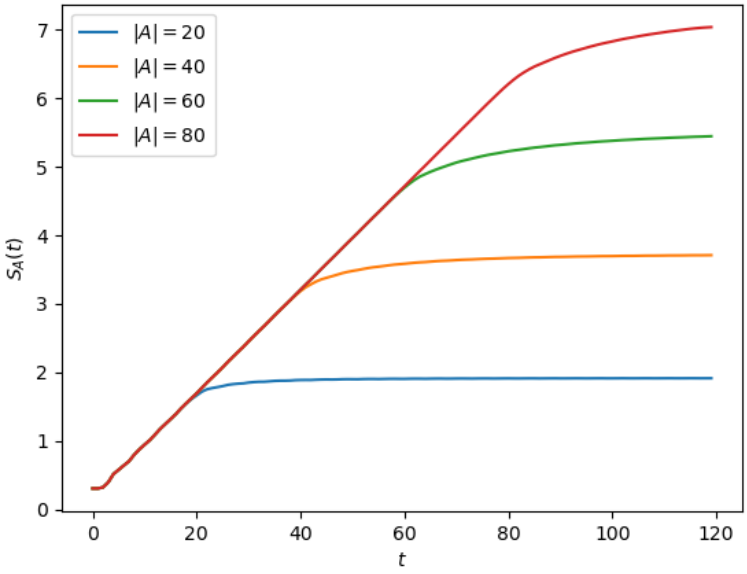

Figure 4.1: Growth of the entanglement entropy of different partitions in the transverse field Ising model. We consider the quenched dynamics of the Hamiltonian (3.122) with $N = 200$ and $g_F = 1$, with the quench $\theta : \frac{\pi}{128} \to \frac{\pi}{8}$. The system is divided in two complementary partitions A and B. We plot the von Neumann entropy of partition A at times $0.25t$. The entropy grows linearly until it saturates to a value proportional to the dimension of the partition. A linear growth of entanglement corresponds to an exponential growth of the resources needed to encode the state with matrix product states.

Since the entanglement is bounded by the logarithm of the bond dimension (see (2.45)), a linear growth of entanglement corresponds to an exponential growth of the resources needed to encode the states with standard tensor network techniques.

Standard tensor network techniques fail to describe out-of-equilibrium states.

As an example we consider the quench of the Fermionic Ising tranverse field Hamiltonian introduced at the end of the last paragraph. In figure 4.1 we analyse the dynamical behaviour of the entropy of an increasingly larger partition A of the system analogously to what is done in [156]. We know that for $1D$ systems satisfying an area law the EE is a finite quantity independent from the dimension of the partition. In the first part of the dynamics in figure 4.1 the system satisfies indeed an area law, up to a time $t = 20$ the EE is independent from the dimension of the partition (even if it grows linearly).

In the long-time regime the EE saturates at a value that is proportional to the size of the partition.

4.0.3 Quasi Particle Picture

In order to explain the dynamical behaviour of the entanglement after some quantum quenches and to give a general intuition of the results explained in the last section, in many cases one can rely on the quasi-particle picture [59, 149, 156, 164–168] (see [169] for a system not admitting quasi-particle picture, but with linear growth of entanglement). In the quasi-particle picture one imagines that the energy injected in the system by the quantum quench creates couples of entangled quasi-particles evenly distributed in the lattice. During the evolution these quasi-particles move ballistically with constant velocity and spread through the system. Because of conservation of momentum, each pair of entangled particles is expected to be created with opposite momenta (zero momentum conservation).

Following the scheme of figure 4.2 we can see how the linear growth of entanglement and the area law can be easily understood from the quasi-particle picture. At time $t = 0$ on each site we have a couple of entangled quasi-particles. As soon as the dynamics kicks in, the particles belonging to each couple start spreading in the system with opposite velocities. We fix a partition of the system A of dimension ℓ. At short times $t = t_1$, some couples of entangled particles, in particular the ones generetaed near the boundaries of the two partitions, have the left moving particles inside of A and the right moving particles inside the complementary partition and vice-versa.

Each shared couple of entangled particles contributes to the total amount of entanglement between the two partitions, thus at time t the entropy $S_A(t)$ of partition A is proportional to the total number of quasi particles pairs that are shared between A and the complementary partition. Specifically one has that, if there is just one kind of quasi-particles identified by their quasi-momentum λ, moving with velocity $v(\lambda)$ [168],

$$S_A(t) \propto 2t \int_{2|v|t<\ell} d\lambda v(\lambda) f(\lambda) + \ell \int_{2|v|t>\ell} d\lambda f(\lambda), \tag{4.2}$$

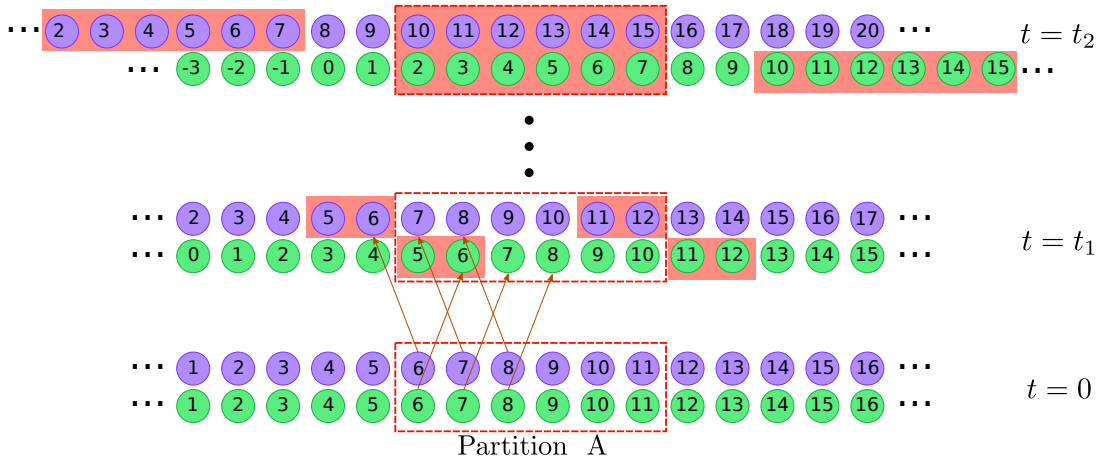

Figure 4.2: Representation of the quasi particle picture. From bottom to top we represent an infinite system at three different times with $0 < t_1 < t_2$. At every time each site of the system is represented as a column with a violet and a green circle. The green and violet circles represent the quasi-particles. Red filled boxes highlight the quasi-particles that contributes to the entanglement between A and its complement. Violet quasi-particles move left with a fixed speed v, green quasi-particles moves in the opposite direction at the same speed so that the total momentum for each couple of quasi particles is conserved. Particles with the same number are entangled. At time $t = 0$ in each site of the system a couple of entangled quasi-particles is created. All the quasi-particles inside of A have their entangled partner inside of A. At time $t = t_1$ the quasi particles moved. Particles $5, 6, 11, 12$ have their entangled partner outside the partition. Each quasi-particle in A with entangled partner outside A contributes to the entanglement of the partition with the rest of the system. We note that in this picture the first sites to contribute to the entanglement are the sites at the boundaries. At time $t = t_2$ the entanglement between partition A and the system is saturated as all the quasi-particles inside of A have the entangled partner outside of A. We note that for an infinite system the entropy of partition A at this point is fixed for the rest of the evolution, but the entangled partners are moving further away from A.

where $f(\lambda)$ depends on the production rate of the quasi-particle in the quench. Equation (4.2) holds exactly in the limit $t, \ell \to \infty$ with $t\ell$ fixed. In figure 4.2 we represent a system with quasi-particles with one single velocity v and we consider equation (4.2) as holding exactly, thus we have that

$$S_A(t) = \min(2|v|t, \ell) \cdot f(v). \tag{4.3}$$

From this equation and from figure 4.2, we see that after enough time has passed (a time proportional to the dimension of the partition) the entropy is expected to saturate

as all the quasi particles in the partition are entangled with a quasi-particle outside the partitition. This picture gives a clear intuition of the reason why entanglement is expected to grow at most linearly in time and tells us that the entropy of a partition can saturate to a value proportional to the dimension of the partition. In fact, the entropy of a partition is saturated when the partition is saturated with entangled quasi-particles. If we assume a finite Hilbert space for the constituents, the number of entangled quasi-particle that fits in a partition is proportional to the volume of the partition.

The validity of equation (4.2) has been verified for free models, it has been proved for rational Conformal Field Theories [170] and it has been studied in interacting integrable models [171, 172].

An important insight we get from the quasi-particle picture is that we can consider the contribution to the entanglement of each partition with the rest of the system as coming from regions further away from the partitions as time passes (see the red rectangles in figure 4.2) . We will investigate further this idea in the paragraph on the equilibration of quadratic sytems 4.1.4 and in chapter 6.

4.1 Equilibration

The linear growth of entanglement during the post quench dynamics is a curse for the simulation of many-body systems out of equilibrium. MPS compression techniques would require an exponential amount of resources to store the istantaneous information of the state during the evolution.

However, many-body quantum systems seemingly relax to equilibrated states, and, in particular cases, they relax to thermal or almost thermal states [64, 173–176]. This suggests that the long-time regime many-body quantum states can be efficiently encoded.

The topic of equilibration of closed quantum systems is broad and we will cover just a small fraction of it. A good review for the interested reader is [64] together with the seminal articles [174–176].

We start by considering an initial state ρ, we call $\rho(t)$ the time evolved state with Hamiltonian H. We are interested in the possible equilibration of the state. It is clear

that, in finite systems, it is impossible for $\rho(t)$ to reach a steady value. The dynamics is unitary and for long enough times we will have recurrence effects, thus unless $\rho(t) = \rho$ at every time, the state will never equilibrate.

Unitarity is not incompatible, though, with the relaxation of some observables to their expectation values or even to the relaxation of *reduced* density matrices to steady states.

For closed-quantum systems we can then define thermalisation focussing on particular properties of the system. A quantum system is said to equilibrate if, on average, during the time evolution the reduced density matrix of the state over a small partition or the expectation value of some observables is close to a steady density matrix or a steady value respectively. The fact that many-body quantum systems are expected to thermalise in this sense is supported by the two results summarised in [177] (see also [178–180]). Defining the steady equilibrium state $\mathcal{JJ}_H(\rho)$ ("katana$_H(\rho)$"), we have that the time-averaged fluctuation of an equilibrating observable A around the equilibrium value are bounded by

$$\overline{(\langle A\rangle_{\rho(t)} - \langle A\rangle_{\mathcal{JJ}_H(\rho)})^2} \leq ||A||^2 e^{-S_2(\mathcal{JJ}_H(\rho))} \tag{4.4}$$

where S_2 denotes the $2-$Reny entropy and $\langle A\rangle_\rho = \mathrm{Tr}\,[\rho A]$. In a similar fashion focussing on the reduced density matrices one has that the time-average distance between the reduced state on partition S, $\rho_S(t) = \mathrm{Tr}_{S^c}[\rho(t)] \in \mathcal{H}_S$ and the reduced density state $\mathcal{JJ}_H(\rho)_S = \mathrm{Tr}_{S^c}[\mathcal{JJ}_H(\rho)]$ (where S^c is the partition of the system complementary to S) is

$$\overline{||\rho_S(t) - \mathcal{JJ}_H(\rho)_S||_1} \leq 2d_s e^{-S_2(\mathcal{JJ}_H(\rho)_S)/2}, \tag{4.5}$$

where d_s is the dimension of the Hilbert space associated to the partition S.

4.1.1 Diagonal Ensemble

We study the time evolution of the expectation value of an observable O. We call $\langle O(t)\rangle = \mathrm{Tr}\,[\rho(t)O]$ the expectation value of O at time t. We say that the value of $\langle O(t)\rangle$ equilibrate if, for most of the time, $\langle O(t)\rangle$ is close to a steady value that we call

$\overline{O}$.

If the steady value $\overline{O}$ exists, it must be equal to infinite time average of $\langle O(t)\rangle$

$$\overline{O} \coloneqq \lim_{T\to\infty}\frac{1}{T}\int_0^T dt\langle O(t)\rangle = \mathrm{Tr}\left[\left(\lim_{T\to\infty}\int_0^T dt\frac{\rho(t)}{T}\right)O\right] = \mathrm{Tr}\left[\mathcal{DJ}_H(\rho)O\right], \tag{4.6}$$

where $\mathcal{DJ}_H(\rho) = \lim_{T\to\infty}\int_0^T dt\frac{\rho(t)}{T}$, is the *diagonal ensemble* of ρ with respect to the Hamiltonian H.

Since the state of quantum state is convex, the diagonal ensemble is a valid correlation matrix and it is the state that encodes all the information on the equilibrium values of every observable. The diagonal ensemble of a state ρ with respect to the Hamiltonian H is obtained by the application of the decohering or dephasing operator $\mathcal{DJ}_H(\cdot)$ defined as

$$\mathcal{DJ}_H(\rho) \coloneqq \sum_E |E\rangle\langle E|\rho|E\rangle\langle E| \tag{4.7}$$

where $\{|E\rangle\}_E$ is the set of eigenvalues of H.

It is clear that, in order to compute $\mathcal{DJ}_H(\rho)$ we have to be able to diagonalise the whole Hamiltonian, a task that requires an exponential amout of the resources in the dimension of the system. Furthermore, being able to diagonalise the complete Hamiltonian, would allow us to compute the complete microscopic out-of-equilibrium dynamics, thus eliminating the need of approximating the equilibrium state.

We can see how, for non degenerate H, this definition corresponds to the form of the diagonal ensemble of equation (4.6) expanding e^{iHt} on the diagonal basis of H as $e^{iHt} = \sum_E e^{iEt}|E\rangle\langle E|$, where

$$\begin{aligned}
&\lim_{T\to\infty}\int_0^T dt\frac{\rho(t)}{T} = \lim_{T\to\infty}\frac{1}{T}\int_0^T dt e^{-iHt}\rho e^{iHt} = \\
&= \lim_{T\to\infty}\int_0^T dt\frac{e^{-i(E-E')t}}{T}\sum_{E,E'}|E\rangle\langle E|\rho|E'\rangle\langle E'| = \\
&= \sum_E |E\rangle\langle E|\rho|E\rangle\langle E| = \mathcal{DJ}_H(\rho),
\end{aligned} \tag{4.8}$$

that is exactly the identity used in eq (4.6).

4.1.2 Maximum Entropy Principle

In 1957 Jayne [136, 137] introduced in statistical mechanics the principle of maximum entropy. This principle states that, given a prior knowledge, the probability distribution that best represents the current state of knowledge is the one that maximise the entropy. The principle of maximum entropy, or Jayne's principle, is now seen as a foundational principle of statistical mechanics.

We can see how statistical ensembles can be constructed by a direct application of the principle. Suppose, for example, that our prior knowledge of the state consists in knowing the expectation value $\{\langle I^{(n)}\rangle\}_n$ of a set of observables $\{I^{(n)}\}_n$. Then Jayne's principle says that the state ρ_J that best describes the system is the solution of the maximisation problem

$$\begin{aligned} \max_{\rho} \quad & S(\rho) \\ \text{s.t.} \quad & \mathrm{Tr}\left[\rho I^{(n)}\right] = \langle I^{(n)}\rangle \quad \forall n, \end{aligned} \tag{4.9}$$

and it has the general form

$$\rho_J = \frac{e^{-\sum_n \lambda_n I^{(n)}}}{\mathrm{Tr}\left[e^{-\sum_n \lambda_n I^{(n)}}\right]}, \tag{4.10}$$

where $\lambda_n \in \mathbb{R}$ are such that $\mathrm{Tr}\left[\rho_J I^{(n)}\right] = \langle I^{(n)}\rangle \ \forall n$.

4.1.3 Generalised Gibbs Ensemble

To every Hamiltonian H it corresponds a set of observables $\{I_n\}_n$ such that $[H, I_n] = 0$ for every n. These are conserved quantities (see section 2.2.1) and their expectation value does not change during the dynamics. If the state we are considering is going to equilibrate, we can be sure that in the diagonal ensemble $\mathcal{DJ}_H(\rho)$ the expectation value of each of these conserved observables is the same as the one computed on the initial state ρ.

This observation connects the diagonal ensemble to the Jayne's principle. It can be shown that the diagonal ensemble is the unique state that maximises the von Neumann entropy given the expectation value of all the conserved quantities [179], thus, the

diagonal ensemble can be computed as the solution of the maximisation problem (4.9) with $\{I_n\}_n$ the set of *all* the conserved quantities imposing $\langle I^{(n)}\rangle = \mathrm{Tr}\left[\rho I^{(n)}\right]$, $\forall n$.
In the previous sections we have seen how being able to compute the diagonal ensemble corresponds to be able to diagonalise the Hamiltonian. This complexity can be seen also in the construction of the diagonal ensemble from the Jayne's principle. In fact, in quantum systems the number of conserved quantities scales exponentially with the number of constituents (indeed it scales as the dimension of the Hilbert space). To see this, it is sufficient to consider the basis of the eigenstates $\{|E\rangle\}_E$ of the Hamiltonian H. The number of eigenvectors of H are expected to scale as the dimension of the Hilbert space. Building a projector $P_E = |E\rangle\langle E|$ out of each eigenvector we obtain an exponentially large set of conserved quantities since $[P_E, H] = 0$.
The Jayne's perspective, nonetheless, leads us to the question if it is really necessary to preserve *all* the conserved quantities or if it is possible to obtain a good approximation of the equilibrium state preserving only a subset of conserved quantities.

In particular, we remind that we are interested in the equilibration of a system with respect to the expectation values of local operators, thus we are not interested in the full information encoded in the diagonal ensemble. Starting from Jayne's principle, it would be desirable to characterise a restricted set of conserved operators $\{I^{(n)}\}_n$ such that the state that maximise the entropy given the set of constraint on the expectation values of all $\{I^{(n)}\}_n$ is going to reproduce, with good approximation, the expectation value of local observables in the diagonal ensemble, that is, in the equilibrated state. This state is called *Generalised Gibbs Ensemble* (GGE) [181–185] (In section 4.2 we will introduce the Gibbs Ensemble, and the reason for the name *generalised* Gibbs ensemble will be clear).
The characterisation of the set $\{I^{(n)}\}_n$, and thus of the GGE, has been longly debated. The GGE has been firstly introduced in the context of free systems [184], where the set of conserved quantities has been individuated as the occupations of the free modes (a set of conserved quantities polynomially large in the system size). Extending this notion of GGE to interacting systems [176], the GGE is constructed from the set of conserved operators constituted by the projectors on the energy eigenstates of the Hamiltonian.

This, de facto, identified the diagonal ensemble with the GGE (an identification that appears also in [186]). It has subsequently been suggested that in interacting and not intergacting systems, the conserved quantities defining the GGE should be just local quantities [181,182]. It can be shown [181] that, for free systems, the GGE formulations based on the set of conserved free modes and the GGE formulation based on local conserved quantities are equivalent. Here we are going to consider the formulation of the GGE based on *local* conserved quantities. For a mathematical precise formulation of this GGE see e.g. [64].

The validity of the GGE, as a state that locally well approximates the equilibrium state, has been confirmed by many results (see for example [64, 181, 182] and references therein).

The set of *local* conserved quantities generally grows linearly with the number of constituents of the system. This allows us to deal with bigger system, but in the case of infinite systems, the number of constraints would be infinite nevertheless (see [187] for an example where this infinite set is explicitly computed). In these cases a notion of *truncated* GGE, where just a part of the the infinite set of local conserved quantities is conserved, has been adopted [182, 184, 188], showing that even the information about all the local conserved quantities can be redundant.

4.1.4 Equilibration of quadratic systems

Here we present the formulation and the properties of the GGE in the particular case of free systems. A complete treatise of free Hamiltonians, for Fermionic systems is given in Chapter 3. We use here the same notation.

One key property of Fermionic Gaussian systems is that the set of Fermionic Gaussian states is closed under the the evolution induced by a quadratic Hamiltonian. Thus one expects that, if a Gaussian state is going to equilibrate, it should equilibrate to a Gaussian state.

The definition of diagonal ensemble does not capture this property. In fact, the diagonal ensemble can be defined as an infinite-time average (see eq (4.6)), but a convex combination of Gaussian states is not a Gaussian state [189]. One can still

compute the projection of the diagonal ensemble to the space of Gaussian states, that is the Gaussian state characterised by the correlation matrix of the diagonal ensemble. We construct it now, explicitly, in an example. Let us consider a Fermionic quadratic Hamiltonian H and an initial Fermionic Gaussian state Γ. With an abuse of notation we denote the density matrix associated to a correlation matrix Γ as $\rho(\Gamma)$ and the correlation matrix computed from a (not necessarily Gaussian) state ρ as $\Gamma(\rho)$. The diagonal ensemble is $\mathcal{J}_H(\rho)$. The projection on the Gaussian state is $\Gamma(\mathcal{J}_H(\rho))$ or $\rho(\Gamma(\mathcal{J}_H(\rho)))$. In general $\mathcal{J}_H(\rho) \neq \rho(\Gamma(\mathcal{J}_H(\rho)))$. In order to compute $\Gamma(\mathcal{J}_H(\rho))$ directly from Γ we can just compute the infinite-time average of the correlation matrices. In particular, we firstly move Γ in the diagonal basis of H. In this basis the Hamiltonian is a free Hamiltonian of the form (3.20)

$$H = \sum_k \epsilon_k b_k^\dagger b_k. \tag{4.11}$$

Considering just the first quadrant of the correlation matrix $\Gamma^{b^\dagger b}_{i,j} = \mathrm{Tr}\left[\rho b_i^\dagger b_j\right]$, its time evolution is

$$\Gamma^{b^\dagger b}_{i,j}(t) = \mathrm{Tr}\left[\rho b_i^\dagger b_j\right] e^{i2(\epsilon_i - \epsilon_j)t}. \tag{4.12}$$

In the case of no degenerancies taking the infinite-time average of $\Gamma^{b^\dagger b}$ corresponds to setting all the out-of-diagonal elements of $\Gamma^{b^\dagger b}$ to 0. This procedure corresponds to building the Gaussian state that in the eigenbasis of H preserves all the free occupations ($\mathrm{Tr}\left[\rho b_i^\dagger b_i\right]$) and has set to zero all the other elements of the correlation matrix. We define the ensemble built following these steps the *Gaussian diagonal ensemble* (GDE), we refer to it has ρ_{GDE} or Γ_{GDE} or $\Gamma(\mathcal{J}_H(\rho))$.

From section 3.3.2, we know that Gaussian states are the states that maximise the entropy for a given set of fixed expectation value for the two points correlators.

For free theories, it can be showed [181] that the state that maximise the entropy for a given set of occupations of the free modes is the GGE. Thus for free theories we have the equivalence between the GGE and the GDE.

Entanglement Contour Dynamics

With the quasi-particle picture we got an intuition on the behaviour of entanglement during the post-quench dynamics. In particular we have seen that, if we consider a bipartite system (A, B), with partition B bigger then partition A (see fig. 4.2), the contribution in B to the entanglement between partition A and B moves further from partition A.

In the context of free systems, this intuition can be strengthened by the study of the dynamics of the entanglement contour (see 2.3.2 and 3.3.10).

We consider again the Hamiltonian (3.122) with $g_F = 1$ corresponding to a system with periodic boundary conditions as in figure 4.3. We choose the system size to be $N = 200$ and we consider the quench from $\theta = \frac{\pi}{128}$ to $\theta = \frac{\pi}{8}$, each timestep t correponds to $\delta = 0.25$. In figure 4.4 we study the dynamics of the contour out of equilibrium for two complementary partitions A of dimension $N_A = 40$ and B of dimension $N_B = 160$.

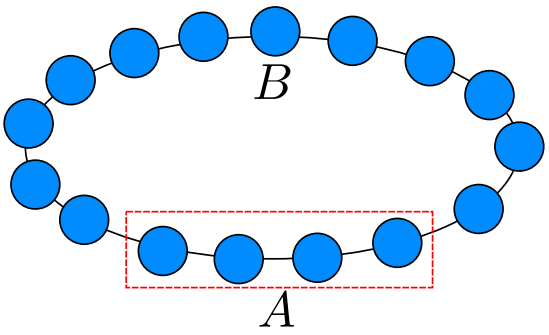

Figure 4.3: A system with periodic boundary conditions divided in two complementary partitions A and B.

From figure 4.1 we know the entanglement entropy of partition A is going to saturate to a value proportional to $|A|$. Since the von Neumann entropy of complementary partitions of a pure state is symmetric (2.21), we know that the value to which the von Neumann entropy of B saturates is dictated by partition A.

In the left panel of figure 4.4 we see the entanglement contour dynamics for partition A. At time $t = 0$ the only sites that contribute to the entanglement are those at the boundaries. This is expected. In fact, we know that this state obeys an area law, thus, for every partition we choose, the scaling of the entanglement is proportional to

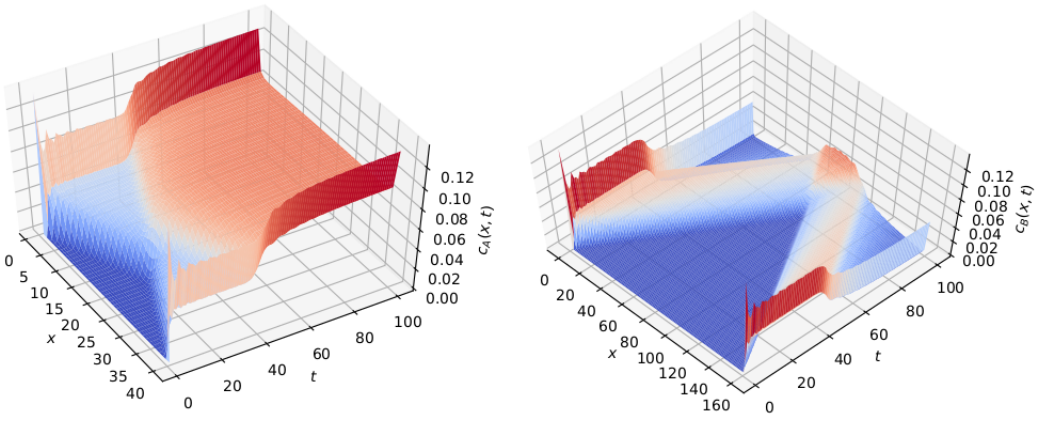

Figure 4.4: Out of equilibrium dynamics of the entanglement contour for two partitions of different dimensions. In the small partition A on the left, at saturation of the EE, the entanglement contour is flat in the middle of the partition. In the big partition B on the right the entanglement contour propagates being always localised.

the scaling of the boundaries of the partition and we have seen that this is a direct consequence of the exponential decay of the correlations. Therefore we expect that the leading contribution to the entanglement should come from the boundaries of the partition. Proceeding with the evolution the entanglement entropy of partition A grows linearly and the contour starts spreading in the bulk of the partition. Each site of the partition is starting to contribute to the total entanglement of the partition. When the entanglement entropy of the partition is saturated, the profile of the entanglement contour is flat in the bulk and has two spikes at the boundary. It looks like the profile at time $t = 0$, with the difference that the contribution of each site is higher, thus a constant term of entropy is added.

In the right panel of figure 4.4 we see the dynamics of the entanglement contour for the bigger partition B. At time $t = 0$ the contour is localised at the boundaries as expected. During the dynamics the contribution to the entanglement spreads inside of the partition entering inside of B from both sides because of the two boundaries. In perfect accordance with the quasi-particle picture, we notice that the contribution to the entanglement spreads further from the boundaries, thus partition A results to be effectively entangled with increasingly distant parts of the system. In figure 4.5 we focus on the contour of partition B at three different timesteps $t = 0$, $t = 70$ and $t = 90$.

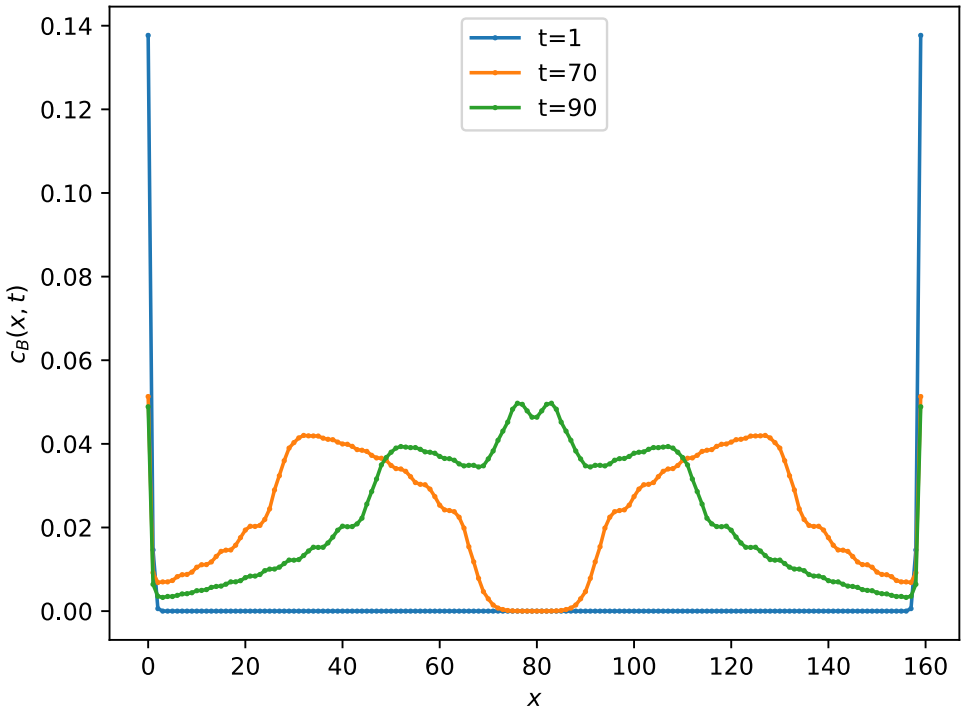

Figure 4.5: Entanglement contour inside of partition B at three different times. At initial time the entanglement is localised at the boundaries of the partition. The entanglement then starts spreading in the partition, always being localised, as it is evident from the two orange peaks. The green curve represents the entanglement contour at the moment when the two entanglement fronts meet.

We notice how at $t > 0$ the contour at the boundaries is comparable to the peak of the contour in the bulk. We notice also how the contribution at the boundaries rapidly decays in space, making the contribution in the bulk extremely localised.

Equilibration times and Gaussification

For systems evolving with a quadratic Fermionic Hamiltonian there exists general, and mathematically rigorous statements about the equilibration of the systems towards the GGE [190, 191].

The framework in which these theorems hold is that of a generic $1D$ fermionic system of N sites with translational invariant local Hamiltonian H with periodic boundary

conditions, with the additional assumption that the derivative of the dispersion relation $\epsilon(k)$ have not coinciding roots (there is not a k such that $\frac{d^2}{dk^2}\epsilon(k) = \frac{d^3}{dk^3}\epsilon(k) = 0$). In this context, for every initial state ρ of the system with finite correlation lenght and no long-wavelength dislocations in the two points correlators of Dirac operators (see chapter 3), there exists a constant relaxation time t_0 and a time of recurrence t_R proportional to the system size N such that, for all $t \in [t_0, t_R]$, the state locally equilibrate to a GGE with

$$|\langle O\rangle_{\rho(t)} - \langle O\rangle_{GGE}| \leq Ct^{-\gamma}, \tag{4.13}$$

with O a local observable and $C, \gamma > 0$ independent from N.

It is important to notice that no assumptions on the Gaussianity of the initial state have been made. It is indeed possible to choose as initial state a state that is not Gaussian, it is the quadratic form of the Hamiltonian H that, through a process called *gaussification* [190], transforms the state to a state locally indistinguishable from a Fermionic Gaussian state.

Gaussification is a general result conferring even more relevance to Fermionic Gaussian states.

Following again [191] we have that for an initial Fermionic state ρ with exponential decay of correlations and a non-interacting translational invariant Hamiltonian H with the derivative of the dispersion relation with not coinciding roots (there is not a k such that $\frac{d^2}{dk^2}\epsilon(k) = \frac{d^3}{dk^3}\epsilon(k) = 0$), there exists a constant relaxation time t_0 and and a recurrence time t_R proportional to N such that, for all $t \in [t_0, t_R]$,

$$|\langle O\rangle_{\rho(t)} - \langle O\rangle_{\rho(\Gamma(\rho(t)))}| \leq Ct^{-1/6}, \tag{4.14}$$

where $C > 0$. This shows that, under these conditions, the expectation value of the local observable O converges with a power law in time towards the same value computed with the Gaussian projection of the state.

Equilibration of occupations in the Fermionic transverve Field Ising model

In some cases it is possible to explicitly compute the equilbration of some local observables.

In chapter 3.5.3 we compute the time evolution of the single site occupation $\langle a_1^\dagger a_1\rangle$ during the out-of-equilibrium dynamics of a translational invariant state with Hamiltonian (3.122) where $g_F = -1$ and N is even.

We are now interested to verify if this observable equilibrates.

In order to avoid recurrence effects we compute the limit of expression (3.143) in the case of the number of sites going to infinity $N \to \infty$. Defining the quantity $p = -\frac{2\pi}{N}$ we can write

$$\begin{aligned}
&\langle a_1^\dagger a_1\rangle(t) = \\
&= \lim_{N\to\infty} \frac{1}{N} \sum_{k=\frac{-N+1}{2}}^{\frac{N+1}{2}} \left[s_k^2 \langle b_k^\dagger b_k\rangle + t_k^2 \langle b_{-k} b_{-k}^\dagger\rangle + i s_k t_k (e^{i\epsilon_k t}\langle b_{-k} b_k\rangle - e^{-i\epsilon_k t}\langle b_k^\dagger b_{-k}^\dagger\rangle)\right] = \\
&= -\int_{-\pi}^{\pi} dp \left[s_{-p}^2 \langle b_{-p}^\dagger b_{-p}\rangle + t_{-p}^2 \langle b_p b_p^\dagger\rangle + i s_{-p} t_{-p} (e^{i\epsilon(p)t}\langle b_p b_{-p}\rangle - e^{-i\epsilon(p)t}\langle b_{-p}^\dagger b_p^\dagger\rangle)\right],
\end{aligned} \tag{4.15}$$

with

$$\begin{aligned}
s_p &= \frac{\sin(p)}{\sqrt{\epsilon_k(\epsilon_p/2 + \cot(\theta) + \cos(p))}}, \\
t_p &= \frac{\epsilon_p/2 + \cot(\theta) + cos(p)}{\sqrt{\epsilon_p(\epsilon_p/2 + \cot(\theta) + cos(p)}}, \\
\epsilon(p) &= 2\sqrt{1 + \cot(\theta)^2 - 2\cot(\theta)\cos(p)}.
\end{aligned} \tag{4.16}$$

The two time-dependent terms of the integral (4.15) have the same form, thus it suffices to study the long-time behaviour of the integral

$$I(t) = \int_{-\pi}^{\pi} dp e^{i\epsilon(p)t} s_{-p} t_{-p} \langle b_p b_{-p}\rangle. \tag{4.17}$$

In order to study the long-time beaviour of $I(t)$ we use the result about oscillatory integral in [192] chapter VII proposition 3. Having that $\frac{d}{dp}\epsilon(p)\Big|_{p=0} = 0$ and $\frac{d^2}{dp^2}\epsilon(p)\Big|_{p=0} \neq 0$, for large values of t, the integral can be approximated as

$$I(t) \sim t^{-1/2} \sum_{j=0}^{\infty} a_{2j} t^{-j}, \tag{4.18}$$

where each a_j depends only on finitely many derivatives of both $\epsilon(p)$ and $s_{-p}t_{-p}\langle b_p b_{-p}\rangle$ at $p = 0$. Computing a_j explicitly we find that $a_0 = 0$, thus we have that at large t

$$I(t) \sim t^{-3/2}. \tag{4.19}$$

Plugging this result into (4.15) we find out that the single site occupation, in the long-time regime, equilibrates as $t^{-3/2}$ to the asymptotic value of

$$\langle a_1^\dagger a_1\rangle = -\int_{-\pi}^{\pi} dp \left[s_{-p}^2 \langle b_{-p}^\dagger b_{-p}\rangle + t_{-p}^2 \langle b_p b_p^\dagger\rangle\right], \tag{4.20}$$

that is exactly the one predicted by the GDE.

4.2 Thermalisation

In the last sections we have been studying ensembles depending on less and less conserved quantities. Starting from the diagonal ensemble, the state that maximises the entropy given all the conserved quantities, we moved to the GGE, for which one considers just the local conserved quantities, and we finished with the truncated GGE, the state constructed out of a selection of local conserved quantities. Taking this process to the limit, we end up introducing the state that maximise the entropy given just one single conserved quantity, the total energy of the system. This state is called *thermal state* or *Gibbs state*. Given a Hamiltonian H and a fixed E, a thermal

state is defined as the state that solve the maximisation problem

$$\begin{aligned} \max_{\tilde{\rho}} \quad & S(\tilde{\rho}) \\ \text{s.t.} \quad & \mathrm{Tr}\left[\tilde{\rho}H\right] = E. \end{aligned} \tag{4.21}$$

The solution of this problem has the form

$$\rho_{\beta,H} = \frac{e^{-\beta H}}{\mathrm{Tr}\left[e^{-\beta H}\right]} \tag{4.22}$$

where the inverse temperature β is chosen in order to satisfy the constraint $\mathrm{Tr}\left[\rho_{\beta,H}H\right] = E$.

Whenever a state equilibrates to an equilibrium state that is close to a thermal state (in the local sense explained before) we say that the system *thermalise*.

The choice of the energy of the state as the only conserved quantity is the most natural. Other than the considerations on classical and statistical mechanics, we note that a quantum system is characterised by two operators: the state ρ and the Hamiltonian H. The state ρ is not a conserved quantity (we are studying the dynamics), while the expectation value of H is a conserved quantity. Concurrently, H is the starting point for finding all the other conserved quantities as operators that commutes with H.

Following this, one can argue that energy conservation is actually the only conserved quantity necessary to be considered as all the operators commuting with (a non degenerate) H are functionally dependent on H [193], but, as explained in [176], even if the operators are functionally dependent their expectation values are generally not.

4.2.1 Eigenstate Thermalisation Hypotesis

At the core of the theory of thermalisation of closed quantum systems there is the Eigenstate Thermalisation Hypothesis (ETH). The ETH was first introduced in the two independent works of Deutsch and Srednicki [174, 175], suggesting that thermalisation in quantum mechanics has a different nature from thermalisation in classical mechanics.

Differently from classical mechanics, for the ETH, thermalisation is not strictly connected to the dynamics, but it is, instead, derived from the properties of the eigenstates of the Hamiltonian [176]. The ETH is a hypothesis on two properties of the energy eigenstates of many-body interacting Hamiltonians that, if satisfied, lead the system to thermalise.

ETH [174, 175, 194] Consider H the Hamiltonian of a quantum system with N constituents. Let $\{|\alpha\rangle\}_\alpha$ be the set of eigenstates of H with eigenvalue $\{E_\alpha\}_\alpha$ respectively and let O be a few-body observable. The set of eigenstates is sorted such that to close values of α corresponds close values of the eigenvalues, or energies, E_α. Then the elements $\langle\alpha|O|\beta\rangle$ satisfy the ETH if:

1. $O_{\alpha,\alpha} \coloneqq \langle\alpha|O|\alpha\rangle$ changes slowly with the state, with the difference between neighboring values $O_{\alpha+1,\alpha+1} - O_{\alpha,\alpha}$ exponentially small in N
2. $O_{\alpha,\beta} \coloneqq \langle\alpha|O|\beta\rangle$, with $\alpha \neq \beta$ are exponentially small in N.

To see how the ETH implies thermalisation we first show that, in the hypothesis that the systems thermalise, the ETH implies a correspondence between the diagonal ensemble and the microcanonical ensemble.
For doing so, let us consider a non degenerate Hamiltonian H and the collection of its eigenstates $\{|\alpha\rangle\}_\alpha$, where with E_α we indicate their eigenvalues, the energies. We consider a state $|\psi\rangle = \sum_{(\alpha|E_\alpha\in\mathcal{E})} C_\alpha|\alpha\rangle$ that is the linear combination of eigenstates of H with corresponding energies in the interval $\mathcal{E} \coloneqq [E_0 - \Delta E, E_0 + \Delta E]$.

The expectation value of an observable O in the diagonal ensemble $\mathcal{J}\mathrm{J}_H(|\psi\rangle\langle\psi|)$ will be

$$\langle O\rangle_{DE} = \mathrm{Tr}\left[\mathcal{J}\mathrm{J}\left(|\psi\rangle\langle\psi|\right)O\right] = \sum_{\alpha|E_\alpha\in\mathcal{E}} |C_{\alpha,\alpha}|^2 O_{\alpha,\alpha}, \tag{4.23}$$

Assuming that the eigestates of H satisfy the ETH and that ΔE is small enough, the value of $O_{\alpha,\alpha}$ with $\alpha|E_\alpha \in \mathcal{E}$ will be approximately constant, we call this constant value O_{E_0}. We then have

$$\langle O\rangle_{DE} = O_{E_0} \sum_{E\in\mathcal{E}} |C_{E,E}|^2 = O_{E_0}. \tag{4.24}$$

Computing the same value assuming that we are in the microcanonical ensemble (that is the equally weighted mixture of all energy egeinstates with energy in $\mathcal{E}$) we would have the equally weighted sum

$$\langle O\rangle_{micro} \coloneqq \frac{1}{\mathcal{N}} \sum_{\alpha|E_\alpha\in\mathcal{E}} O_{\alpha,\alpha}, \tag{4.25}$$

with $\mathcal{N} = |\{|\alpha\rangle|E_\alpha \in \mathcal{E}\}|$ the number of eigenstates in the considered energy window. Considering the ETH even in this case we have that

$$\langle O\rangle_{micro} = O_{E_0} \frac{1}{\mathcal{N}} \sum_{\alpha|E_\alpha\in\mathcal{E}} 1 = O_{E_0}. \tag{4.26}$$

The diagonal ensemble and the microcanonical thus give the same prediction for the equilibration value of O.

This proof relied only on the point (1) of the ETH. Point (2) is required for the system to equilibrate [175,176]. Different versions of the ETH exist, we refer to [64] for a version of the ETH valid for degenerate Hamiltonians that leads to thermal Gibbs states.

It is still an open question under wich conditions the ETH holds. Rigorous proofs exist that the ETH holds for special models as for example [195] and that conditions similar to the ETH hold for more general models [196].

Chapter 5

Quantum conformal field theories

In this chapter we introduce and review some of the main concepts and tools of conformal field theories. Exploiting conformal symmetries we are able to encode relevant and universal properties of quantum systems in just a few parameters describing the theory. In chapter 7 we will use these ideas to characterise states in the long-time out-of-equilibrium dynamics.

5.1 Conformal transformations (in 2D)

A conformal transformation is defined as a function that locally preseserves the angles. If we denote with $g_{\mu,\nu}$ the metric tensor of a manifold of dimension d, then a conformal transformation is the invertible coordinate transformation $r \to r' = r'(r)$ that changes the metric as

$$g'_{\alpha,\beta}(r') = \frac{\partial r^\mu}{\partial r'^\alpha}\frac{\partial r^\nu}{\partial r'^\beta} g_{\mu,\nu}(r) \coloneqq \Omega(r) g_{\alpha,\beta}, \tag{5.1}$$

that is, the coordinate transformation that scales the metric by a position-dependent factor $\Omega(r)$.

If we consider the infinitesimal transformation $r^\mu \to r^\mu + \epsilon^\mu(r)$, then we have that the first order transformation of the metric is

$$g_{\mu,\nu} \to g_{\mu,\nu} - (\partial_\mu \epsilon_v + \partial_\nu \epsilon_\mu). \tag{5.2}$$

If we ask for this infinitesimal transformation to be conformal (that is, to obey eq (5.1)) we obtain that

$$\partial_\mu \epsilon_\nu + \partial_\nu \epsilon_\mu = \frac{2}{d} \partial_\eta \epsilon^\eta g_{\mu,\nu}. \tag{5.3}$$

In dimensions $d = 2$ the characterisation of the infinitesimal conformal mapping (5.3) becomes the Cauchy-Riemann equations. In fact expanding (5.3) on the indices $(\mu, \nu, \eta = 1, 2)$ and solving the system we obtain

$$\partial_1 \epsilon_1 = \partial_2 \epsilon_2, \qquad \partial_1 \epsilon_2 = -\partial_2 \epsilon_1. \tag{5.4}$$

If we introduce the complex coordinate

$$z = r_1 + i r_2, \qquad \bar{z} = r_1 - i r_2, \tag{5.5}$$

as new coordinates in $d = 2$, we denote the partial derivatives as

$$\partial_z = \frac{1}{2}(\partial_0 - i\partial_1), \qquad \partial_{\bar{z}} = \frac{1}{2}(\partial_0 + i\partial_1), \tag{5.6}$$

and we denote the infinitesimal transformations $\epsilon(z)$ and $\bar{\epsilon}(\bar{z})$ as

$$\epsilon(z) = \epsilon_1 + i\epsilon_2, \qquad \bar{\epsilon}(\bar{z}) = \epsilon_1 - i\epsilon_2, \tag{5.7}$$

we find that the conformal transformations in two dimensions can be identified by the holomorphic functions $z \to w(z)$ and $\bar{z} \to \bar{w}(\bar{z})$.
Unless global properties of some functions are explicitly needed one may treat z and $\bar{z}$ as separate, independent coordinates [197].
We can express the infinitesimal transformations as $z' = z + \epsilon(z)$ where, because of its analyticity, $\epsilon(z)$ admits the Laurent expansion

$$\epsilon(z) = \sum_{-\infty}^{\infty} c_n z^{n+1}. \tag{5.8}$$

As functions of $z, \bar{z}$ these infinitesimal transformations are generated by the differential

operators

$$l_n = -z^{n+1}\partial_z, \qquad and \qquad \bar{l}_n = -\bar{z}^{n+1}\partial_{\bar{z}} \tag{5.9}$$

respectively as can be seen considering a field $\phi(z)$ and its expansion after a transformation of the coordinates

$$\begin{aligned}\delta(\phi) = \phi'(z', \bar{z}') - \phi(z', \bar{z'}) = -\epsilon(z)\partial\phi - \bar{\epsilon}(\bar{z})\bar{\partial}\phi = \\ = \sum_n \left[c_n l_n \phi(z, \bar{z}) + \bar{c}_n \bar{l}_n \phi(z, \bar{z})\right],\end{aligned} \tag{5.10}$$

where

$$\begin{aligned}\phi'(z'\bar{z}') = \phi(z, \bar{z}) = \\ = \phi(z', \bar{z}') - \epsilon(z')\partial'\phi(z', \bar{z}') - \bar{\epsilon}(\bar{z}')\bar{\partial}'\phi(z', \bar{z}').\end{aligned} \tag{5.11}$$

The generators (5.9) form the so called *Witt algebras* characterised by the following commutation relations

$$\begin{aligned}[l_n, l_m] = (n-m)l_{n+m}, \\ [\bar{l}_n, \bar{l}_m] = (n-m)\bar{l}_{n+m}, \\ [l_n, \bar{l}_m] = 0.\end{aligned} \tag{5.12}$$

If one is interested in global conformal transformation, then one has to require for $\epsilon(z)$ (and $\bar{\epsilon}(\bar{z})$) to be analytic everywhere. To check the analyticity of $\epsilon(z)$ we study its Laurent expansion 5.8.

We see that the series diverges at $z = 0$ for $n < -1$. In order to study the singularities at $z = \infty$ we map $z \to (\frac{1}{w})$ obtaining

$$\frac{\partial}{\partial z} = \frac{\partial w}{\partial z}\frac{\partial}{\partial w} = -w^2\frac{\partial}{\partial w}, \tag{5.13}$$

thus in term of w the generators have the form

$$l_n = -\left(-\frac{1}{w}\right)^{n-1} \partial_w, \tag{5.14}$$

and the singularity at $w = 0$ ($z = \infty$) occur for $n > 1$. From this we derive that global conformal transformations are generated by the set of generators $\{l_{-1}, l_0, l_{+1}\}$. Global conformal transformations are also called *Mobius transformations* (see figure 5.1). In general Mobius transformations $z \to w = w(z)$ are characterised by four parameters a, b, c, d and are written as

$$w(z) = \frac{az + b}{cz + d}, \tag{5.15}$$

with the constraint that $ad - bc = 1$.

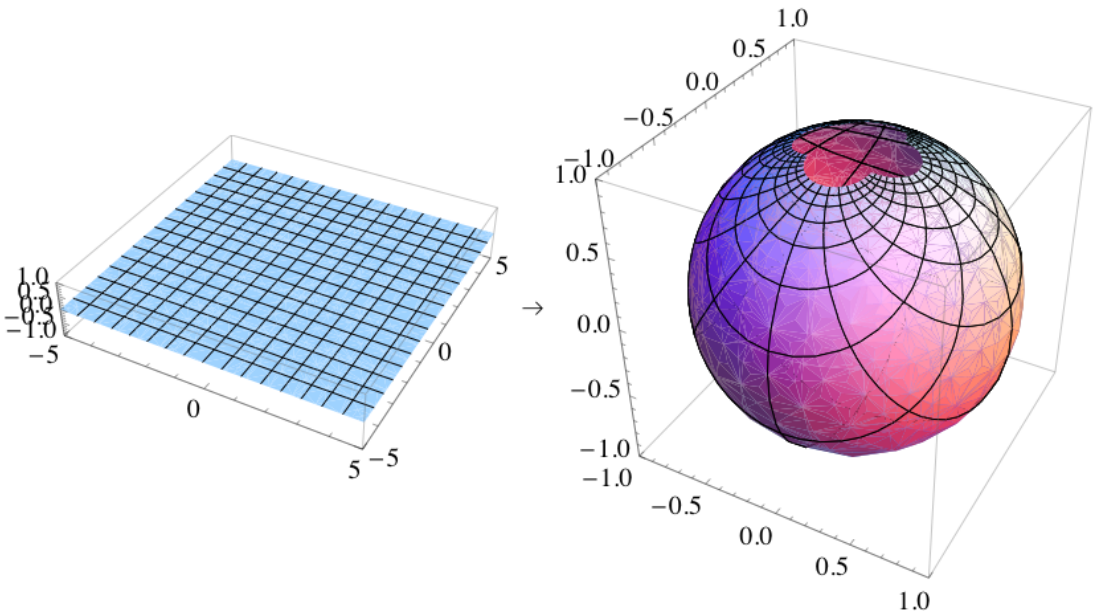

Figure 5.1: The stereographic projection is a conformal map. On the left we see a grid on the complex plane mapped onto a sphere, on the right, via stereographic projection. The intersection between the lines of the grid are still perpendicular. A general Mobius transformation (see equation (5.15)) can be built from a stereographic projection of the plane onto the sphere, followed by a rotation and translation of the sphere, subsequently followed by a projection of the points of the sphere onto the complex plane.

5.2 Conformal field theories (in 2D)

5.2.1 Primary fields and restriction on correlation functions

In $2D$ there is a special set of local fields $\{\phi(z,\bar{z})\}$ called *primary fields* (or primary operators) characterised by their transformation after a conformal mapping of the coordinates $z \to w = w(z)$. In particular a local field $\{\phi(z,\bar{z})\}$ is said to be a primary field, if, for any conformal transformation $w(z)$, it transforms as

$$\phi(w(z),\bar{w}(\bar{z})) = \left(\frac{dw}{dz}\right)^{-h}\left(\frac{d\bar{w}}{d\bar{z}}\right)^{\bar{h}}\phi(z,\bar{z}), \tag{5.16}$$

where $(h,\bar{h})$ are the *conformal dimensions* of the field.
For two primary fields ϕ_1 and ϕ_2, with conformal dimensions $(h_1,\bar{h}_1)$ and $(h_2,\bar{h}_2)$ respectively, the two points correlation function is fixed to

$$\langle\phi_1(z_1,\bar{z}_1)\phi_2(z_2,\bar{z}_2)\rangle = \frac{C_{1,2}}{(z_1-z_2)^{2h}(\bar{z}_1-\bar{z}_2)^{2\bar{h}}} \qquad \text{if} \qquad \begin{cases} h_1 = h_2 = h \\ \bar{h}_1 = \bar{h}_2 = \bar{h} \end{cases}, \tag{5.17}$$

with $C_{1,2}$ a numerical constant. In the case of two fields with different conformal dimensions the correlators vanishes. Constraints for more-points correlation functions exists too (see e.g. [197, 198]). If we have a field theory that is invariant under the group of conformal transformations, this invariance manifests itself in the correlation functions as expressed for example in (5.17). Fields that are not primary fields are called *secondary fields*. For example, if ϕ is a primary field, derivatives like $\partial_z^n\phi$ are called secondary fields over the primary field ϕ.

5.2.2 Quantum conformal field theories on the cylinder

In order to get a quantum Conformal Field Theory (CFT) first of all we need a quantum field theory. The main ingredients of a quantum field theory are an Hilbert space $\mathcal{H}$, a vacuum vector $|0\rangle$ and a set of relevant observables $\{\phi\}$, that is a selected subset of operators on $\mathcal{H}$ that, in $1+1$ dimensions, are labelled by (x,t) .
Until now we have considered field theories on a manifold with coordinates $z,\bar{z}$, that is

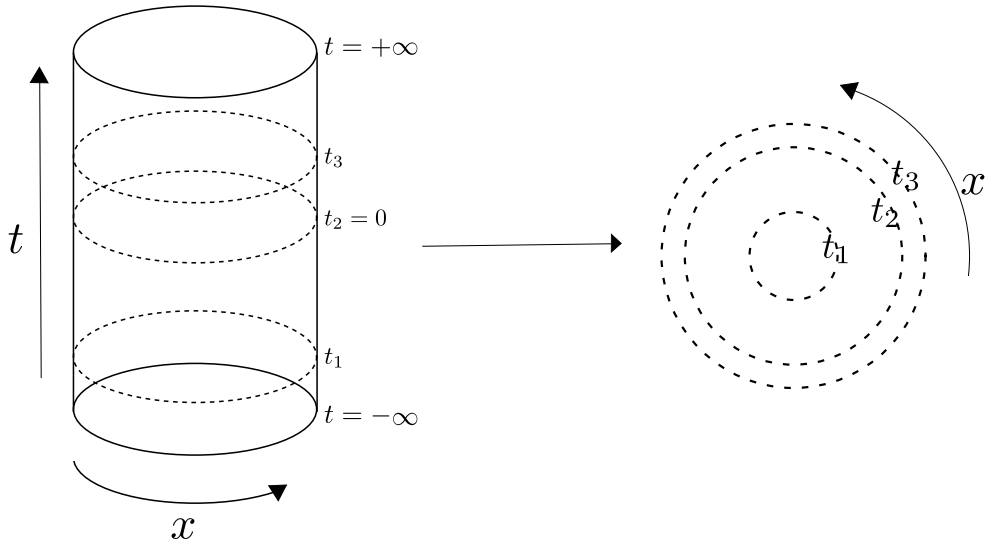

Figure 5.2: Mapping from the cylinder to the complex plane.

in a space of $2+0$ dimensions, a 2 dimensional euclidean space. The standard technique for connecting the two description consists in considering the analytical continuation of the quantum field theory in complex time and thus move to a quantum field theory in $2+0$ dimensions via Wick rotation.

With this procedure we obtain a quantum field theory in euclidean space time, where we associate one dimension with (imaginary) time and one with space.

Similarly to what is done for regularising a quantum system by putting it in a finite box in space, it is convenient to make the space direction finite by imposing periodic boundary conditions [198]. We decide to compactify the space dimension x by imposing $x = x + 2\pi$. With this compactification we describe the physical theory on an infinite cylinder, with the periodic dimension corresponding to the space dimension x and the infinite dimension corresponding to the time t going from $-\infty$ to $+\infty$.

With a convenient conformal transformation we then map the cylinder to the complex plane $(z, \bar{z})$. To do so we use the mapping

$$z = e^{t+ix}, \qquad \bar{z} = e^{t-ix}. \tag{5.18}$$

In the complex plane the time flows along the radial direction and space moves changing the angle coordinate (see figure 5.2). The entire circle of the system at time $t = -\infty$ is mapped to the single point at the origin of the complex plane (this particularity allows for a direct correspondence between states and operators [67] in conformal field theories). We have now a quantum CFT of a one dimensional system with periodic boundary conditions.

5.2.3 Virasoro Algebra and CFT Hamiltonian

In the Hilbert space description, the algebra of the generators of the conformal mappings is not the Witt Algebra (5.9) of the generators $\{l_n, \bar{l}_m\}_{n,m}$, but instead we have that the generators of local conformal transformation in the Hilbert space are now $\{L_n, \bar{L}_m\}_{n,m}$, and these generators obey the commutations rules

$$\begin{aligned}
[L_n, L_m] &= (n-m)L_{n+m} + \frac{c}{12} n(n^2-1)\delta_{n+m,0}, \\
[\bar{L}_n, \bar{L}_m] &= (n-m)\bar{L}_{n+m} + \frac{\bar{c}}{12} n(n^2-1)\delta_{n+m,0}, \\
[L_n, \bar{L}_m] &= 0,
\end{aligned} \tag{5.19}$$

where c, $\bar{c}$ are called *central charges*. The algebras of L_n and $\bar{L}_n$ are two copies of the so called *Virasoro Algebra*, they are identical to the Witt algebra, except for the central term characterised by the value of the central charges c, $\bar{c}$. There are different ways of introducing the Virasoro Algebra. If one for example asks for a projective representation of the Witt Algebra (this is a reasonable request, since in quantum mechanics we most often encounter projective representations, in fact we talk about rays in the Hilbert space and not about vectors in the Hilbert space), then the Virasoro Algebra is the central extension of the Witt Algebra and its representation is equivalent to a projective representation of the Witt Algebra [199, 200]. For a complete introduction we refer to the seminal article [67] as well as the many introductory textbooks [68, 198, 201]. Going back to our physical CFT we note that the operator $L_0 + \bar{L}_0$ generates the dilations $(z, \bar{z}) \to \lambda(z, \bar{z})$. It is easy to see that dilations correspond to translations along the radial dimension. After the mapping of the cylinder to the plane we have that time

level	**Eigenvalue**	**states**
0	h	$\|h\rangle$
1	$h+1$	$L_{-1}\|h\rangle$
2	$h+2$	$L_{-2}\|h\rangle$, $L_{-1}^2\|h\rangle$
3	$h+3$	$L_{-3}\|h\rangle$, $L_{-1}L_{-2}\|h\rangle$, $L_{-1}^3\|h\rangle$
$\vdots$	$\vdots$	$\vdots$

Table 5.1: Example of primary state and its first descendants, the complete set of states is called *Verma module*. The collection of the eigenvalues of L_0 of the not null states of the Verma module for a given primary state is called *Virasoro tower* or *Conformal tower*

.

flows along the radial direction, thus we have that $L_0 + \bar{L}_0$ generates time translations in the coordinate system of the complex plane.

This considerations leads us to consider $L_0 + \bar{L}_0$ proportional (up to a factor) to the Hamiltonian of the system, or, as we will call it, to the CFT Hamiltonian [67, 68, 198, 202].

5.2.4 The Hilbert space and Verma module

Suppose we have a state $|h\rangle$ that is eigenstate of L_0 (and $\bar{L}_0$) with eigenvalues h (respectively $\bar{h}$)

$$L_0|h\rangle = h|h\rangle \qquad (\bar{L}_0|h\rangle = \bar{h}|h\rangle). \tag{5.20}$$

Because of the commutation rules of the Virasoro algebra we have that

$$L_0 L_n|h\rangle = (h-n)L_n|h\rangle, \tag{5.21}$$

thus L_n are raising and lowering operators for $n < 0$ and $n > 0$ respectively.

We remind that the Hamiltonian is proportional (up to a factor) to $L_0 + \bar{L}_0$. In order for the energy of the system to be bounded from below there must exists a state that is annihilated by L_n with $n > 0$. Such a state is called *primary state* or *highest weight state* and it is the state of lowest energy.

Acting with the raising operators L_{-n} $(n > 0)$ on the primary states we obtain an infinite tower of states called *descendants* of the primary states that are an irreducible representation of the Virasoro algebra. If we know the eigenvalues of the primary states, we know the spectrum of the whole Hamiltonian. Acting with different raising operators on a primary state we note that the Hilbert space of the conformal states has a nested structure. There exist indeed multiple ways of constructing the descendants corresponding to the eigenvalue $h+2$. We can both act with L_{-2} to obtain the eigenstate $L_{-2}|h\rangle$ or just raising the primary state two times with L_{-1} to obtain the eingestate $L_{-1}L_{-1}|h\rangle$. This property creates an exponential growth of the dimensions of the degenerate L_0 eigenspaces (see table 5.1).

The collection of the primary state together with all its descendants is called Verma module. In constructing the Verma module one has to remember that states in a Verma module are not guranteed to be all linearly independent. The possibility of finding vectors that are a linear combinations of others depends on the structure of the Virasoro algebra for the given choice of the central charge c and of h. Linear combinations of states of the Verma module that vanishes are called *null states*. A great work has been done in analytically characterise null states (see e.g. [203, 204]). The represantion of a Virasoro algebra is constructed from the Verma module deprived of the null states.
The collection of the not null states of the Verma module for a given primary state is called *Virasoro tower* or *Conformal tower*.

Because of the one to one correspondence between operator and states in CFT (see [67]), it is possible to see that primary states are associated to primary fields and that the eigenvalues h are the conformal dimensions h of the primary field associated to the state. In particular, if $|0\rangle$ is the vacuum of the theory, the primary state $|h\rangle$ associated to the primary field $\phi(z)$ of conformal dimenions h is $|h\rangle = \phi(0)|0\rangle$.
The existence of a primary state implies the existence of a primary field and vice versa.

Unitary minimal models

In the last section we supposed the existence of at least one primary field. It possible though, that a theory with a primary field is impossible to build, as well as it is possible that every CFT results having an infinite number of primary fields. An answer to these doubts is found by restricting to unitary representation of conformal field theories with central charge $c < 1$ [205]. In this case one considers *unitary minimal models*. In particular, using the notation of [203], one parametrise a family of central charges with a parameter $\mathbb{N} \ni m > 2$ with the formula

$$c = 1 - \frac{6}{m(m+1)}. \tag{5.22}$$

For each value of c there are $m(m-1)/2$ primary fields, one for each value of

$$h_{r,s}(m) = \frac{[(m+1)r - ms]^2 - 1}{4m(m+1)}, \tag{5.23}$$

where r, s are the two positive integers $r = 1, \ldots, m-1$ and $s = 1, \ldots, m$.
Models characterised by central charges and primary fields defined by these formulas are known as *unitary minimal models*. Because of (5.22) and (5.23) unitary minimal models with $c < 1$ have only a *finite* number of primary fields.
The model corresponding to $m = 3$ is associated to the Ising model at the critical point [116,206]. In particular, in the case of the critical Ising model on the cylinder one consider also the generators $\bar{L}_n$ of the Virasoro algebra with central charge $\bar{c} = c = \frac{1}{2}$. The primary fields are thus described by two conformal dimensions $(h, \bar{h})$. It can be seen that the allowed primary states are $|0,0\rangle$, $|\frac{1}{2}, \frac{1}{2}\rangle$, $|\frac{1}{16}, \frac{1}{16}\rangle$, knowing their associated Virasoro Towers allows us to compute the spectrum of the CFT Hamiltonian of the Ising model.
At last, we note that the primary state $|0,0\rangle$ is always present as it is built out of the action of the identity operator on the vacuum $|0\rangle$ (and $|0\rangle$ is defined in any field theory). Because of the symmetry property of the vacuum $|0\rangle$, we have that $|0,0\rangle$ is annihilated by the generator of *global* conformal transformations $L_n, \bar{L}_n$ for $n = -1, 0, +1$.

Virasoro Tower for the minimal model $m = 3$

In [68] we can find a catalog for the degenerancies of the first level of the Virasoro towers for the three primary states $|0\rangle$, $|\frac{1}{2}\rangle$, $|\frac{1}{16}\rangle$. If we denote with $d(h, N)$ the degenerancies at level N of the Virasoro tower of the primary state corresponding to the conformal dimension h we have that, for the unitary minimal model $m = 3$, the degenerancies in the Virasoro towers are as in table 5.2.

N	0	1	2	3	4	5	6	7
$d(0, N)$	1	0	1	1	2	2	3	3
$d(1/16, N)$	1	1	1	2	2	3	4	5
$d(1/2, N)$	1	1	1	1	2	2	3	4

Table 5.2: Degenerancies at the low levels of the Virasoro towers of each of the primary state of the minimal model $c = \frac{1}{2}$, $m = 3$.

Conformal spectrum of the CFT Ising model

The CFT Ising model is the product of two copies of the Virasoro algebra $m = 3$ with generators L_n and $\bar{L}_n$. From table 5.2 it is possible to compute the low levels of the Virasoro towers associated to the primary states $|0\rangle$, $|1/16\rangle$, $|1/2\rangle$ of each of the two single Virasoro algebras. As we said in section 5.2.4 there are just three primary states $|0, 0\rangle$, $|\frac{1}{2}, \frac{1}{2}\rangle$ and $|\frac{1}{16}, \frac{1}{16}\rangle$ for the CFT Ising.

Joining the results of each single Virasoro algebra in a suitable way [198, 201], we obtain the towers of eingevalues of $L_0 + \bar{L}_0$ for the primaries and low descendants as reported in figure 5.3. Since the CFT Hamiltonian is proportional (up to a factor) to $L_0 + \bar{L}_0$, considering the three towers together we obtain the conformal spectrum of the Ising critical model.

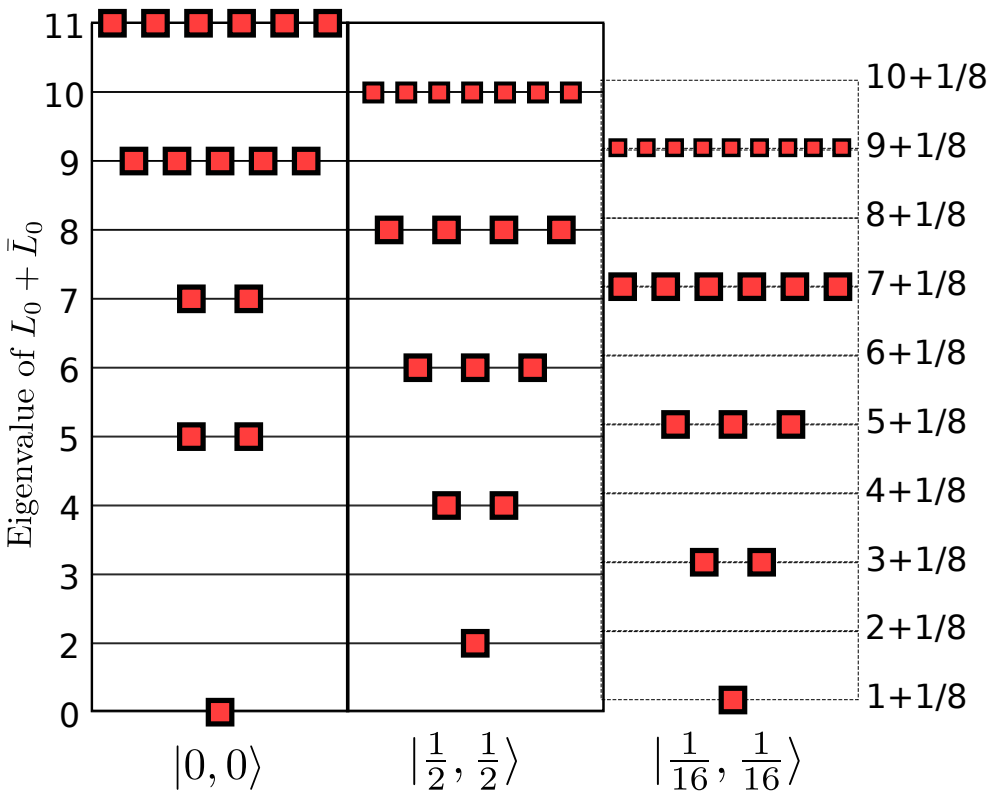

Figure 5.3: Conformal spectrum of the CFT Ising model Hamiltonian organised in Virasoro towers. On the right we use dashed line to highlight the positive $\frac{1}{8}$ shifting of all the horizontal line from their closest integer value.

5.3 The continuum limit of the Ising model

In section 3.5 we have seen how to map the transverse field Ising model Hamiltonian to the quadratic Fermionic Hamiltonian (3.120)

$$\begin{aligned}\hat{H}(g_F) = -J\Big(&\sum_{n=1}^{N-1}(a_n^\dagger - a_n)(a_{n+1} + a_{n+1}^\dagger) \\ &- g_F(a_N^\dagger - a_N)(a_1 + a_1^\dagger) - \cot(\theta)\sum_{n=1}^{N}(a_n^\dagger a_n - a_n a_n^\dagger)\Big),\end{aligned} \tag{5.24}$$

where $J > 0$ is a multiplicative factor, N is the number of sites of the chain, $g_F \in \{-1, 0, +1\}$ encodes the fermionic boundary conditions and $\theta \in [0, \frac{\pi}{2}]$ is the

parameter that control the strength of the transverse field. The relation between boundary conditions of the Ising Hamiltonian in terms of spins and the fermionised Ising Hamiltonian is explained in section 3.5. In the following we will consider the case $g_F = 1$. In this section, we want to compute the continuum limit of this Hamiltonian.

Already in chapter 4 we have studied the behaviour of some quantities related to this Hamiltonian in the limit for $N \to \infty$. Here we consider a different limit procedure. Denoting with s the lattice spacing, with continuum limit at the critical point we refer to the procedure of taking simultaneously the limit for $N \to \infty$, $s \to 0$, and $J \to \infty$ for some fixed value L of the product $Ns = L$ and for $Js = 1$. In our treatment we always considered the lattice spacing equal to 1, thus it was never explicitly appearing in the expressions. We start denoting the Dirac operators with the continuum (in the limit $s \to \infty$) Fermi fields

$$\Psi(x_i) = \frac{1}{\sqrt{s}} a_i, \qquad \Psi^\dagger(x_j) = \frac{1}{\sqrt{s}} a_i^\dagger, \tag{5.25}$$

where $x_i = si$ thus, for example, $\Psi(x_{i+1}) = \Psi(x_i + s)$, and where the factor $\frac{1}{\sqrt{s}}$ is chosen in order to obtain the correct commutation relations in the limit $s \to \infty$. In fact, in the limit $s \to 0$, $N \to \infty$ with $Ns = L$ fixed, Ψ and $\Psi^\dagger$ satisfy the anticommutation relation

$$\lim_{\substack{s\to 0 \\ N\to\infty}} \{\Psi(x_i), \Psi^\dagger(x_j)\} = \lim_{s\to 0} \frac{\delta_{i,j}}{s} = \delta(x_i - x_j), \tag{5.26}$$

where $\delta(x_i - x_j)$ is the Dirac delta function.

We substitute (5.25) in (5.24), take the limits explained above, and we obtain [207]

$$\hat{H}_F = \int dx \left[\Psi^\dagger \frac{\partial \Psi^\dagger}{\partial x} - \Psi \frac{\partial \Psi}{\partial x} \right]. \tag{5.27}$$

The procedure for obtaining this field theory from the TFI Hamiltonian is often called *scaling limit*.

In order to see the connection between this Hamiltonian and its underlying CFT model it is necessary to represent the dynamics induced by H_F with the formalism of path integral. The full derivation can be found in [198]. We report here that the action in euclidean time is

$$S = \frac{1}{2\pi}\int dz d\bar{z}\left(\psi(z,\bar{z})\partial_{\bar{z}}\psi(z,\bar{z}) + \bar{\psi}(z,\bar{z})\partial_z\bar{\psi}(z,\bar{z})\right), \tag{5.28}$$

that is the action of a free massless real fermion model.
We can see that if Ψ and $\bar{\Psi}$ have conformal weight $(h,\bar{h}) = (\frac{1}{2},0)$ and $(h,\bar{h}) = (0,\frac{1}{2})$ respectively, then the action is conformal invariant

$$\begin{aligned}
S' &= \frac{1}{2\pi}\int dz d\bar{z}\left[\Psi'(z,\bar{z})\partial_{\bar{z}}\Psi'(z,\bar{z}) + \bar{\Psi}'(z,\bar{z})\partial_z\bar{\Psi}'(z,\bar{z})\right] = \\
&= \frac{1}{2\pi}\int \frac{\partial z}{\partial w}\frac{\partial \bar{z}}{\partial \bar{w}} dw d\bar{w} (\frac{\partial w}{\partial z})^{1/2}\frac{\partial \bar{w}}{\partial \bar{z}}\Psi(w,\bar{w})\partial_{\bar{w}}(\frac{\partial w}{\partial z})^{1/2}\Psi(w,\bar{w}) + \\
&+ (\frac{\partial \bar{w}}{\partial \bar{z}})^{1/2}\frac{\partial w}{\partial z}\bar{\Psi}(w,\bar{w})\partial_w(\frac{\partial \bar{w}}{\partial \bar{z}})^{1/2}\bar{\Psi}(w,\bar{w}) = \\
&= \frac{1}{2\pi}\int dw d\bar{w}\left[\Psi'(w,\bar{w})\partial_{\bar{w}}\Psi'(w,\bar{w}) + \bar{\Psi}'(w,\bar{w})\partial_w\bar{\Psi}'(w,\bar{w})\right].
\end{aligned} \tag{5.29}$$

This conformally invariant action leads to a theory with central charge $c_{\text{Ising}} = \frac{1}{2}$ that corresponds to the CFT Ising Model [198, 206, 208].
As we said in the last section the CFT Ising model is characterised by the three primary states $|0,0\rangle$, $|\frac{1}{2},\frac{1}{2}\rangle$ and $|\frac{1}{16},\frac{1}{16}\rangle$ thus its conformal spectrum will be the union of the three conformal towers associated to the three primary states (see figure 5.3). From section 3.5 we know that the spectrum of the Ising model is divided in two parity sectors. The same division appears also in the case of the free fermions theories on a circle. Here the two sectors are individuated by the realisation of different primary fields. In the sector with periodic boundary conditions, called Neveu-Schwarz sector, are realised the Virasoro towers associated to $h = 0$ and $h = 1/2$, while in the sector with antiperiodic boundary condition, called Ramond sector, is realised the Virasoro tower associated to $h = 1/16$.

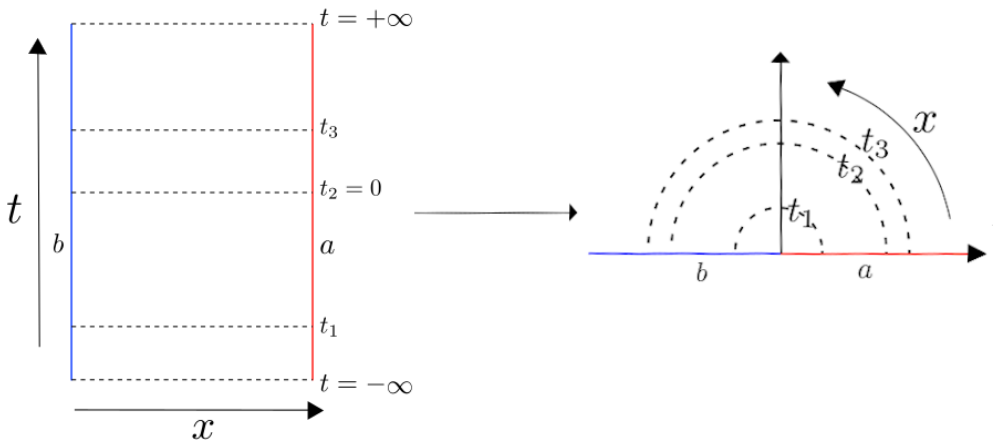

Figure 5.4: Mapping from the strip to the upper half complex plane. The boundary conditions are highlighted in blue and red.

5.4 Conformal field theories with boundaries

In the previous sections we have studied conformal field theories on a cylinder with periodic boundary conditions. In many different cases one is interested in physical systems with open boundary conditions. CFT defined for specfic boundary conditions are called Boundary CFT (BCFT) [209–212].

The request for specific boundary conditions on the systems are introduced during the step of compactification of the space dimension. In the case of open boundary conditions one restricts the spatial coordinate to $x \in [0, \pi]$, obtaining the geometry of an infinite strip instead of that of an infinite cyilinder. One then proceed applying the same mapping to the complex plane $z = e^{(t+ix)}$ used precedently and finds that the system is now mapped to the upper half part of the complex plane and the two boundary conditions a, b are defined on the positive and negative real axis (see figure 5.4).

One consequence of considering a CFT defined only on the upper half complex plane, is that, in this case, it is possible to consider just a single set of Virasoro generators L_n [213]. Consider for example the critical Ising model with open boundary conditions, the Hamiltonian in this case is proportional to L_0 and it is described by a single copy

of the Virasoro algebra of the unitary minimal model with $c = \frac{1}{2}$.

Differently from CFTs on the whole plane, these will be specified not just by the central charge, but by the knowledge of the boundary conditions a, b. For the Ising model on the upper half complex plane we thus have that the Hamiltonian is proportional (up to a factor) to L_0 and just three different values for the boundary conditions a and b are admitted. In chapter 7 we will report the conformal spectrum of the Hamiltonian of the BCFT Ising on the upper half complex plane for different combinations of the boundary conditions.

Chapter 6

Finding the low parts of the entanglement wall trading entanglement with mixture

In chapter 2 we have seen two clashing properties of many-body quantum systems out of equilibrium. We have seen how moving out of equilibrium the resources needed to describe a state grow exponentially in time. Concurrently, we have seen that many-body quantum systems are expected to locally equilibrate in the long-time regime. The equilibrium states so reached can be efficiently approximated with the encoding tools described in chapter 2.

This puts us in the situation where starting from an efficiently encodable state, evolving it out of equilibrium we have to pass through a stage of the evolution requiring an enormous amount of computational resources in order to obtain an equilibrium state that is again efficiently encodable.

Being a curse for the out-of-equilibrium simulations, this high complexity middle phase, got the infamous name of *entanglement wall* [214–216].

The growth of computational resources is due to the the linear growth of entanglement out of equilibrium, linear growth that is due to the spreading of correlations in the system. As we have seen in chapter 4 correlations spread inside the system in a localised fashion.

In this chapter we are going to exploit this locality property in order to surpass the entanglement wall. In particular we exploit the idea of transforming entanglement due to long-distance correlations into local entropy. We present our proposal [217] for a novel algorithm that allows to systematically approximate the equilibration value of local operators after a quantum quench.

6.1 Introduction

Simulating the time evolution of many-body quantum systems by classical means is hard. In fact, simulating an N constituents system requires storage and computation time that scale exponentially with N.

In order to understand how this exponential growth can limit our simulations, consider for example a system of N qubits. Characterising a state $|\psi\rangle$ requires to specify 2^N complex coefficients. Now suppose we want to store the information about the state in a computer. We decide to encode each real number with a `Float64`, so that storing a single complex coefficient requires 2^7 `bit`. This implies that storying the whole state would require $\sim 1.6 \cdot 10^{-8} \cdot 10^{0.3N}$ `Gigabytes`. This is a requirement of almost 20.000 `Gigabyte` of memory for just 40 qubits.

The problem of the exponential growth of the resources needed to completely describe a many-body system is not exclusive to quantum mechanics. Already in statistical mechanics the number of possible configurations grows exponentially with the number of constituents of the system. In this context, exploiting the specific structure of some systems has led to the creation of efficient classical algorithms for the simulation of classical many-body systems. We remind, for example, how in classical statistical mechanics, using Monte-Carlo techniques, one is able to simulate a system efficiently sampling only on a polynomially-large set of configurations [218]. Efficient algorithms have been devised also for quantum mechanical systems, we showed in chapter 2 how, with MPS and MPO ansatzes, we are able to efficiently compress the ground and thermal states of gapped local Hamiltonians, as we are able to simulate the short time evolution of some systems out of equilibrium.

Traditional tensor networks techniques are a powerful tool for describing states with

local correlations [18, 19, 109], but they fail as soon as the locality of correlation is lost. This is what happens in the context of many-body quantum systems out-of-equilibrium. Consider for example a dynamics obtained with a quench process. Here initially localised correlations spread across the system [52, 53] leading to a fast growth of entanglement. Since the resources needed to describe a system with tensor network techniques strongly depend on the amount of entanglement present in the state, soon enough, the resources needed to describes the current state are grown too much. Simulating the time evolution from this point forward results unaffordable if we want a good approximation. It is said that the evolution just hit the "entanglement wall".

The quest of getting on top of the wall is, in its most general form, quite hard, if not even impossible. Here we will focus to the specific case of systems that, in the long-time regime, are expected to locally equilibrate to some state well approximated with traditional tensor network techniques. In this scenario, we will focus of finding a locally consistent approximate dynamics as schematised in figure 6.1. We know, in some sense, that what we want to obtain is behind the wall and not above it, so we just decide to pass through the wall.

6.2 Robust aspects of quantum quenches

We will focus on the out-of-equilbrium dynamics that follows a quantum quench (see section 4.0.1 and [219]). Consider a local Hamiltonian $H(\theta)$ dependent on the parameter θ. As explained in section 4.0.1 a quench protocol is composed by two steps. We take the ground state $|\psi(\theta_0)\rangle$ of $H(\theta_0)$ and we evolve it with the new Hamiltonian $H(\theta_1)$. This evolution is described by:

$$|\psi(t)\rangle = e^{-itH(\theta_1)}|\psi\rangle. \tag{6.1}$$

Cardy and Calabrese [52] showed that in this setting the entanglement entropy between two different partitions of $|\psi(t)\rangle$ grows linearly in time, a footprint of the

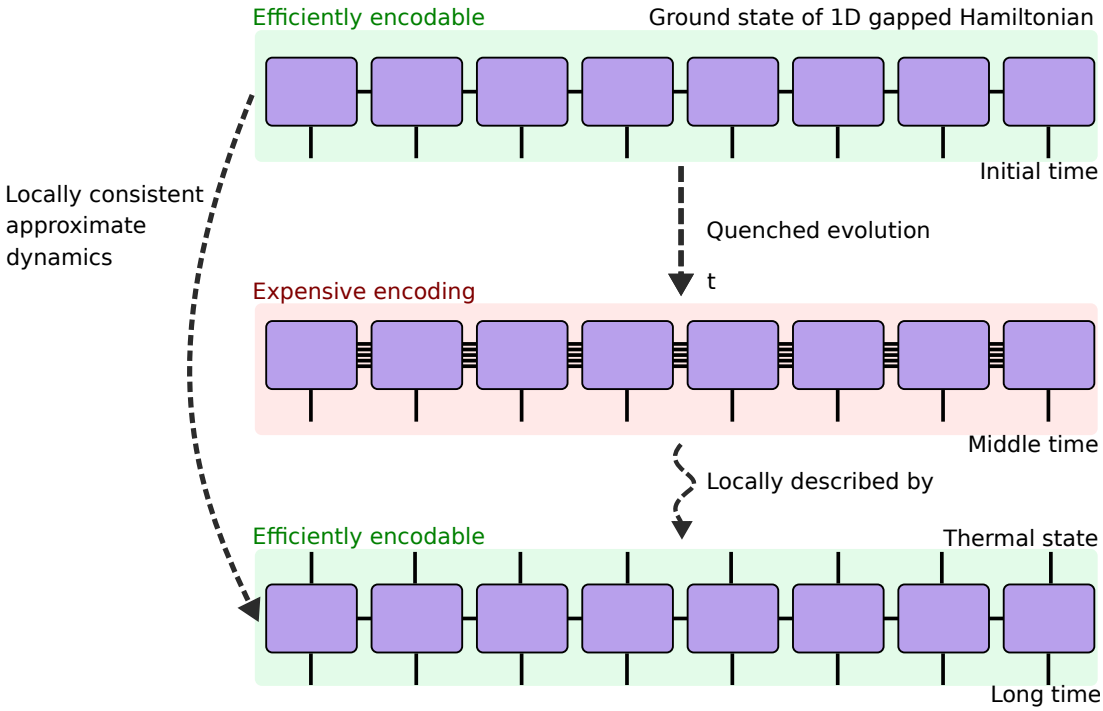

Figure 6.1: From top to bottom the three time scales of the dynamics out of equilibrium after a quantum quench. At the initial time the state is the ground state of a 1D Gapped Hamiltonian, it is easily encondable with an MPS. The entanglement grows during the dynamics (represented by the growing number of connections between the purple boxes), gradually the state becomes too expensive to be represented with an MPS. We hit the entanglement wall. In the long-time regime the state equilibrate to a state locally well approximated by an easy to describe equilibrium state (as for example a thermal state). Thermal states have an efficient representation as MPO. The aim of the presented algorithm is finding a locally consistent approximate dynamics that would allow to go from the initial time to the long-time regime, avoiding the entanglement wall.

radiation of the correlation as pseudo-particles [52, 149, 163, 164, 168]. This leads the corresponding states to become too entangled and hard to represent with standard tensor network algorithms after relatively short times [31, 43] [1]. The quenched system hits the entanglement wall.

We have to give up trying to compute a complete description of the state at each step of the dynamics.

We focus instead on the robust features of the out-of-equilibrium dynamics after a

[1] Here we consider only systems whose excitations are extended and can be described using pseudo particles.

quench, that is, features that are not too sensitive to the specific details of the quench. One of such features is the equilibration of local observables occurring at long times after the quench.

As motivated in chapter 4, if a closed quantum system equilibrates, the value of the relaxed local observables is predicted by its diagonal ensemble. The DE of a state ρ with respect to the Hamiltonian H is defined as

$$\rho_{DE(H)} \coloneqq \mathcal{J}\mathrm{J}_H(\rho), \tag{6.2}$$

where $\mathcal{J}\mathrm{J}_H$ is the complete dephasing map with respect to the eigenbasis of H (see eq (4.7)).

We remind here that, in order to construct the diagonal ensemble $\mathcal{J}\mathrm{J}_H(\rho)$, one needs to be able to build the completely dephasing map $\mathcal{J}\mathrm{J}_H$ and this requires to diagonalise the Hamiltonian H. This is an exponentially hard task in the number of constituents of the system. In the case of ETH Hamiltonians (see section 4.2.1) the DE is locally approximated by the Gibbs Ensemble

$$\rho_H(\beta) \coloneqq \frac{e^{-\beta H}}{Z}, \tag{6.3}$$

where $Z \coloneqq \mathrm{Tr}\left[e^{-\beta H}\right]$. The inverse temperature β of the approximating Gibbs ensemble is defined by imposing $\mathrm{Tr}\left[\mathcal{J}\mathrm{J}_H(\rho)H\right] = \mathrm{Tr}\left[\rho_H(\beta)H\right]$ and thus, only depends on the energy of the initial state ρ. This suggests us that, as long as we are conserving the information about the initial energy of the state, we should have enough information to be able to build a good approximation of the state that approximate the value of the relaxed local observables. For those systems described by a local Hamiltonian, the energy is conserved if we conserve short-range correlations. As a result, by designing an approximated dynamics conserving short-range correlations, the robustness of the thermalisation process forces the convergence to the correct state, in spite of discarding the long-range correlations.

We will benchmark our algorithm with free Fermions. As explained in section 3.6 non-interacting systems are often used as a first benchmark for tensor network

algorithms, see for example [220]. Following this methodology one is able to study the relevant effects of the approximation using larger systems with respect to the use of tensor network techniques. Nonetheless, in order for the benchmark to be informative, one has to pay attention to the special characteristic of the system considered. In our case, non interacting Fermionic systems do not satisfy the ETH. The relaxed state of a Fermionic system depends on the initial occupation of all the free modes since these are conserved during all the evolution (see chapters 4 and 3). Containing more information about the initial state than just the total energy, the system of the relaxed state cannot be approximated by the Gibbs ensemble. Instead, the equilibrated state is locally described by the *Generalised Gibbs Ensembles* (GGE). If the Gibbs ensemble is defined as the state that maximise the entropy at fixed value of the energy, the GGE can be defined as the state that maximise the entropy at a fixed value of all the conserved quantities (see section 4.1.3 for a discussion about the possible definitions of the GGE [149, 163, 182, 184, 221–227]) . Luckily a weaker notion of robustness can be recovered. The occupation of the free modes can be re-expressed as the conservation of charges whose densities are defined on bounded regions of the lattice. This corrseponds to the equivalence of the construction of the GGE discussed in chapter 4. We can thus sort the conserved charges by the dimension of the support of their density. Charges whose densities have support on smaller blocks are more local than those with support on larger blocks.

This methods defines a weaker notion of robusteness on which our benchmark relies. Any algorithm correctly describing short-range correlations is forced by this weaker robustness to convergence to a truncated version of the GGE. We both design and characterise such an algorithm in the following sections. Before moving to the next section we want to remind here the relations between the GGE and the DE explained in chapter 4.

It is known that the set of Fermionic Gaussian states is not a convex set (see chapter 3 and [189]). This tells us that the DE, being an infinite average of Gaussian states is not guaranteed to be a Gaussian state. At the same time since the space of Fermionic Gaussian states is closed under the evolution with Fermionic quadratic Hamiltonian,

we expect that at any time the state we are going to deal with must be Gaussian, even the relaxed state. For this reason, instead of considering the full DE, we are going to consider its projection on the space of Fermionic Gaussian state. We are going to call this projected state Gaussian Diagonal Ensemble (GDE). It is interesting to note that, in the case we are going to consider, the GDE corresponds to the GGE. Since the projection on the space of Fermionic Gaussian states preserves the expected value of all the two point correlators, we have that the value of the two point correlators of the GGE corresponds to the same value computed with the GDE, that are the same value computed with the DE.

6.3 The algorithm

Taking inspiration from the TEBD [11], t-DMRG [228, 229] and their more recent developments (see for example [230]), the algorithm we introduce is designed to work with tensor network states.
In particular the algorithm exploits the ablities of tensor network techniques, to encode efficiently slightly correlated states and the ability to perform, almost exactly, their short-time dynamics.

Concurrently, the algorithm differs from traditional tensor network techniques for two main reasons:

1. MPS ansatz rely on a repeated application of the singular value decomposition followed by a truncation of some singular values. The Eckart-Young-Mirsky theorem tells us that this is the best fixed rank approximation with respect to the Frobenius norm distance (see section 2.3.4). The Frobenius norm distance does not encodes any notion of locality. Our algorithm, instead, ensures that the approximated state has the short-range correlations of the state we want to approximate.

2. The approximate state computed by our algorithm can be encoded with available resources even after the short-time dynamics.

3. The approximated state computed by our algorithm is a mixed state, as the one that we expect to locally approximate the equilibrated state. The ideas is to trade entanglement with mixture. TEBD algorithms on pure states returns pure states.

By using 1) we exploit the idea of robustness; with 2) we make sure that the algorithm is practically useful, also at long times. The choice of 3) is because we want to obtain an approximation of the state that approximate the equilibrium state, namely the GGE.

In Fig. 6.2 we present our algorithm in the case of a 1D system using standard tensor network notation. The algorithm is divided in three steps, each represented in a panel.
The initialisation step is in panel a).

We start by the encoding the initial state with an MPS, the blue rectangles at the top of the panel, and the time evolution as an MPO, the light-blue circles in the middle of the panel. At the bottom of the panel we have the MPS of the state after one step of the time evolution. Evolving the state for a sufficient time, the computational resources needed to encode the state as an MPS would exceed our resources. We have to approximate the state if we want to proceed with the evolution.

At the top of panel b) we have the MPS that we want to approximate with a mixed state $\rho(0)$ encoded in the MPO (the orange circles in the second line). In order to find the tensors of the MPO representation of $\rho(0)$ we force the local reduced density matrix to be indistinguishable up to a fixed precision. This can be done variationally. This step is illustrated in the third line of panel b) where the $m = 3$ sites reduced density matrix of the MPS state is forced to be indistinguishable to the $m = 3$ sites reduced density matrix of the MPO state. The size m of the reduced density matrix forced to be indistinguishable is our refinement parameter. In the case of $m = N$, where N is the dimension of the system, we obtain a t-DMRG simulation. In the fourth line of panel b) we compute a time step of the evolution of the MPO.

In panel c), after having evolved the MPO for enough time, the computational resources needed to describe the state exceed again our capabilities. We approximate the state again with another MPO of fixed operator Schmidt rank imposing the

indistinguishability of the $m = 3$ sites reduced density matrices of the state before and after the approximation. We proceed iterating the step of panel c) until local variables equilibrate.

The main idea of the algorithm consist in trading the evolved state with a mixed state, precedure that can be interpreted as transforming the entanglement present in the initial state into mixture. This is exactly what is done when approximating the long-time equilibrium state with a thermal state. The difference, is that here we are performing this transformation already at relatively short times, and then repeating it iteratively.

This procedure of increasing the entropy at each step can be interpreted as an iterative implementation of Jayne's principle [136, 137].

At the same time, the local conserved quantities (relevant in the construction of the GGE) are protected from the approximations and thus kept constant. We thus expect that, as a consequence of the robustness of the equilibration, the process will equilibrate to a state locally indistinguishable from the DE.

It is clear that at very long times this approximation procedure is possible. It corresponds to building the maximum entropy mixed state that is locally identical to the locally equilibrated state. This would be a truncated generalised Gibbs ensamble [188]. In our case we do not know if the process of repeatedly applying the approximation, starting from the early stages of the evolution, is going to converge to the desired state anyway. We thus need to understand if mixed states that are locally indistinguishable from the states produced in early stages of the evolution exist, how to construct them, and the effects they induce once used at a given time as the starting point for the subsequent evolution.

Benchmarking with free Fermions allows us to separate any methodological difficulty associated with a tensor network algorithm from the physical effects that such approximation will produce. In fact, working directly with MPO would require, for example, choosing the norm to use in order to force the equalities in Fig. 6.2, we would not know how to construct an initial guess for it that can be variationally improved or how to design a tensor network algorithm guaranteed to converge to the

optimal MPO starting from this initial guess. We do not have clear control on the effect of the truncation of an MPO.

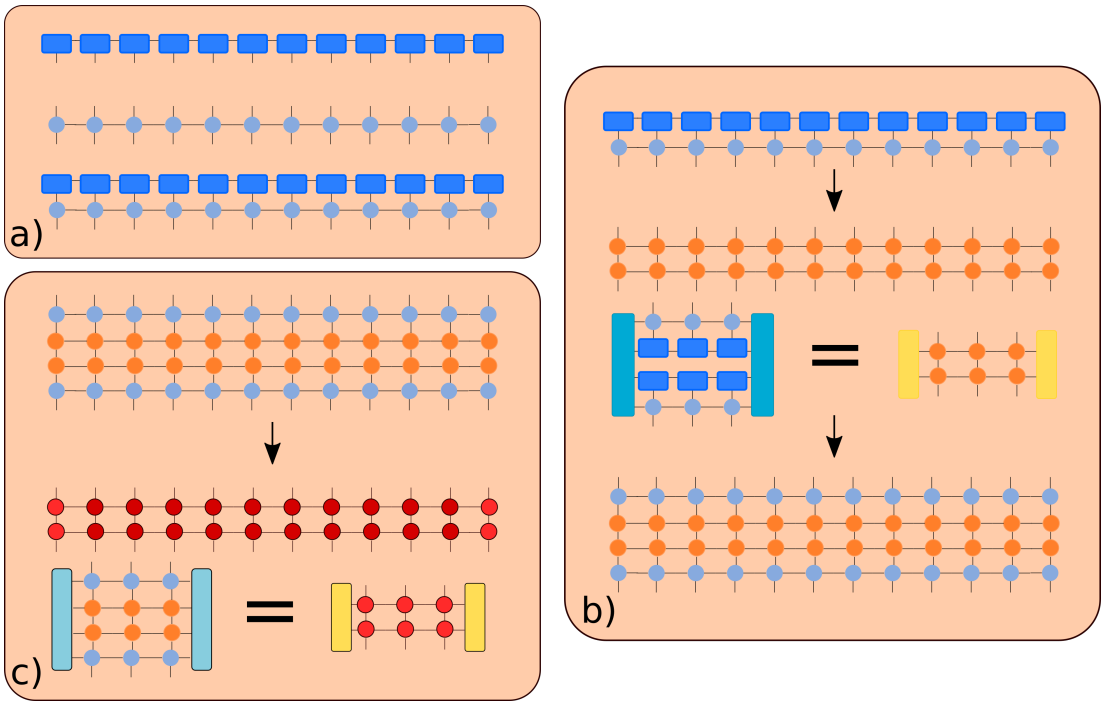

Figure 6.2: Tensor network scheme for the proposed algorithm. **a)** An initial state, represented by the MPS with blue boxes, is evolved for a short time applying the pale-blue MPO encoding the evolution. The evolved system is represented by the contraction of the MPS and the MPO. **b)** The evolved state becomes highly entangled, we decide to approximate it with a mixed state represented here by the orange MPO. In order to obtain the MPO we variationally search for it by imposing that its reduced density matrices up to distance m coincide exactly with those of the evolved state. Here $m = 3$. Subsequentely the best MPO approximation of the evolved state is evolved again for short times. **c)** The dynamics increases again the amount of computational resources needed beyond the one we can deal with. We approximate the MPO with an MPO with lower operator-Schmidt rank (in red in the figure). The key point of the approximation is always forcing the local indistinguishability of the approximate state and the evolved one, for all the contiguous blocks of size up to m.

We will benchmark the algorithm with Fermionic quadratic Hamiltonians and Fermionic Gaussian states. As a specific example we will consider the Fermionic transverse field Ising model (3.122)

$$H(\theta) = -\sum_{i=0}^{N-1}\left[a_i^\dagger a_{i+1} - a_i a_{i+1}^\dagger + a_i^\dagger a_{i+1}^\dagger - a_i a_{i+1}\right] + \\ - \cot(\theta)\sum_{i=0}^{N-1}\left[a_i^\dagger a_i - a_i a_i^\dagger\right]. \tag{6.4}$$

The ground state of this Hamiltonian can be completely characterised by its correlation matrix

$$\Gamma_{i,j} = \langle \vec{\alpha}_i \vec{\alpha}_j^\dagger \rangle, \tag{6.5}$$

where $\vec{\alpha}^\dagger = \left(a_1, a_2, \ldots, a_N, a_1^\dagger, a_2^\dagger, \ldots, a_N^\dagger\right)$ is the collection of annihilation and creations operators for every site.

We study the case of the out-of-equilibrium evolution generated by a sudden quench of the Hamiltonian. We start from the ground state Γ_0 of the Hamiltonian (6.4) for a given θ_0, $H(\theta_0)$ and we evolve it with the Hamiltonian $H(\theta)$, where $\theta \neq \theta_0$.

We are now interested in translating the algorithm of Fig. 6.2 in the language of Fermionic Gaussian states, in a similar fashion of what we do in section 3.6. In particular we need to translate the truncation step. In the language of f.g.s. the truncation step corresponds to defining a truncated matrix $\mathcal{TJ}_{\{a^\dagger a\},m}(\Gamma)$, with $m \in \left[0, \lfloor \frac{N}{2} \rfloor\right]$, obtained from Γ expressed in the basis of the Dirac operators $\{a^\dagger, a\}$ by setting all the matrix elements corresponding to correlations at distances $d > m$ to zero. We remark that for denoting the truncation operator we used the same symbol used for denoting the total dephasing operator (4.7), as the truncation with $m = 0$ of a correlation matrix is the analogous of the dephasing on the space of the correlation matrices. Whether $\mathcal{TJ}$ corresponds to the truncation operator or the dephasing operator will be understood from its argument.

Consider for example Γ, the correlation matrix of the f.g.s ρ, if $\{b^\dagger, b\}$ are the modes that express the f.q.h. H in diagonal form, we have

$$\mathcal{TJ}_{\{b^\dagger,b\},m=0}(\Gamma) = \Gamma(\mathcal{TJ}_H(\rho)). \tag{6.6}$$

In the following we will drop the basis specification $\{a^\dagger, a\}$ as it is implicitly specified

by Γ and denote the truncation operator just as $\mathcal{TJ}_m(\cdot)$. For every finite-size system made by N constituents, as m grows to $\tilde{m} = \lfloor \frac{N}{2} \rfloor$, $\mathcal{TJ}_{\tilde{m}}(\Gamma) = \Gamma$ and thus the approximation becomes exact.

We see that $\mathcal{TJ}_m(\Gamma)$ preserves all the reduced density matrices consisting of $m+1$ sites and, consequently, all the expectation values of local operators with support on $m+1$ contiguous sites. This corresponds to the implementation of the equality of panels b) and c) of 6.2.

With `F_utilities` it is possible to obtain $\mathcal{TJ}_m(\Gamma)$ using `Katana(Γ,m)`.

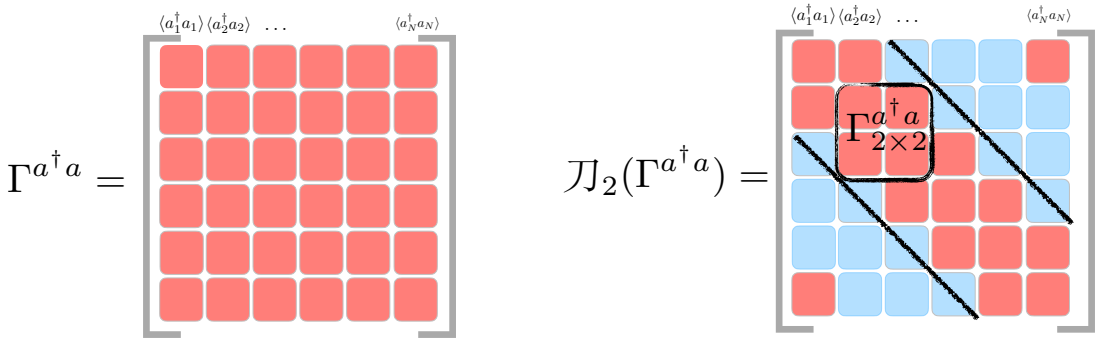

Figure 6.3: The action of the truncation operator on the top left quadrant of the correlation matrix Γ. The red squares indicate elements of the matrix with a definite value, the light blue squares indicate elements of the correlation matrix that are set to 0. Truncating at a fixed value of m preserves all the reduced correlation matrices of dimension $m \times m$, in the picture we represent a truncation at $m = 2$.

For the transverse field Ising Hamiltonian we are considering, setting $m \geq 1$ is enough to conserve the total energy of the state. From equation (6.4) we see that the information about the energy of a state is encoded in the nearest neighbour correalators. For a generic f.q.h. sum of operators with support on at most l neighbouring sites, the truncation preserves the energy if we choose $m \geq (l-1)$.

Furthermore, the truncation maps translational invariant states to translational invariant states, thus preserving translation invariance for every choice of m. We are now able to build the approximate time evolution algorithm by approximating Γ with $\mathcal{TJ}_m(\Gamma)$ at every step of the evolution. The translation of the algorithm of Fig. 6.2 in pseudo-code for f.g.s is reported in Algorithm 1.

Algorithm 1 Truncated time evolution of precision m

procedure TRUNC-EVOLV($\Gamma, N_s, \delta t, m$)
  $t \coloneqq 0$
  while $t < N_s$ **do**
    $\Gamma \coloneqq Katana(\Gamma, m)$ ▷ Truncation step
    $\Gamma \coloneqq Evolve(\Gamma, (H(\theta_1)), \delta t)$ ▷ Evolution step
    $t \coloneqq t + 1$
  end while
  return Γ
end procedure.

The `Evolve` step is performed with the `Evolve` function of `F_utilities`.

As a first observation, we remark that at each truncation step we are erasing some information, loosing in this way the unitarity of the exact dynamics. This process is reminescent of what happens during open dynamics that lead to thermalisation. We are indeed trying to obtain a good approximation of the Gaussian diagonal ensemble ρ_{GDE}.

As a second observation, we note that we do not have full control on the effect of the truncation effect on the state. Even if we are sure to preserve the local reduced density matrices of the sytem we do not know how the global state is changed. It can be even possible that the truncated correlation matrix is not a valid correlation matrix (a problem reminescent of the positivity problem after a Schmidt rank truncation in the MPO formalism).

Let us consider a simple example of the effect of the truncation. Consider the positive definite matrix

$$M = \begin{pmatrix} 4 & 3 & 2 & 1 \\ 3 & 4 & 3 & 2 \\ 2 & 3 & 4 & 3 \\ 1 & 2 & 3 & 4 \end{pmatrix} \tag{6.7}$$

this matrix has eigenvalues $\lambda_{1,2} = 6 \pm \sqrt{26}$ and $\lambda_{3,4} = 2 \pm \sqrt{2}$. The eigenvalues of $\mathcal{J}_1(M)$ are instead $\tilde{\lambda}_{1,2} = \frac{1}{2}(11 \pm 3\sqrt{5})$ and $\tilde{\lambda}_{3,4} = \frac{1}{2}(5 \pm 3\sqrt{5})$ and thus the positivity is lost.

We see that, in general, the truncation operation modifies the eigenvalues of the matrix. Since, in order to check this changes, we should diagonalise the whole correlation matrix before and after the truncation, we do not have real control on this changes. This means that we cannot know if the truncation step preserves the positivity of the state. The possibility of obtaining a not positive correlation matrix, implies that it is possible that a locally indistiguishable global mixed state could not exist or it is hard to identify. In the numerical analysis we will adress the question about the positivity.

Our exact results refer both to the full out-of-equilibrium dynamics of the system and to the GDE. Because of the local identification of the DE with the GDE explained at the end of section 6.2, with a slight abuse of notation we will refer to the GDE as DE.

6.4 Numerical results

We study in detail the dynamics for the quench in the ferromagnetic phase $\theta : \frac{\pi}{4} + 0.1 \to \frac{\pi}{4} + 0.3$ of the Hamiltonian (6.4). We compare the results with the one obtained for different quenches, both in the disordered phase and across the phase transition and we show that qualitatively similar results are obtained.

We use systems of three differents sizes.

We choose a large system with $N = 1500$ as our model for the dynamics in the thermodynamics limit. For this system we compare the long-time dynamics up to its recurrence time. For testing the dynamics induced by the algorithm we choose a system of dimension $N = 200$. This intermediate dimension allows us to study the effects of the truncation for many values of the refinement parameter m.

We then choose a small system of dimension $N = 41$. This system is used for the comparisons with a specific truncated dynamics that requires similar computational resources.

In all the numerical simulations we set the length of the time step to $\delta t = 0.25$.

We study the dynamics induced by the algorithm introduced in the last section.

Chosen the quench, the output state of the algorithm depends on three parameters: N the total dimension of the system, t the time for wich we want to compute the approximated dynamics and m the refinement parameter specifying the magnitude of the truncation. We denote the state as $\rho_N(t, m)$. In the case of the exact dynamics we simply omit m and denote the time evolved state with $\rho_N(t)$.
The first analysis we perform is on the behaviour of the single site occupation $n = a^\dagger a$ (we remind that the system is translationally invariant, thus the choice of a specific site is irrelevant). In particular we study the deviation of the dynamics of n from its expected equilibrated value computed in the GDE

$$\Delta_{N,m}(t) \coloneqq \langle n \rangle_{\rho_N(t,m)} - \langle n \rangle_{GDE}, \tag{6.8}$$

where we use the notation $\langle O \rangle_\rho = \mathrm{Tr}\,[\rho O]$.

In figure 6.4 we plot the evolution of $\Delta_{N,m}(t)$ for the systems we decided to analyse. Inspecting the blue curve, the one associated with the big system of $N = 1500$, we see the local equilibration towards the GDE in action. This is a consequence of the general results about the equilibration rate (measured as the damping of the envelope of the oscillations in figure 6.4). For this specific system we have that the envelope of the oscillations of the blue line converges towards $\langle n \rangle_{GDE}$ as a power law proportional to $t^{-\frac{3}{2}}$, in agreement with the predictions for the infinite system limit contained in section 4.1.4.
In the exact dynamics of the small and medium systems ($N = 41$ and $N = 200$) we can clearly identify the recurrence effects by the rebirth of large oscillations at later times. It is worth noting that before the recurrence effects become evident, the dynamics of the local observable is the same for all the sizes of the systems we have considered. In the inset of figure 6.4 we show the details of the dynamics in the first time part of the evolution. We can further appreciate the fact that, as expected, the recurrence time is proportional to the size of the system. In the thermodynamic limit the recurrence time is proportional to the maximum group velocity of the pseudo particles as it is the minimum time for the correlations to spread across the entire system [52, 149, 163, 164].

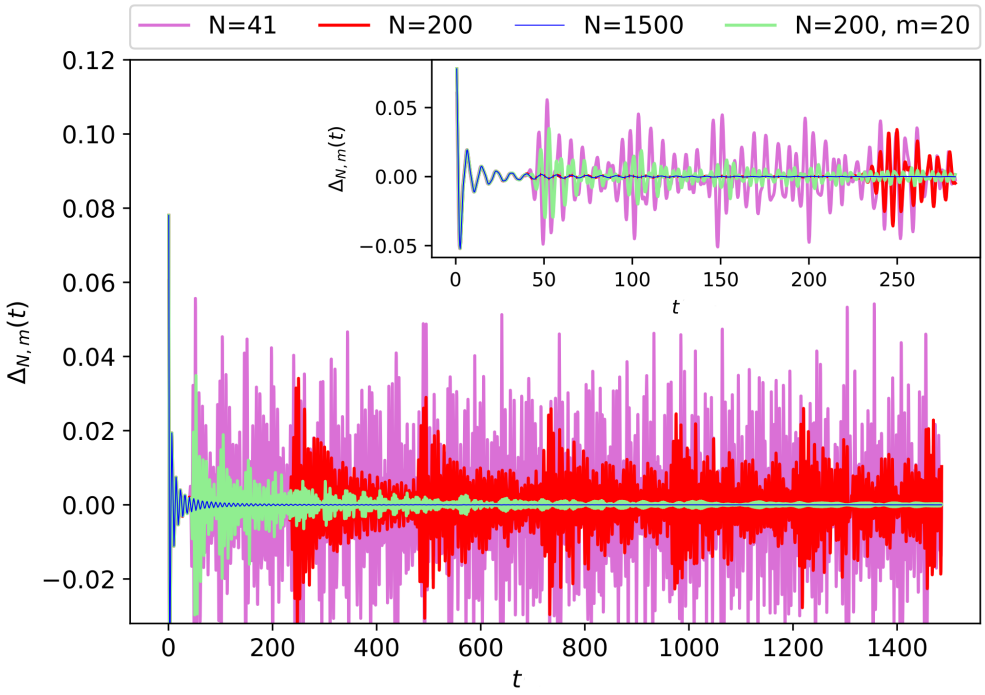

Figure 6.4: Time evolution of the quantity $\Delta_{N,m}(t) := \langle n \rangle_{\rho_N(t,m)} - \langle n \rangle_{GDE}$ for different values of the parameters N and m. In the inset a zoom on the first part of the dynamics where the recurrence effects for two exacts evolution and the approximation error deriving from the truncations are visible. In the main picture we plot the evolution for long-times. The truncated dynamic converges towards the GDE more slowly than the exact one.

The light green line in figure 6.4 represents the truncated dynamics $\langle n \rangle_{\rho_N(t,m=20)}$. As we can see from figure 6.3, the choice $m = 20$ implies that the truncation step always preserves the reduced density matrices of all the sub-systems of $N = m + 1 = 21$ consecutive sites and for each site it preserves all the correlations with $2m + 1 = 41$ sites. This explains our choice of $N = 41$ for the dimension of the small system. For the exact evolution of the small system, when correlations spreads at greater distances than 41, they meet again because of the periodic boundary conditions. This disturb the local equilibration process. The dynamics is unitary, no information on the initial state is lost and we have recurrence effects. For the truncated evolution, when correlations spreads at greater distances than 41 they get erased. Information is lost and the dynamics is not unitary anymore.

In the inset of figure 6.4, we compare $\langle\rho\rangle_{\rho_{200}(t,20)}$ with $\langle\rho\rangle_{\rho_{200}(t)}$. Because we chose as initial state the ground state of Hamiltonian (6.4) for $\theta = \frac{\pi}{4} + 0.1$, we see that the truncation does not affect the dynamics at short times. In fact the ground state of a gapped Hamiltonian has correlations that decay exponentially with the distance [18, 109, 231].

Focussing on the long-time dynamics of the truncated evolution, we see that erasing correlations spreaded at great distances completely changes the dynamics. The approximated dynamics deviates both from the one of the small system and from the one of the larger system (considered in our simulation as the system in the thermodynamic limit). We see for example that the envolope of the light green line in figure 6.4 shrinks with time even after the recurrence time expected for system of dymension $N = 41$ and $N = 200$. The approximated dynamics converges towards a value close to the one predicted by the GDE, we call this value $e(m = 21)$. In general, we call $e(m)$ the value towards which each truncated evolution with parameter m converges. We are interested in characterising the dependence of $e(m)$ from m and the trend of convergence of the truncated dynamics towards $e(m)$. We adress this analysis in figure 6.5. In the main figure we consider the trend of convergence during the truncated dynamics of the local occupations n towards its equilibration value $e(m)$. We plot the quantity $\log|\langle\rho\rangle_{\rho_N(t,m)} - e(m)|$ versus the logarithm of time, for the exact evolution of the big system and the truncated evolution of the medium system with $m = 10$. A linear behaviour highlights a power law convergence. In the case of the exact dynamics, we expect the equilibration value to be $e(\infty) = \langle n\rangle_{GDE}$. The linear fit on the exact dynamics returns a slope $\sim -\frac{3}{2}$ in complete accordance with the analytical prediticiton for system of infinite dimension in section 4.1.4 where the system equilibrates towards the GDE as $t^{-3/2}$. The linear fit for the truncated evolution has a slope qualitatively similar to the one of the exact dynamics.

In the inset of figure 6.5 we study the convergence of $e(m)$ towards the equilibration value predicted by the GDE.

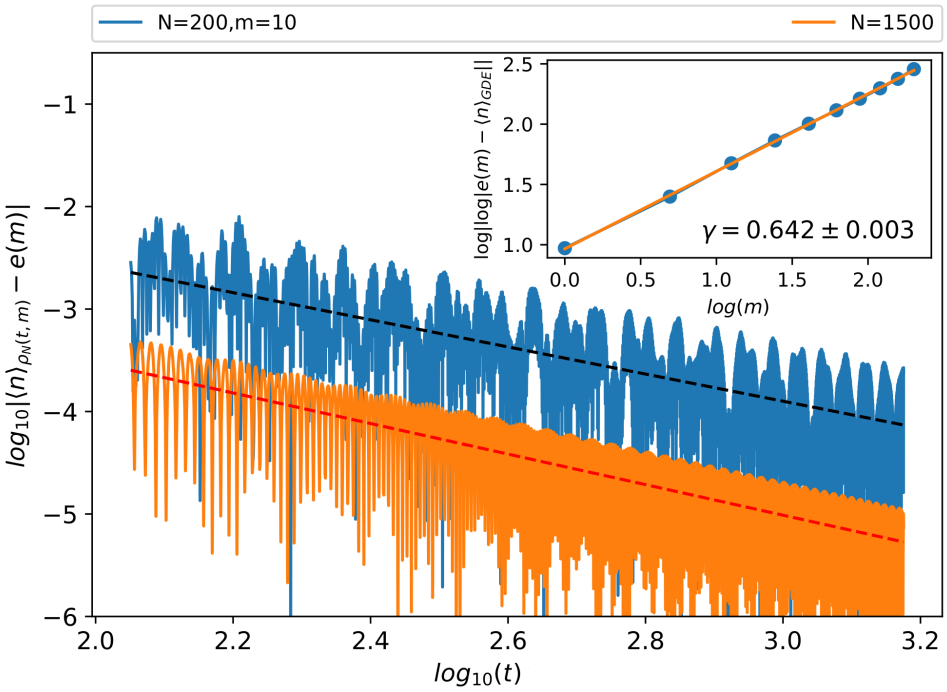

Figure 6.5: **(Main)** Logarithmic difference between $\langle n\rangle_{\rho_N(t,m)}$ and the expected equilibration value at a given m, $e(m)$, as a function of the logarithm of time. The exact dynamics converges algebraically to $\langle n\rangle_{GDE}$. The approximate dynamics converges algebraically to $e(10)$. The two dotted lines are linear fits to the data of the dynamics. The quantity $\langle n\rangle_{\rho_N(t)}$ converges to $\langle n\rangle_{GDE}$ as $t^{-\frac{3}{2}}$ for $t < T_R$, where T_R is the recurrence time for the given N. We qualitatively see that the truncated dynamics converges towards $e(10)$ with a similar trend. **(Inset)** Here we address the dependence of $e(m)$ on m. We plot the log-log difference between the equilibration values $e(m)$ and $\langle n\rangle_{GDE}$ as a function of $\log(m)$. The linear dependence suggests that $e(m)$ converges towards $\langle n\rangle_{GDE}$ as $(e(m) - \langle n\rangle_{GDE}) \sim e^{-m^\gamma}$. Our best fit gives an estimate $\gamma = 0.642 \pm 0.003$.

The data suggest a dependence

$$e(m) = e^{-m^{\gamma}} + \langle n \rangle_{GDE}, \tag{6.9}$$

where the value of γ, extracted numerically, is found to be $\gamma = 0.642 \pm 0.003$.

We perform an analogous analysis for different quenches. As shown in figure 6.6 the truncated dynamics of the local occupation for different quenches is qualitatively similar. With the process of equilibration we are expecting the system to locally

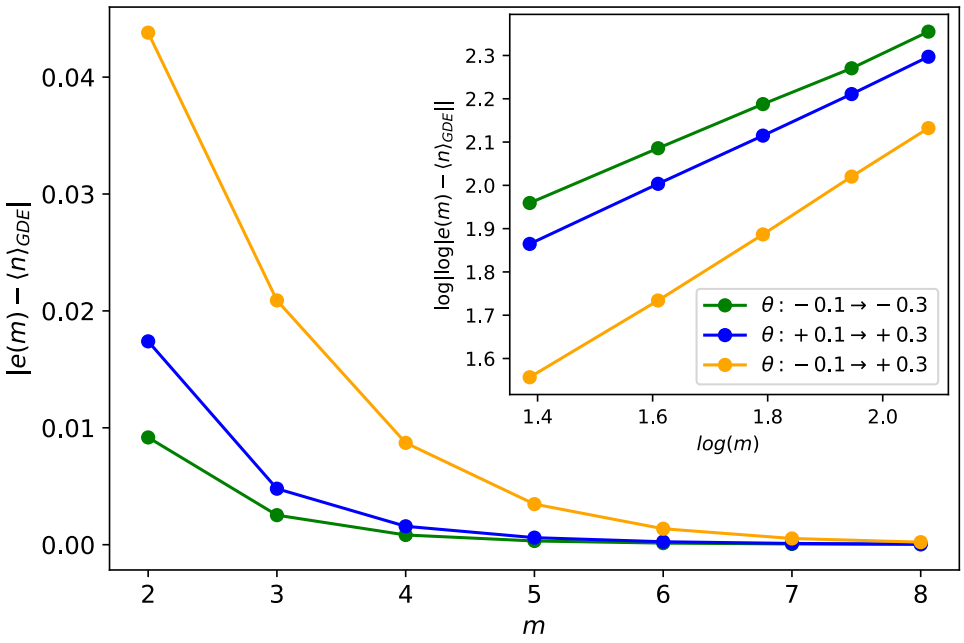

Figure 6.6: (**Main**) The difference $|e(m) - \langle n \rangle_{GDE}|$, where $e(m)$ is the equilibrium value of the local observable n for the truncated evolution with parameter m in the corresponding quench (different quenches correspond to different colours) and $\langle n \rangle_{GDE}$ is the value of n computed on the corresponding GDE. (**Inset**) We plot the same data of the main figure, with a suitable scale, in order to check the validity of the ansatz

equilibrate. In order to check if the algorithm is able to correctly capture this phenomenon, checking the dynamics of the local occupation is not enough. We thus turn to check the local convergence of the 2−sites reduced density matrices $\rho_N^{[2]}(m,t) := \mathrm{Tr}_{[3,\ldots,N]}[\rho_N(,t)]$ towards the 2− sites reduced density matrices of the GDE

$\rho^{[2]}_{GDE} \coloneqq \mathrm{Tr}_{[3,\dots,N]}[\rho_{GDE}]$. We report the results of this analysis in figure 6.7. In figure 6.7 we plot the time evolution of the trace distance

$$\mathcal{D}\left(\rho^{[2]}_N(m,t), \rho^{[2]}_{GDE}\right) = \frac{1}{2} Tr\left[\left|\rho^{[2]}_N(m,t) - \rho^{[2]}_{GDE}\right|\right] \tag{6.10}$$

in log-log scale.

The numerical values returned by the trace distance corresponds to the maximum probability of distinguishing between $\rho^{[2]}_N(m,t)$ and $\rho^{[2]}_{GDE}$ with a local measurement. From figure 6.7 we see that the 2−sites reduced density matrices, both of the exact as well as the truncated dynamics, converge towards the value predicted by the GDE with a behaviour qualitatively similar as the one of the local occupations of figure 6.5.

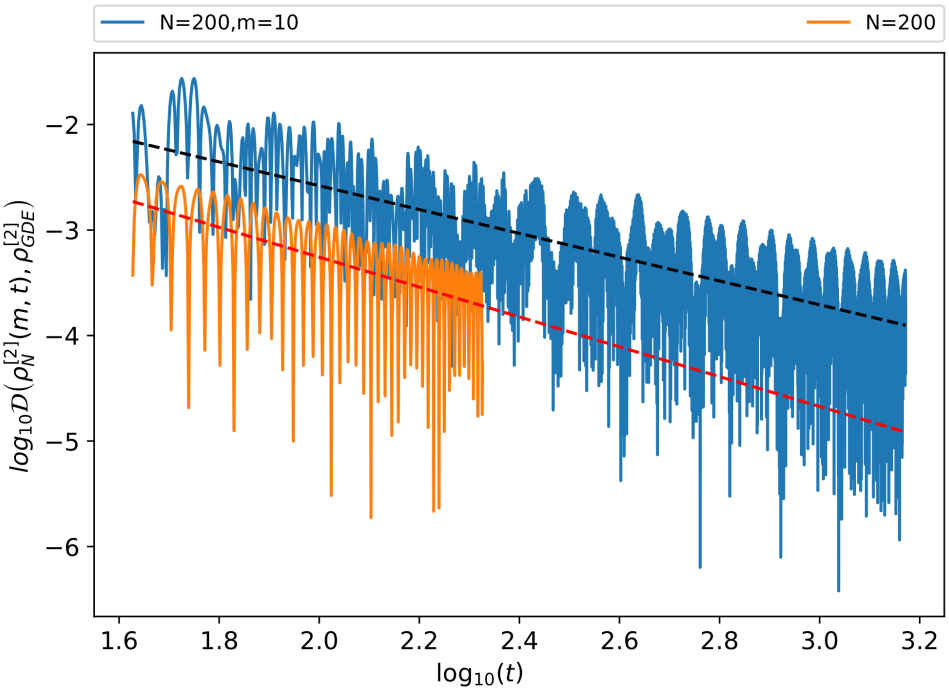

Figure 6.7: Time evolution of the logarithm of the trace distance $\mathcal{D}\left(\rho^{[2]}_N(m,t), \rho^{[2]}_{GDE}\right)$. Both the exact dynamics and the truncated dynamics locally converge towards the GDE.

Having found that the algorithms is able to predict an approximation of the local equilibration values, we are now interested in the effect of the truncated dynamics on

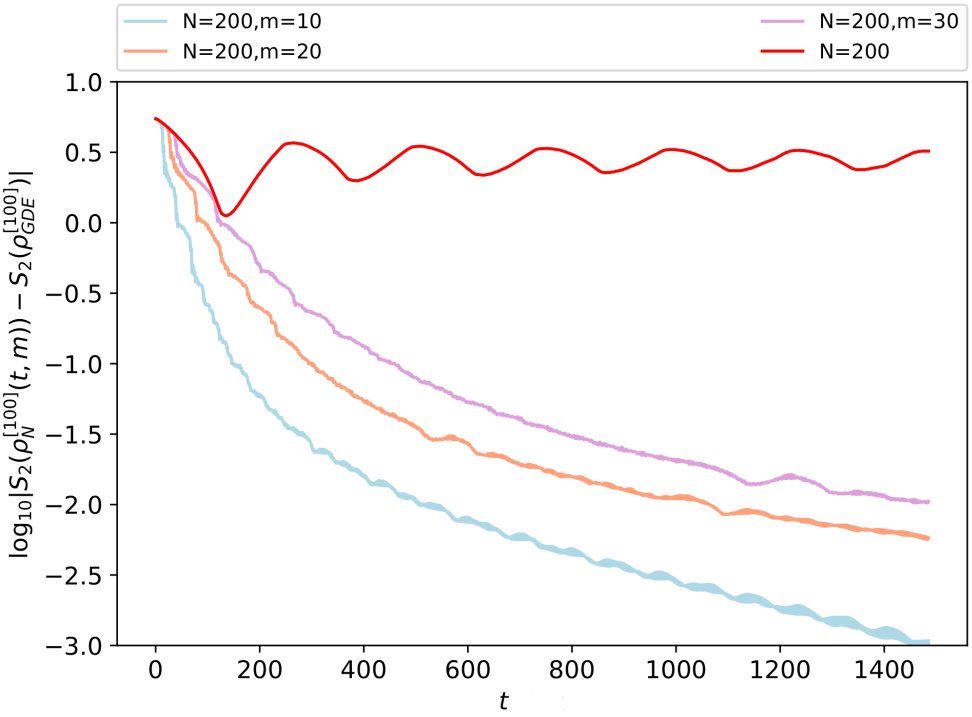

Figure 6.8: Logarithm of the time evolution of the difference between the second Reny entropy of the truncated state and the second Reny entropy of the GDE for a fixed partition of 100 sites and different values of m.

the state.

One of the ideas behind the algorithm is trading entanglement for mixture. A misure of mixedness of the state $\rho_N(m,t)$ is its purity. As we expect, the exact dynamic mantains the purity of the state. The truncated dynamics decrease the purity of the state, indeed transforming the state in a mixed state. As explained in the last section, the truncation step of the algorithm adds mixedness to the global system, while at the same time (for $m > 1$) conserving local densities, in perfect accordance with Jayne's principle.

We then consider the dynamics of a block of 100 consecutive sites described by the reduced density matrix $\rho_N^{[100]}(t,m) = \mathrm{Tr}_{101,\dots,N}[\rho_N(tm,)]$.

In figure 6.8 we study the time evolution of the second Reny entropy of $\rho_N^{[100]}(t,m)$. The second Reny entropy is defined for a generic density matrix ρ as

$S_2(\rho) = -\log(\mathrm{Tr}\left[\rho^2\right])$.
In particular we plot the quantity $|S_2\left(\rho_N^{[100]}(t,m)\right) - S_2(\rho_{GDE}^{[100]})|$ in logarithmic scale, for different values of the parameters N and m.

For the exact dynamics with $N = 200$, S_2 grows close to the value of $S_2(\rho_{GDE}^{[100]})$ before starting to decrease as a result of the recurrence. It then oscillates, with a frequency fixed by the size of the system.

In the truncated dynamics, correlations are not allowed to return into the partition, therefore, once spread outside, they are lost forever. We see that, indeed, the entropy always increases getting closer to $S_2(\rho_{GDE}^{[100]})$.
An interesting question, is wether or not the truncated algorithm preserves the physicality of the state. It is in fact not guaranteed that the matrix $\mathcal{J}\mathrm{J}_m(\Gamma)$ is a valid correlation matrix. The analogous of this question, in the language of density matrices, is asking if the $2^N \times 2^N$ Hermitian matrix $\rho(t,m)$ with trace 1 is positive or not. Checking if a matrix is positive requires diagonalising it. Diagonalising a $2^N \times 2^N$ is an unfeasible task already for small values of N. Even in the case of tensor networks, it has been shown that checking for the positivity is a task NP-hard in the dimension of the system [125].
In the case of Fermionic Gaussian states, checking the physicality of the state corresponds to check if the eigenvalues of the $2N \times 2N$ correlation matrix Γ lie between 0 and 1. Because of the properties of Γ, the eigenvalues of Γ appear in couples $(\lambda_i, 1-\lambda_i)$ (see chapter 3), thus to check the physicality it will be sufficient that no eigenvalues are negative.
We check if the physicality is conserved on average. In doing so we compute the truncated evolution for every allowed value of m for N_s number of steps. For every truncated evolution, we consider the average correlation matrix

$$\bar{\Gamma}(m) = \frac{1}{N_S}\sum_{t=1}^{N_s}\Gamma(t\cdot\delta t, m). \tag{6.11}$$

For each of the average truncated correlation matrix $\bar{\Gamma}(m)$ we consider the quantity

$$\mathcal{N}(x,m) = 1 - \frac{||\bar{\Gamma}(m)_x||_{l=1} - 1}{2} = 1 - \sum_i \frac{|\lambda_i| - \lambda_i}{2}, \tag{6.12}$$

where $\bar{\Gamma}(m)_x$ is the restriction of $\bar{\Gamma}(m)$ to the sites $[1,\ldots,x]$ (an analogous of the reduced density matrix on the first x sites if the global state were physical), and $\{\lambda_i\}_i$ are the eigenvalues of $\bar{\Gamma}(m)_x$. If the state is physcal, and thus Γ_m does not have negative eigenvalues, each term of the sum $\sum_i \frac{|\lambda_i|-\lambda_i}{2}$ is zero. Thus $\mathcal{N}(x,m) = 1$ for physical states. In general $\mathcal{N}(x,m)$ decreases as the absolute value of the sum of the negative eigenvalues of $\Gamma(m)_x$ increases.

In Figure 6.9 we plot $\mathcal{N}(m,x)$ versus m for different values of x. Each colour represents a different dimension of the reduced system we are considering. The value of m where a line reaches the value of 1 corresponds to the minimum value of m required for the truncated algorithm to preserve the physicality on average. The fact that for large enough m all the lines are at 1 tells us that for big values of m the correlation matrix $\overline{\Gamma}(m)$ is physical for every size x. In the inset, we plot the value of m where for the first time each line interesects the horizontal line $y = 1$. This is the minimum value of precision m_{phys} required for $\overline{\Gamma}(m)_x$ to be physical for every choice of its size x.

This fact should be related to the finite correlation length present in the GDE. In order to describe correctly the expectation value of a local operator we just need to embed the local system into a larger system whose size exceeds the correlation length of the desired state (see e.g. [129, 232–235]).

6.5 Conclusion

We have designed an algorithm for the efficient prediction of the approximated relaxed values of local operators in the out-of-equilibrium dynamics. The existence of such algorithm is explained by the presence of robust aspects in the out-of-equilibrium dynamics, that is, the presence of features that are not too sensitive to the specific details of the quench. One of such features is the equilibration

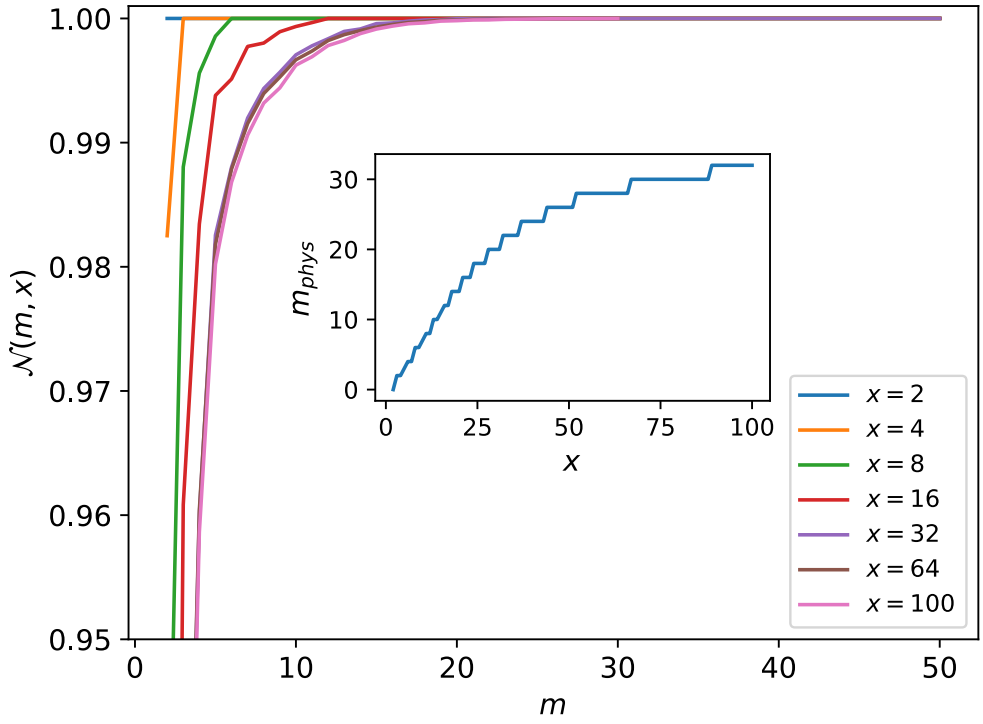

Figure 6.9: **(Main)** The value of $\mathcal{N}(m,x)$ versus m is plotted for different dimensions x of the reduced matrix $\overline{\Gamma}(m)_x$. When $\mathcal{N}(m,x)=1$ then $\overline{\Gamma}(m)_x$ is physical. **(Inset)** Minimum value of the precision m_{phys} for a specific x such that $\overline{\Gamma}(m)_x$ is physical. It is remarkable that, already for moderate values of m, the average approximate state is physical over a large range of distances.

of local observables occurring at long-times after the quench. As long as the relevant conserved quantities are protected from the approximation, it is possible to manipulate the description of the state for making it computationally affordable. In our algorithm the relevant conserved quantities are defined as the conserved quantities built out of local densities. The degree of locality of such conserved quantities naturally acts as the refinement parameter of the algorithm allowing to increase the precision of the results by increasing the computational cost.

We provided a benchmark of the algorithm with Fermionic Gaussian systems. In this context the approximation required by the algorithm corresponds to setting to zero the elements of the correlation matrix that encodes correlations at distances larger than a certain refinement parameters m.

We have observed that, in most cases, for moderate values of the refinement parameter m, our algorithm provides a good local approximation to the DE, by practically generating a dynamics that monotonically increases the entropy while exactly protecting the local conserved quantities. Furthermore, the precision of the approximation improves exponentially as we increase the value of m and, hence, the computational cost of the algorithm.

The results can be extendend checking if the same algorithm would give good results in the presence of strong interactions implementing the variational version of the algorithm using tensor networks as anticipated in the scheme presented in Fig. 6.2. Another possible further step in the development of these ideas would be relating this approach with the other proposed ideas for surpassing the entanglement wall [58, 236–241].

Chapter 7

Universal data in the entanglement spectrum of systems out of equilibrium

The equilibrium states of $1D$ gapped many-body quantum systems contain a limited amount of entanglement. In chapter 2 we have seen how the limited amount of entanglement can be exploited for the efficient encoding of these states. During the out-of-equilibrium evolution the entanglement grows. In chapter 6 we have investigated how to efficiently encodes states in this scenario.

At the Quantum Critical Point (QCP) Hamiltonians become gapless.

The equilibrium states of non-gapped quantum many-body systems are more complex, their entanglement grows with the dimension of the partition. This growth of the entanglement follows universal laws [65, 66] encoded in an underlying conformal field theory (CFT) model (see chapter 5). In this chapter we are going to see how the out-of-equilibrium evolution of the entanglement spectrums encodes information on the CFT describing the system at the quantum critical point.

7.1 Universality out of equilibrium

Approaching a quantum critical point can be dangerous if we want to faithfully and efficently simulate the system with standard tensor network techniques. It has been found that the entanglement entropy of a partition A of the ground state of a $1D$ gapped Hamiltonian tends to be a finite number independent from the dimension $|A|$ (this is an instance of the area law described in chapter 2). Approaching a quantum critical point, though, this finite number grows becoming, at the critical point, proportional to $\log(|A|)$.

This is where standard tensor networks techniques fail already at equilibrium.

This failiure does not imply an impossibility of describing the system in a compact way, it tells us, instead, that we should change the language of the description.

Moving closer to a quantum critical point, the correlation length is expected to grow much larger than the lattice spacing. In this regime, it is believed that, for the ground state of a quantum spin chain, the low-lying eigenstates and the behaviour of the correlations at long distance are described by a quantum field theory [69]. In particular, exactly at the quantum critical point, where the correlation length diverges, it is believed that the properties of these systems follow universal laws dictated by an underlying Conformal Field Theory (CFT). For example, for a CFT theory, in Ref. [110] it has been computed that

$$S(A) = \frac{c + \overline{c}}{6} \log_2(|A|), \tag{7.1}$$

where c is the central charge of the CFT. For the quantum transverse field Ising model at the Quantum Critical Point (QCP) it has been found by [66] that

$$S(A) \sim \frac{1}{6} \log_2(|A|) + k, \tag{7.2}$$

where k is a fixed numerical constant. The proportionality of entanglement to the logarithm of the dimension of the system is indeed in perfect agreement with the predictions of the CFT calculation as showed in the seminal works [66, 67, 69, 110, 242].

Often the specific data characterising the underlying CFT model are not known, but they can be found studying the behaviour of the system.

Because of the power of the universality, even studying the system in a really coarse way, we can retreive these universal data. For example we can make the choice of discretizing the space on a finite lattice and performing finite size scaling [243] or we can choose to study an infinite system restricting to a limited amount of entanglement in the ground state and performing finite-entanglement scaling [244].

As previously showed, the central charge of the CFT underlying the quantum Ising model can be deduced to be $c = \frac{1}{2}$ from the study of the entanglement entropy [69, 242].

The remaining data describing the underlying CFT are encoded in the entanglement entropy when the geometry of the partition A is more complicated [245–249].

We see again how entanglement happens to be a fundamental quantity, able to reveal information about the system we want to study. In this case it gives us access to universal information, without the necessity of understanding the details of the model, such as, e.g., the presence of an order parameter. Driven by these facts, several theoretical proposals on how to measure entanglement in experiments have led to the first experimental measures in the context of cold atoms and trapped ions [250–261]. Such experiments are able to measure entanglement not only of equilibrium states, but even during the out of equilibrium dynamics. This put experimental results ahead of theoretical predictions, in fact the entanglement wall prevents us from extracting reliable prediticton for the long-time out-of-equilibrium dynamics.

Even though exact solutions of the out-of-equilibrium dynamics are generally computationally too expensive, there exist several approximate methods, as the one presented in the previous chapter and the others cited therein, for approximating the dynamics. For every approximate method it is important to understand if it is able to retain information about relevant physical properties of the dynamics. Building our intuition on equilibrium phenomena, we can say that, if we are able to identify a form of out-of-equilibrium universality, this out-of-equilibrium universality should be detectable even through these approximate methods, after appropriate scaling

analysis. In the following we are going to discuss a form of universality based on the dynamics out of equilibrium. Universality out of equilibrium has been previously studied and observed in some specific scenarios. In [262] (see references therein for other examples) it is reported how the scaling of the spatio-temporal evolution of the system can be described by universal exponents and functions.

We are going to consider the quenched evolution of the transverse Ising field model in 1 dimension, providing numerical evidences that in various quench scenarios the entanglement spectrum of the evolved state contains informations about the specific conformal field theory describing the QCP.

7.2 Setup and relevant quantities

We are going to consider the quantum transverse field Ising model (see sections 3.5 and 5) described by the one parameter Hamiltonian (3.119)

$$H(\theta) = -\sum_{n=1}^{N-1} \sigma_n^x \sigma_{n+1}^x - \cot(\theta) \sum_{n=1}^{N} \sigma_n^z - g_I \sigma_N^x \sigma_1^x, \tag{7.3}$$

where N is the number of sites, σ_i^α with $\alpha = x, y, z$ are the Pauli matrices at the i-th site, and $\cot(\theta)$ is the magnetic field, with $0 \leq \theta \leq \frac{\pi}{2}$. The parameter g_I encodes the boundary conditions of the lattice. In the following we are going to consider systems with Open Boundary Conditions (OBC) and Periodic Boundary Conditions (PBC) corresponding to the choices of $g_I = 0$ and $g_I = 1$ respectively.

At zero temperature this system exhibits two phases: an ordered (ferromagnetic) phase for $\theta \in (\frac{\pi}{4}, \frac{\pi}{2}]$ and disordered (paramagnetic) phase for $\theta \in [0, \frac{\pi}{4})$. The two phases are separated by a QCP at $\theta = \frac{\pi}{4}$.

We consider every system divided in two complementary partitions, a partition A made by ℓ contiguos sites and the complementary partition B made by $N - \ell$ contiguous sites. We are going to study two quantities. The first one is the Entanglement Entropy (EE), defined as the von Neumann entropy $S(A)$ (3.87) of the reduced density matrix $\rho_A = \mathrm{Tr}_B\,[\rho]$

$$S_A \coloneqq -\mathrm{Tr}\,[\rho_A \log(\rho_A)]\,. \tag{7.4}$$

The second quantity we are interested in, is the Entanglement Spectrum (ES) (see section 2.3.2 and [97]) , defined as the ordered collection $\{\xi_i\}_i$ of the negative logarithm of the eigenvalues $\{\lambda_i \coloneqq e^{-\xi_i}\}$ of ρ_A. By definition $\xi_{2^{|A|}-1} \geq \cdots \geq \xi_{i+1} \geq \xi_i \geq \cdots \geq \xi_0 \geq 0$.
In particular we will study the gaps $\{g_r\}_r$ in the low-lying entanglement spectrum, defined as

$$g_r \coloneqq \xi_r - \xi_0 \geq 0, \tag{7.5}$$

for the first 16 eigenvalues $r \in [1, 15]$. We are going to consider the dynamics induced by a quench. We evolve the state $\rho_0 = |\psi_0\rangle\langle\psi_0|$, the ground state of the Hamiltonian $H(\theta_0)$, with the Hamiltonian $H(\theta)$. At each time t the evolved state will be $\rho(t) = e^{-iH(\theta)t}\rho_0 e^{iH(\theta)t}$. In particular we will focus on results for quenches to the critical point, quenches across the critical point and quenches within the same phase.

As seen in chapter 5, in the continuum limit, at the critical point, the transverse field Ising model becomes a free Fermions massless field theory describeed by the Dirac action

$$S = \frac{1}{2\pi}\int(\psi\bar{\partial}\psi + \bar{\psi}\partial\psi). \tag{7.6}$$

This action is conformally invariant and the two fields ψ and $\bar{\psi}$ have conformal weight of $(h, \bar{h}) = (\frac{1}{2}, 0)$ and $(h, \bar{h}) = (0, \frac{1}{2})$. This can be described by a CFT with Virasoro algebra with central charge $c = \frac{1}{2}$ and it is in general associated to the unitary minimal model $m = 3$ called two dimensional critical Ising model (see section 5.2.4) for which the space state is generated by just three primary fields called identity (conformal dimension 0), spin (conformal dimension $\frac{1}{16}$), and energy (conformal dimension $\frac{1}{2}$).

As observed by Läuchli with numerical studies on the ground state of finite systems [263], the entanglement spectrum can be related to the conformal spectrum of a conformal field theory with boundaries (BCFT) defined by proper Conformal Boundary Conditions (CBC). In the presence of boundaries, the conformal symmetry of the Ising BCFT allows only three CBC for each boundary spin [210, 212]. Denoting these three boundary conditions with $(+)$, $(-)$ and (f), in figure 7.1 we report the

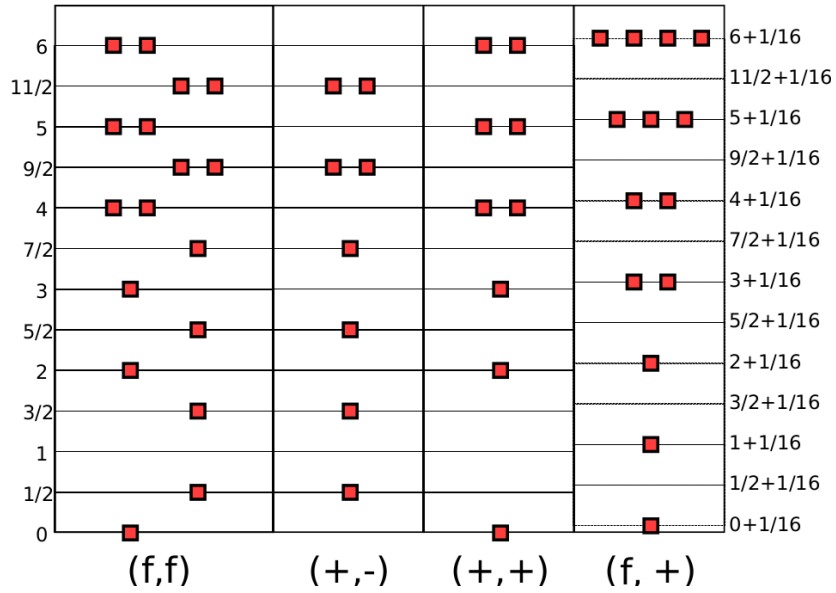

Figure 7.1: Catalog of the conformal spectrum for the Ising BCFT for different combinations of boundary conditions at the two boundaries.

low-lying conformal spectrum for the possible combinations of boundary conditions for two boundaries.

We are going to compare the numerical results with the analytical results of the CFT analysis of the out-of-equilibrium dynamics for a quench to the QCP for half of an infinite line [264]. Here Cardy and Tonni predicts that the quantity g_r/g_1, $(\ell g_r)^{-1}$ and $g_r S_A$ encode the conformal weights of the theory (a similar analysis has been performed for an infinite harmonic chain and for free fermions systems at half filling [265]). Comparing these results we will be able to identify the appropriate configuration of the boundary conditions of the BCFT and to find out that the entanglement spectrum in the post quench dynamics encodes information about the CFT model underlying the QCP of the evolution Hamiltonian.

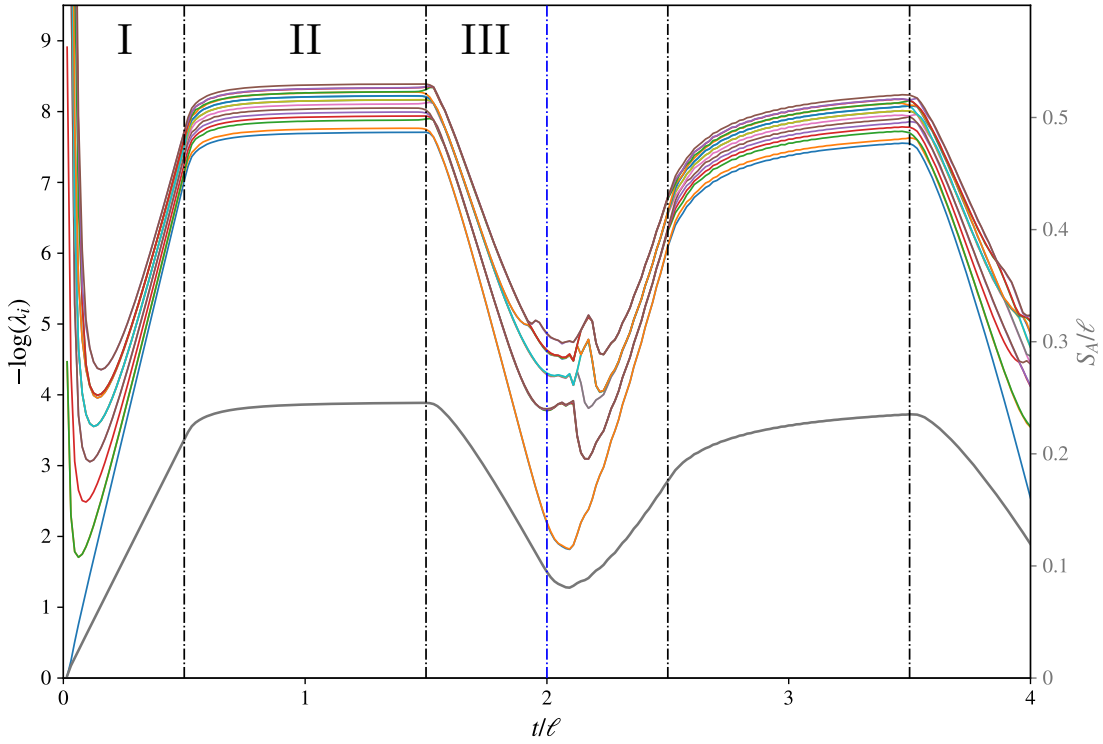

Figure 7.2: Time evolutions of the first 16 eigenvalues $\lambda_{\max} \geqslant \lambda_1 \geqslant \lambda_2 \geqslant \cdots \geqslant \lambda_{15}$ of the ES and of the EE (grey line) for an interval with $\ell = 64$ sites in the chain with $L = 256$ sites and PBC after the quench $\theta = \pi/8 \to \theta = \pi/4$ to the QCP. Different degeneracies are observed in regimes I, II and III within the period.

7.3 Numerical Analysis

7.3.1 Quenches at the quantum critical point

We start with the results for a system with PBC for which we consider the time evolution induced by the quench $\theta_0 = \frac{\pi}{8} \to \frac{\pi}{4}$ from the ordered phase to the QCP. In figure 7.2 we report the time evolution of the first 16 elements of the entanglement spectrum for $\ell = 64$ and $N = 256$, together with the time evolution of the EE.

Referring to the quasi-particle picture of section 4.0.3, we identify three different regimes for the evolution, which we separate with vertical dashed-dotted lines. Immediately after the quench the entangled couples of quasi particles separate and start traveling in opposite directions with velocity $v_{\mathrm{q}} = \min(1, \cot\theta)$

[104, 266]. As long as at least one of the quasi-particles initially belonging to the same couple in A are still crossing the boundaries of partition A the EE keeps growing linearly in time. We identify this as the first regime (regime I) of the time evolution.

The system enters in the second regime (regime II) of the time evolution in the moment when all the quasi particles in partition A have their entangled partner outside of partition A. For what explained in chapter 4, we will refer to the time at which regime II starts as equilibration time.

After enough time the quasi-particles spreading in the system will be both again in partition A. When the first couple of quasi particles are again present in partition A, the system enters in third regime (regime III). Since the system is finite, we observe recurrences effects. Indeed, after a time that can be easily calculated to be an integer multiple of $t_3^{PBC} = \frac{L/2}{v_q}$ (for PBC) the quasi-particle partners will meet again as at time $t = 0$. This is when phase I starts again. In the case of OBC, where the quasi particles will be reflected by the borders of the system, recurrence time is $t_3^{OBC} = \frac{L}{v_q}$, because the quasi particles need to travel double the distance, with respect to the PBC case, in order to be back again in partition A.
We can identify the three regimes as starting at the times $t_1 = n\frac{L/2}{v_q}$, $t_2 = \frac{\ell/2}{v_q} + t_1$ (equilibration time), and $t_3 = \frac{(L-\ell)/2}{v_q} + t_1$ where $n \in \mathbb{N}_0$. In the case of OBC we identify the same three regimes, but the times are doubled.
The three different regimes can be easily identified by the value of the first derivative of the EE.

We remind that a CFT analytic expression of the entanglement spectrum for the dynamics we are going to consider is not available in the literature. Referring to the CFT results in [267] and adopting the BCFT approach to global quantum quenches with the critical evolution Hamiltonian [52, 59, 268–270] (see [271] for a recent review) we want to identify the two CBC (a, b_0) (see [272] for a detailed description of the CFT analysis and interpretation) of the underlying BCFT. A similar analysis has been done by Läuchli [263] for systems at equilibrium, where it has been found the correspondence with a (f, f) Ising BCFT on a strip. Here we study, instead, systems out of equilibrium

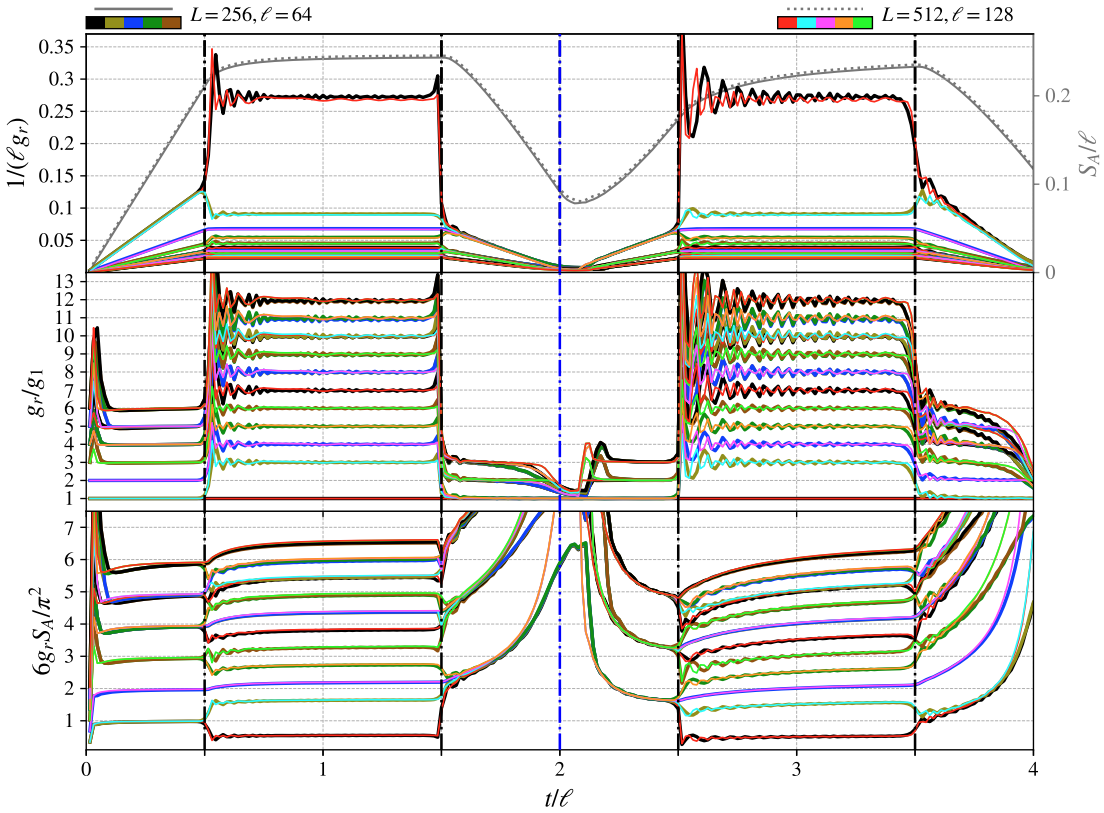

Figure 7.3: Time evolution of $(\ell g_r)^{-1}$ (top), g_r/g_1 (middle), $g_r S_A$ (bottom), and S_A/ℓ (in grey) after the quench $\theta_0 = \pi/8 \to \theta = \pi/4$ for an interval in the chain with PBC.

with the quench dynamics of a system that thermalise. For systems of this kind we consider the following CFT predictions [156, 267]

$$S_A \propto \begin{cases} \frac{2\pi c}{3\tau_0} t & \text{at short times (regime I)} \\ \frac{c}{6} W & \text{at equilibration time (regime II),} \end{cases} \tag{7.7}$$

and

$$g_r \propto \begin{cases} \frac{\pi \tau_0 c}{2t} \Delta_r & \text{at short times (regime I)} \\ \frac{2\pi^2 \Delta_r}{W} & \text{at equilibration times (regime II),} \end{cases} \tag{7.8}$$

where

$$W = 2 \log\left(\frac{\beta}{\pi \tau_0} \sinh\left(\frac{\pi \ell}{\beta}\right)\right), \tag{7.9}$$

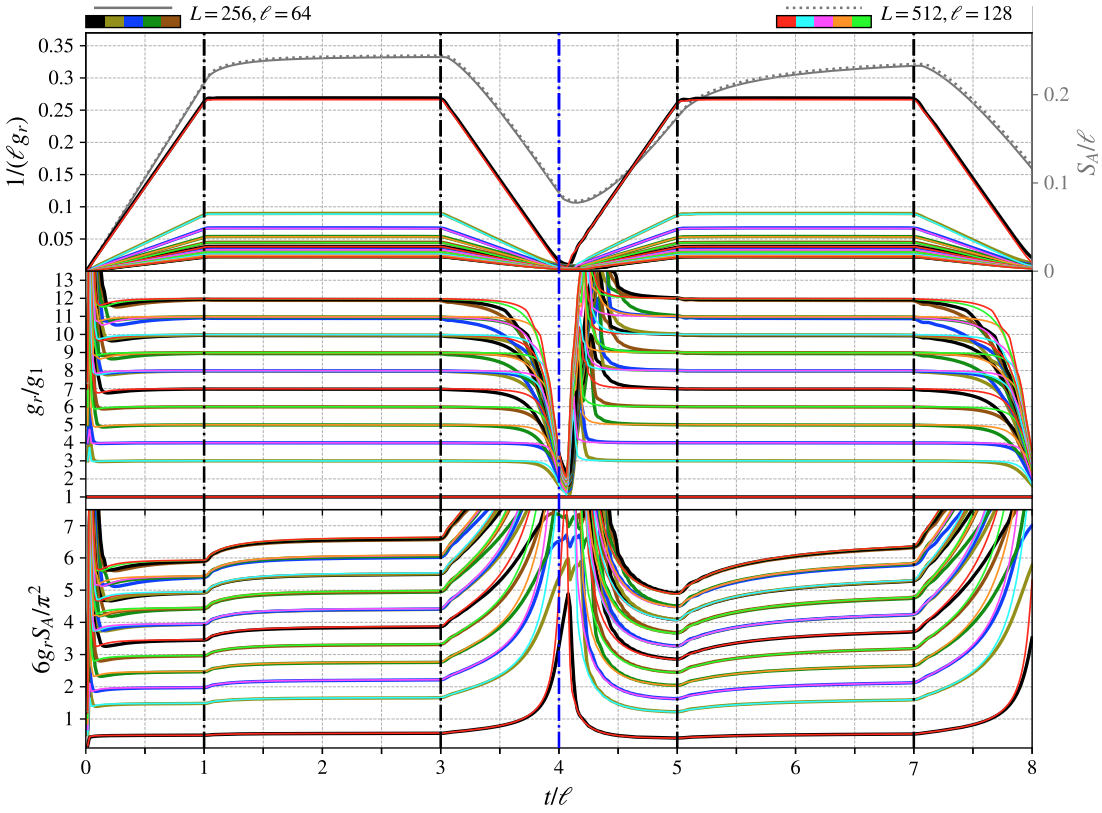

Figure 7.4: Time evolution of $(\ell g_r)^{-1}$ (top), g_r/g_1 (middle), $g_r S_A$ (bottom), and S_A/ℓ (in grey) after the quench $\theta_0 = \pi/8 \to \theta = \pi/4$ for an interval in the chain with OBC.

with β the temperature to which the system thermalise, $\Delta_r \in \mathcal{S}(a, b_0) \setminus \{0\}$ are the element of the conformal towers of the primary fields and of their descendants of the BCFT with CBC (a, b_0) (collected in figure 7.1 including the vanishing values for the Ising BCFT), and the parameter τ_0 encodes information about the initial state [267]. We see that from the quantities g_r/g_1 and $g_r S_A$ we can extract the conformal spectrum of the underlying BCFT [272]. In fact

$$\frac{g_r}{g_1} = \frac{\Delta_r}{\Delta_1}, \tag{7.10}$$

and

$$g_r S_A \propto \begin{cases} \frac{\pi^2}{3} c^2 \Delta_r & \text{at short times (regime I)} \\ \frac{\pi^2}{3} c \Delta_r & \text{at equilibration time (regime II).} \end{cases} \tag{7.11}$$

We are going to infer the CBC (a, b_0) from the consistency of the data for the ES compared with the table in figure 7.1.

In figure 7.3 and figure 7.4 we report the post quench dynamics of the quantities we want to study (S_A, $\frac{1}{\ell g_r}$, $\frac{g_r}{g_1}$, and $\frac{6 g_r S_A}{\pi^2}$) for systems with PBC and OBC respectively and quench $\theta_0 = \frac{\pi}{8} \to \theta = \frac{\pi}{4}$ (quench to the QCP).

For both boundary conditions we observe a linear growth of $1/\ell g_r$ in regime I as expected while in regime II it equilibrates to a static value. We are now interested in extracting the values of Δ_r in each regime. To do so we study the time evolution of the ratio of the gaps g_r/g_1. We expect this ratio to be constant in all regimes. From figure 7.3 and figure 7.4 we can see that this is indeed the case, except for an abrupt change (followed by some oscillations) passing from regime I to regime II in the case of PBC. We compare the value of g_r/g_1, the ratios of the gaps, with Δ_r/Δ_1, the value of the ratios of the gaps in the conformal spectrum for the free-free boundary conditions in figure 7.5 computed from the elements of the conformal towers in figure 7.1.

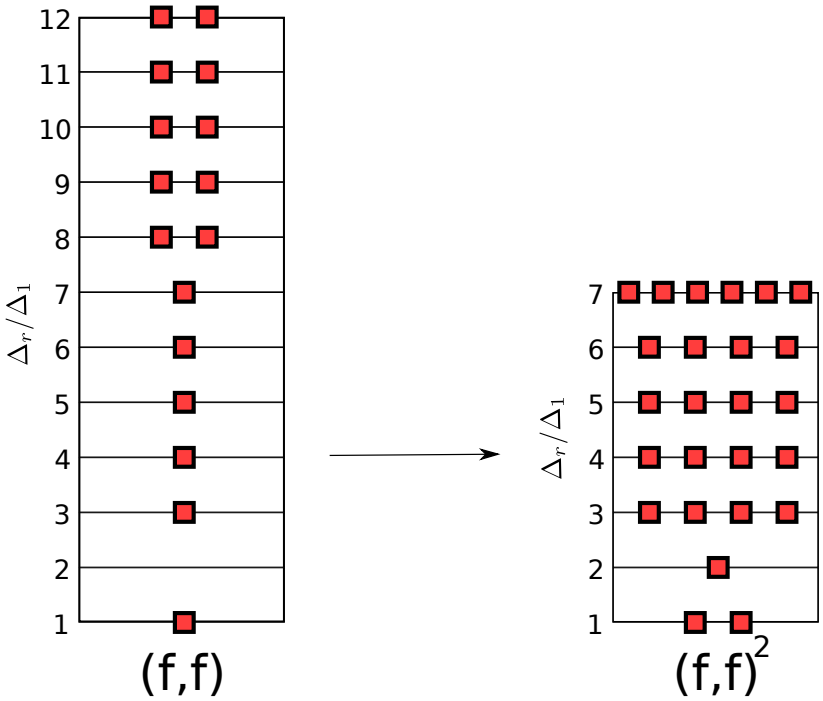

Figure 7.5: Catalog of the ratios of the gaps in the conformal spectrum of one and two copies of the Ising BCFT with free-free boundary conditions.

We see that the time evolution of the spectral gaps in regime I of the OBC case and regime II of the PBC and OBC case seem determined by the gaps of the conformal spectrum given by a BCFT with free-free boundary conditions (f, f). Regime I of the dynamics of the system with PBC can be interpreted as encoding the information of two copies of the conformal spectrum given by a BCFT with free-free boundary conditions $(f, f)^2$.

7.3.2 Thermalisation in regime II

The results we presented show that the low-entanglement part of the entanglement spectrum of the reduced density matrix of a block in regime II of the quenches, the equilibrated regime, coincides with the low-energy spectrum of a given Hamiltonian. Given this, one would be tempted to extend this result saying that for the reduced density matrix of a partition of ℓ spins $\rho(\ell) \simeq \exp(-\beta H_\ell)$, that is our equilibrated state is thermal, it is described by a Gibbs Ensemble (GE). This temptation should be resisted since it obviously contradicts what is known about the equilibration of integrable systems that equilibrate to Generalized Gibbs Ensemble (GGE) (see chapter 4). At the same time, this observation is an insightful intuition. We remind and stress the fact that we are only looking at the very low entanglement energies. The relation between the GGE and the GE in this regime, that is by projecting them at very low energies, has not yet been studied. It is known indeed, that for small blocks the GGE and the GE are distinguishable and the GE fails to correctly reproduce the expectation values of local operators when these operators equilibrate after the quench [273]. This is apparent also by comparing the eigenvalues of the two ensemble as we do in Fig. 7.6. The two ensembles are well distinguishable if one considers the full spectrum, but they are very close to each other in the lower part of the spectrum. In the first panel of Fig.7.6 we plotted the spectrum for $\ell = 4$, for this size of the partition we just have 16 eigenvalues in total. We can appreciate how the lower eigenvalues of the GGE deviate from those of the GE already after 5 eigenvalues. The situation changes as we increase ℓ, and as a result the number of eigenvalues increases as 2^ℓ. Focussing on the first 16 eigenvalues we are thus focussing on an exponentially small relative low energy

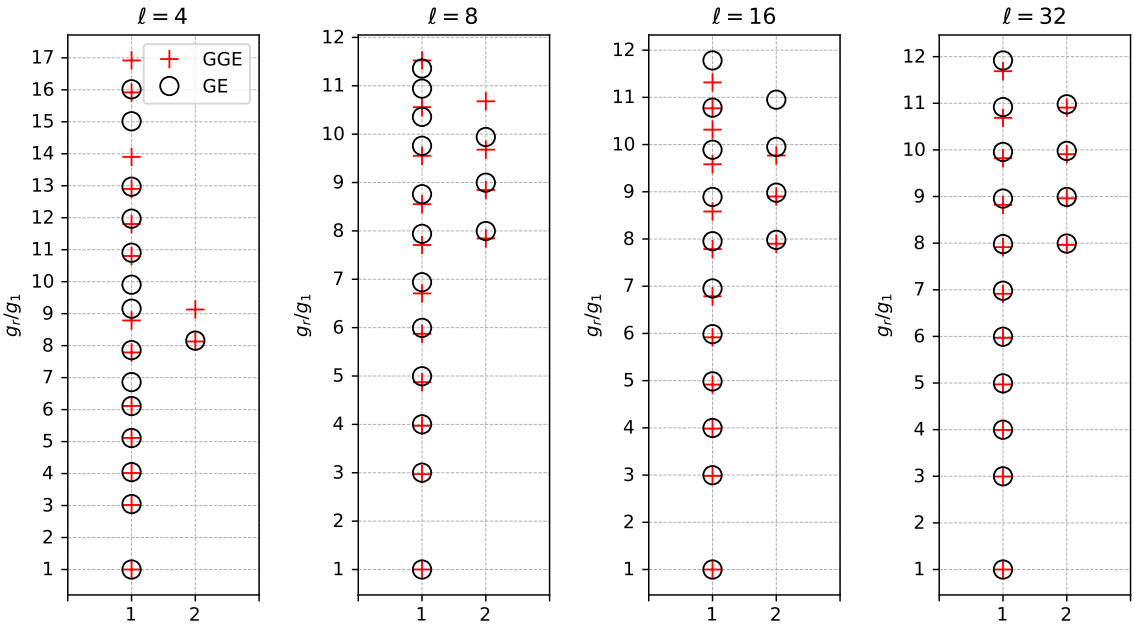

Figure 7.6: First 16 gap ratios of GE versus GGE spectra for different dimensions ℓ of the reduced density matrix at the temperature obtained from the quench $\frac{\pi}{8} \to \frac{\pi}{4}$, in a chain of $L = 256$ with PBC. In each of the four plots, in the case of two ratios with almost the same value (as for example the case of $g_r/g_1 \sim 8$ in the leftmost plot), we plot the second one on a second column labelled by 2. Moving from left to right the red crosses moves inside the black circles. On the left we consider a partition of dimension $\ell = 4$, thus, plotting 16 eigenvalues, we are plotting its whole spectrum. We see that in this case the GE and the GGE are different as expected. On the right we consider a partition of $\ell = 32$ sites, thus, plotting the first 16 eigenvalues we are considering only the first $\sim 4 \cdot 10^{-7}\%$ of its spectrum. Here the GE approximates the GGE.

subset. In this subset the two ensembles become less and less distinguishable as shown for $\ell = 32$ where they almost coincide through all the range. As a result we can safely confirm that our results are in agreement with the generalised thermalisation to the GGE of the states after a quench.

7.3.3 Quenches across the quantum critical point

Quenches to the critical points encode the information about the CFT underlying the Hamiltonian at the critical point, that is the Hamiltonian inducing the dynamics. We investigate now the scenario of quenches *across* the QCP. In this scenario neither the initial Hamiltonian nor the post-quench Hamiltonian are critical. Knowing that

the system is going to equilibrate though, tells us that the starting state and the equilibrated state of the system are two equilibrium states of two Hamiltonian in two different phases. We expect thus, that the state, *in some way*, passes across the critical point. By quenching across the quantum critical point of the Ising model we encounter a dynamical quantum phase transition [274]. Dynamical quantum phase transition occurs at those times when the return probability to the original state after the quench vanishes (see [275] for a recent review). Usual quantum phase transitions induce a universal behaviour of correlation functions. Although the return probability to the ground state bares similarities with a boundary partition function at complex temperature, the presence of dynamical quantum phase transition does not have the same universal consequences on time dependent correlation functions.

Here we show that the entanglement spectrum still becomes universal when crossing the dynamical quantum phase transitions. The results of a typical quench across the QCP are shown in Fig. 7.7, where qualitatively different ES are observed when quenching in the two different directions between the two phases.

In regimes I and III for the quench having $\theta_0 < \frac{\pi}{4}$ and $\theta > \frac{\pi}{4}$ we see spikes in the plots on the left panel in Fig. 7.7. They identify the points in time where the first gap vanishes and hence the ratios g_r/g_1 diverge. In regime I, these times coincide with the times when the Loschmidt echo is singular [276]. This implies that these are the times that identify the location of dynamical quantum phase transitions.

For quenches in the other direction (right panels) across the QCP the spikes are absent. Still, the ES becomes gapless as witnessed by the linear increase of the inverse gaps (modulo the spikes we have discussed) in the regimes I of the quenches in both directions (see [276,277]). When we quench from larger to smaller θ this is more visible due to the absence of spikes.

In the next section we will see that for generic quenches in the same phase indeed the entanglement spectrum remains gapped.

We try to identify the spectrum we observe even in this context. The ratios g_r/g_1 display surprising behaviour, they approach integer values in regimes I and II in the right panel of Fig. 7.7. Furthermore, similar steady integer values are present also in

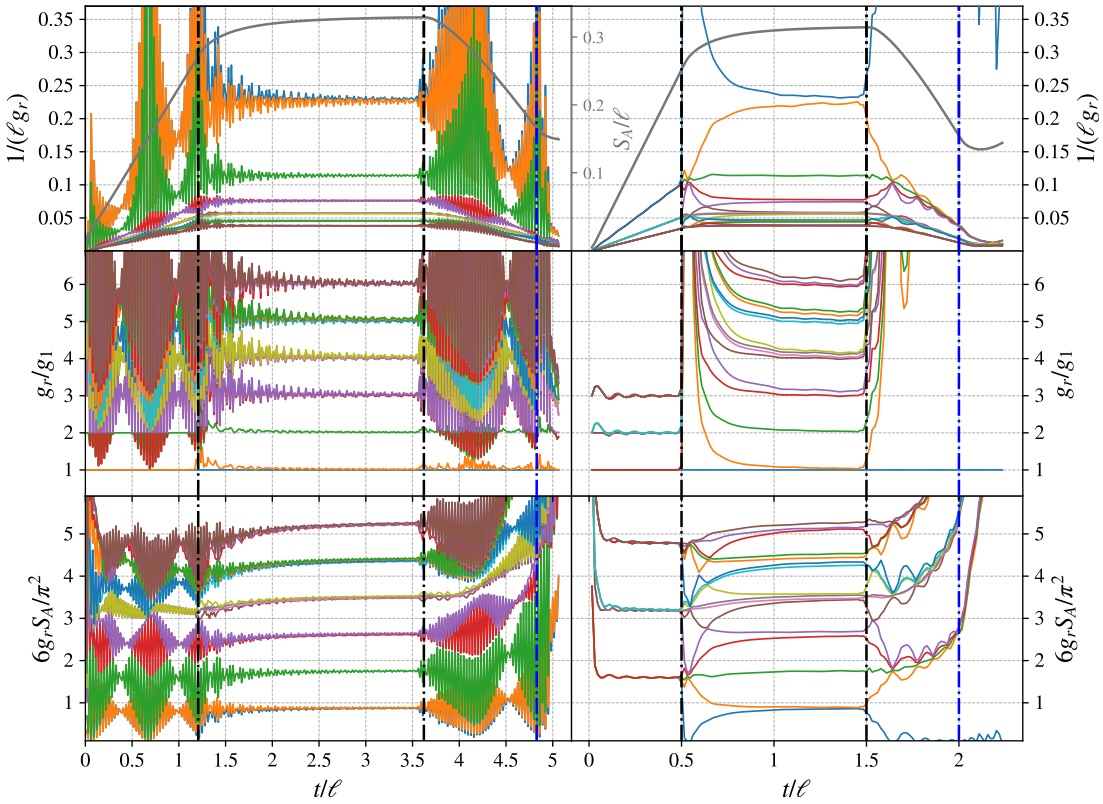

Figure 7.7: Time evolution of $(\ell g_r)^{-1}$ (top), g_r/g_1 (middle), $g_r S_A$ (bottom), and S_A/ℓ (in grey) after quenches such that H and H_0 belong to different phases given by $\theta_0 = \pi/8 \to \theta = \pi/2 - \pi/8$ (left) and $\theta_0 = \pi/2 - \pi/8 \to \theta = \pi/8$ (right), for an interval having $\ell = 128$ sites in the chain with PBC having $L = 512$ sites.

regime II in the left panel. This feature is the same observed in the quenches at the QCP (see regime I in Fig. 7.3) and could be attributed to the crossing of the QCP. Indeed, comparing to the case when the QCP is not crossed (see Fig. 7.8), we see that plateaux at integer values for g_r/g_1 in regime II are not observed if the QCP is not at least crossed. We observe that the convergence of the curves of g_r/g_1 to the integer plateaux in regime II for the quench from the paramagnetic phase to the ferromagnetic phase improves as $|\theta - \theta_0|$ increases.

Comparing again to figure 7.5, these integer values can be related to two copies of the Ising BCFT with free-free boundary conditions.

The appearance of a universal entanglement spectrum when crossing several dynamical quantum phase transitions, seems to suggest the possibility of defining

scaling and universality there, something that as of today was still considered an open question as discussed e.g. in [275].

7.3.4 Quenches in the same phase

Both quenches at the QCP or across the QCP encode universal information about the conformal spectrum of the Ising boundary conformal field theory with the proper CBC. Here we investigate if this information is encoded even in quenched dynamics where the initial and the equilibrium state are inside the same phase. The dynamics of the entanglement spectrum for this kind of quenches is showed in Fig. 7.8 both inside the paramagnetic phase (panel on the left) and inside the ferromagnetic phase (panel on the right).

Comparing Fig. 7.8 with the data of figures 7.1 and 7.5, the gaps ratios g_r/g_1 seem to not encode any information about the quantum critical point.

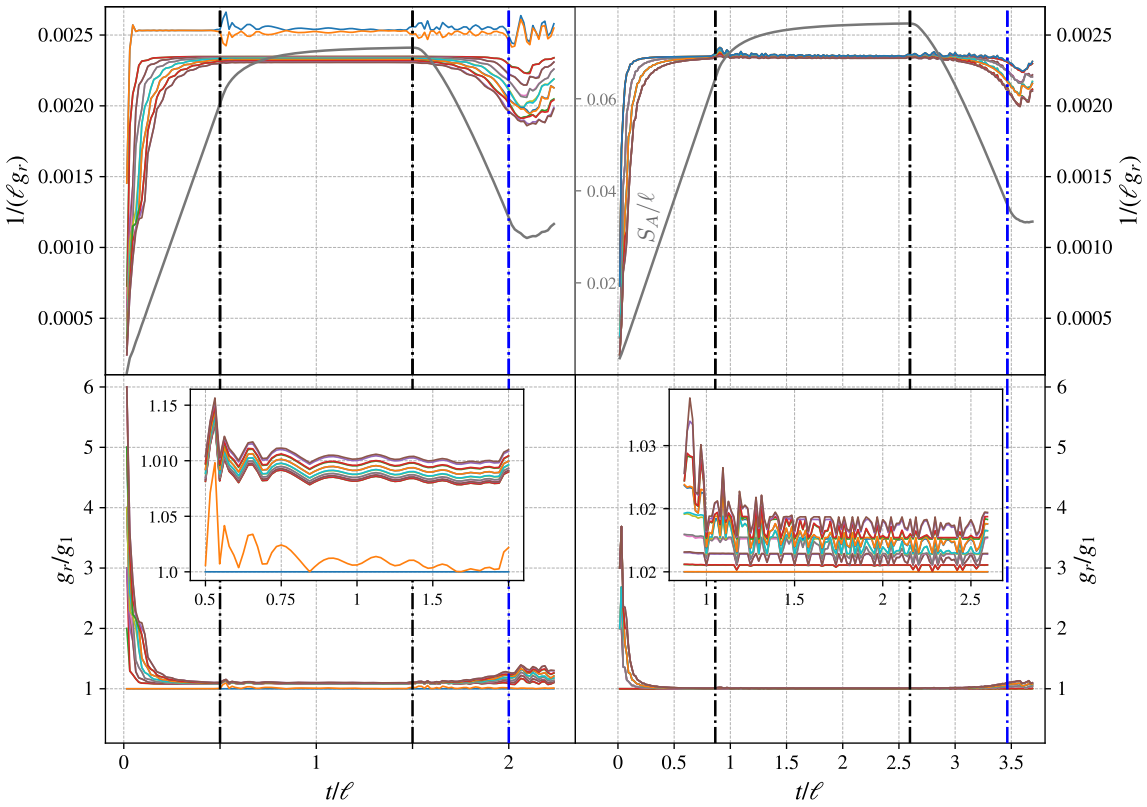

Figure 7.8: (color online). Time evolution of $(\ell g_r)^{-1}$ (top), g_r/g_1 (bottom), and S_A/ℓ (in grey) after the quench $\theta_0 = \pi/12 \to \theta = \pi/4 - \pi/12$ within the paramagnetic phase (left) and $\theta_0 = \pi/2 - \pi/12 \to \theta = \pi/4 + \pi/12$ within the ferromagnetic phase (right), for an interval with $\ell = 128$ sites in chain with PBC having $L = 512$ sites.

7.4 Conclusion

We studied the dynamics of the gaps of the entanglement spectrum in the post quench dynamics of the transverse field Ising model with periodic and open boundary conditions.

Analysing the ratios of the gaps in the low energy part of the spectrum, we found that they take constant values in different time regimes.

In particular we found that, in the first thermalisation regime (regime II), the ratios of the gaps encode information about the conformal boundary conditions of the underlying Ising BCFT. The appearence of this feature, even during the dynamics induced by quenches across the QCP, suggests the possibility of a form of universality

out-of-equilibrium.

Our results are robust under a reasonable change of the parameters of the quench.

The results are double-sided. From one side the numerical analysis suggests us the proper conformal boundary conditions to adopt in the boundary conformal field theory approach to global quenches. From the other side it tells us that we can adopt a BCFT approach to obtain information about the results of the numerical analysis.

A possible extension of this work would be considering different BC, different protocols for the quenches, different bipartition schemes and different interacting spin chains models.

Another research direction suggested by the numerical analysis is studying quantitatively the role of the GGE in our analysis, in particular the differences between the low energy spectrum of the GE and GGE.

This results also suggest a more quantitative study of the connections between the features of the dynamical quantum phase transition and the entanglement spectrum dynamics in quenches across the quantum critical point.

At last, our results suggest that critical exponents could be possibly measured by experiments on entanglement spectroscopy of correlated many-body quantum systems out of equilibrium.

Chapter 8

Conclusions

In this thesis, we have explored the evolution of many-body quantum systems out of equilibrium. We have focussed on understanding if the fast growth of entanglement really prevents a classical treatment of these systems or if it is just a clue that we are focussing on a wrong description. We have assumed, as a research hypothesis, that this growth can be overcome by appropriate algorithms and encodings. To answer this question, we developed proper tools for the exploration of the out-of-equilibrium dynamics and used them in different scenarios. These tools are presented in chapter 3 together with the documentation, and with practical examples for the usage of the package `F_utilities`. With this package, it is possible to perform simulations with Fermionic Gaussian states using the programming language `Julia`. It includes standard algorithms for the manipulation of Fermionic Gaussian states (as partial trace, time evolution etc.) as well as algorithm from the modern literature (as the product formula [143], the reduction of bond dimension a la White [154] etc.). We have also implemented algorithms for mimicking tensor networks with Fermionic Gaussian states, as for example a version of the time evolving block decimation, used widely in the context of matrix product states. The next steps in the development of the package include implementing tools for the manipulation of reduced density matrices of infinite Fermionic Gaussian states (see e.g. [66]) and possibly extending it to Bosonic systems.

In chapter 6 we designed and benchmarked a numerical algorithm for the prediction

of the long-time expectation value of local observables in the quantum many-body dynamics out of equilibrium.

For translationally invariant systems described by local Hamiltonians entanglement spreads in the system. As a consequence the constituents belonging to a small region of contiguous sites become entangled with constituents further away from them as time passes. We thus argue that to describe their dynamics it is not necessary to preserve information about their entangled partners.

Trading the entanglement of the state for mixture we obtain a local description of the state as viewed by the local terms of the Hamiltonian. The state so obtained is efficiently encodable in a computer. We translate these ideas into a working algorithm that we show provides good predictions of the equilibrated expectation values of the system. A natural extension, on which we are working, is to check that the same algorithm works in the presence of strong interactions. This requires implementing the generic version of the algorithm using tensor networks.

In chapter 7 we explored the dynamics of the transverse field Ising model, a model that at the critical point is described by a quantum conformal field theory. We discovered that during the out-of-equilibrium dynamics for quenches to the critical point, and across the critical point, the entanglement spectrum encodes information of the conformal field theory of the system at the critical point. Thus, even if the entanglement grows during the evolution, we see that, in the appropriate basis, at low-entanglement, the systems looks thermal with time dependent temperature. We can interpret this as another clue that the growth of entanglement does not imply the loss of the ability to describe the system.

In order to accumulate more evidences of the appropriateness of this simplified picture we need to perform more numerical simulations focussing in particular on interacting systems. As a side result, we have observed that at low entanglement the GE and GGE are locally indistinguishable. This is an interesting observation that we need to further extend and explore.

In conclusion, we have accumulated a growing set of evidences that, although entanglement grows out of equilibrium, we may still be able to describe many-body

quantum systems using numerical simulations, thus confirming our initial research hypothesis.

Appendix A

Appendix to F_utilities

A.1 Extended calculations

A.1.1 Eigenvalues of Γ and H_α

We consider the state $\rho = \frac{e^{-\vec{\alpha}^\dagger H \vec{\alpha}}}{Z}$, we diagonalise H changing the basis to $\vec{\beta} = U^\dagger \vec{\alpha}$. Thus we have

$$\rho = \frac{e^{-\vec{\beta}^\dagger H_D \vec{\beta}}}{Z} = \frac{e^{-\sum_{k=1}^{N} \epsilon_k \left(b_k^\dagger b_k - b_k b_k^\dagger\right)}}{Z}. \tag{A.1}$$

We change the basis of the correlation matrix too

$$\Gamma^b_{i,j} = \left(U^\dagger \Gamma U\right)_{i,j} = Tr\left[\rho \vec{\beta}_i \vec{\beta}_j{}^\dagger\right]. \tag{A.2}$$

Now we want to explicitly compute the elements of Γ^b. First of all we compute the normalisation constant

$$Z = Tr\left[e^{-\sum_{k=1}^{N} \epsilon_k \left(b_k^\dagger b_k - b_k b_k^\dagger\right)}\right] = 2^N \prod_{k=1}^{N} \left(\cosh\left(\epsilon_k\right)\right). \tag{A.3}$$

To compute the numerator part this equalities will result useful

- For $x \neq y$

$$Tr\left[e^{-\sum_{k=1}^{N}\epsilon_k\left(b_k^\dagger b_k - b_k b_k^\dagger\right)} b_x^\dagger b_y\right] = \sum_{v\in\{0,1\}^N} \langle v|e^{-\sum_{k=1}^{N}\epsilon_k\left(b_k^\dagger b_k - b_k b_k^\dagger\right)} b_x^\dagger b_y|v\rangle =$$
$$= \sum_{v\in\{0,1\}^N} \langle v|e^{-\sum_{k=1}^{N}\epsilon_k\left(b_k^\dagger b_k - b_k b_k^\dagger\right)}|\tilde{v}\rangle = \tag{A.4}$$
$$= \sum_{v\in\{0,1\}^N} e^{-\sum_{k=1}^{N}(-1)^{v_k+1}\epsilon_k}\langle v|\tilde{v}\rangle = 0$$

$$Tr\left[e^{-\sum_{k=1}^{N}\epsilon_k\left(b_k^\dagger b_k - b_k b_k^\dagger\right)} b_x b_y^\dagger\right] = 0 \tag{A.5}$$

- $\forall x, y$

$$Tr\left[e^{-\sum_{k=1}^{N}\epsilon_k\left(b_k^\dagger b_k - b_k b_k^\dagger\right)} b_x b_y\right] = 0 \tag{A.6}$$

$$Tr\left[e^{-\sum_{k=1}^{N}\epsilon_k\left(b_k^\dagger b_k - b_k b_k^\dagger\right)} b_x^\dagger b_y^\dagger\right] = 0 \tag{A.7}$$

Thus the numerator can be explicitly written as

$$Tr\left[e^{-\sum_{k=1}^{N}\epsilon_k\left(b_k^\dagger b_k - b_k b_k^\dagger\right)} \vec{\alpha}_i \vec{\alpha_j}^\dagger\right] = \tag{A.8}$$

$$= \sum_{l=1}^{2N}\sum_{m=1}^{2N} U_{i,l}U_{m,j}^\dagger Tr\left[e^{-\sum_{k=1}^{N}\epsilon_k\left(b_k^\dagger b_k - b_k b_k^\dagger\right)} \vec{\beta}_l \vec{\beta_m}^\dagger\right] =$$

$$= \sum_{l=1}^{N} U_{i,l}U_{l,j}^\dagger Tr\left[e^{-\sum_{k=1}^{N}\epsilon_k\left(b_k^\dagger b_k - b_k b_k^\dagger\right)} b_l^\dagger b_l\right] + \sum_{l=1}^{N} U_{i,l+N}U_{l+N,j}^\dagger Tr\left[e^{-\sum_{k=1}^{N}\epsilon_k\left(b_k^\dagger b_k - b_k b_k^\dagger\right)} b_l b_l^\dagger\right] =$$

$$= \sum_{l=1}^{N} U_{i,l}U_{l,j}^\dagger e^{-\epsilon_l}\prod_{k\neq l} 2\cosh(\epsilon_k)) + \sum_{l=1}^{N} U_{i,l+N}U_{l+N,j}^\dagger e^{\epsilon_l}\prod_{k\neq l} 2\cosh(\epsilon_k))$$

I can divide by Z and obtain

$$\begin{aligned}\Gamma_{i,j} &= \sum_{l=1}^{N} U_{i,l} U^{\dagger}_{l,j} \frac{e^{-\epsilon_l}}{e^{\epsilon_l}+e^{-\epsilon_l}} + \sum_{l=1}^{N} U_{i,l+N} U^{\dagger}_{l+N,j} \frac{e^{\epsilon_l}}{e^{\epsilon_l}+e^{-\epsilon_l}} \\ &= \sum_{l=1}^{N} U_{i,l} U^{\dagger}_{l,j} \frac{1}{1+e^{2\epsilon_l}} + \sum_{l=1}^{N} U_{i,l+N} U^{\dagger}_{l+N,j} \frac{1}{1+e^{-2\epsilon_l}} = \\ &= (U\Gamma^{D}U^{\dagger})_{i,j}.\end{aligned} \tag{A.9}$$

So the same transformation U that moves to the free Hamiltonian H_D is also the transformation that diagonalise the correlation matrix. The eigenvalues ν_i of the correlation matrix Γ are related to the eigenvalues of the parent Hamiltonian H by

$$\nu_i = \frac{1}{1+e^{2\epsilon_i}}, \tag{A.10}$$

$$\epsilon_i = \frac{1}{2} ln\left(\frac{1-\nu_i}{\nu_i}\right), \tag{A.11}$$

since $\nu_i \in [0,1]$ the eigenvalues ϵ_i∈[-∞,+∞].

A.1.2 Purity

From the previous paragraph we have:

$$Z^2 = \prod_{k=1}^{N} \left(2\cosh\left(\epsilon_k\right)\right)^2 \tag{A.12}$$

and

$$Tr\left[e^{-\sum_{k=1}^{N}\epsilon_k\left(b_k^{\dagger}b_k - b_k b_k^{\dagger}\right)}\right] = \prod_{k=1}^{N}\left(2\cosh\left(2\epsilon_k\right)\right). \tag{A.13}$$

Thus the purity is:

$$\text{Purity} = \prod_{k=1}^{N} \frac{1}{\text{sech}(\epsilon_k)+1} \tag{A.14}$$

A.1.3 Real Time Evolution

We want to compute the time evolution in the Heisenberg picture of the annihilation operator b_k induced by the Hamiltonian $\hat{H} = \sum_{l=1}^{N} \epsilon_l (b_l^\dagger b_l - b_l b_l^\dagger)$. First we simplify the expression exploiting the commuting terms

$$b_k(t) = e^{i\hat{H}t} b_k e^{-i\hat{H}t} = e^{it\sum_{l=1}^{N} \epsilon_l (b_l^\dagger b_l - b_l b_l^\dagger)} b_k e^{it\sum_{l=1}^{N} \epsilon_l (b_k^\dagger b_l - b_l b_l^\dagger)} = \tag{A.15}$$

$$= e^{it\epsilon_k (b_k^\dagger b_k - b_k b_k^\dagger)} b_k e^{it\epsilon_k (b_k^\dagger b_k - b_k b_k^\dagger)}. \tag{A.16}$$

Secondly applying B.C.H.1 (see B.C.H.1 in A.2.4) we obtain that

$$b_k(t) = \sum_{n=0}^{\infty} \frac{(ie_k t)^n}{n!} \underbrace{[b_k^\dagger b_k - b_k b_k^\dagger, \ldots [v_k^\dagger b_k - b_k b_k^\dagger}_{n}, b_k \underbrace{] \ldots]}\, n, \tag{A.17}$$

and using the fact that

$$[b_k^\dagger b_k - b_k b_k^\dagger, b_k] = -2b_k, \tag{A.18}$$

we obtain

$$b_k(t) = \sum_{n=0}^{\infty} \frac{(2ie_k t)^n}{n!} b_k = e^{-i2e_k t} b_k. \tag{A.19}$$

A.1.4 Circulant Matrices

An $N \times N$ circulant matrix C is a matric of the form

$$C = \begin{pmatrix} c_0 & c_1 & c_2 & \ldots & c_{N-1} \\ c_{N-1} & c_0 & c_1 & \ldots & c_{N-2} \\ c_{N-2} & c_{N-1} & c_0 & \ldots & c_{N-3} \\ \vdots & \vdots & \vdots & \ddots & \vdots \\ c_1 & c_2 & c_3 & \ldots & c_0 \end{pmatrix}. \tag{A.20}$$

A circulant matrix is completely specified by the *circulant vector* $\vec{c}$, that is its first row.

$$\vec{c} = (c_0, c_1, c_2, \ldots, c_{N-1}). \tag{A.21}$$

All the other rows of the matrix are cyclic permutations of $\vec{c}$ with offset increasing by one going down with the rows.

Since each descending diagonal from left to right is constant, circulant matrices are a special case of Toeplitz matrices.

Because of their special structure, circulant matrices are diagonalised by taking their Fourier transform.

Given a vector $\vec{v}$ of length N its Fourier transform is expressed as $\vec{w} = W\vec{v}$, with W defined as

$$W = \frac{1}{\sqrt{N}} \begin{pmatrix} \omega & \omega^2 & \omega^3 & \cdots & \omega^{N-1} & 1 \\ \omega^2 & \omega^4 & \omega^6 & \cdots & \omega^{2(N-1)} & 1 \\ \omega^3 & \omega^6 & \omega^9 & \cdots & \omega^{3(N-1)} & 1 \\ \vdots & \vdots & \vdots & \ddots & \vdots & 1 \\ \omega^{N-1} & \omega^{2(N-1)} & \omega^{3(N-1)} & \cdots & \omega^{(N-1)(N-1)} & 1 \\ 1 & 1 & 1 & 1 & \cdots & 1 \end{pmatrix}, \tag{A.22}$$

with $\omega = e^{-i\frac{2\pi}{N}}$.

The columns of W are the normalised eigenvectors $|\lambda_i\rangle$ of every circulant matrix of dimension $N \times N$.

The corresponding eigenvalues depend on the specific circulant vector $\vec{c}$ specifying the circulant matrix and are given by

$$\lambda_j = c_0\omega^j + c_1\omega^j + c_2\omega^{j2} + \cdots + c_{N-2}\omega^{j(N-2)} + c_{N-1}\omega^{j(N-1)}. \tag{A.23}$$

A.1.5 Block diagonal form of skew-symmetric matrices

Let h be a $N \times N$ skew-symmetric matrix of rank $2m$, where $N \geq 2m$.

Then there exist a $N \times N$ unitary matrix U such that [134]

$$U^T h U = \begin{pmatrix} 0 & \lambda_1 \\ -\lambda_1 & 0 \end{pmatrix} \oplus \begin{pmatrix} 0 & \lambda_2 \\ -\lambda_2 & 0 \end{pmatrix} \oplus \cdots \oplus \begin{pmatrix} 0 & \lambda_m \\ -\lambda_m & 0 \end{pmatrix} \oplus \hat{0}_{N-2m}, \tag{A.24}$$

where $\hat{0}_{N-2m}$ is a $(N-2m) \times (N-2m)$ matrix with all elements equal to zero and where the real and positive-definite $\{\lambda_i\}_{i=1,m}$ are the singular values of h.
Since a skew-symmetric matrix h is similar to its own transposeh^T, then h and h^T must have the same eigenvalues. Thus, the eigenvalues of a skew-symmetric matrix of even dimension will always come in pairs $\pm\tilde{\lambda}$ (for the case of odd dimension there will be an unpaired eigenvalue equal to 0).

A.1.6 Jordan-Wigner transformation

The Jordan-Wigner transformation, introduced in the original paper [278], is a transformation that maps spin-$\frac{1}{2}$ systems to fermionic systems.
Suppose we have a system of N spins-$\frac{1}{2}$ with the usual Pauli matrices σ_j^x, σ_j^y and σ_j^z acting on the j-th spin of the system The Jordan-Wigner transformation defines the operator a_j as

$$a_j = -\left(\otimes_{k=1}^{j-1}\sigma_k^z\right) \otimes \sigma_j^+ \left(\otimes_{k=j+1}^{N}\mathbb{I}_k\right), \tag{A.25}$$

where $\sigma_j^{\pm} = \frac{\sigma_j^x \pm i\sigma_j^y}{2}$ and $\mathbb{I}_j$ is the identity acting on the j-th spin. Taking the adjoint obtains

$$a_j^\dagger = -\left(\otimes_{k=1}^{j-1}\sigma_k^z\right) \otimes \sigma_j^- \left(\otimes_{k=j+1}^{N}\mathbb{I}_k\right). \tag{A.26}$$

Computing the anticommutator of these two operators we notice that they obey the CAR, thus using this transformation for every site j we are able to build a legitimate set of Dirac fermionic operators starting from a set of Pauli matrices.
Knowing the expression for the creation and annihilation operators, we can easily find the mapping of the single site occupation operator in term of Pauli operators:

$$a_j^\dagger a_j = \left(\otimes_{k=1}^{j-1}\mathbb{I}_k\right) \otimes \frac{\mathbb{I}_j - \sigma_j^z}{2} \left(\otimes_{k=j+1}^{N}\mathbb{I}_k\right). \tag{A.27}$$

Finally there are two important remarks. We notice that the mapping from spins to fermions is not local, in the sense that equation A.25 maps a string of Pauli operators acting non trivially on j spins to a Dirac operator local only on site j.
We even notice that in the definition of the annihilation operator A.25 it is encoded

some information on the geometrical structure of the spin system, in particular it is encoded the distance of site j from the border.
When using the Jordan-Wigner transformation one has to be careful about these two observations.

In the main text we are interested in mapping the transverse field Ising Hamiltonian to a fermionic system, thus we need the inverse Jordan-Wigner transformation. We have that the Pauli operator σ_j^z is easily mapped to fermionic annihilation and creation operators as

$$\sigma_j^z = a_j a_j^\dagger - a_j^\dagger a_j = 1 - 2a_j^\dagger a_j. \tag{A.28}$$

We see that for this transformation local spin operators are mapped to local fermionic operators. We know nonetheless that the Jordan-Wigner transformation does not preserve locality in general, indeed we have that the Pauli operators σ_j^x and σ_j^y maps to fermionic operators as

$$\begin{aligned}
\sigma_j^x &= -\left(\otimes_{k=1}^{j-1}\sigma_k^z\right) \otimes (a_j + a_j^\dagger) \left(\otimes_{k=j+1}^{N}\mathbb{I}_k\right) \\
\sigma_j^y &= i\left(\otimes_{k=1}^{j-1}\sigma_k^z\right) \otimes (a_j^\dagger - a_j) \left(\otimes_{k=j+1}^{N}\mathbb{I}_k\right),
\end{aligned} \tag{A.29}$$

where for each σ_k^z one should use the substitution (A.28).
Fortunately, if we consider the product of Pauli operators, as for example are the spin-spin interactions in the TFI model we have

$$\begin{aligned}
\sigma_j^x\sigma_{j+1}^x &= (a_j^\dagger - a_j)(a_{j+1} + a_{j+1}^\dagger), \\
\sigma_j^y\sigma_{j+1}^y &= -(a_j^\dagger + a_j)(a_{j+1}^\dagger - a_{j+1}), \\
\sigma_j^x\sigma_{j+1}^y &= i(a_j^\dagger - a_j)(a_{j+1}^\dagger - a_{j+1}), \\
\sigma_j^y\sigma_{j+1}^x &= i(a_j^\dagger + a_j)(a_{j+1}^\dagger + a_{j+1}),
\end{aligned} \tag{A.30}$$

nearest neighbour interactions are mapped to nearest neighbour interactions.
It easy to see that an interaction of this kind between two arbitrary spins at site j and k will map to a string of Dirac operators acting non trivially on all sites between

j and k.

We have seen that the Jordan-Wigner transformation defines an isomorphism from a system of n fermions to a system of n spins. One should ask why we cannot completely identify spin systems with fermionic systems or vice versa. To answer to this question we remind that, as specified above, the Jordan-Wigner mapping does not preserve the locality. One of the consequence of this fact is that the procedure of partial tracing does not generally commute with the Jordan-Wigner mapping [1, 135]. Consider for example a state of N fermions ρ_{AB} defined on a system divided in two complementary partitions A and B. We map ρ_{AB} with a Jordan-Wigner transformation to a state $\tilde{\rho}_{AB}$ of N spins. Now we consider the reduced states ρ_A and $\tilde{\rho}_A$ on partition A of the states ρ_{AB} and $\tilde{\rho}_{AB}$. If, using a Jordan-Wigner transformation, we map the state ρ_A to the spin state $\tilde{\tilde{\rho}}_A$, we will generally have that $\tilde{\rho}_A \neq \tilde{\tilde{\rho}}_A$ as shown schematically in figure A.1.6.

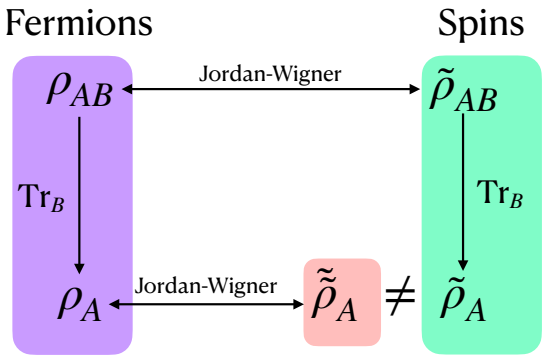

Figure A.1: The mapping of the reduced state is different from the reduced state of the mapping [1]

For a detailed and very well explained treatment of this question see [1]. We end this subsection pointing out that, the fact that the well defined trace for fermionic system is not consistent with the mapping between fermions and qubits, leads to many interesting questions on entanglement in fermionic systems, see e.g. [279–284]

A.2 Useful relations

A.2.1 Pauli Matrices

1. $\sigma^+ = \begin{pmatrix} 0 & 1 \\ 0 & 0 \end{pmatrix}$, $\sigma^- = \begin{pmatrix} 0 & 0 \\ 1 & 0 \end{pmatrix}$, $\sigma^z = \begin{pmatrix} 1 & 0 \\ 0 & -1 \end{pmatrix}$, $\sigma^y = \begin{pmatrix} 0 & -i \\ i & 0 \end{pmatrix}$, $\sigma^x = \begin{pmatrix} 0 & 1 \\ 1 & 0 \end{pmatrix}$, $|+\rangle_x = \frac{1}{\sqrt{2}} \begin{pmatrix} 1 \\ 1 \end{pmatrix}$, $|-\rangle_x = \frac{1}{\sqrt{2}} \begin{pmatrix} 1 \\ -1 \end{pmatrix}$, $|+\rangle_y = \frac{1}{\sqrt{2}} \begin{pmatrix} 1 \\ i \end{pmatrix}$, $|-\rangle_y = \frac{1}{\sqrt{2}} \begin{pmatrix} 1 \\ -i \end{pmatrix}$, $|0_-\rangle_z = \begin{pmatrix} 0 \\ 1 \end{pmatrix}$, $|1_+\rangle_z = \begin{pmatrix} 1 \\ 0 \end{pmatrix}$
2. $\sigma^z\sigma^- = -\sigma^-$
3. $\sigma^z\sigma^+ = \sigma^+$
4. $\sigma^-\sigma^z = \sigma^-$
5. $\sigma^+\sigma^z = -\sigma^+$
6. $\sigma^+\sigma^- = \frac{\sigma^z+\mathbb{I}}{2}$
7. $\sigma^-\sigma^+ = \frac{\mathbb{I}-\sigma^z}{2}$

A.2.2 Operators obeying CAR

1. $\{a_i, a_j^\dagger\} = \mathbb{I}\delta_{i,j} \qquad \{a_i, a_j\} = \{a_i^\dagger, a_j^\dagger\} = 0$
2. $a_i a_j = -a_j a_i; \qquad a_i^\dagger a_j^\dagger = -a_j^\dagger a_i^\dagger$
3. $a_i^2 = \left(a_j^\dagger\right)^2 = 0$
4. $a_i a_j^\dagger = \delta_{i,j} - a_j^\dagger a_i$
5. $a_i a_j = \frac{a_i a_j - a_j a_i}{2}$
6. $a_i a_j^\dagger = \frac{a_i a_j^\dagger - a_j^\dagger a_i}{2} + \frac{\delta_{i,j}}{2}$
7. $a_i^\dagger a_j = \frac{a_i^\dagger a_j - a_j a_i^\dagger}{2} + \frac{\delta_{i,j}}{2}$

Commutators

1. $[a_i^\dagger, a_j] = \delta_{i,j} - 2a_j a_i^\dagger = a_i^\dagger a_j - \delta_{i.j}$
2. $[a_i, a_j^\dagger] = \delta_{i,j} - 2a_j^\dagger a_i = a_i a_j^\dagger - \delta_{i,j}$
3. $[a_i, a_j] = 2a_i a_j$
4. $[a_i^\dagger, a_j^\dagger] = 2a_i^\dagger a_j^\dagger$

Majorana operators

1. $x_i^2 = p_i^2 = \frac{1}{2}$
2. $a^\dagger a = \frac{i}{2}(xp - px) + \frac{1}{2} = ixp + \frac{1}{2}$
3. $aa^\dagger = \frac{i}{2}(px - xp) + \frac{1}{2} = ipx + \frac{1}{2}$
4. $xp = -\frac{i}{2}\left(a^\dagger a - aa^\dagger\right) = -i\left(a^\dagger a - \frac{1}{2}\right)$

A.2.3 Jordan-Wigner Transformations

spinless fermions → spins

1. $a_j = -\bigotimes_{k=1}^{j-1} \sigma_k^z \otimes \sigma_j^- \bigotimes_{k=j+1}^{N} \mathbb{I}_k$
2. $a_j^\dagger = -\bigotimes_{k=1}^{j-1} \sigma_k^z \otimes \sigma_j^+ \bigotimes_{k=j+1}^{N} \mathbb{I}_k$
3. $a_j^\dagger a_j = \otimes_{k=1}^{j-1} \mathbb{I}_k \otimes \frac{\sigma_j^z + \mathbb{I}_j}{2} \otimes_{k=j+1}^{N} \mathbb{I}_k$

spins → spinless fermions

1. $\sigma_j^z = a_j^\dagger a_j - a_j a_j^\dagger$
2. $\sigma_j^x = -\bigotimes_{k=1}^{j-1} \sigma_j^z \otimes (a_j + a_j^\dagger) \bigotimes_{k=j+1}^{N} \mathbb{I}_j$
3. $\sigma_j^x = i \bigotimes_{k=1}^{j-1} \sigma_j^z \otimes (a_j^\dagger - a_j) \bigotimes_{k=j+1}^{N} \mathbb{I}_j$
4. $\sigma_j^x \sigma_{j+1}^x = (a_j^\dagger - a_j)(a_{j+1} + a_{j+1}^\dagger)$
5. $\sigma_j^y \sigma_{j+1}^y = -(a_j^\dagger + a_j)(a_{j+1}^\dagger - a_{j+1})$
6. $\sigma_j^x \sigma_{j+1}^y = i(a_j^\dagger - a_j)(a_{j+1}^\dagger + a_{j+1})$
7. $\sigma_j^y \sigma_{j+1}^x = i(a_j^\dagger + a_j)(a_{j+1}^\dagger + a_{j+1})$

A.2.4 Formulas

1. B.C.H. 1: $e^A e^B = e^Z$ with $Z = A + B + \frac{1}{2}[A,B] + \frac{1}{12}[A,[A,B]] + \frac{1}{12}[B,[A,B]] +$ ... higher commutators of A and B

2. B.C.H 2: $e^A B e^{-A} = \sum_{n=0}^{\infty} \frac{1}{n!} \underbrace{[A,\ldots[A}_{n},B\underbrace{]\ldots]}_{n}$ where $[A,B] = AB - BA$.

3. B.C.H 3: $e^A B e^A = \sum_{n=0}^{\infty} \frac{1}{n!} \underbrace{\{A,\ldots\{A}_{n},B\underbrace{\}\ldots\}}_{n}$ where $\{A,B\} = AB + BA$.

4. Kronecker Delta: $\delta_{n,m} = \frac{1}{N}\sum_{k=1}^{N} e^{i\frac{2\pi}{N}k(n-m)}$.

Bibliography

[1] N. Friis, "Reasonable fermionic quantum information theories require relativity," *New J. Phys.*, vol. 18, no. 3, 2016.

[2] M. H. Anderson, J. R. Ensher, M. R. Matthews, C. E. Wieman, and E. A. Cornell, "Observation of Bose-Einstein Condensation in a Dilute Atomic Vapor," *Science*, vol. 269, pp. 198–201, July 1995.

[3] K. B. Davis, M. O. Mewes, M. R. Andrews, N. J. van Druten, D. S. Durfee, D. M. Kurn, and W. Ketterle, "Bose-Einstein Condensation in a Gas of Sodium Atoms," *Phys. Rev. Lett.*, vol. 75, pp. 3969–3973, Nov. 1995.

[4] C. C. Bradley, C. A. Sackett, J. J. Tollett, and R. G. Hulet, "Evidence of Bose-Einstein Condensation in an Atomic Gas with Attractive Interactions," *Phys. Rev. Lett.*, vol. 75, pp. 1687–1690, Aug. 1995.

[5] H. J. Metcalf, P. van der Straten, and P. van der Straten, *Laser Cooling and Trapping*. Graduate Texts in Contemporary Physics, New York: Springer-Verlag, 1999.

[6] W. Ketterle and N. J. V. Druten, "Evaporative Cooling of Trapped Atoms," in *Advances In Atomic, Molecular, and Optical Physics* (B. Bederson and H. Walther, eds.), vol. 37, pp. 181–236, Academic Press, Jan. 1996.

[7] F. Schreck, G. Ferrari, K. L. Corwin, J. Cubizolles, L. Khaykovich, M.-O. Mewes, and C. Salomon, "Sympathetic cooling of bosonic and fermionic lithium gases towards quantum degeneracy," *Phys. Rev. A*, vol. 64, p. 011402, June 2001.

[8] D. C. McKay and B. DeMarco, "Cooling in strongly correlated optical lattices: Prospects and challenges," *Rep. Prog. Phys.*, vol. 74, p. 054401, Apr. 2011.

[9] I. Bloch, J. Dalibard, and W. Zwerger, "Many-body physics with ultracold gases," *Rev. Mod. Phys.*, vol. 80, pp. 885–964, July 2008.

[10] S. R. White, "Density matrix formulation for quantum renormalization groups," *Phys. Rev. Lett.*, vol. 69, pp. 2863–2866, Nov. 1992.

[11] G. Vidal, "Efficient Classical Simulation of Slightly Entangled Quantum Computations," *Phys. Rev. Lett.*, vol. 91, p. 147902, Oct. 2003.

[12] G. Vidal, "Efficient simulation of one-dimensional quantum many-body systems," *Phys. Rev. Lett.*, vol. 93, p. 040502, July 2004.

[13] I. Affleck, T. Kennedy, E. H. Lieb, and H. Tasaki, "Valence bond ground states in isotropic quantum antiferromagnets," *Commun. Math. Phys.*, vol. 115, pp. 477–528, Sept. 1988.

[14] M. Fannes, B. Nachtergaele, and R. F. Werner, "Exact Antiferromagnetic Ground States of Quantum Spin Chains," *EPL*, vol. 10, pp. 633–637, Dec. 1989. Publisher: IOP Publishing.

[15] M. Fannes, B. Nachtergaele, and R. F. Werner, "Finitely correlated states on quantum spin chains," *Commun.Math. Phys.*, vol. 144, pp. 443–490, Mar. 1992.

[16] S. Rommer and S. Östlund, "Class of ansatz wave functions for one-dimensional spin systems and their relation to the density matrix renormalization group," *Phys. Rev. B*, vol. 55, pp. 2164–2181, Jan. 1997.

[17] M. B. Hastings, "An Area Law for One Dimensional Quantum Systems," *J. Stat. Mech.*, vol. 2007, no. 08, p. P08024, 2007.

[18] M. M. Wolf, F. Verstraete, M. B. Hastings, and J. I. Cirac, "Area Laws in Quantum Systems: Mutual Information and Correlations," *Phys. Rev. Lett.*, vol. 100, p. 070502, Feb. 2008.

[19] J. Eisert, M. Cramer, and M. B. Plenio, "Colloquium: Area laws for the entanglement entropy," *Rev. Mod. Phys.*, vol. 82, pp. 277–306, Feb. 2010.

[20] R. Orús, "A practical introduction to tensor networks: Matrix product states and projected entangled pair states," *Ann. Phys. (N. Y.)*, vol. 349, pp. 117–158, Oct. 2014.

[21] J. C. Bridgeman and C. T. Chubb, "Hand-waving and Interpretive Dance: An Introductory Course on Tensor Networks," *J. Phys. A: Math. Theor.*, vol. 50, p. 223001, June 2017.

[22] S.-J. Ran, E. Tirrito, C. Peng, X. Chen, L. Tagliacozzo, G. Su, and M. Lewenstein, *Tensor Network Contractions: Methods and Applications to Quantum Many-Body Systems*. Lect. Notes Phys., Springer International Publishing, 2020.

[23] J. Biamonte and V. Bergholm, "Tensor Networks in a Nutshell," *arXiv:1708.00006*, July 2017.

[24] B. Pirvu, V. Murg, J. I. Cirac, and F. Verstraete, "Matrix product operator representations," *New J. Phys.*, vol. 12, p. 025012, Feb. 2010.

[25] M. Zwolak and G. Vidal, "Mixed-State Dynamics in One-Dimensional Quantum Lattice Systems: A Time-Dependent Superoperator Renormalization Algorithm," *Phys. Rev. Lett.*, vol. 93, p. 207205, Nov. 2004.

[26] I. P. McCulloch, "From density-matrix renormalization group to matrix product states," *J. Stat. Mech.*, vol. 2007, p. P10014, Oct. 2007.

[27] G. M. Crosswhite, A. C. Doherty, and G. Vidal, "Applying matrix product operators to model systems with long-range interactions," *Phys. Rev. B*, vol. 78, p. 035116, July 2008.

[28] I. P. McCulloch, "Infinite size density matrix renormalization group, revisited," *arXiv:0804.2509*, Apr. 2008.

[29] T. Koffel, M. Lewenstein, and L. Tagliacozzo, "Entanglement Entropy for the Long-Range Ising Chain in a Transverse Field," *Phys. Rev. Lett.*, vol. 109, p. 267203, Dec. 2012.

[30] V. Nebendahl and W. Dür, "Improved numerical methods for infinite spin chains with long-range interactions," *Phys. Rev. B*, vol. 87, p. 075413, Feb. 2013.

[31] F. Verstraete, J. J. García-Ripoll, and J. I. Cirac, "Matrix Product Density Operators: Simulation of Finite-Temperature and Dissipative Systems," *Phys. Rev. Lett.*, vol. 93, p. 207204, Nov. 2004.

[32] J. v. Neumann, "Beweis des Ergodensatzes und des H-Theorems in der neuen Mechanik," *Z. Physik*, vol. 57, pp. 30–70, Jan. 1929.

[33] E. Schrödinger, "Energieaustausch nach der Wellenmechanik," *Ann. Phys. (Berl.)*, vol. 388, no. 15, pp. 956–968, 1927.

[34] H. Tasaki, "From Quantum Dynamics to the Canonical Distribution: General Picture and a Rigorous Example," *Phys. Rev. Lett.*, vol. 80, pp. 1373–1376, Feb. 1998.

[35] P. Reimann, "Foundation of Statistical Mechanics under Experimentally Realistic Conditions," *Phys. Rev. Lett.*, vol. 101, p. 190403, Nov. 2008.

[36] N. Linden, S. Popescu, A. J. Short, and A. Winter, "Quantum mechanical evolution towards thermal equilibrium," *Phys. Rev. E*, vol. 79, p. 061103, 2009.

[37] A. Acín, I. Bloch, H. Buhrman, T. Calarco, C. Eichler, J. Eisert, D. Esteve, N. Gisin, S. J. Glaser, F. Jelezko, S. Kuhr, M. Lewenstein, M. F. Riedel, P. O. Schmidt, R. Thew, A. Wallraff, I. Walmsley, and F. K. Wilhelm, "The quantum technologies roadmap: A European community view," *New J. Phys.*, vol. 20, p. 080201, Aug. 2018.

[38] M. Lostaglio, "An introductory review of the resource theory approach to thermodynamics," *Rep. Prog. Phys.*, vol. 82, p. 114001, Oct. 2019.

[39] T. Kinoshita, T. Wenger, and D. S. Weiss, "Observation of a One-Dimensional Tonks-Girardeau Gas," *Science*, vol. 305, pp. 1125–1128, Aug. 2004.

[40] T. Kinoshita, T. Wenger, and D. S. Weiss, "Local Pair Correlations in One-Dimensional Bose Gases," *Phys. Rev. Lett.*, vol. 95, p. 190406, Nov. 2005.

[41] A. H. van Amerongen, J. J. P. van Es, P. Wicke, K. V. Kheruntsyan, and N. J. van Druten, "Yang-Yang Thermodynamics on an Atom Chip," *Phys. Rev. Lett.*, vol. 100, p. 090402, Mar. 2008.

[42] S. Hofferberth, I. Lesanovsky, B. Fischer, T. Schumm, and J. Schmiedmayer, "Non-equilibrium coherence dynamics in one-dimensional Bose gases," *Nature*, vol. 449, pp. 324–327, Sept. 2007.

[43] S. Trotzky, Y.-A. Chen, A. Flesch, I. P. McCulloch, U. Schollwöck, J. Eisert, and I. Bloch, "Probing the relaxation towards equilibrium in an isolated strongly correlated one-dimensional Bose gas," *Nat. Phys.*, vol. 8, pp. 325–330, Apr. 2012.

[44] M. Cheneau, P. Barmettler, D. Poletti, M. Endres, P. Schauß, T. Fukuhara, C. Gross, I. Bloch, C. Kollath, and S. Kuhr, "Light-cone-like spreading of correlations in a quantum many-body system," *Nature*, vol. 481, pp. 484–487, Jan. 2012.

[45] L. Hackermüller, U. Schneider, M. Moreno-Cardoner, T. Kitagawa, T. Best, S. Will, E. Demler, E. Altman, I. Bloch, and B. Paredes, "Anomalous Expansion of Attractively Interacting Fermionic Atoms in an Optical Lattice," *Science*, vol. 327, pp. 1621–1624, Mar. 2010.

[46] M. Gring, M. Kuhnert, T. Langen, T. Kitagawa, B. Rauer, M. Schreitl, I. Mazets, D. A. Smith, E. Demler, and J. Schmiedmayer, "Relaxation and Prethermalization in an Isolated Quantum System," *Science*, vol. 337, pp. 1318–1322, Sept. 2012.

[47] T. Langen, R. Geiger, M. Kuhnert, B. Rauer, and J. Schmiedmayer, "Local emergence of thermal correlations in an isolated quantum many-body system," *Nat. Phys.*, vol. 9, pp. 640–643, Oct. 2013.

[48] I. Bloch, "Ultracold quantum gases in optical lattices," *Nat. Phys.*, vol. 1, pp. 23–30, Oct. 2005.

[49] R. Jördens, N. Strohmaier, K. Günter, H. Moritz, and T. Esslinger, "A Mott insulator of fermionic atoms in an optical lattice," *Nature*, vol. 455, pp. 204–207, Sept. 2008.

[50] T. Kinoshita, T. Wenger, and D. S. Weiss, "A quantum Newton's cradle," *Nature*, vol. 440, pp. 900–903, Apr. 2006.

[51] A. Polkovnikov, K. Sengupta, A. Silva, and M. Vengalattore, "Colloquium: Nonequilibrium dynamics of closed interacting quantum systems," *Rev. Mod. Phys.*, vol. 83, pp. 863–883, Aug. 2011.

[52] P. Calabrese and J. Cardy, "Evolution of entanglement entropy in one-dimensional systems," *J. Stat. Mech.*, vol. 2005, no. 04, p. P04010, 2005.

[53] G. De Chiara, S. Montangero, P. Calabrese, and R. Fazio, "Entanglement entropy dynamics of Heisenberg chains," *J. Stat. Mech.: Theory Exp.*, vol. 2006, no. 3, p. P03001, 2006.

[54] A. M. Läuchli and C. Kollath, "Spreading of correlations and entanglement after a quench in the one-dimensional Bose–Hubbard model," *J. Stat. Mech.*, vol. 2008, p. P05018, May 2008.

[55] H. Kim and D. A. Huse, "Ballistic Spreading of Entanglement in a Diffusive Nonintegrable System," *Phys. Rev. Lett.*, vol. 111, p. 127205, Sept. 2013.

[56] M. Fagotti and M. Collura, "Universal prethermalization dynamics of entanglement entropies after a global quench," *arXiv:1507.02678*, July 2015.

[57] M. Kormos, M. Collura, G. Takács, and P. Calabrese, "Real-time confinement following a quantum quench to a non-integrable model," *Nat. Phys.*, vol. 13, pp. 246–249, Mar. 2017.

[58] C. W. von Keyserlingk, T. Rakovszky, F. Pollmann, and S. L. Sondhi, "Operator Hydrodynamics, OTOCs, and Entanglement Growth in Systems without Conservation Laws," *Phys. Rev. X*, vol. 8, p. 021013, Apr. 2018.

[59] P. Calabrese and J. Cardy, "Time-dependence of correlation functions following a quantum quench," *Phys. Rev. Lett.*, vol. 96, p. 136801, Apr. 2006.

[60] A. J. Short, "Equilibration of quantum systems and subsystems," *New J. Phys.*, vol. 13, p. 053009, May 2011.

[61] A. J. Short and T. C. Farrelly, "Quantum equilibration in finite time," *New J. Phys.*, vol. 14, p. 013063, Jan. 2012.

[62] J. Eisert, M. Friesdorf, and C. Gogolin, "Quantum many-body systems out of equilibrium," *Nat. Phys.*, vol. 11, pp. 124–130, Feb. 2015.

[63] A. Polkovnikov, K. Sengupta, A. Silva, and M. Vengalattore, "Colloquium: Nonequilibrium dynamics of closed interacting quantum systems," *Rev. Mod. Phys.*, vol. 83, pp. 863–883, Aug. 2011.

[64] C. Gogolin and J. Eisert, "Equilibration, thermalisation, and the emergence of statistical mechanics in closed quantum systems," *Rep. Prog. Phys.*, vol. 79, p. 056001, Apr. 2016.

[65] A. Pelissetto and E. Vicari, "Critical phenomena and renormalization-group theory," *Phys. Rep.*, vol. 368, pp. 549–727, Oct. 2002.

[66] G. Vidal, J. I. Latorre, E. Rico, and A. Kitaev, "Entanglement in Quantum Critical Phenomena," *Phys. Rev. Lett.*, vol. 90, p. 227902, June 2003.

[67] A. A. Belavin, A. M. Polyakov, and A. B. Zamolodchikov, "Infinite conformal symmetry in two-dimensional quantum field theory," *Nucl. Phys. B*, vol. B241, pp. 333–380, 1984.

[68] M. Henkel, *Conformal Invariance and Critical Phenomena*. Theoretical and Mathematical Physics, Berlin Heidelberg: Springer-Verlag, 1999.

[69] P. Calabrese and J. Cardy, "Entanglement entropy and quantum field theory," *J. Stat. Mech.: Theory Exp.*, vol. 2004, p. P06002, June 2004.

[70] P. Corboz and G. Vidal, "Fermionic multiscale entanglement renormalization ansatz," *Phys. Rev. B*, vol. 80, p. 165129, Oct. 2009.

[71] G. Evenbly and G. Vidal, "Entanglement renormalization in free bosonic systems: Real-space versus momentum-space renormalization group transforms," *New J. Phys.*, vol. 12, p. 025007, Feb. 2010.

[72] G. Evenbly and G. Vidal, "Entanglement renormalization in noninteracting fermionic systems," *Phys. Rev. B*, vol. 81, p. 235102, June 2010.

[73] M. T. Fishman and S. R. White, "Compression of correlation matrices and an efficient method for forming matrix product states of fermionic Gaussian states," *Phys. Rev. B*, vol. 92, p. 075132, Aug. 2015.

[74] G. Evenbly and S. R. White, "Entanglement Renormalization and Wavelets," *Phys. Rev. Lett.*, vol. 116, p. 140403, Apr. 2016.

[75] J. Haegeman, B. Swingle, M. Walter, J. Cotler, G. Evenbly, and V. B. Scholz, "Rigorous Free-Fermion Entanglement Renormalization from Wavelet Theory," *Phys. Rev. X*, vol. 8, p. 011003, Jan. 2018.

[76] J. Demmel, I. Dumitriu, and O. Holtz, "Fast linear algebra is stable," *Numer. Math.*, vol. 108, pp. 59–91, Nov. 2007.

[77] W. H. Press, S. A. Teukolsky, W. T. Vetterling, and B. P. Flannery, *Numerical Recipes 3rd Edition: The Art of Scientific Computing*. USA: Cambridge University Press, third ed., 2007.

[78] R. M. Noack and S. R. Manmana, "Diagonalization- and Numerical Renormalization-Group-Based Methods for Interacting Quantum Systems," *AIP Conference Proceedings*, vol. 789, pp. 93–163, Sept. 2005.

[79] Y. Saad, *Numerical Methods for Large Eigenvalue Problems*. Classics in Applied Mathematics, SIAM, Jan. 2011.

[80] C. Lanczos, "An iteration method for the solution of the eigenvalue problem of linear differential and integral operators," *J. Res. Natl. Bur. Stan.*, vol. 45, p. 255, Oct. 1950.

[81] I. U. Ojalvo and M. Newman, "Vibration modes of large structures by an automatic matrix-reductionmethod," *AIAA Journal*, vol. 8, pp. 1234–1239, July 1970.

[82] C. C. Paige, *The Computation of Eigenvalues and Eigenvectors of Very Large Sparse Matrices*. London: C.C. Paige, 1971.

[83] M. Grinfeld, *Mathematical Tools for Physicists*. John Wiley & Sons, Jan. 2015.

[84] H. F. Trotter, "On the product of semi-groups of operators," *Proc. Amer. Math. Soc.*, vol. 10, no. 4, pp. 545–551, 1959.

[85] M. Suzuki, "Generalized Trotter's formula and systematic approximants of exponential operators and inner derivations with applications to many-body problems," *Commun.Math. Phys.*, vol. 51, pp. 183–190, June 1976.

[86] N. Hatano and M. Suzuki, "Finding Exponential Product Formulas of Higher Orders," in *Quantum Annealing and Other Optimization Methods* (A. Das and B. K. Chakrabarti, eds.), Lect. Notes Phys., pp. 37–68, Berlin, Heidelberg: Springer, 2005.

[87] D. A. Huffman, "A Method for the Construction of Minimum-Redundancy Codes," *Proceedings of the IRE*, vol. 40, pp. 1098–1101, Sept. 1952.

[88] T. M. Cover and J. A. Thomas, *Elements of Information Theory 2nd Edition*. Hoboken, N.J: Wiley-Interscience, 2 edition ed., July 2006.

[89] J. Biamonte, "Lectures on Quantum Tensor Networks," *arXiv:1912.10049*, Jan. 2020.

[90] R. Horodecki, P. Horodecki, M. Horodecki, and K. Horodecki, "Quantum entanglement," *Rev. Mod. Phys.*, vol. 81, pp. 865–942, June 2009.

[91] E. Chitambar and G. Gour, "Quantum resource theories," *Rev. Mod. Phys.*, vol. 91, p. 025001, Apr. 2019.

[92] Y. Chen and G. Vidal, "Entanglement contour," *J. Stat. Mech. Theory Exp.*, vol. 2014, p. P10011, Oct. 2014.

[93] A. Coser, C. D. Nobili, and E. Tonni, "A contour for the entanglement entropies in harmonic lattices," *J. Phys. A: Math. Theor.*, vol. 50, p. 314001, July 2017.

[94] E. Tonni, J. Rodríguez-Laguna, and G. Sierra, "Entanglement hamiltonian and entanglement contour in inhomogeneous 1D critical systems," *J. Stat. Mech.: Theory Exp.*, vol. 2018, p. 043105, Apr. 2018.

[95] X. Wen, S. Ryu, and A. W. W. Ludwig, "Entanglement Hamiltonian evolution during thermalization in conformal field theory," *J. Stat. Mech.*, vol. 2018, p. 113103, Nov. 2018.

[96] E. Pavarini, ed., *Emergent phenomena in correlated matter: lecture notes of the Autumn School Correlated Electrons 2013 at Forschungszentrum Jülich, 23 –27 September 2013*. No. 3 in Schriften des Forschungszentrums Jülich Reihe Modeling and Simulation, Jülich: Forschungszentrum Jülich, 2013.

[97] H. Li and F. D. M. Haldane, "Entanglement Spectrum as a Generalization of Entanglement Entropy: Identification of Topological Order in Non-Abelian Fractional Quantum Hall Effect States," *Phys. Rev. Lett.*, vol. 101, p. 010504, July 2008.

[98] P. Calabrese and A. Lefevre, "Entanglement spectrum in one-dimensional systems," *Phys. Rev. A*, vol. 78, p. 032329, Sept. 2008.

[99] D. Poilblanc, "Entanglement Spectra of Quantum Heisenberg Ladders," *Phys. Rev. Lett.*, vol. 105, p. 077202, Aug. 2010.

[100] J. I. Cirac, D. Poilblanc, N. Schuch, and F. Verstraete, "Entanglement spectrum and boundary theories with projected entangled-pair states," *Phys. Rev. B*, vol. 83, p. 245134, June 2011.

[101] J. Dubail, N. Read, and E. H. Rezayi, "Real-space entanglement spectrum of quantum Hall systems," *Phys. Rev. B*, vol. 85, p. 115321, Mar. 2012.

[102] M. B. Hastings, "Decay of Correlations in Fermi Systems at Non-zero Temperature," *Phys. Rev. Lett.*, vol. 93, Sept. 2004.

[103] M. B. Hastings and T. Koma, "Spectral Gap and Exponential Decay of Correlations," *Commun. Math. Phys.*, vol. 265, pp. 781–804, Aug. 2006.

[104] O. Bratteli and D. W. Robinson, *Operator Algebras and Quantum Statistical Mechanics II: Equilibrium States Models in Quantum Statistical Mechanics.* Theoretical and Mathematical Physics, Berlin Heidelberg: Springer-Verlag, 1981.

[105] F. G. S. L. Brandão and M. Horodecki, "Exponential Decay of Correlations Implies Area Law," *Commun. Math. Phys.*, vol. 333, pp. 761–798, Jan. 2015.

[106] J. D. Bekenstein, "Black Holes and Entropy," *Phys. Rev. D*, vol. 7, pp. 2333–2346, Apr. 1973.

[107] M. B. Plenio, J. Eisert, J. Dreißig, and M. Cramer, "Entropy, Entanglement, and Area: Analytical Results for Harmonic Lattice Systems," *Phys. Rev. Lett.*, vol. 94, p. 060503, Feb. 2005.

[108] M. M. Wolf, "Violation of the Entropic Area Law for Fermions," *Phys. Rev. Lett.*, vol. 96, p. 010404, Jan. 2006.

[109] M. B. Hastings, "An area law for one-dimensional quantum systems," *J. Stat. Mech.*, vol. 2007, p. P08024, Aug. 2007.

[110] C. Holzhey, F. Larsen, and F. Wilczek, "Geometric and renormalized entropy in conformal field theory," *Nucl. Phys. B*, vol. 424, pp. 443–467, Aug. 1994.

[111] M. Cramer and J. Eisert, "Correlations, spectral gap and entanglement in harmonic quantum systems on generic lattices," *New J. Phys.*, vol. 8, pp. 71–71, May 2006.

[112] M. Cramer, J. Eisert, and M. B. Plenio, "Statistics Dependence of the Entanglement Entropy," *Phys. Rev. Lett.*, vol. 98, p. 220603, May 2007.

[113] L. Masanes, "Area law for the entropy of low-energy states," *Phys. Rev. A*, vol. 80, p. 052104, Nov. 2009.

[114] S. K. Foong and S. Kanno, "Proof of Page's conjecture on the average entropy of a subsystem," *Phys. Rev. Lett.*, vol. 72, pp. 1148–1151, Feb. 1994.

[115] G. Vidal, "Efficient Classical Simulation of Slightly Entangled Quantum Computations," *Phys. Rev. Lett.*, vol. 91, p. 147902, Oct. 2003.

[116] G. Vidal, J. I. Latorre, E. Rico, and A. Kitaev, "Entanglement in Quantum Critical Phenomena," *Phys. Rev. Lett.*, vol. 90, p. 227902, June 2003.

[117] U. Schollwöck, "The density-matrix renormalization group in the age of matrix product states," *Annals of Physics*, vol. 326, pp. 96–192, Aug. 2011.

[118] C. Eckart and G. Young, "The approximation of one matrix by another of lower rank," *Psychometrika*, vol. 1, pp. 211–218, Sept. 1936.

[119] L. Mirsky, "Symmetric gauge functions and unitarily invariant norms," *Q. J. Math.*, vol. 11, pp. 50–59, Jan. 1960.

[120] N. Srebro and T. Jaakkola, "Weighted low-rank approximations," in *Proceedings of the Twentieth International Conference on International Conference on Machine Learning*, ICML'03, (Washington, DC, USA), pp. 720–727, AAAI Press, Aug. 2003.

[121] I. Razenshteyn, Z. Song, and D. P. Woodruff, "Weighted low rank approximations with provable guarantees," in *Proceedings of the Forty-Eighth Annual ACM Symposium on Theory of Computing*, STOC '16, (Cambridge, MA, USA), pp. 250–263, Association for Computing Machinery, June 2016.

[122] F. Verstraete and J. I. Cirac, "Matrix product states represent ground states faithfully," *Phys. Rev. B*, vol. 73, p. 094423, Mar. 2006.

[123] N. Schuch, M. M. Wolf, F. Verstraete, and J. I. Cirac, "Entropy Scaling and Simulability by Matrix Product States," *Phys. Rev. Lett.*, vol. 100, p. 030504, Jan. 2008.

[124] B. Pirvu, V. Murg, J. I. Cirac, and F. Verstraete, "Matrix product operator representations," *New J. Phys.*, vol. 12, p. 025012, Feb. 2010.

[125] M. Kliesch, D. Gross, and J. Eisert, "Matrix-Product Operators and States: NP-Hardness and Undecidability," *Phys. Rev. Lett.*, vol. 113, p. 160503, Oct. 2014.

[126] M. B. Hastings, "Solving gapped Hamiltonians locally," *Phys. Rev. B*, vol. 73, p. 085115, Feb. 2006.

[127] M. Kliesch, C. Gogolin, M. J. Kastoryano, A. Riera, and J. Eisert, "Locality of Temperature," *Phys. Rev. X*, vol. 4, p. 031019, July 2014.

[128] A. Molnar, N. Schuch, F. Verstraete, and J. I. Cirac, "Approximating Gibbs states of local Hamiltonians efficiently with projected entangled pair states," *Phys. Rev. B*, vol. 91, p. 045138, Jan. 2015.

[129] M. Kliesch and A. Riera, "Properties of Thermal Quantum States: Locality of Temperature, Decay of Correlations, and More," in *Thermodynamics in the Quantum Regime: Fundamental Aspects and New Directions*, Fundamental Theories of Physics, pp. 481–502, Springer International Publishing, 2018.

[130] M. A. Nielsen, "The Fermionic canonical commutation relations and the Jordan-Wigner transform," *http://michaelnielsen.org/blog/archive/notes/fermions_and_jordan_wigner.pdf*, p. 8.

[131] S. Bravyi, "Lagrangian representation for fermionic linear optics," *arXiv:quant-ph/0404180*, Apr. 2004.

[132] E. Lieb, T. Schultz, and D. Mattis, "Two soluble models of an antiferromagnetic chain," *Ann. Phys. (N. Y.)*, vol. 16, pp. 407–466, Dec. 1961.

[133] B. Zumino, "Normal Forms of Complex Matrices," *J. Math. Phys.*, vol. 3, pp. 1055–1057, Sept. 1962.

[134] R. A. Horn and C. R. Johnson, *Matrix Analysis*. Cambridge: Cambridge University Press, second ed., 2012.

[135] N. Friis, A. R. Lee, and D. E. Bruschi, "Fermionic-mode entanglement in quantum information," *Phys. Rev. A*, vol. 87, p. 022338, Feb. 2013.

[136] E. T. Jaynes, "Information theory and statistical mechanics," *Phys. Rev.*, vol. 106, pp. 620–630, May 1957.

[137] E. T. Jaynes, "Information theory and statistical mechanics. II," *Phys. Rev.*, vol. 108, no. 2, pp. 171–190, 1957.

[138] L. G. Molinari, "Notes on Wick's theorem in many-body theory," *arXiv:1710.09248*, Oct. 2017.

[139] R. Vein and P. Dale, *Determinants and Their Applications in Mathematical Physics*. Applied Mathematical Sciences, New York: Springer-Verlag, 1999.

[140] I. Peschel, "Calculation of reduced density matrices from correlation functions," *J. Phys. A: Math. Gen.*, vol. 36, pp. L205–L208, Mar. 2003.

[141] S.-A. Cheong and C. L. Henley, "Many-body density matrices for free fermions," *Phys. Rev. B*, vol. 69, p. 075111, Feb. 2004.

[142] J. Zhang, P. Calabrese, M. Dalmonte, and M. A. Rajabpour, "Lattice Bisognano-Wichmann modular Hamiltonian in critical quantum spin chains," *arXiv:2003.00315*, Feb. 2020.

[143] M. Fagotti and P. Calabrese, "Entanglement entropy of two disjoint blocks in XY chains," *J. Stat. Mech. Theory Exp.*, vol. 2010, p. P04016, Apr. 2010.

[144] V. Bach, E. H. Lieb, and J. P. Solovej, "Generalized Hartree-Fock theory and the Hubbard model," *J Stat Phys*, vol. 76, pp. 3–89, July 1994.

[145] T. D. Schultz, D. C. Mattis, and E. H. Lieb, "Two-dimensional Ising model as a soluble problem of many fermions," *Rev. Mod. Phys.*, vol. 36, pp. 856–871, July 1964.

[146] P. Pfeuty, "The one-dimensional Ising model with a transverse field," *Ann Phys (N Y)*, vol. 57, pp. 79–90, Mar. 1970.

[147] D. C. Mattis, "Solvable spin systems with random interactions," *Phys. Lett. A*, vol. 56, pp. 421–422, Apr. 1976.

[148] G. G. Cabrera and R. Jullien, "Role of boundary conditions in the finite-size Ising model," *Phys. Rev. B*, vol. 35, pp. 7062–7072, May 1987.

[149] P. Calabrese, F. H. L. Essler, and M. Fagotti, "Quantum Quench in the Transverse Field Ising chain I: Time evolution of order parameter correlators," *J. Stat. Mech. Theory Exp.*, vol. 2012, p. P07016, July 2012.

[150] S. Suzuki, J.-i. Inoue, and B. K. Chakrabarti, *Transverse Ising Chain (Pure System)*, vol. 862, pp. 13–46. Berlin, Heidelberg: Springer Berlin Heidelberg, 2013.

[151] N. N. Bogoljubov, "On a new method in the theory of superconductivity," *Nuovo Cim*, vol. 7, pp. 794–805, Mar. 1958.

[152] J. G. Valatin, "Comments on the theory of superconductivity," *Nuovo Cim*, vol. 7, pp. 843–857, Mar. 1958.

[153] Y. He and H. Guo, "The boundary effects of transverse field Ising model," *J. Stat. Mech.*, vol. 2017, p. 093101, Sept. 2017.

[154] M. T. Fishman and S. R. White, "Compression of correlation matrices and an efficient method for forming matrix product states of fermionic Gaussian states," *Phys. Rev. B*, vol. 92, p. 075132, Aug. 2015.

[155] J. v. Neumann, "Beweis des Ergodensatzes und des H-Theorems in der neuen Mechanik," *Z. Physik*, vol. 57, pp. 30–70, Jan. 1929.

[156] P. Calabrese and J. Cardy, "Evolution of entanglement entropy in one-dimensional systems," *J. Stat. Mech.*, vol. 2005, p. P04010, Apr. 2005.

[157] G. D. Chiara, S. Montangero, P. Calabrese, and R. Fazio, "Entanglement entropy dynamics of Heisenberg chains," *J. Stat. Mech.*, vol. 2006, Mar. 2006.

[158] M. Collura, M. Kormos, and G. Takács, "Dynamical manifestation of the Gibbs paradox after a quantum quench," *Phys. Rev. A*, vol. 98, p. 053610, Nov. 2018.

[159] S. Bravyi, M. B. Hastings, and F. Verstraete, "Lieb-Robinson Bounds and the Generation of Correlations and Topological Quantum Order," *Phys. Rev. Lett.*, vol. 97, p. 050401, July 2006.

[160] J. Eisert and T. J. Osborne, "General Entanglement Scaling Laws from Time Evolution," *Phys. Rev. Lett.*, vol. 97, p. 150404, Oct. 2006.

[161] K. Van Acoleyen, M. Mariën, and F. Verstraete, "Entanglement Rates and Area Laws," *Phys. Rev. Lett.*, vol. 111, p. 170501, Oct. 2013.

[162] E. H. Lieb and D. W. Robinson, "The finite group velocity of quantum spin systems," *Commun.Math. Phys.*, vol. 28, pp. 251–257, Sept. 1972.

[163] P. Calabrese, F. H. Essler, and M. Fagotti, "Quantum quench in the transverse-field ising chain," *Phys. Rev. Lett.*, vol. 106, Apr. 2011.

[164] P. Calabrese, F. H. L. Essler, and M. Fagotti, "Quantum Quench in the Transverse Field Ising Chain II: Stationary State Properties," *J. Stat. Mech. Theory Exp.*, 2012.

[165] S. Sachdev and A. P. Young, "Low Temperature Relaxational Dynamics of the Ising Chain in a Transverse Field," *Phys. Rev. Lett.*, vol. 78, pp. 2220–2223, Mar. 1997.

[166] M. Fagotti and P. Calabrese, "Evolution of entanglement entropy following a quantum quench: Analytic results for the XY chain in a transverse magnetic field," *Phys. Rev. A*, vol. 78, p. 010306, July 2008.

[167] I. Peschel and V. Eisler, "Reduced density matrices and entanglement entropy in free lattice models," *J. Phys. A: Math. Theor.*, vol. 42, p. 504003, Dec. 2009.

[168] V. Alba and P. Calabrese, "Entanglement and thermodynamics after a quantum quench in integrable systems," *PNAS*, vol. 114, pp. 7947–7951, July 2017.

[169] A. Nahum, S. Vijay, and J. Haah, "Operator Spreading in Random Unitary Circuits," *Phys. Rev. X*, vol. 8, p. 021014, Apr. 2018.

[170] C. T. Asplund, A. Bernamonti, F. Galli, and T. Hartman, "Entanglement scrambling in 2d conformal field theory," *J. High Energ. Phys.*, vol. 2015, p. 110, Sept. 2015.

[171] B. Bertini, M. Collura, J. De Nardis, and M. Fagotti, "Transport in Out-of-Equilibrium XXZ Chains: Exact Profiles of Charges and Currents," *Phys. Rev. Lett.*, vol. 117, p. 207201, Nov. 2016.

[172] O. A. Castro-Alvaredo, B. Doyon, and T. Yoshimura, "Emergent Hydrodynamics in Integrable Quantum Systems Out of Equilibrium," *Phys. Rev. X*, vol. 6, p. 041065, Dec. 2016.

[173] R. V. Jensen and R. Shankar, "Statistical Behavior in Deterministic Quantum Systems with Few Degrees of Freedom," *Phys. Rev. Lett.*, vol. 54, pp. 1879–1882, Apr. 1985.

[174] J. M. Deutsch, "Quantum statistical mechanics in a closed system," *Phys. Rev. A*, vol. 43, pp. 2046–2049, Feb. 1991.

[175] M. Srednicki, "Chaos and quantum thermalization," *Phys. Rev. E*, vol. 50, pp. 888–901, Aug. 1994.

[176] M. Rigol, V. Dunjko, and M. Olshanii, "Thermalization and its mechanism for generic isolated quantum systems," *Nature*, vol. 452, pp. 854–858, Apr. 2008.

[177] A. J. Short, "Equilibration of quantum systems and subsystems," *New J. Phys.*, vol. 13, p. 053009, May 2011.

[178] N. Linden, S. Popescu, A. J. Short, and A. Winter, "Quantum mechanical evolution towards thermal equilibrium," *Phys. Rev. E*, vol. 79, p. 061103, June 2009.

[179] C. Gogolin, M. P. Müller, and J. Eisert, "Absence of Thermalization in Nonintegrable Systems," *Phys. Rev. Lett.*, vol. 106, p. 040401, Jan. 2011.

[180] H. Wilming, M. Goihl, I. Roth, and J. Eisert, "Entanglement-Ergodic Quantum Systems Equilibrate Exponentially Well," *Phys. Rev. Lett.*, vol. 123, p. 200604, Nov. 2019.

[181] F. H. L. Essler and M. Fagotti, "Quench dynamics and relaxation in isolated integrable quantum spin chains," *J. Stat. Mech.*, vol. 2016, p. 064002, June 2016.

[182] M. Fagotti and F. H. L. Essler, "Reduced Density Matrix after a Quantum Quench," *Physical Review B*, vol. 87, June 2013.

[183] L. Vidmar and M. Rigol, "Generalized Gibbs ensemble in integrable lattice models," *J. Stat. Mech.*, vol. 2016, p. 064007, June 2016.

[184] M. Rigol, V. Dunjko, V. Yurovsky, and M. Olshanii, "Relaxation in a completely integrable many-body Quantum system: An Ab initio study of the dynamics of the highly excited states of 1D lattice hard-core bosons," *Phys. Rev. Lett.*, vol. 98, no. 5, 2007.

[185] G. Mussardo, "Infinite-Time Average of Local Fields in an Integrable Quantum Field Theory After a Quantum Quench," *Phys. Rev. Lett.*, vol. 111, p. 100401, Sept. 2013.

[186] C. Gogolin, M. P. Müller, and J. Eisert, "Absence of Thermalization in Nonintegrable Systems," *Phys. Rev. Lett.*, vol. 106, p. 040401, Jan. 2011.

[187] M. Grady, "Infinite set of conserved charges in the Ising model," *Phys. Rev. D*, vol. 25, pp. 1103–1113, Feb. 1982.

[188] F. H. L. Essler, G. Mussardo, and M. Panfil, "On truncated generalized Gibbs ensembles in the Ising field theory," *J. Stat. Mech.*, vol. 2017, p. 013103, Jan. 2017.

[189] F. de Melo, P. Ćwikliński, and B. M. Terhal, "The Power of Noisy Fermionic Quantum Computation," *New J. Phys.*, vol. 15, p. 013015, Jan. 2013.

[190] M. Gluza, C. Krumnow, M. Friesdorf, C. Gogolin, and J. Eisert, "Equilibration via Gaussification in Fermionic Lattice Systems," *Phys. Rev. Lett.*, vol. 117, p. 190602, Nov. 2016.

[191] M. Gluza, J. Eisert, and T. Farrelly, "Equilibration towards generalized Gibbs ensembles in non-interacting theories," *SciPost Phys.*, vol. 7, p. 038, Sept. 2019.

[192] E. M. Stein and T. S. Murphy, *Harmonic Analysis: Real-Variable Methods, Orthogonality, and Oscillatory Integrals. (PMS-43).* Princeton University Press, 1993.

[193] B. Sutherland, *Beautiful Models: 70 Years of Exactly Solved Quantum Many-Body Problems.* World Scientific, June 2004.

[194] M. Rigol and M. Srednicki, "Alternatives to Eigenstate Thermalization," *Phys. Rev. Lett.*, vol. 108, p. 110601, Mar. 2012.

[195] H. Tasaki, "From Quantum Dynamics to the Canonical Distribution: General Picture and a Rigorous Example," *Phys. Rev. Lett.*, vol. 80, pp. 1373–1376, Feb. 1998.

[196] M. P. Müller, E. Adlam, L. Masanes, and N. Wiebe, "Thermalization and Canonical Typicality in Translation-Invariant Quantum Lattice Systems," *Commun. Math. Phys.*, vol. 340, pp. 499–561, Dec. 2015.

[197] M. Henkel, *Conformal Invariance and Critical Phenomena.* Theoretical and Mathematical Physics, Berlin Heidelberg: Springer-Verlag, 1999.

[198] P. Francesco, P. Mathieu, and D. Sénéchal, *Conformal Field Theory.* Graduate Texts in Contemporary Physics, New York: Springer-Verlag, 1997.

[199] J. D. Qualls, "Lectures on Conformal Field Theory," *arXiv:1511.04074*, May 2016.

[200] S. Ribault, "Conformal field theory on the plane," *arXiv:1406.4290*, June 2019.

[201] G. Mussardo, *Statistical Field Theory: An Introduction to Exactly Solved Models in Statistical Physics*. Oxford University Press.

[202] P. Ginsparg, "Applied Conformal Field Theory," *arXiv:hep-th/9108028*, Nov. 1988.

[203] V. G. Kac, A. K. Raina, and N. Rozhkovskaya, *Bombay Lectures On Highest Weight Representations Of Infinite Dimensional Lie Algebras*. Hackensack, New Jersey: Wspc, 2nd revised ed. edition ed., July 2013.

[204] M. Schottenloher, *A Mathematical Introduction to Conformal Field Theory*. Lect. Notes Phys., Berlin Heidelberg: Springer-Verlag, second ed., 2008.

[205] D. Friedan, Z. Qiu, and S. Shenker, "Conformal Invariance, Unitarity, and Critical Exponents in Two Dimensions," *Phys. Rev. Lett.*, vol. 52, pp. 1575–1578, Apr. 1984.

[206] D. Boyanovsky, "Field theory of the two-dimensional Ising model: Conformal invariance, order and disorder, and bosonization," *Phys. Rev. B*, vol. 39, pp. 6744–6756, Apr. 1989.

[207] S. Sachdev, *Quantum Phase Transitions*. Cambridge: Cambridge University Press, second ed., 2011.

[208] Y. A. Bashilov and S. V. Pokrovsky, "A conformally invariant limit of the critical lattice Ising model," *Commun.Math. Phys.*, vol. 113, pp. 115–136, Mar. 1987.

[209] J. L. Cardy, "Conformal invariance and surface critical behavior," *Nucl. Phys. B*, vol. 240, pp. 514–532, Nov. 1984.

[210] J. Cardy, "Boundary conditions, fusion rules and the Verlinde formula," *Nucl. Phys. B*, vol. 324, pp. 581–596, Oct. 1989.

[211] J. L. Cardy and D. C. Lewellen, "Bulk and boundary operators in conformal field theory," *Phys. Lett. B*, vol. 259, pp. 274–278, Apr. 1991.

[212] J. Cardy, "Boundary Conformal Field Theory," *arXiv:hep-th/0411189*, Feb. 2008.

[213] D. Tong, *Cambridge Lecture Notes on String Theory.* https://www.damtp.cam.ac.uk/user/tong/string.html.

[214] M. M. Rams and M. Zwolak, "Breaking the Entanglement Barrier: Tensor Network Simulation of Quantum Transport," *Phys. Rev. Lett.*, vol. 124, p. 137701, Mar. 2020.

[215] L. Pastori, M. Heyl, and J. C. Budich, "Disentangling sources of quantum entanglement in quench dynamics," *Phys. Rev. Research*, vol. 1, p. 012007, Aug. 2019.

[216] C. Krumnow, J. Eisert, and Ö. Legeza, "Towards overcoming the entanglement barrier when simulating long-time evolution," *arXiv:1904.11999*, Apr. 2019.

[217] J. Surace, M. Piani, and L. Tagliacozzo, "Simulating the out-of-equilibrium dynamics of local observables by trading entanglement for mixture," *Phys. Rev. B*, vol. 99, p. 235115, June 2019.

[218] G. Parisi, *Statistical Field Theory.* Addison-Wesley, 1988.

[219] A. Polkovnikov, K. Sengupta, A. Silva, and M. Vengalattore, "Colloquium : Nonequilibrium dynamics of closed interacting quantum systems," *Rev. Mod. Phys.*, vol. 83, pp. 863–883, Aug. 2011.

[220] P. Corboz and G. Vidal, "Fermionic multiscale entanglement renormalization ansatz," *Phys. Rev. B*, vol. 80, p. 165129, Oct. 2009.

[221] M. Rigol, V. Dunjko, and M. Olshanii, "Thermalization and its mechanism for generic isolated quantum systems," *Nature*, vol. 452, no. 7189, pp. 854–858, 2008.

[222] M. Cramer, C. M. Dawson, J. Eisert, and T. J. Osborne, "Exact Relaxation in a Class of Nonequilibrium Quantum Lattice Systems," *Phys. Rev. Lett.*, vol. 100, p. 030602, Jan. 2008.

[223] T. Barthel and U. Schollwöck, "Dephasing and the Steady State in Quantum Many-Particle Systems," *Phys. Rev. Lett.*, vol. 100, p. 100601, Mar. 2008.

[224] M. Cramer and J. Eisert, "A quantum central limit theorem for non-equilibrium systems: Exact local relaxation of correlated states," *New J. Phys.*, vol. 12, no. 5, p. 055020, 2010.

[225] T. Langen, S. Erne, R. Geiger, B. Rauer, T. Schweigler, M. Kuhnert, W. Rohringer, I. E. Mazets, T. Gasenzer, and J. Schmiedmayer, "Experimental observation of a generalized Gibbs ensemble," *Science*, vol. 348, pp. 207–211, Apr. 2015.

[226] E. Ilievski, J. De Nardis, B. Wouters, J.-S. Caux, F. H. L. Essler, and T. Prosen, "Complete Generalized Gibbs Ensembles in an Interacting Theory," *Phys. Rev. Lett.*, vol. 115, p. 157201, Oct. 2015.

[227] L. Vidmar and M. Rigol, "Generalized Gibbs ensemble in integrable lattice models," *J. Stat. Mech. Theory Exp.*, vol. 2016, no. 6, p. 64007, 2016.

[228] A. J. Daley, C. Kollath, U. Schollwöck, and G. Vidal, "Time-dependent density-matrix renormalization-group using adaptive effective Hilbert spaces," *J. Stat. Mech.: Theory Exp.*, vol. 2004, no. 04, p. P04005, 2004.

[229] S. R. White and A. E. Feiguin, "Real-Time Evolution Using the Density Matrix Renormalization Group," *Phys. Rev. Lett.*, vol. 93, p. 076401, Aug. 2004.

[230] S. Paeckel, T. Köhler, A. Swoboda, S. R. Manmana, U. Schollwöck, and C. Hubig, "Time-evolution methods for matrix-product states," *Annals of Physics*, vol. 411, p. 167998, Dec. 2019.

[231] J. Eisert, "Entanglement and tensor network states," *Model. Simul.*, vol. 3, no. 520, p. 39, 2013.

[232] S. Hernández-Santana, A. Riera, K. V. Hovhannisyan, M. Perarnau-Llobet, L. Tagliacozzo, and A. Acín, "Locality of temperature in spin chains," *New J. Phys.*, vol. 17, Aug. 2015.

[233] A. De Pasquale, D. Rossini, R. Fazio, and V. Giovannetti, "Local quantum thermal susceptibility," *Nat. Commun.*, vol. 7, p. 12782, Sept. 2016.

[234] A. García-Saez, A. Ferraro, and A. Acín, "Local temperature in quantum thermal states," *Phys. Rev. A*, vol. 79, p. 052340, May 2009.

[235] A. Ferraro, A. García-Saez, and A. Acín, "Intensive temperature and quantum correlations for refined quantum measurements," *EPL*, vol. 98, p. 10009, Apr. 2012.

[236] E. Leviatan, F. Pollmann, J. H. Bardarson, D. A. Huse, and E. Altman, "Quantum thermalization dynamics with Matrix-Product States," *arXiv:1702.08894*, Oct. 2017.

[237] C. D. White, M. Zaletel, R. S. K. Mong, and G. Refael, "Quantum dynamics of thermalizing systems," *Phys. Rev. B*, vol. 97, p. 035127, Jan. 2018.

[238] J. Wurtz and A. Polkovnikov, "Quantum diffusion in spin chains with phase space methods," *Phys. Rev. E*, vol. 101, p. 052120, May 2020.

[239] J.-S. Caux and F. H. L. Essler, "Time Evolution of Local Observables After Quenching to an Integrable Model," *Phys. Rev. Lett.*, vol. 110, p. 257203, June 2013.

[240] J. D. Nardis, L. Piroli, and J.-S. Caux, "Relaxation dynamics of local observables in integrable systems," *J. Phys. A Math. Theor.*, vol. 48, no. 43, p. 43FT01, 2015.

[241] J.-S. Caux, "The Quench Action," *J. Stat. Mech.*, vol. 2016, no. 6, p. 064006, 2016.

[242] C. Callan and F. Wilczek, "On geometric entropy," *Physics Letters B*, vol. 333, pp. 55–61, July 1994.

[243] J. L. Cardy, ed., *Finite-Size Scaling*, vol. 2 of *Current Physics–Sources and Comments*. Elsevier, Jan. 1988.

[244] L. Tagliacozzo, T. R. de Oliveira, S. Iblisdir, and J. I. Latorre, "Scaling of entanglement support for matrix product states," *Phys. Rev. B*, vol. 78, p. 024410, July 2008.

[245] P. Calabrese, J. Cardy, and E. Tonni, "Entanglement entropy of two disjoint intervals in conformal field theory," *J. Stat. Mech.: Theory Exp.*, vol. 2009, p. P11001, Nov. 2009.

[246] P. Calabrese, J. Cardy, and E. Tonni, "Entanglement entropy of two disjoint intervals in conformal field theory: II," *J. Stat. Mech.: Theory Exp.*, vol. 2011, p. P01021, Jan. 2011.

[247] V. Alba, L. Tagliacozzo, and P. Calabrese, "Entanglement entropy of two disjoint intervals in c=1 theories," *J. Stat. Mech.: Theory Exp.*, vol. 2011, p. P06012, June 2011.

[248] A. Coser, L. Tagliacozzo, and E. Tonni, "On Rényi entropies of disjoint intervals in conformal field theory," *J. Stat. Mech.: Theory Exp.*, vol. 2014, p. P01008, Jan. 2014.

[249] C. De Nobili, A. Coser, and E. Tonni, "Entanglement entropy and negativity of disjoint intervals in CFT: Some numerical extrapolations," *J. Stat. Mech.: Theory Exp.*, vol. 2015, p. P06021, June 2015.

[250] J. Cardy, "Measuring Entanglement Using Quantum Quenches," *Phys. Rev. Lett.*, vol. 106, p. 150404, Apr. 2011.

[251] D. A. Abanin and E. Demler, "Measuring Entanglement Entropy of a Generic Many-Body System with a Quantum Switch," *Phys. Rev. Lett.*, vol. 109, p. 020504, July 2012.

[252] A. J. Daley, H. Pichler, J. Schachenmayer, and P. Zoller, "Measuring Entanglement Growth in Quench Dynamics of Bosons in an Optical Lattice," *Phys. Rev. Lett.*, vol. 109, p. 020505, July 2012.

[253] R. Islam, R. Ma, P. M. Preiss, M. Eric Tai, A. Lukin, M. Rispoli, and M. Greiner, "Measuring entanglement entropy in a quantum many-body system," *Nature*, vol. 528, pp. 77–83, Dec. 2015.

[254] P. Hauke, M. Heyl, L. Tagliacozzo, and P. Zoller, "Measuring multipartite entanglement through dynamic susceptibilities," *Nat. Phys.*, vol. 12, pp. 778–782, Aug. 2016.

[255] H. Pichler, G. Zhu, A. Seif, P. Zoller, and M. Hafezi, "Measurement Protocol for the Entanglement Spectrum of Cold Atoms," *Phys. Rev. X*, vol. 6, p. 041033, Nov. 2016.

[256] A. M. Kaufman, M. E. Tai, A. Lukin, M. Rispoli, R. Schittko, P. M. Preiss, and M. Greiner, "Quantum thermalization through entanglement in an isolated many-body system," *Science*, vol. 353, pp. 794–800, Aug. 2016.

[257] M. Dalmonte, B. Vermersch, and P. Zoller, "Quantum simulation and spectroscopy of entanglement Hamiltonians," *Nat. Phys.*, vol. 14, pp. 827–831, Aug. 2018.

[258] A. Elben, B. Vermersch, M. Dalmonte, J. I. Cirac, and P. Zoller, "Renyi Entropies from Random Quenches in Atomic Hubbard and Spin Models," *Phys. Rev. Lett.*, vol. 120, p. 050406, Feb. 2018.

[259] B. Vermersch, A. Elben, M. Dalmonte, J. I. Cirac, and P. Zoller, "Unitary n-designs via random quenches in atomic Hubbard and spin models: Application to the measurement of Renyi entropies," *Phys. Rev. A*, vol. 97, p. 023604, Feb. 2018.

[260] T. Brydges, A. Elben, P. Jurcevic, B. Vermersch, C. Maier, B. P. Lanyon, P. Zoller, R. Blatt, and C. F. Roos, "Probing Rényi entanglement entropy via randomized measurements," *Science*, vol. 364, pp. 260–263, Apr. 2019.

[261] A. Lukin, M. Rispoli, R. Schittko, M. E. Tai, A. M. Kaufman, S. Choi, V. Khemani, J. Léonard, and M. Greiner, "Probing entanglement in a many-body–localized system," *Science*, vol. 364, pp. 256–260, Apr. 2019.

[262] M. Prüfer, P. Kunkel, H. Strobel, S. Lannig, D. Linnemann, C.-M. Schmied, J. Berges, T. Gasenzer, and M. K. Oberthaler, "Observation of universal dynamics in a spinor Bose gas far from equilibrium," *Nature*, vol. 563, pp. 217–220, Nov. 2018.

[263] A. M. Läuchli, "Operator content of real-space entanglement spectra at conformal critical points," *arXiv:1303.0741*, Mar. 2013.

[264] J. Cardy and E. Tonni, "Entanglement Hamiltonians in two-dimensional conformal field theory," *J. Stat. Mech.: Theory Exp.*, vol. 2016, p. 123103, Dec. 2016.

[265] G. D. Giulio, R. Arias, and E. Tonni, "Entanglement Hamiltonians in 1D free lattice models after a global quantum quench," *J. Stat. Mech.*, vol. 2019, p. 123103, Dec. 2019.

[266] D. W. Robinson, "Properties of propagation of quantum spin systems," *J. Aust. Math. Soc.*, vol. 19, p. 387, Dec. 1976.

[267] J. Cardy and E. Tonni, "Entanglement Hamiltonians in two-dimensional conformal field theory," *J. Stat. Mech.: Theory Exp.*, vol. 2016, p. 123103, Dec. 2016.

[268] P. Calabrese and J. Cardy, "Quantum quenches in extended systems," *J. Stat. Mech.: Theory Exp.*, vol. 2007, p. P06008, June 2007.

[269] J. Cardy, "Thermalization and Revivals after a Quantum Quench in Conformal Field Theory," *Phys. Rev. Lett.*, vol. 112, p. 220401, June 2014.

[270] J. Cardy, "Quantum revivals in conformal field theories in higher dimensions," *J. Phys. A: Math. Theor.*, vol. 49, p. 415401, Sept. 2016.

[271] P. Calabrese and J. Cardy, "Quantum quenches in 1 + 1 dimensional conformal field theories," *J. Stat. Mech.: Theory Exp.*, vol. 2016, p. 064003, June 2016.

[272] J. Surace, L. Tagliacozzo, and E. Tonni, "Operator content of entanglement spectra in the transverse field Ising chain after global quenches," *Phys. Rev. B*, vol. 101, p. 241107, June 2020.

[273] M. Fagotti and F. H. L. Essler, "Reduced density matrix after a quantum quench," *Phys. Rev. B*, vol. 87, p. 245107, June 2013.

[274] M. Heyl, A. Polkovnikov, and S. Kehrein, "Dynamical Quantum Phase Transitions in the Transverse-Field Ising Model," *Phys. Rev. Lett.*, vol. 110, p. 135704, Mar. 2013.

[275] M. Heyl, "Dynamical quantum phase transitions: A brief survey," *EPL*, vol. 125, p. 26001, Feb. 2019.

[276] G. Torlai, L. Tagliacozzo, and G. De Chiara, "Dynamics of the entanglement spectrum in spin chains," *J. Stat. Mech.: Theory Exp.*, vol. 2014, p. P06001, June 2014.

[277] M. Fagotti, "Dynamical Phase Transitions as Properties of the Stationary State: Analytic Results after Quantum Quenches in the Spin-1/2 XXZ Chain," *arXiv:1308.0277*, Aug. 2013.

[278] P. Jordan and E. Wigner, "Über das Paulische Äquivalenzverbot," *Z. Phys.*, vol. 47, pp. 631–651, Sept. 1928.

[279] Y. S. Li, B. Zeng, X. S. Liu, and G. L. Long, "Entanglement in a two-identical-particle system," *Phys. Rev. A*, vol. 64, p. 054302, Oct. 2001.

[280] J. Schliemann, J. I. Cirac, M. Kuś, M. Lewenstein, and D. Loss, "Quantum correlations in two-fermion systems," *Phys. Rev. A*, vol. 64, p. 022303, July 2001.

[281] M. M. Wolf, "Violation of the Entropic Area Law for Fermions," *Phys. Rev. Lett.*, vol. 96, p. 010404, Jan. 2006.

[282] M.-C. Bañuls, J. I. Cirac, and M. M. Wolf, "Entanglement in fermionic systems," *Phys. Rev. A*, vol. 76, p. 022311, Aug. 2007.

[283] E. Sindici and M. Piani, "Simple class of bound entangled states based on the properties of the antisymmetric subspace," *Phys. Rev. A*, vol. 97, p. 032319, Mar. 2018.

[284] J. Becher, E. Sindici, R. Klemt, S. Jochim, A. Daley, and P. Preiss, "Measurement of Identical Particle Entanglement and the Influence of Antisymmetrization," *Phys. Rev. Lett.*, vol. 125, p. 180402, Oct. 2020.